



# University of HUDDERSFIELD

## University of Huddersfield Repository

Zhang, Hongyu

The Influence of Stem Design and Fixation Methods on the Lifetime of Total Hip Replacement

### Original Citation

Zhang, Hongyu (2009) The Influence of Stem Design and Fixation Methods on the Lifetime of Total Hip Replacement. Doctoral thesis, University of Huddersfield.

This version is available at <http://eprints.hud.ac.uk/id/eprint/6965/>

The University Repository is a digital collection of the research output of the University, available on Open Access. Copyright and Moral Rights for the items on this site are retained by the individual author and/or other copyright owners. Users may access full items free of charge; copies of full text items generally can be reproduced, displayed or performed and given to third parties in any format or medium for personal research or study, educational or not-for-profit purposes without prior permission or charge, provided:

- The authors, title and full bibliographic details is credited in any copy;
- A hyperlink and/or URL is included for the original metadata page; and
- The content is not changed in any way.

For more information, including our policy and submission procedure, please contact the Repository Team at: [E.mailbox@hud.ac.uk](mailto:E.mailbox@hud.ac.uk).

<http://eprints.hud.ac.uk/>

**The Influence of Stem Design and Fixation Methods  
on the Lifetime of Total Hip Replacement**

**Hongyu Zhang**

**Direct Supervisor: Professor Liam Blunt**

**Centre for Precision Technologies  
School of Computing and Engineering  
University of Huddersfield**

**A thesis submitted to the University of Huddersfield in accordance with  
the requirements for the degree of Doctor of Philosophy**

**January 2009**

## Abstract

Total hip replacement is one of the most common surgical procedures performed both in the UK and worldwide, with aseptic loosening cited as the primary reason for revision. Aseptic loosening is attributed to the wear debris generated by wear of the components. Recently, as great progress has been achieved in reducing wear at the head–cup interface, there has been a shift of research interest to other load bearing surfaces.

The main purpose of this thesis is to study fretting wear mechanisms at the polished femoral stem–bone cement interface.

The initial studies have investigated the bond strength at the stem–cement interface using seven brands of bone cement and femoral stems with different surface finishes. It can be confirmed that debonding at this interface is inevitable, which subsequently facilitates generation of fretting wear on the stem surface.

A new test methodology has been developed to reproduce fretting wear clinically seen on polished stems through *in vitro* wear simulations, and it shows great success in comparison with previous attempts. In addition, migration of the stem within the cement mantle has been investigated, and it has been indicated that the simulation setup more realistically mimics clinical situations.

The influence of two factors on generation of fretting wear, i.e. the duration of *in vivo* service of the hip implant and bone cement brand, has been studied. A potential fretting wear initiator that is concerned with polymerisation of bone cement has been identified, with both experimental (the results of wear simulations) and theoretical (finite element analysis) evidence being provided.

In summary, the overall contribution of this research is that it has gained a deep insight into the fretting wear mechanism between polished femoral stem and bone cement.

## **Acknowledgements**

I would firstly like to thank my director of studies Prof. Liam Blunt for his great supervision and professional guidance during this research. I am most indebted to him and I am deeply impressed by his erudition in knowledge and attitude in science which promote me to keep on going.

I would also like to show my grateful appreciation to the other members of the supervisory team, Prof. Xiang qian (Jane) Jiang, Dr. Leigh Brown and Dr. Simon Barrans for their continuous suggestions and aspiring assistance, which are certainly one of the key elements in the completion of this thesis.

Additionally, I would like to express my deepest thanks to Dr. Shaojun Xiao, Dr. Feng Xie, Dr. Paul Bills, Dr. Philip Harrison, and Mr. Allan Kennedy, Centre for Precision Technologies, School of Computing and Engineering, The University of Huddersfield, who have been so supportive over the years.

From a more practical view, Mr. Peter Norman, Mr. Dennis Town and other technicians, School of Computing and Engineering, The University of Huddersfield, have provided substantial technical assistance throughout the duration of this research. I would like to thank them from the bottom of my heart.

Many thanks are due for the support from Mr. Ian Johnson and Dr. Howard Williams, School of Applied Science, The University of Huddersfield, who trained me on scanning electron microscopy and provided me an access whenever available.

Lastly, I would like to show my sincere gratitude to my family and all of the friends in Centre for Precision Technologies, The University of Huddersfield, but especially my beloved wife Yan Zhao for her tendance in my life and continued belief in me.

<b>Abstract.....</b>	<b>1</b>
<b>Acknowledgements .....</b>	<b>2</b>
<b>List of figures.....</b>	<b>7</b>
<b>List of tables.....</b>	<b>13</b>
<b>Abbreviations .....</b>	<b>14</b>
<b>Chapter 1 Introduction.....</b>	<b>15</b>
<b>1.1 Project background.....</b>	<b>15</b>
1.1.1 Total hip replacement .....	15
1.1.2 Failure of total hip replacement .....	16
1.1.3 The stem–cement interface .....	17
<b>1.2 Project aims and objectives .....</b>	<b>18</b>
1.2.1 Aims.....	18
1.2.2 Objectives .....	18
<b>Chapter 2 Total hip replacement .....</b>	<b>20</b>
<b>2.1 Chapter summary .....</b>	<b>20</b>
<b>2.2 The loading regime of the hip joint .....</b>	<b>20</b>
2.2.1 Anatomy of the hip .....	20
2.2.2 Hip joint force.....	22
<b>2.3 Uncemented and cemented total hip replacement .....</b>	<b>23</b>
2.3.1 Uncemented total hip replacement.....	23
2.3.2 Cemented total hip replacement.....	24
<b>2.4 Metal femoral stem .....</b>	<b>25</b>
2.4.1 General introduction .....	25
2.4.2 Design properties .....	27
<b>2.5 Acrylic bone cement.....</b>	<b>29</b>
2.5.1 General introduction .....	29
2.5.2 Mechanical and physical properties.....	31
2.5.3 Current controversies.....	33
<b>2.6 Failure mechanisms of cemented total hip replacement.....</b>	<b>34</b>
2.6.1 General introduction .....	34
2.6.2 Wear debris induced bone resorption.....	35
2.6.3 Stress shielding .....	36
<b>2.7 Wear at the stem–cement interface .....</b>	<b>37</b>
2.7.1 General introduction .....	37
2.7.2 Evidence of wear on the stem .....	38
2.7.3 Wear mechanism at the stem–cement interface .....	39
<b>2.8 Fretting wear and <i>in vitro</i> simulation .....</b>	<b>42</b>
2.8.1 Fretting wear .....	42
2.8.2 <i>In vitro</i> simulation of fretting wear .....	43
<b>Chapter 3 Metrology strategy .....</b>	<b>45</b>
<b>3.1 Chapter summary .....</b>	<b>45</b>
<b>3.2 The challenge for metrology in hip orthopaedic industry .....</b>	<b>45</b>
3.2.1 The head–cup interface.....	45
3.2.2 The stem–cement interface .....	46

3.2.3 Summary .....	47
<b>3.3 Instrumentation employed throughout the research of the project .....</b>	<b>47</b>
3.3.1 Contacting stylus measurement—Talysurf PGI Series 2 .....	48
3.3.2 Non-contacting optical measurement—Talysurf CCI 3000.....	49
3.3.3 Scanning electron microscope—JEOL JSM-6060 .....	51
<b>3.4 Characterisation technology .....</b>	<b>54</b>
3.4.1 The limitations of 2D surface characterisation .....	54
3.4.2 3D surface characterisation.....	55
<b>Chapter 4 The stem–cement interfacial strength.....</b>	<b>57</b>
<b>4.1 Chapter summary .....</b>	<b>57</b>
<b>4.2 The stem–cement interfacial gap .....</b>	<b>57</b>
4.2.1 Background and aims.....	57
4.2.2 Materials and methods .....	58
4.2.3 Results and discussion .....	59
4.2.4 Conclusions.....	60
<b>4.3 Interfacial strength between polished stem and bone cements .....</b>	<b>60</b>
4.3.1 Background and aims.....	60
4.3.2 Materials and methods .....	61
4.3.3 Results.....	65
4.3.4 Discussion.....	72
4.3.5 Conclusions.....	73
<b>4.4 Influence of stem surface finish on stem–cement interfacial strength.....</b>	<b>74</b>
4.4.1 Background and aims.....	74
4.4.2 Materials and methods .....	74
4.4.3 Results.....	76
4.4.4 Discussion.....	82
4.4.5 Conclusions.....	84
<b>4.5 Summary .....</b>	<b>84</b>
<b>Chapter 5 Reproduction of fretting wear on the femoral stem.....</b>	<b>86</b>
<b>5.1 Chapter summary .....</b>	<b>86</b>
<b>5.2 Initial attempt to replicate fretting wear at the stem–cement interface (Simulation I).....</b>	<b>86</b>
5.2.1 Background and aims.....	86
5.2.2 Materials and methods .....	87
5.2.3 Results.....	90
5.2.4 Discussion.....	98
5.2.5 Conclusions.....	99
<b>5.3 Consistent reproduction of fretting wear at the stem–cement interface (Simulation II) .....</b>	<b>100</b>
5.3.1 Background and methods.....	100
5.3.2 Results.....	100
5.3.3 Discussion.....	104
<b>5.4 Summary of the <i>in vitro</i> wear simulations .....</b>	<b>105</b>
<b>Chapter 6 Relative micromotion at the stem–cement interface .....</b>	<b>106</b>

<b>6.1 Chapter summary .....</b>	<b>106</b>
<b>6.2 Investigation of relative micromotion at the stem–cement interface (Simulation III)</b>	<b>106</b>
6.2.1 Background and aims.....	106
6.2.2 Materials and methods .....	107
6.2.3 Results.....	109
6.2.4 Discussion.....	112
6.2.5 Conclusions.....	114
<b>6.3 Summary .....</b>	<b>114</b>
<b>Chapter 7 Factors influencing fretting wear on the femoral stem .....</b>	<b>115</b>
<b>7.1 Chapter summary .....</b>	<b>115</b>
<b>7.2 Influence of the duration of <i>in vivo</i> service of the hip prosthesis on generation of fretting wear (Simulation IV).....</b>	<b>115</b>
7.2.1 Background and methods.....	115
7.2.2 Results and discussion .....	116
7.2.3 Conclusions.....	121
<b>7.3 Influence of bone cement brand on generation of fretting wear (Simulation V to VIII).....</b>	<b>121</b>
7.3.1 Background and aims.....	121
7.3.2 Materials and methods .....	121
7.3.2 Results.....	122
7.3.3 Discussion.....	134
7.3.4 Conclusions.....	136
<b>7.4 A summary of all the <i>in vitro</i> wear simulations completed (from Simulation I to VIII, see Appendix IV).....</b>	<b>136</b>
<b>Chapter 8 Initiation and propagation of fretting wear on the femoral stem.....</b>	<b>137</b>
<b>8.1 Chapter summary .....</b>	<b>137</b>
<b>8.2 Finite element analysis of the stem–cement interface .....</b>	<b>137</b>
8.2.1 Background and aims.....	137
8.2.2 Methods .....	138
8.2.3 Results.....	141
8.2.4 Discussion.....	148
8.2.5 Conclusions.....	150
<b>8.3 Summary .....</b>	<b>150</b>
<b>Chapter 9 Discussion .....</b>	<b>151</b>
<b>Chapter 10 Conclusions.....</b>	<b>154</b>
<b>Chapter 11 Future studies .....</b>	<b>155</b>
<b>11.1 Investigation of the influence of storage condition of bone cement on its mechanical properties and long term performance .....</b>	<b>155</b>
<b>11.2 Investigation of the influence of stem geometry and surface finish on generation of fretting wear .....</b>	<b>155</b>
<b>11.3 Development of a method to evaluate the wear debris at the stem–cement interface.....</b>	<b>156</b>
<b>11.4 Further refinement of the simulation rig .....</b>	<b>156</b>

11.5 More detailed study of FEA techniques to investigate the stem–cement interface	156
References	158
Appendix I	167
Three-way ANOVA of static shear strength, interfacial porosity, and micropore size for bone cements (Section 4.3)	167
Appendix II	168
Unpaired student t-test between Simplex P and Simplex P–T (Section 4.3)	168
Appendix III	168
One-way ANOVA of interfacial strength and Tukey–Kramer Post Hoc Test for different surface finish rods (Section 4.4)	168
Appendix IV	169
Summary of the <i>in vitro</i> wear simulations to reproduce fretting wear at the stem–cement interface	169
Appendix V	170
3D surface topography of the worn areas of Gruen zones 6 and 7 on the femoral stem in simulation I (Section 5.2)	170
Appendix VI	171
Surface topography of fretting zone on the femoral stem from Simulation I measured utilising scanning electron microscope (Section 5.2)	171
Appendix VII	171
Fretting wear scar generated on the femoral stem from Simulation II (Section 5.3)	171
Appendix VIII	172
Calibration of the new custom-made micromotion sensor (Section 6.2)	172
Appendix IX	172
One-way ANOVA of 3D surface parameters of the fretting zones on the stem (Section 7.2)	172
Appendix X	173
Microhardness test of the bone cements from the <i>in vitro</i> wear simulations (Section 7.3)	173
Appendix XI	174
Shrinkage bumps present on Simplex P and Corioplast 3 bone cements following polymerisation (Section 8.3)	174
Appendix XII	174
A selection of publications resulting from this project	174

## List of figures

- Figure 1.1: (a) Osteoarthritis at the hip (b) Total hip replacement with a metal prosthesis
- Figure 1.2: (a) Uncemented total hip replacement (b) Cemented total hip replacement
- Figure 1.3: Typical periprosthetic bone resorption
- Figure 2.1: The structure of a natural hip
- Figure 2.2: Definition of degree of freedom of hip motions
- Figure 2.3: Hip joint reaction force in terms of body weight through one walking cycle (1) Vertical force (2) Entraining velocity (Paul 1967)
- Figure 2.4: Typical procedures of total hip replacement
- Figure 2.5: Different designs of femoral implants
- Figure 2.6: (a) Example of a modular femoral stem design—Exeter (b) Example of a monoblock femoral stem design—Charnley
- Figure 2.7: Load transfer patterns (a) Within the natural femur (b) Around the C stem
- Figure 2.8: The formation of polymer chains (a) Radical for initiation of polymerisation and MMA monomer (b) Growing polymer chain with reactive site at the end (c) Final polymer molecule
- Figure 2.9: Fractures present in bone cement mantle: c=cement; p=prosthesis; b=bone
- Figure 2.10: Reasons for revision of THR (a) Stem fracture (b) Prosthesis dislocation
- Figure 2.11: Migration of wear debris to bone tissues through gaps at the stem–cement interface
- Figure 2.12: Effect of stress shielding
- Figure 2.13: Evidence of abrasive wear present on matt Exeter femoral stems
- Figure 2.14: Fretting wear on an explanted polished Exeter femoral stem measured by SEM
- Figure 2.15: Grazing incidence SEM images showing increasing degrees of polishing wear on matt-surfaced stems (a) An unworn area (b) An area of slight polishing wear (c) An area of marked polishing wear (Howell et al. 2004)
- Figure 2.16: The axonometric plots showing progressive stages of abrasive wear on an Exeter matt-surfaced stem, the asperities present on the unworn surface are removed during the wear process (Brown 2006)
- Figure 2.17: The schematic appearance of fretting damage on metal surfaces
- Figure 2.18: (a) The model of simplified pin-on-plate device, the arrows show axial force on the pin and sliding motion of the plate (b) The model of simplified pin-on-disk device, the arrows show axial force on the pin and rotating motion of the disk
- Figure 3.1: The plot showing range and resolution for the available measurement techniques
- Figure 3.2: The schematic diagram showing the principle of RCHD grating transducer
- Figure 3.3: The contacting stylus measurement instrument—Talysurf PGI
- Figure 3.4: The non-contacting optical measurement instrument—Talysurf CCI 3000
- Figure 3.5: The basic principle showing how Talysurf CCI 3000 works
- Figure 3.6: The schematic diagram showing the main components of a scanning electron microscope
- Figure 3.7: Various signals generated by the interaction between the electron beam and the specimen
- Figure 3.8: The scanning electron microscope—JEOL JSM–6060
- Figure 3.9: Three surfaces with evidently different height distributions but the same Ra

Figure 3.10: A 2D trace taken from an areal surface measurement shows the ambiguity of 2D surface characterisation

Figure 3.11: The 3D field parameter set to describe functional performance of a surface

Figure 4.1: The schematic diagram to describe the steps to prepare the experimental specimen

Figure 4.2: The experimental specimen to test fluid flow along the stem–cement interface

Figure 4.3: Observation of the blue ink at the bottom of the shot-blasted stainless steel rod

Figure 4.4: (a) Dimension of the stainless steel rods (b) Design of the steel holder

Figure 4.5: Preparation of specimen using a milling machine chuck to ensure axial positioning

Figure 4.6: Set up of pull out test on a Hounsfield Test Machine H20K–W

Figure 4.7: The Leica optical stereomicroscope

Figure 4.8: Micropores detection based on grey scale threshold (a) Original image (b) Detected image

Figure 4.9: The model of three-way analysis of variance

Figure 4.10: Static shear strength for the 12mm diameter stainless steel rod

Figure 4.11: Interfacial porosity for the 12mm diameter stainless steel rod

Figure 4.12: Micropore size at the interface for the 12mm diameter stainless steel rod

Figure 4.13: Static shear strength for the 8mm diameter stainless steel rod

Figure 4.14: Interfacial porosity for the 8mm diameter stainless steel rod

Figure 4.15: Micropore size at the interface for the 8mm diameter stainless steel rod

Figure 4.16: A typical load–displacement plot for the pull out test

Figure 4.17: (a) Pull out test performed on Instron Test Machine (b) Transfer films on the rod surface

Figure 4.18: (a) Transfer films detected for CMW 3 bone cement in the pull out test by Instron (b) 2D profile showing height of transfer films for CMW 3 bone cement in a pull out test by Instron

Figure 4.19: The flow diagram showing the pull out process of the rod from the cement mantle

Figure 4.20: Pull out test of a cylindrical fibre from a resin disk (a) The fibre embedded in the resin disk (b) Typical load–displacement curve

Figure 4.21: (a) Transfer films detected for CMW 3 bone cement in a pull out test by Hounsfield (b) 2D profile showing height of transfer films for CMW 3 bone cement in a pull out test by Hounsfield

Figure 4.22: 3D surface topography of stainless steel rods before pull out test (a) Polished (b) Glass bead-blasted (c) Shot-blasted (d) Grit-blasted

Figure 4.23: Interfacial strength between Simplex P bone cement and different surface finish rods

Figure 4.24: Typical load–displacement plot for pull out test of glass bead-blasted stainless steel rods

Figure 4.25: Typical load–displacement plot for pull out test of shot-blasted stainless steel rods

Figure 4.26: Typical load–displacement plot for pull out test of grit-blasted stainless steel rods

Figure 4.27: Stainless steel rod surface after pull out test (a) Polished rod, the black substrate is the polished rod, and the lighter areas are the transfer films (b) Glass bead-blasted rod, no cement is present on the surface (c) Shot-blasted rod, no cement is present on the surface (d) Grit-blasted rod, the shiny substrate is the grit-blasted rod, and the grey covering is cement debris

Figure 4.28: Micropores formed in the cement surface interfaced with polished rods

Figure 4.29: 3D surface topography of bone cement interfaced with stainless steel rods (a) Polished (b) Glass bead-blasted (c) Shot-blasted (d) Grit-blasted

Figure 4.30: Metallic debris embedding within the cement mantle originating from the grit-blasted rod pull out test

Figure 5.1: Preparation of specimen for fretting wear simulation

Figure 5.2: Oscilloscope displaying the sine wave force applied to femoral head (Channel 1) and the corresponding displacement of the experimental specimen (Channel 2) of Instron test machine

Figure 5.3: Definition of Gruen zones of the stem surface

Figure 5.4: The grid coordinate system to relocate the position of femoral stem

Figure 5.5: Validation of the relocation system by two measurements taken at different time

Figure 5.6: Fretting wear generated on the femoral stem surface (Simulation I, use Simplex P cement)

Figure 5.7: Detection of worn areas on the stem surface based on grey scale threshold

Figure 5.8: Change of stem surface at the same position pre and post simulation (Simulation I, use Simplex P cement)

Figure 5.9: (a) Comparison of fretting wear area and undamaged area on the femoral stem (b) 2D surface topography of the worn areas (Simulation I, use Simplex P cement)

Figure 5.10: The thresholding process to remove potential wear debris above the original stem surface

Figure 5.11: Histogram showing change of  $S_q$  pre and post simulation of selected area on the stem

Figure 5.12: Histogram showing change of  $S_z$  pre and post simulation of selected area on the stem

Figure 5.13: Histogram showing change of  $S_{dq}$  pre and post simulation of selected area on the stem

Figure 5.14: Histogram showing change of  $S_{dr}$  pre and post simulation of selected area on the stem

Figure 5.15: Comparison of fretting zones between (a) Simulated Exeter femoral stem and (b) Explanted Exeter femoral stem (Simulation I, use Simplex P cement) (two micrographs at optimal magnification to show fretting effects)

Figure 5.16: Comparison of worn and unworn areas on the Simplex P cement surface (Simulation I)

Figure 5.17: (a) SEM micrograph showing fretting debris located in the micropores (b) Corresponding EDX analysis (Simulation I, use Simplex P cement)

Figure 5.18: (a) Optical micrograph showing “undamaged islands” on the stem surface and (b) Corresponding micropores in the cement surface (Simulation I, use Simplex P cement)

Figure 5.19: Initiation of fretting wear on the stem surface and micropores in the cement surface (Simulation II, use Simplex P cement)

Figure 5.20: Initiation of fretting wear on the stem surface and micropores in the cement surface (Simulation II, use Simplex P cement)

Figure 5.21: Propagation of fretting wear on the stem surface and micropores in the cement surface (Simulation II, use Simplex P cement)

Figure 5.22: (a) Interferometric micrograph of the worn areas showing propagation of fretting wear on the stem surface (b) 2D surface topography of the worn areas (Simulation II, use Simplex P cement)

Figure 5.23: The maximum and minimum position of the experimental specimen, note that the dashed line is fitted according to the tendency of the data (Simulation II, use Simplex P cement)

Figure 5.24: Shrinkage bumps on the cement surface following polymerisation and its 2D profile

Figure 6.1: The schematic diagram showing the principle of the micromotion sensor

Figure 6.2: Calibration of the micromotion sensor using the extensometer

Figure 6.3: The curve fitted using Least Squares Analysis based on the recorded data

Figure 6.4: The experimental specimen prepared for the present simulation

Figure 6.5: Migration of the polished Exeter stem within the cement mantle, the curves (a) and (b) correspond to the maximum and minimum values of the compressive loading respectively

Figure 6.6: Generation of typical fretting pits on the femoral stem surface (Simulation III)

Figure 6.7: Initiation of fretting wear on the stem surface and micropores in the cement surface (Simulation III)

Figure 6.8: The femoral stem and bone cement surfaces after simulation demonstrating an evident relationship between fretting wear damage and unworn areas on the stem surface and corresponding contact areas on the cement surface (Simulation III)

Figure 7.1: Fretting wear generated on the femoral stem surface (Simulation IV, use Simplex P cement)

Figure 7.2: Talysurf CCI measurement of worn areas on the stem surface (Simulation IV, use Simplex P cement)

Figure 7.3: Comparison of 3D surface parameters of the worn areas on the femoral stem between two wear simulations (Simulation I and Simulation IV)

Figure 7.4: Optical micrograph of cement surface showing the highly reflective sites around the micropores (Simulation IV, use Simplex P cement)

Figure 7.5: (a) SEM micrograph of the micropores in the cement surface (b) EDX analysis (Simulation IV, use Simplex P cement)

Figure 7.6: Micro-cracks initiated at the edge of the micropores in the Simplex P cement surface (Simulation IV)

Figure 7.7: Magnification of the two micro-cracks in figure 7.6

Figure 7.8: Optical micrograph showing undamaged areas on the stem surface and micropores in the cement surface (Simulation IV, use Simplex P cement)

Figure 7.9: The Micromet 2101 microhardness tester

Figure 7.10: Fretting wear generated on the femoral stem surface (Simulation V, use CMW 3 cement)

Figure 7.11: Fretting wear generated on the femoral stem surface (Simulation VI, use CMW 3 cement)

Figure 7.12: Talysurf CCI measurement of worn areas on the stem surface (Simulation V, use CMW 3 cement)

Figure 7.13: Talysurf CCI measurement of worn areas on the stem surface (Simulation VI, use

CMW 3 cement)

Figure 7.14: Initiation of fretting wear on the stem surface and micropores in the cement surface (Simulation V, use CMW 3 cement)

Figure 7.15: Propagation of fretting wear on the stem surface and micropores in the cement surface (Simulation V, use CMW 3 cement)

Figure 7.16: Initiation of fretting wear on the stem surface and micropores in the cement surface (Simulation VI, use CMW 3 cement)

Figure 7.17: Propagation of fretting wear on the stem surface and micropores in the cement surface (Simulation VI, use CMW 3 cement)

Figure 7.18: Optical micrograph of cement surface showing areas of potential metallic debris around the micropores (Simulation V, use CMW 3 cement)

Figure 7.19: (a) SEM micrograph of the micropores in the cement surface (b) EDX analysis (Simulation V, use CMW 3 cement)

Figure 7.20: Optical micrograph of cement surface showing areas of potential metallic debris around the micropores (Simulation VI, use CMW 3 cement)

Figure 7.21: (a) SEM micrograph of the micropores in the cement surface (b) EDX analysis (Simulation VI, use CMW 3 cement)

Figure 7.22: Fretting wear generated on the femoral stem surface (Simulation VII, use Palacos R cement)

Figure 7.23: Fretting wear generated on the femoral stem surface (Simulation VIII, use Palacos R cement)

Figure 7.24: Comparison of fretting wear area and undamaged area on the femoral stem (Simulation VII, use Palacos R cement)

Figure 7.25: Comparison of fretting wear area and undamaged area on the femoral stem (Simulation VIII, use Palacos R cement)

Figure 7.26: Optical micrograph showing undamaged areas on the stem surface and micropores in the cement surface (Simulation VII, use Palacos R cement)

Figure 7.27: Optical micrograph showing undamaged areas on the stem surface and micropores in the cement surface (Simulation VIII, use Palacos R cement)

Figure 7.28: Optical micrograph of cement surface showing areas of potential metallic debris around the micropores (Simulation VII, use Palacos R cement)

Figure 7.29: (a) SEM micrograph of the micropores in the cement surface (b) EDX analysis (Simulation VII, use Palacos R cement)

Figure 7.30: Optical micrograph of cement surface showing areas of potential metallic debris around the micropores (Simulation VIII, use Palacos R cement)

Figure 7.31: (a) SEM micrograph of the micropores in the cement surface (b) EDX analysis (Simulation VIII, use Palacos R cement)

Figure 8.1: Shrinkage bumps present on the common bone cement surfaces following polymerisation (a) Simplex P with tobramycin (b) Palacos R (c) CMW 1 (d) CMW 3

Figure 8.2: 2D finite element model simulating the interaction between the stem and the bumps

Figure 8.3: 2D finite element model simulating the interaction between the stem and the micropores

Figure 8.4: The schematic diagram showing the interaction between the stem and the shrinkage

bumps when pressing the stem to the cement (a) The stem and the bumps contact without any deformation (b) The bumps are badly deformed upon loading (c) There exits a gap at the edge of the bumps (d) The stem and the bumps are in full contact

Figure 8.5: The relative micromotion along the stem–cement interface between the stem and the shrinkage bumps

Figure 8.6: The contact pressure normal to the cement surface between the stem and the shrinkage bumps

Figure 8.7: The schematic diagram showing the interaction between the stem and the micropore (1) when pressing the stem to the cement

Figure 8.8: The relative micromotion along the stem–cement interface between the stem and the micropores

Figure 8.9: The contact pressure normal to the cement surface between the stem and the micropores

Figure 8.10: The maximum relative micromotion along the stem–cement interface between the stem and the micropores with different sizes. The red line shows the tendency for micropore (1) and the blue line shows the tendency for micropore (2)

Figure 8.11: The maximum contact pressure normal to the cement surface between the stem and the micropores with different sizes

Figure 8.12: The maximum relative micromotion along the stem–cement interface between the stem and micropores with different loading levels, the red line shows the tendency for micropore (1) and the blue line shows the tendency for micropore (2)

Figure 8.13: The maximum contact pressure normal to the cement surface between the stem and the micropores with different loading levels

Figure 8.14: The 2D surface profile of a commercial highly polished femoral stem with the variation in amplitude of about 40nm

## List of tables

- Table 2.1: The three degrees of freedom of the hip joint
- Table 2.2: Typical studies on hip joint forces during different human normal activities
- Table 2.3: The five most commonly used bone cements
- Table 2.4: Typical characteristics of three generations of cementing techniques
- Table 3.1: The typical specifications of Talysurf PGI Series 2
- Table 3.2: The typical specifications of Talysurf CCI 3000
- Table 3.3: The typical specifications of JEOL JSM-6060
- Table 4.1: Relative viscosity and composition of the seven commercial PMMA bone cements
- Table 4.2: Static shear strength, porosity, and micropore size for each cement brand (mean±std)
- Table 4.3: Expatriation of 3D surface parameters to assess a surface in height deviation
- Table 4.4: 3D surface parameters of stainless steel rods with differing surface finishes (mean±std)
- Table 4.5: 3D surface parameters of bone cement interfaced with the four kinds of surface finish rod (mean±std)
- Table 5.1: A summary of the instruments used to analyse femoral stem wear
- Table 5.2: Coverage of fretting wear area in each Gruen zone on the stem surface (%)—Simulation I, use Simplex P cement
- Table 5.3: The maximum and minimum position of the experimental specimen—Simulation II, use Simplex P cement
- Table 7.1: Coverage of fretting wear area in each Gruen zone on the stem surface (%)—Simulation IV, use Simplex P cement
- Table 7.2: Elemental composition of the wear debris at the edge of the micropores (% , m/m)—Simulation IV, use Simplex P cement
- Table 7.3: Chemical composition of stainless steel REX 734 specified in BS 7252-9 (% , m/m)
- Table 7.4: Coverage of fretting wear area in each Gruen zone on the stem surface (%)—Simulation V, use CMW 3 cement
- Table 7.5: Coverage of fretting wear area in each Gruen zone on the stem surface (%)—Simulation VI, use CMW 3 cement
- Table 7.6: Coverage of fretting wear area in each Gruen zone on the stem surface (%)—Simulation VII, use Palacos R cement
- Table 7.7: Coverage of fretting wear area in each Gruen zone on the stem surface (%)—Simulation VIII, use Palacos R cement
- Table 7.8: Microhardness of the bone cements from the in vitro wear simulations

## Abbreviations

ANOVA: analysis of variance  
BEI: backscattered electron image  
BPO: benzoylperoxide  
BW: body weight  
CCI: coherence correlation interferometer  
CRT: cathode ray tube  
DMPT: dimethyl para toluidine  
EDM: electrical discharge machining  
EDX: energy dispersive X-ray  
EU: European Union  
FEA: finite element analysis  
HA: hydroxyapatite  
HQ: hydroquinone  
HV: Vickers microhardness  
LVDT: linear variable differential transformer  
MMA: methylmethacrylate  
PGI: phase grating interferometer  
PMMA: polymethylmethacrylate  
PSI: phase shift interferometry  
RSA: roentgen stereophotogrammetric analysis  
SEI: secondary electron image  
SEM: scanning electron microscope  
SPM: scanning probe microscope  
STM: scanning tunnelling microscope  
THR: total hip replacement  
UHMWPE: ultra high molecular weight polyethylene  
VSI: vertical scanning interferometry

## Chapter 1 Introduction

### 1.1 Project background

#### 1.1.1 Total hip replacement

Total hip replacement (THR) is one of the most common and effective orthopaedic procedures performed both in the UK and worldwide, with the purpose of dramatically improving quality of life of patients suffering from debilitating hip disorders, such as osteoarthritis, rheumatoid arthritis and avascular necrosis. This procedure can bring almost immediate relief to the unremitting pain due to which the functional capacity of the lower limb has been greatly decreased. Especially to those patients with an end stage degenerative joint disease, THR is often the final attempt that the surgeons can resort to in terms of pain relief and increasing mobility. The first tentative steps toward restoration of function and alleviation of pain for patients with an arthritic hip involved many researchers and ideas, but a significant contribution to the routine success of today was undoubtedly the concept of the low-friction arthroplasty proposed by Sir John Charnley (1911–1982) (Wroblewski *et al.* 2005). Since its introduction as a pioneering method in the 1960s, the basic structure of THR has remained unchanged, involving replacing the affected articulating hip joint with the use of a femoral component, which consists of a femoral stem with a femoral head on the neck, and a shell and liner system that acts as an acetabular cup, figure 1.1.

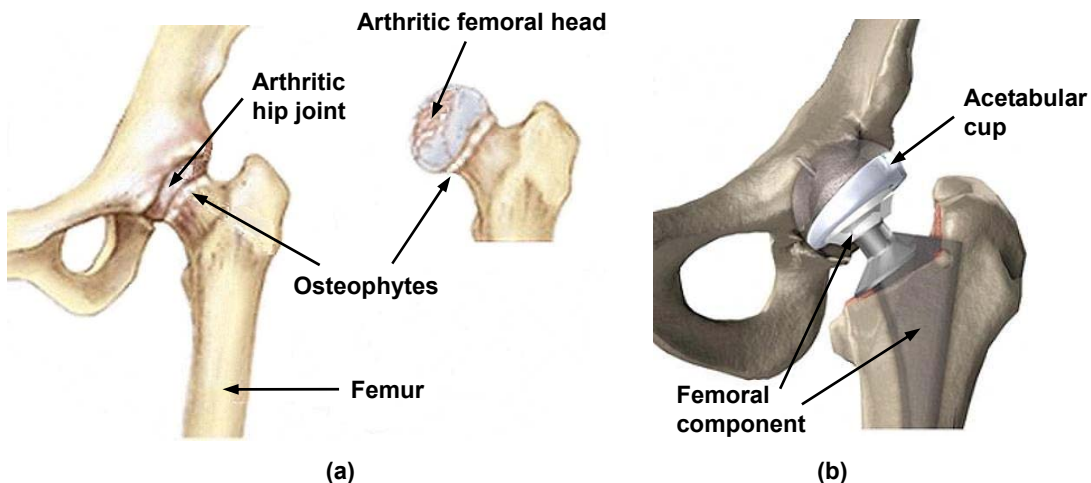


**Figure 1.1:** (a) Osteoarthritis at the hip (b) Total hip replacement with a metal prosthesis

There are primarily two fixation methods to secure the femoral stem into position in the femoral cavity, relying on either an uncemented method which depends on bone ingrowth into a porous or hydroxyapatite (HA) coating on the stem surface, or more common a cemented method which utilises acrylic bone cement for fixation. Bone cement functions as an intermediary agent between the prosthesis and the bone, to mechanically stabilise the femoral stem and to effectively transfer physiological loading from the prosthesis to the bone, figure 1.2. The acetabular cup is held into place in the same way as the femoral stem, either using an uncemented or a cemented technique. In the uncemented variety, the acetabular cup is simply stabilised by the tightness of the fit or with screws, whereas in the cemented variety, bone cement is used to fix the acetabular cup to the bone. The choice of uncemented versus cemented method remains highly personal and varies noticeably from one country to another. Even within countries, individual surgeons and research centres also

have different criteria for selecting the type of fixation method. Across Europe, national variations range from 91% cemented THR in the UK to 10% in Austria (Wirz *et al.* 2005). However, the Hybrid THR, i.e. the combination of a cemented femoral stem with an uncemented acetabular cup, has nowadays become more and more popular for a large number of orthopaedic surgeons to treat the patients, especially those older than 50–60 years. The rationale for the hybrid THR is based on the experience that with the assistance of “modern cementing techniques”, the results on the stem side could be greatly improved, whereas on the acetabular side, clinical results with uncemented cup designs are more promising. The present research mainly concentrates on cemented THR regarding the fixation of the femoral stem.

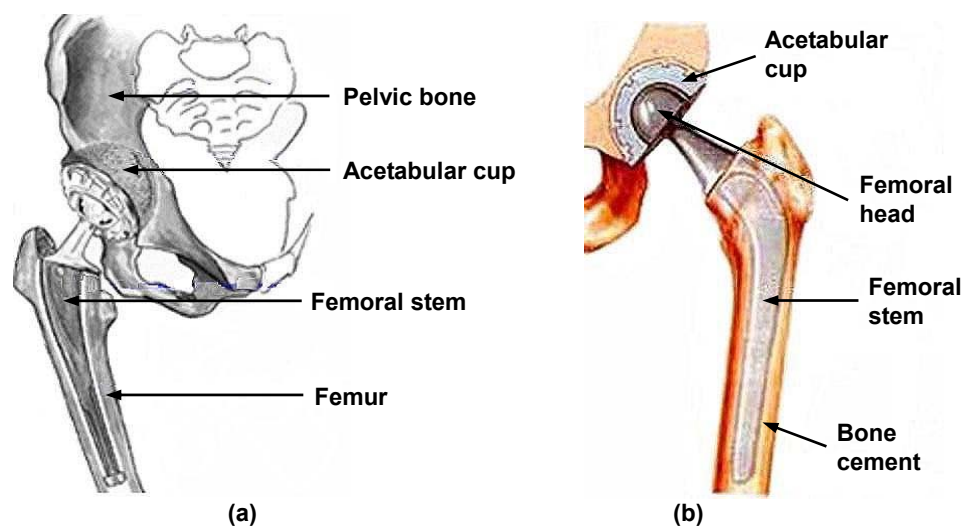


**Figure 1.2:** (a) Uncemented total hip replacement (b) Cemented total hip replacement

### 1.1.2 Failure of total hip replacement

With a progressively increasing prevalence of THR performed in younger and more active people coupled with a longer life expectancy, it is hoped that hip prosthesis will function well for at least 15–20 years. Although the clinical success of THR has been well documented, especially with the improvement in implant design and the use of “modern cementing techniques”, revision does occur and it is required when one or more components fail. It is reported that up to 10% of the 65,000 operations carried out in the UK in 2007 are to revise those prostheses which have failed prematurely (National Joint Registry, 4<sup>th</sup> annual report, 2007). In comparison with the primary arthroplasty, revision is not only exposed to a considerably higher cost, but also associated with a decisively lower longevity and a higher rate of complication and morbidity. Consequently, great efforts have been made to investigate the scenario behind failure of THR. Nowadays, it has been generally accepted that this is mainly attributed to aseptic loosening, which dominates mechanical malfunctioning of the total joint system. Aseptic loosening of the hip prosthesis, usually with the symptom of a radiolucent line wider than 2mm around the prosthesis, has been identified as the predominant long term complication. It can occur in the absence of clinical or microbiological evidence of infection, and it is influenced by many factors such as periprosthetic bone resorption, poor initial fixation or alignment (Sutherland *et al.* 1982, Malchau *et al.* 1993, Johnsson *et al.* 1994, Mohler *et al.* 1995). Consequently, in spite of the long history of THR and the enormous research carried out, the mechanical aspects of aseptic loosening are still not entirely elucidated.

This indicates that a deep insight into the etiology of aseptic loosening of THR should be gained and this would require much more fortitude and endeavour in research.

Notwithstanding, it has been shown from autopsy retrieved hip prosthesis that, with regard to cemented THR, periprosthetic bone resorption acts as the primary reason for aseptic loosening, associated with debonding at the femoral stem–bone cement interface (Jasty *et al.* 1991, Mjoberg 1997, Maloney *et al.* 2002). Bone resorption can be mainly attributed to an immune system response to particulate debris generated by wear of the hip prosthesis, and also to stress shielding because of changed loading conditions at the bone stock after implantation of the hip prosthesis. As the particles are liberated from the implant, stimulated macrophages attempt to clear them, resulting in an inflammatory reaction. This leads to the production of foreign body giant cells that release chemical mediators, such as prostaglandin E<sub>2</sub>, cytokines interleukin–1 and interleukin–6. These chemical mediators activate osteoblasts which will absorb bone from around the prosthesis, figure 1.3.



**Figure 1.3: Typical periprosthetic bone resorption**

### **1.1.3 The stem–cement interface**

Previously, wear between the femoral head and the acetabular cup has been regarded as the primary source responsible for the generation of particulate debris as this interface is designed to allow for movement and to offer the patients flexibility. Recently, however, great progress has been made in reducing wear at this articulating interface with the advent of cross-linked ultra high molecular weight polyethylene (UHMWPE) (Wroblewski *et al.* 1996) and the renaissance of hard-on-hard bearing systems, e.g. metal-on-metal and ceramic-on-ceramic artificial hip joints (Firkins *et al.* 2001, Hatton *et al.* 2002).

Therefore, this current research has transferred attention to another site which also contributes to wear—the stem–cement interface. Historically, this interface has consistently been noted as a weak link in the stem–cement–bone structure, being a transitional zone between two materials with significantly different stiffness, hardness and elastic modulus (Stone *et al.* 1989, Wang *et al.* 2003). Due to the wear reduction at the head–cup interface, it is now considered that wear at the

stem–cement interface is showing an increasing significance in the overall wear of cemented THR. However, in spite of its potential importance, such wear has only received relatively little concern and its contribution to failure of cemented THR has been greatly overlooked. Previous studies have indicated that mechanical debonding at the stem–cement interface may be inevitable for almost all stem designs and this can result in subsidence of the femoral stem within the cement mantle (Karrholm *et al.* 2000). It is further suggested that, under cyclical physiological loading *in vivo*, the typical low-amplitude oscillatory micromotion at the stem–cement interface can lead to subsequent generation of fretting wear at this interface. Although fretting wear has been clinically detected on polished femoral stems, *in vitro* simulation to reproduce it has seldom been attempted and even then with only limited success. Additionally, it is demonstrated that wear mechanism at the stem–cement interface is mainly determined by femoral stem surface finish, with differing wear characteristics and severity of damage to bone cement in spite of similar wear locations on the femoral stem (Howell *et al.* 1999), but other factors such as stem geometry and bone cement brand may also influence the corresponding wear at this interface. Furthermore, the initiation and propagation process of this wear has never been established across previously published literature, and accordingly research needs to be undertaken to address these issues.

## **1.2 Project aims and objectives**

### **1.2.1 Aims**

The overall aims of this current study are to give a better understanding of the characteristics of the stem–cement interface, to successfully and consistently reproduce fretting wear through *in vitro* wear simulations and to ascertain the influence of the potential contributory factors on the generation of fretting wear and on the wear mechanism. In addition, a model is to be developed to give a more detailed description of fretting wear generated on the stem surface. As a consequence, the work consists of a number of experimental studies and theoretical analysis.

### **1.2.2 Objectives**

The specific objectives are given below in detail to fulfil the above aims, these include:

- To investigate the static bond strength of the stem–cement interface utilising polished femoral stems and several commercially available bone cements, with the purpose of validating that debonding at the stem–cement interface is commonplace.
- To study the influence of stem surface finish on the static bond strength of the stem–cement interface, using Simplex P bone cement and femoral stems with different surface finishes.
- To design a test fixture connected with an Instron test machine and to establish a test regime to enable *in vitro* wear simulation of the hip prosthesis.
- To successfully and consistently reproduce fretting wear through development of *in vitro* wear simulations, using polished Exeter femoral stems and Simplex P bone cement.
- To develop an effective method to investigate the relative micromotion at the stem–cement interface during the *in vitro* wear simulation.
- To analyse the potential contributory factors on generation of fretting wear and on the wear mechanism, such as duration of *in vivo* service of the hip prosthesis and bone cement brand.
- To develop a model to describe the fretting process at the stem–cement interface, including

the initiation site and the locations of fretting wear, development of surface topography of the fretting zones, and generation of fretting debris, etc.

- To investigate the use of finite element analysis to model the stem–cement interface, aiming to provide theoretical support for describing the initiation and progression of fretting wear on the femoral stem.

## Chapter 2 Total hip replacement

### 2.1 Chapter summary

In the five decades since Sir John Charnley first advanced his revolutionary concept of a totally artificial hip joint consisting of a metal-on-plastic articulation, literally millions of people have had their lives dramatically and remarkably improved by this innovation. Equally to improve the basic design, many researchers have poured various ideas, efforts, and experience into this area. Understandings have developed significantly and new insights now abound to augment Charnley's original design. It is considered essential to review the state of art of THR in order to make it clear where we are before carrying out any further research. The overall aim of this chapter is to obtain a general background of THR and to summarise the critical issues that need to be addressed through a comprehensive literature review, specifically concentrating on the characteristics at the stem–cement interface of cemented THR.

Firstly a fundamental knowledge of the loading regime of the hip joint is given, which is regarded as the basis that the configuration of *in vitro* wear simulation depends upon. The chapter then describes in detail two stem fixation methodologies based on two different principles. These two methods overwhelmingly predominate in modern THR procedure. As the cemented method is the one that this project is interested in, the characteristics of its two main components, i.e. metal femoral stem and acrylic bone cement, are further expatiated. Later in the chapter, the two primary reasons resulting in aseptic loosening of THR are outlined, these are summarised as wear debris induced bone resorption and stress shielding. Finally, the recognition and evaluation of femoral stem wear as a consequence of the fretting process at the stem–cement interface are introduced chronologically, and the initial attempts to reproduce fretting wear on the femoral stem through *in vitro* simulations are discussed.

### 2.2 The loading regime of the hip joint

#### 2.2.1 Anatomy of the hip

The hip is a ball and socket joint connecting the torso to the legs. It is surrounded by a joint capsule and kept stabilised through tendons, ligaments and muscles. Basically, this structure consists of a hip ball, also called the femoral head, which is situated right at the top of the femur, and a hip socket, also called the acetabulum, which is a part of the pelvis. The joint operates with the femoral head articulating with the acetabulum. In a healthy hip, both the femoral head and the acetabulum are covered with a layer of articular cartilage which acts as a cushion to prevent the bones from rubbing against each other. In addition, the joint space between the femoral head and the acetabulum is filled with synovial fluid. It works in collaboration with the articular cartilage to ensure the femoral head glides as smoothly as possible inside the acetabulum without any pain, figure 2.1. This enables the hip joint to remain stable to support the weight of the human body, and unrestricted enough to allow for the full range of leg motion, which is virtually friction free since the well-cushioned ball and socket do not rub together. However, as the hip joint is a major weight bearing system subjected to locomotion, the articular cartilage and synovial fluid can dissipate gradually due to wear and tear over an extensive period of time, heading to the onset of osteoarthritis. This causes the underlying bone to become exposed, and accompanying pain as the

femoral head and the acetabulum contact directly against each other. Consequently, an age-related degradation is predicted to occur to most people in the late stage with varying severity.

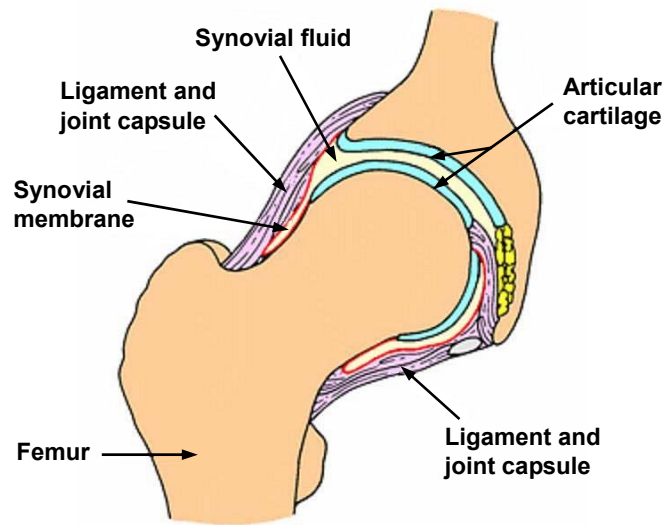


**Figure 2.1: The structure of a natural hip**

Generally speaking, the main functions of the hip joint are to transmit physiological loading from the human body to the thigh bone and then to the lower limb, and also to allow for mobility of the leg in space. It has three degrees of freedom, all of which are rolling, figure 2.2 and table 2.1.

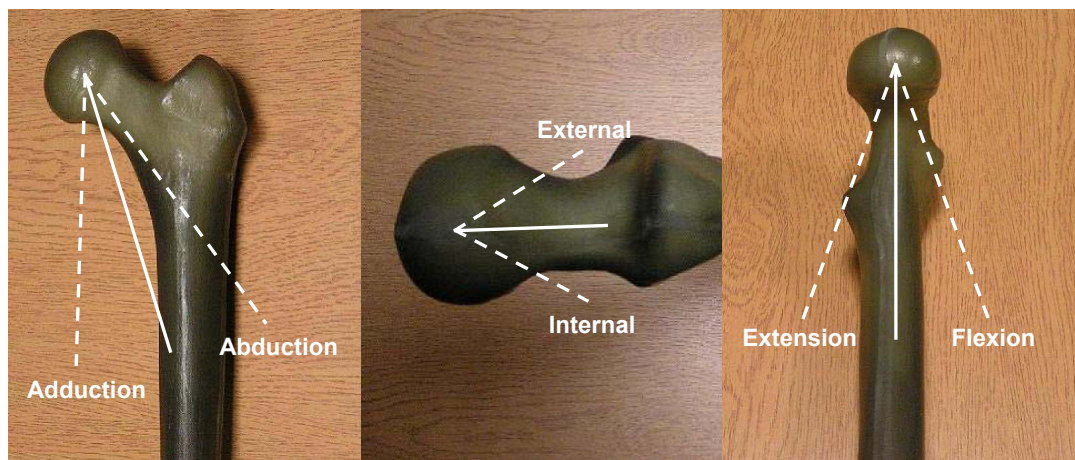


**Figure 2.2: Definition of degree of freedom of hip motions**

**Table 2.1: The three degrees of freedom of the hip joint**

Hip movement	Explanation	Plane of motion	Axis of rotation	Range
Abduction/adduction	Spin with inferior/superior glide of the femoral head inside the acetabulum	Frontal plane	A sagittal axis passing through the centre of the femoral head	Up to 90°
Internal/external	Spin with inward/outward glide of the femoral head inside the acetabulum	Transverse plane	A vertical axis passing through the centre of the femoral head	Up to 90°
Flexion/extension	Spin with posterior/anterior glide of the femoral head inside the acetabulum	Sagittal plane	A frontal axis passing through the centre of the femoral head	Up to 145° and 30° respectively

Due to the little restriction to rotation, the hip joint is considered to be inherently unstable. It would finally lead to a complete loss of function of the lower limb if often subjected to excessive loading. A fundamental knowledge of the variation in these three degrees of freedom is essential in replicating normal human activities, in evaluating curative effects of THR and also in designing a hip simulator. For example, the hip joint is flexed 30°, adducted 3° and internally rotated 5° at heel strike of a gait cycle, and extended 15°, adducted 3° and internally rotated 5° at toe off.

### 2.2.2 Hip joint force

The success of THR largely depends on its ability to transmit physiological loading of the human body without failure, therefore an insight into the forces acting on the hip joint is required. It is well known that the hip joint force applied on the femoral head is considerably greater than the human body weight (BW) during walking, and it is even higher in other situations such as stair climbing, running and stumbling (Davy *et al.* 1988).

To date there have been a great deal of investigations performed concerning hip joint force. The first study of *in vivo* measurement of the force is considered to be the one carried out by Rydell in 1966. In that study he employed a metal prosthesis instrumented with strain gauges and collected data through subcutaneous leads. The peak force value was found to be about 3.3BW during walking for dynamic measurements. Another area of early research on the forces transmitted by hip joint in the human body completed by Paul in 1967 resulted in a curve that is still regarded as one of the standard loading configurations for modern hip simulators. He obtained a peak hip force value of around 3.9BW at a relatively low velocity in one walking cycle, figure 2.3. English and Kilvington in 1979 recorded similar values employing a telemetry system implanted in a hip prosthesis. More recently, Bergmann *et al.* (1993) measured *in vivo* hip forces in two patients, using a telemetering total hip prosthesis. They recorded that the peak force value during walking ranged between 2.8BW and 4.8BW, and it was as high as 5.5BW when jogging and 8.7BW when stumbling. This data is summarised in table 2.2.

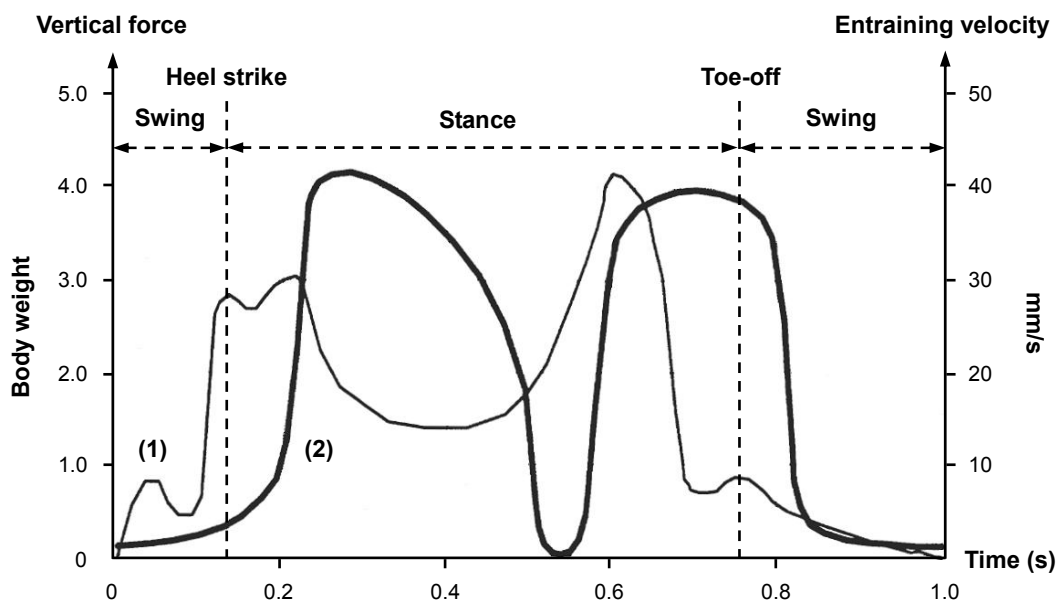


Figure 2.3: Hip joint reaction force in terms of body weight through one walking cycle (1) Vertical force (2) Entraining velocity (Paul 1967)

**Table 2.2: Typical studies on hip joint forces during different human normal activities**

Authors	Activities	Resultant forces
Rydell (1966)	Walking	3.3BW
Paul (1967)	Walking	3.9BW
English and Kilvington (1979)	Walking One-legged stance	2.56BW 3.59BW
Bergmann et al (1993)	Walking Jogging Stumbling	Between 2.8BW and 4.8BW 5.5BW 8.7BW

Although there are some variations among these studies, they all have confirmed that the hip joint is a weight bearing interface that experiences high physiological loading during human normal activities. As a result, there is no doubt that a gradual degradation in the function of the hip joint will occur if it is always being overworked. It follows that, if the articular cartilage is worn, an implicated hip disorder, commonly osteoarthritis, would be likely to be accelerated, leading to extensive impairment to people's quality of life. In such a case, a THR operation may have to be subsequently carried out to reconstruct function of the hip joint and to relieve the pain. This procedure is considered to be the most effective treatment in comparison with other methods, e.g. anti-inflammatory medications, as it allows the patients who have struggled with the simple action of walking once again to participate in most ordinary daily activities following a relatively short period of rehabilitation.

### **2.3 Uncemented and cemented total hip replacement**

THR is deemed as one of the major advances in medicine of the 20<sup>th</sup> century and it is typically required when osteoarthritis results in severe discomfort and disability to the patients. Basically, a THR procedure involves several steps, including removal of the affected femoral head, reaming of the acetabulum and subsequent insertion of a metal shell and an acetabular cup, reaming of the femur and securing of a femoral stem with a ball on the neck into the femoral cavity, figure 2.4.

#### **2.3.1 Uncemented total hip replacement**

Despite the overwhelming prevalence of this surgical procedure, debate still continues concerning the optimal choice of fixation method for the primary THR. As has been mentioned previously, there are primarily two methods for fixation of the femoral stem: the uncemented method and the cemented method. The primary aim of the uncemented method is to improve long term success of THR in younger patients. Ideally it can achieve stable fixation in terms of osseointegration by coating the femoral stem with a biological material which could promote bone ingrowth. Potential benefits with this type of fixation are its ability to remodel activity and to repair itself over time. Three major strategies are pursued in this regard, namely the formation of porous-coated metallic implants with surface coatings prepared by sintered porous metallic powders or fibres over bone-interfacing surfaces of metal substrates, plasma-sprayed deposition of metallic or ceramic coatings (nominally HA) over solid metal substrates, and specialised methods for directly forming implants with irregular or textured surfaces (Pilliar 2005).

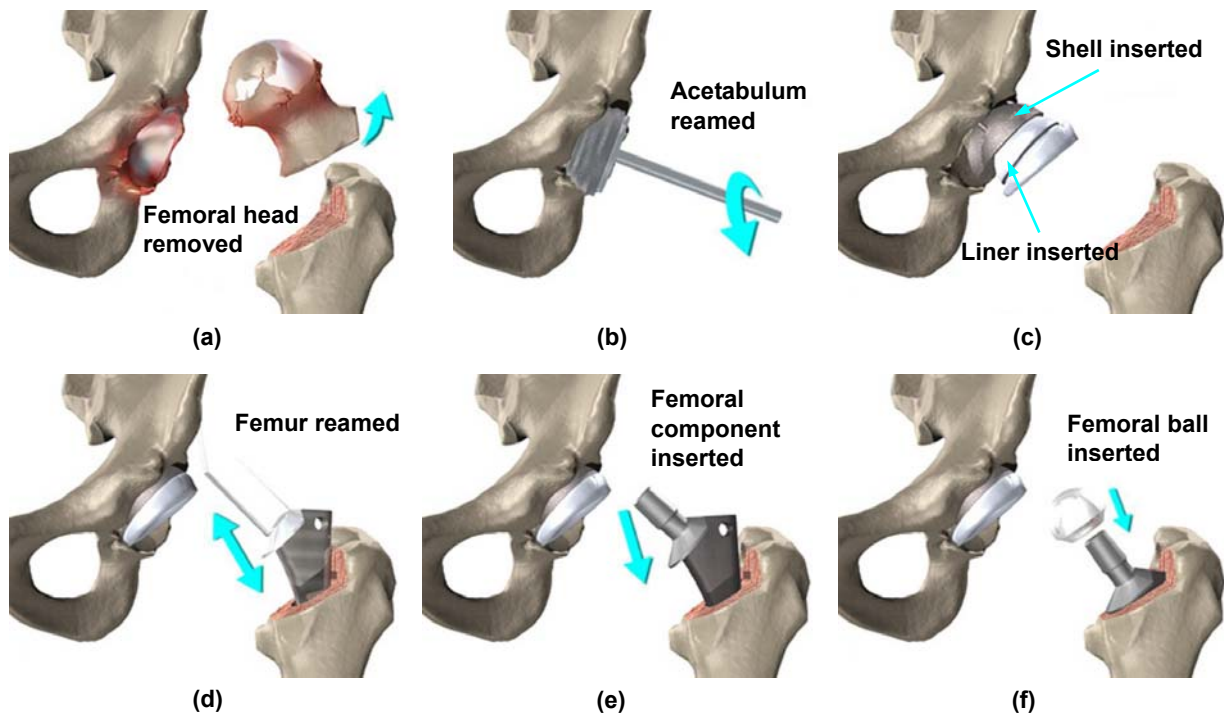


**Figure 2.4: Typical procedures of total hip replacement**

Sintered porous-coated and plasma-sprayed HA coated implants have now been comprehensively used to allow for mechanical interlock and fixation of the stem to the surrounding bone, especially the osteoconductive HA coated implant which was initially introduced by Geesink *et al.* in 1987. The early prognosis of uncemented THR has been reported as good, which promotes direct bone apposition. The long term clinical success, however, is of major concern. The potential problems involved in these implants such as delamination or fragmentation of the coatings and subsequent exposition of metal beneath may become predominant during its *in vivo* service (Porter *et al.* 2004), releasing particulate debris and invoking a foreign body host response. The particulate debris would also migrate into the joint articulation regions where they can act as third-body particles causing higher wear rates of the bearing surfaces and further consequences from the greater volumes of liberated wear debris. Additionally, subsidence of the stem relative to the bone is considered to be extremely detrimental to bone ingrowth, and it is indicated that bone ingrowth will not occur if the initial micromotion is excessive (Pilliar *et al.* 1981). In summary, uncemented hip prostheses offer the advantage of fixation by direct bone-to-implant osseointegration, therefore avoiding the use of a synthetic intermediary material with limited mechanical strength, such as acrylic bone cement. As a consequence, uncemented THR is preferably performed for the younger patients with good bone quality. However, severe thigh pain or discomfort emerges as a long term challenge and sequela for uncemented THR, and successful osseointegration depends on several multifactorial conditions being satisfied, including the need for limited early loading which will hopefully lead to minimal relative movement at the stem–bone interface.

### **2.3.2 Cemented total hip replacement**

The rationale behind the cemented method is to employ acrylic bone cement as a medium for fixation of the stem. Given the demographics in many countries, it seems in all probability that there must be a period of at least two decades in the new millennium for the use of bone cement,

even with the progress in uncemented fixation and tissue engineering (Smith 2005). Therefore, there is great requirement to gain a deep insight into this biomaterial, especially its application in the area of THR. Actually, cemented THR has been accepted as the more popular mode for stem fixation throughout Europe and it is in part why this current research focuses on cemented THR. Bone cement was originally designed for use in dentistry, and it was Sir John Charnley (1960) who introduced it to orthopaedic surgery. This advance was not simply the utilisation of bone cement but rather a conscious recognition of its ability to completely fill the medullary canal and to adapt to the bone interface, thereby anchoring the hip prosthesis. It was a brand new technique and provided the basis for the development of the Charnley low friction arthroplasty over the following decades.

Bone cement has now been used in cemented THR for more than 40 years. As a grouting material, bone cement allows for almost immediate stabilisation of the femoral stem and smooth transfer of physiological loading from the metal prosthesis to the bone. During the surgical procedure, it is introduced into the femoral cavity prior to insertion of the femoral stem. Upon polymerisation, the bone cement cures into a solid dough state in approximately 15 minutes, which can then steadily hold the stem in position. This procedure is preferably recommended for older patients over age 60, or younger patients with poor bone quality and density who cannot tolerate a long period of rehabilitation. Therefore, these individuals benefit greatly from the relatively short healing time, usually from one to two weeks. The hospital cost of implanting a cemented femoral stem is commonly more than that of implanting an uncemented femoral stem, when adding together the cost of additional operating room time and anaesthesia time, and the cost of stem, cement and other accessories (Barrack *et al.* 1996). Although both short term and long term survivorship of cemented THR has been well documented in part due to the improvement in “modern cementing techniques”, aseptic loosening is generally regarded as a major threat to its durability (Raut *et al.* 1995, Herberts and Malchau 2000), with sometimes an unacceptably high rate of hip implant loosening reported in some centres through 1960s and 1970s. These unsatisfactory results, associated with the intrinsic limitations of acrylic bone cement in mechanical properties, partially resulted in research initiatives intending to develop alternative methods for reliably and durably securing hip prosthesis in bone, i.e. uncemented THR. Over the years, uncemented and cemented methods have proved to be much effective for THR therapy, with the selection of one or the other approach being favored, depending on specific situations.

## **2.4 Metal femoral stem**

### **2.4.1 General introduction**

Since the introduction of cemented THR in the 1960s by Charnley using an original Charnley femoral stem, great changes have occurred to this design, with Elite Plus (DePuy International Ltd., Leeds, UK) being the fifth generation. Evolvments happen not only to one single stem design, but also with the emergence of more and more diverse types of femoral stems, figure 2.5. Hip prosthesis technology has been continuously changing, with new designs and methodologies being introduced. For example, in 1995 there were more than 62 hip prostheses available on the market for the surgeons to choose from, which were provided by 19 different companies (Murray *et al.* 1995).



**Figure 2.5: Different designs of femoral implants**

These stems no doubt offer more flexibility in terms of geometry as well as cost, but they to a certain degree make the optimal choice for the patients very difficult considering that a long term follow up is required to assess the performance of a new stem design. What is worse, some of the new designs met with an extremely unsatisfied survivorship since being used, i.e. the 3M Capital hip system (3M Health Care Ltd., Loughborough, UK). These stems, available in both monoblock and modular forms, were introduced to the UK market in 1991, and shortly adverse reviews reported that between 19% and 21% of patients either had undergone revision surgery or were identified as being in need of revision at less than five years (Medical Devices Agency, hazard notice, 1998). Therefore, a balance needs to be struck between the demand for long term clinical data before a stem is released to market and also the demand for continued development in order to improve longevity of THR. Nowadays, Charnley, Exeter, Stanmore, and Müller stems are generally regarded to be “benchmarks” across all stem designs and the long term durability of these stems has been well evaluated (Shen 1998).

One advent that is worth noting is the introduction of the modular stem design, usually utilising a head–neck Morse taper junction, figure 2.6 (a). Originally the femoral head and the femoral stem were manufactured as a single component, which incurred great difficulty when being implanted in patients with special hip joint anatomy, figure 2.6 (b). Modular design not only provides the ability to vary neck length and femoral head size independently of the femoral stem, but also allows for the best combination of materials to be used, i.e. the femoral head benefits from the wear resistance of cobalt chrome alloy and the femoral stem obtains excellent mechanical properties when manufactured from stainless steel. Before the femoral head is connected to the femoral stem, it is usually polished smooth to facilitate easy rotation within the prosthetic socket. In spite of its great success, modular stem design encounters its own inherent shortcoming due to

more potential wear sites that have been introduced at the Morse taper. However, the benefits given by the modular stem design appears to far outweigh this potential problem, especially with the use of ceramic as a material for the femoral head to further reduce wear.

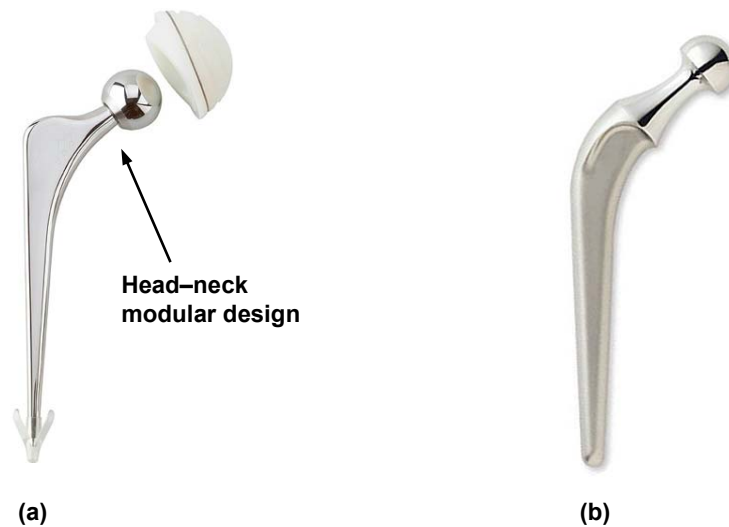


**Figure 2.6: (a) Example of a modular femoral stem design—Exeter (b) Example of a monoblock femoral stem design—Charnley**

## 2.4.2 Design properties

### 2.4.2.1 Stem material

There are many variables when designing a femoral stem, including material, geometry, surface finish, etc. With reference to material selection, biocompatibility and optimal mechanical and tribological properties are of prominent significance, taking into consideration the aggressive physiological environment in the human body as well as the complicated loading regime on the femoral stem *in vivo* (Semlitsch and Willert 1980). The material must be able to withstand physiological loading for the duration of day-to-day utilisation by an active individual. As most materials used in biomedical engineering are much stronger than the requirements for yielding and fatigue, the strength of the material is no longer a critical issue. There is, however, another very important design constraint for material selection, i.e. stress shielding. Stress shielding is the reduction in bone density due to much of the load being carried by a much stiffer implant, which results in a huge stress gradient between the cancellous bone and the lower region of the femur. This is associated with resultant pain and discomfort for the patients. As a consequence, it is ideal to choose those materials with similar strength, stiffness, density and other mechanical properties as the bone to reduce the stress shielding effect. Nowadays, stainless steel, cobalt chrome alloys, and titanium alloys are the three most commonly used materials primarily attributed to their biocompatibility and excellent mechanical and tribological properties. Unfortunately, all of these materials possess yield strength and stiffness much higher than that of bone. Femoral stems made of titanium alloys have gradually received a reputation for failure earlier than the cobalt chrome and stainless steel designs because titanium is susceptible to crevice corrosion, which is driven by the generation of a gap between the stem and the cement, and also between the head and the taper.

Therefore, there are certain concerns when manufacturing a femoral stem utilising titanium alloy, and titanium articulating surfaces are no longer recommended for clinical use.

#### 2.4.2.2 Stem geometry

In addition, stem geometry is also considered to be very important because it may have a direct effect on the *in vivo* behaviour and consequent failure mechanism of THR. Certain unsuccessful stems such as the 3M Capital hip have been removed from the market as a very poor short term survival rate was obtained, and this has been suggested to be highly design-related. The optimal geometry of a stem should transfer axial as well as torsional load through the bone cement and then to the bone without creating destructive peak stresses and without excessive micromotion. Generally speaking, stem geometry design involves the overall shape (symmetrical or anatomical), the cross-section (oval or square), the presence or absence of a collar and a flange, the shape of the stem tip, and the length of the stem. Also, it includes whether the edges are rounded to a greater or lesser degree, and whether the stem is double taper design (e.g. Exeter stem) or triple taper design (e.g. C Stem, figure 2.7). Charnley, Exeter, and Müller stems are all symmetrical designs, with excellent clinical track records. Anatomical stem designs such as Lubinus SP2 can generate different strains within the cement mantle because of their specific shape, which allows for better centralisation of the stem and more even thickness of the cement mantle. The cross-sectional shape influences the distribution of cement within the femoral canal, the rotational stability of the implant, and the stress distribution within the cement mantle. Stems with a square cross-section offer more rotational stability than stems with an oval cross-section. However, the sharp edges create peak stresses in the cement, potentially leading to micro-cracks (Scheerlinck and Casteleyn 2006). Nowadays, although there are still no published results for some of the hip implants on the market, the number of THR designs that are available to surgeons is rapidly increasing. Therefore, an effective early clinical assessment of the performance of a new femoral stem design is greatly necessary.

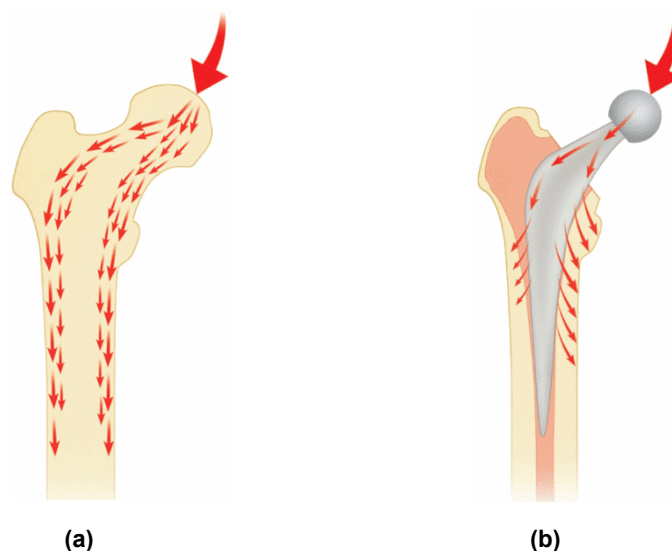


**Figure 2.7: Load transfer patterns (a) Within the natural femur (b) Around the C stem**

#### 2.4.2.3 Stem surface finish

Surface finish is another crucial design property that varies substantially across different femoral

stems. There are currently no standards relating to this and therefore its influence on the reliability and longevity of cemented THR has been debated for a long time. The focus of controversy concentrates mainly on whether matt femoral stems can achieve permanent fixation during long term *in vivo* service. Undoubtedly, the stem surface texture has a direct effect on the interaction with bone cement, which as a consequence functions as a significant factor in influencing the bond strength at the stem–cement interface. From a mechanical perspective, matt stems can form much greater bond strength at this interface than polished stems, mainly owing to the enhanced bone cement attachment. Therefore, a matt femoral stem with a collar and a flange is termed as “shape closed design” which tends to obtain its stability through mechanical interlock between the stem and the cement. By contrast, a polished femoral stem incorporated with a collarless design is termed as “force closed design” which depends on mechanical taper locking of the stem within the cement mantle to accomplish self-tightening (Huiskes *et al.* 1998). This is taken to be the rationale behind the great success of the Exeter polished femoral stem, which has been changed back from the matt surface finish design based on the fact that an inferior clinical outcome was obtained for the matt stems. Originally, the Exeter femoral stems were highly polished before 1976. There was no particular reason for this except that it was “the fashion” for many femoral components of that era. Later from 1976 to 1985, the Exeter femoral stem had a matt surface as it is quite expensive to polish a stem. Whilst the occurrence of stem fracture with the matt-surfaced stems was virtually abolished, there gradually emerged the paradoxical finding of a great increase in the incidence of focal femoral lysis and aseptic loosening (Anthony *et al.* 1990), which directly resulted in the re-introduction of the polished surface at the beginning of 1986. Basically, matt femoral stems are prone to generate more debris and cause severe damage to the cement mantle once debonding at the stem–cement interface occurs. This is considered to be the primary disadvantage involved in matt surface finish design. Although it is still an area of debate for the optimal stem surface finish, more and more documents are being published to support for the use of polished femoral stems (Howie *et al.* 1998) as in some cases matt stems have shown to fail earlier than polished stems of the same type, such as the Exeter stem and the Iowa stem. Matt stems may preferably need a thick, continuous cement mantle of good quality with a strong cement–bone interface to function well.

One would expect that it should not be a problem to distill the optimal design parameters as there has been to date a clinical database representing over two decades survival data of cemented THR. However, it is such a complex matter that from a clinical point of view conclusive evidence for the optimal implant design remains elusive. One design feature would have a negative effect for a particular design, whereas it has none or even a beneficial effect for another prosthetic design. Therefore, it definitely is a combination of inferior design features that result in a bad hip implant. In this respect, it has been suggested that one must consider a certain design philosophy, e.g. “shape closed design” or “force closed design”, rather than in individual design features. When a design philosophy is adopted, all design features can be chosen to match the particular philosophy and to optimise the clinical performance (Verdonschot 2005). Failure to do this would result in arbitrary mixing of design features and potentially a painful lesson in history.

## **2.5 Acrylic bone cement**

### **2.5.1 General introduction**

Acrylic bone cement was initially used in dental surgery, and then in the 1960s Sir John Charnley at Wrightington Hospital pioneered its application as a grouting material to stabilise hip prosthesis in orthopaedic surgery, which is nowadays one of the most frequently performed orthopaedic procedures across the world. In spite of more than 45 years of usage, its basic composition has remained largely unchanged, with a fine polymer powder and a vial of monomer liquid as the general components. The powder consists of pre-polymerised polymethylmethacrylate (PMMA) or PMMA-based copolymers, benzoylperoxide (BPO), and a radiopaque agent, commonly barium sulphate ( $\text{BaSO}_4$ ) or zirconium ( $\text{ZrO}_2$ ). BPO behaves as an initiator for the polymerisation reaction;  $\text{BaSO}_4$  and  $\text{ZrO}_2$  are radiopacifiers to aid in radiological assessment of cemented THR. The liquid is composed of methylmethacrylate (MMA) monomer, N, N dimethyl para toluidine (DMPT), and hydroquinone (HQ). From a chemical point of view, MMA monomer is an ester of methacrylic acid with a polymerisable double bond, and it is a clear, colourless, flammable liquid with intense odor; DMPT is a tertiary aromatic amine that acts as an activator for the polymerisation reaction; HQ is used to prevent spontaneous polymerisation of the monomer due to exposure to heat or light during storage to guarantee a sufficient shelf life. All the bone cements on the market have similar liquid compositions but considerably different powder composition. Upon mixing the powder and the liquid, BPO and DMPT participate in a redox reaction or a so called “initiation reaction”, producing free radicals which initiate additional polymerisation of MMA monomer by adding to the polymerisable double bond of the monomer molecule. Because of the high number of radicals generated, many rapidly growing polymer chains are formed, and there is a fast conversion of MMA to PMMA. If two growing polymer chains meet, they are terminated by combining both, resulting in an unreactive polymer molecule, figure 2.8. During the polymerisation process, the admixture gradually experiences a transition from liquid to solid, and then it is transferred to the reamed femoral cavity which is ready for insertion of a femoral stem.

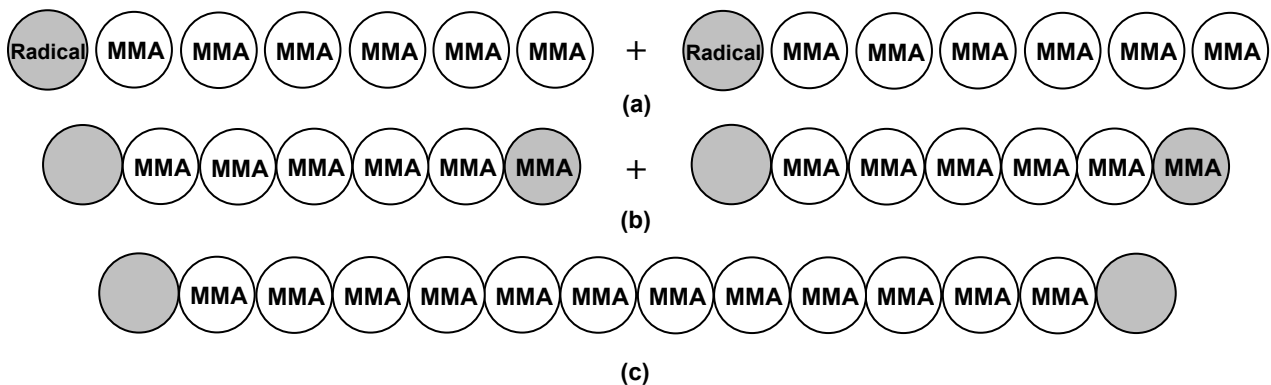


**Figure 2.8: The formation of polymer chains (a) Radical for initiation of polymerisation and MMA monomer (b) Growing polymer chain with reactive site at the end (c) Final polymer molecule**

There are currently numerous brands of acrylic bone cement commercially available on the market. According to the viscosity disparities when they are introduced to the femoral bone cavity, bone cements can be classified into three categorisations: low viscosity (e.g. Cemfix 3, Coriplast 3), medium viscosity (e.g. Simplex P, CMW 3) and high viscosity (e.g. Palacos R, CMW1). Low viscosity bone cements have a long lasting wetting phase and the material usually remains sticky for three minutes or longer. High viscosity bone cements have a relatively short wetting phase and lose their stickiness quickly. The viscosity of bone cements at the dough stage is determined

mainly by the chemical composition and the powder to liquid ratio. However, there is one method to modify the viscosity without changing other characteristics of the cement, i.e. pre-chilling the cement. As pre-chilling the cement can slow down the polymerisation by reducing the maximum temperature during the process of polymerisation, the viscosity is therefore to some extent reduced. Nowadays, there are five most commonly used bone cements, which are summarised in table 2.3.

**Table 2.3: The five most commonly used bone cements**

Bone cement brands	Suppliers
Simplex P	Howmedica International Inc., Limerick, Ireland
Palacos R	Biomet Merck Ltd., Bridgend, UK
CMW	DePuy International Ltd., Leeds, UK
Zimmer	Zimmer Inc., Indiana, USA
Sulfix	Sulzer Brothers Ltd., Winterthur, Switzerland

### 2.5.2 Mechanical and physical properties

Although these commercially available bone cements vary slightly in composition, they possess significantly different mechanical properties. Bone cements endure considerable stresses *in vivo*, therefore sufficient mechanical strength is one of the most important demands to achieve stable fixation and to guarantee long term stability of the hip implant. There are two different measuring principles to determine mechanical properties of bone cement, one applying static stresses and the other applying dynamic stresses. Static tests are destructive tests with a uniaxial single loading, increasing until failure, whereas dynamic tests involve a cyclical loading. In general, acrylic bone cement displays high strength in compression, whilst its brittle characteristic is noticeable under tension and bending. Common bone cements on the market display 75–105MPa for compressive strength, 65–75MPa for bending strength, 50–60MPa for tensile strength. According to the BS ISO standard 5833, the vast majority of commercial antibiotic and plain bone cements are compliant with these requirements. Additionally, it is indicated that fatigue failure of bone cement will occur at a load much lower than the predicted ultimate strength, and bone cement fractures and cracks have been observed from hip retrieval studies and they are suggested to be one potential reason to promote aseptic loosening of the femoral stem (Eliades *et al.* 2003), figure 2.9.

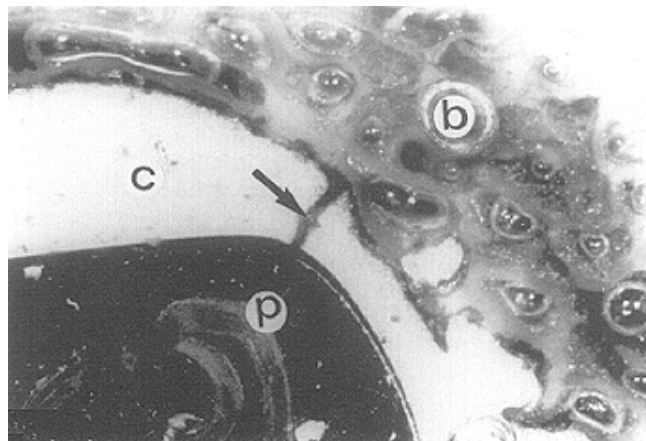


**Figure 2.9: Fractures present in bone cement mantle: c=cement; p=prosthesis; b=bone**

Consequently, great efforts have been made in order to improve the mechanical properties of bone cement and also the mixing technologies. One method that has been comprehensively attempted is the so called “modern cementing techniques”. Table 2.4 shows the typical characteristics of three generations of cementing techniques. Bone cement was originally mixed in a bowl and manually finger-packed into a reamed and irrigated bone cavity. This method would expose the surgeons to noxious fumes released by the MMA monomer. The second generation cementing technique was developed to enhance the interlock between the cement and the surrounding cancellous bone. This as a consequence resulted in a greater scrutiny of the cement itself and the stem–cement interface, which is the main purpose of the third generation cementing technique. It has been indicated that a better reliability and survivorship of cemented THR is achieved through the use of “modern cementing techniques”, probably in part due to the reduction of porosity of the cement mantle (Mulroy and Harris 1990). Porosity is considered to be a major cause of reduced fatigue life of bone cement. The micropores generated and sometimes even the macropores can be introduced through air initially surrounding the powder, and air trapped in the cement during mixing and during transfer from the mixing container to the application device. Those pores are often cited as stress risers to initiate and propagate cracks and fractures within bone cement mantle.

**Table 2.4: Typical characteristics of three generations of cementing techniques**

First generation (1960s)	Second generation (1970s)	Third generation (late 1980s)
Finger packing	Hand mixing	Vacuum mixing
Bulb syringe irrigation	Distal plugging	Distal plugging
	Pulsatile lavage cleaning	Pulsatile lavage cleaning
	Syringe injection	Centrifugation
	Retrograde cement delivery with gun	Centralisation and pressurisation

When considering the mechanical tests that are used to obtain the mechanical properties of bone cement, one fact that should be taken into account is most of these tests are executed with dry specimens at room temperature. However, the cement has to perform its task in the human body, in contact with synovial fluid and at a temperature of 37°C. Mechanical properties of acrylic bone cement vary relative to the variance of test environment. For instance, the cement absorbs water from the synovial fluid, resulting in a decrease in modulus of elasticity as well as stiffness. The water uptake of commercial bone cements is approximately 1%–2% for plain bone cements and slightly higher for antibiotic bone cements. Accordingly, there is a potential relationship between mechanical and physical properties of bone cement. One thing that has to be specially mentioned is the creep characteristic of bone cement as it has a direct influence on the long term behaviour. In nature, acrylic bone cement exhibits a combination of elastic and also viscous behaviour called viscoelasticity. When the cement is subjected to a constant load, the resulting deformation can be divided into two categories, one is immediate elastic deformation and the other is time-dependent continuous deformation. The immediate elastic deformation happens instantaneously by applying loading. It is a recoverable deformation which is essentially independent of time. Following this rapid deformation there is a delayed continuous deformation resulting from stress. One part of this continuous deformation is recoverable in time after releasing the load, and this is called primary creep. The second part is a non-recoverable permanent deformation called secondary creep.

(Kuehn *et al.* 2005). It has been proposed that the creep behaviour of acrylic bone cement may contribute to loosening of cemented THR, allowing for expansion of bone cement mantle and subsequent prosthetic subsidence although it was reported to be small (Verdonschot and Huiskes 1997a). On the other hand, creep of bone cement could relax cement stresses and creates a more favourable stress distribution at the interfaces.

### **2.5.3 Current controversies**

The introduction of acrylic bone cement has undoubtedly contributed to the success of THR, but it also inevitably incurs some intractable problems which should be carefully investigated. Firstly, polymerisation reaction in nature is highly exothermic. The heat gradient can cause shrinkage of the bone cement away from the femoral stem, and even worse thermal necrosis of the bone tissue. Secondly, a certain amount of monomer remains unreacted after polymerisation and this may lead to chemical necrosis of the bone tissue. The content of residual monomer directly after curing is approximately 2% to 6%, and it will decrease slowly *in vivo*. Thirdly, the initial stress state in the cement mantle is complicated and it is considered that the residual stress may result in initial damage to the bone cement or to the stem–cement and cement–bone interfaces, especially when there are abundant micropores located at the interfaces (Lennon and Prendergast 2002). These drawbacks to some extent limit the application of acrylic bone cement.

#### **2.5.3.1 With or without radiopacifiers**

Additionally, although the long term survivorship of cemented THR has been well documented and it still takes predominance in terms of the number of operations carried out in the UK in comparison with uncemented THR, there is no unanimity of support for the use of acrylic bone cement. There are currently several significant issues that controversies have concentrated on. One is concerned with the addition of BaSO<sub>4</sub> or ZrO<sub>2</sub> as radiopacifiers. It is indicated in literature that these additives could cause a decrease of mechanical properties of bone cement (Ginebra *et al.* 1999) and promote generation of wear debris when they are liberated, given that these materials are much harder than both the femoral stem and the bone cement. If they further migrate into the head–cup articulating interface, the femoral head will be more severely damaged by third-body wear. It is also suggested that these additives could contribute to some extent to bone resorption by enhancing macrophage–osteoclast differentiation (Sabokbar *et al.* 1997). On the other hand, it is considered that the influence of these radiopaque agents on mechanical properties of bone cement is insignificant, and the generation of wear debris and noticeable osteolytic lesion are still apparent even if plain bone cements without these additives are used. Without distinct opacity, the surgeons cannot easily monitor the healing process and it is therefore difficult to monitor any failure over time. Taking into account the great contribution that these radiopaque agents have made to aid in radiological assessment of cemented THR, it may be more advisable to conclude that their use as additives to bone cement should be kept.

#### **2.5.3.2 With or without antibiotics**

The other area that research has been focusing on is to add antibiotics to bone cement, commonly gentamicin and tobramycin, with the aim of preventing or treating infection. It has been indicated from the Norwegian National Hip Register that the combination of systemic administration of

antibiotics with the use of antibiotic-loaded bone cements resulted in a lower risk for revision (Havelin *et al.* 1995). The release of antibiotics for all bone cements is rapid at the beginning, followed by an evident decrease within the next few days. It is important to note that the release of antibiotics comes only from a thin layer of the cement surface, and most of the antibiotic is not eluted during the lifetime of the implant. In spite of the application of the antibiotic-loaded bone cements, other studies have demonstrated that, again, the mechanical properties of these bone cements will be modified, exemplified by an alteration in density, bending strength and viscosity, etc (Armstrong *et al.* 2002). Consequently, arguments against incorporating antibiotics into bone cement are still in existence.

### **2.5.3.3 Cement mantle thickness**

A third but not the last issue is concerned with the thickness of bone cement mantle. Conventional wisdom based on the results of theoretical and laboratory work and retrieval studies, especially from research centres in the USA and in the UK, suggests that the cement mantle should have a minimal thickness of 2 to 4mm, and should, moreover, be complete (Fisher *et al.* 1997). It is considered that when the cement mantle fails to match these requirements, mechanical failure may ensue and progress to femoral lysis, resulting in aseptic loosening of the hip prosthesis. This comprehensively accepted technique was challenged by the study carried out by Skinner *et al.* (2003), in which they obtained a clinically better outcome for the cohort of hip prosthesis with thin bone cement mantle. It was further entirely transgressed by two French-designed cemented femoral components, Charnley Kerboul (Aston, St Etienne, France) and Ceraver Osteal (Ceraver Osteal, Roissy, France), which are intended to fully occupy the medullary canal of the femur. The design philosophy of these stems implies that the cement mantle will not only be very thin, but incomplete in certain places. This is termed as the “French paradox” (Langlais *et al.* 2003), and a better understanding of the function of thin cement mantle may be gained from histological studies of post-mortem specimens.

To sum up, there is no doubt that in orthopaedic surgery acrylic bone cement is going to be widely employed in many hospitals and research centres all over the world and it is of potential utility wherever mechanical attachment of biocompatible metal to living bone is necessary. Also there is equally no doubt that its use by different operators will definitely produce complications which might seriously threaten its reputation.

## **2.6 Failure mechanisms of cemented total hip replacement**

### **2.6.1 General introduction**

Despite its great success in providing an appropriate treatment for those patients with hip disorders, THR incurs a high revision rate with aseptic loosening as its end point after a 15–20 years’ follow up, especially when the metal hip prosthesis is improperly implanted. In contrast to the expanding demand of this procedure performed in younger and more active people, the survivorship in these patients has remained poor partly due to an increased activity level. Additionally, the number of THR carried out annually has been continually rising, with a consequent increase of revision operations. This is the case not only in the UK but also all over the world. Accordingly, there is imperative requirement to gain a deeper insight into the scenario behind failure of THR.

With reference to cemented THR, it is generally accepted that meticulous attention should be paid to three elements and two interfaces to achieve long term durability. These are the femoral stem, the stem–cement interface, the bone cement, the cement–bone interface, and the bone. Due to the complexity of this structure, there have been intense contentions concerning the site that aseptic loosening, the prominent failure mode of cemented THR, initially occurs. By definition, aseptic loosening denotes that the prosthesis becomes loosened in the absence of microbiological or clinical evidence of infection or mechanical failure, with severe pain and instability in terms of a radiolucent line, usually wider than 2mm around the hip implant, as its clinical symptoms. Other reasons for revision of THR include stem fracture, prosthesis dislocation, and deep infection, etc, figure 2.10. Stem fracture has almost entirely been eradicated due to improved material selection and processing, and surgical technique and postoperative care have also significantly reduced the percentile of prosthesis dislocation that leads to revision of THR. Additionally, the issue of deep infection has been addressed by employing antibiotic-loaded bone cement and through surgical protocols minimising bacterial exposure. Consequently, aseptic loosening has attracted the most research interest as it involves so many factors that could be controlled through stem design, stem material, bone cement brand and surgical procedures, etc.

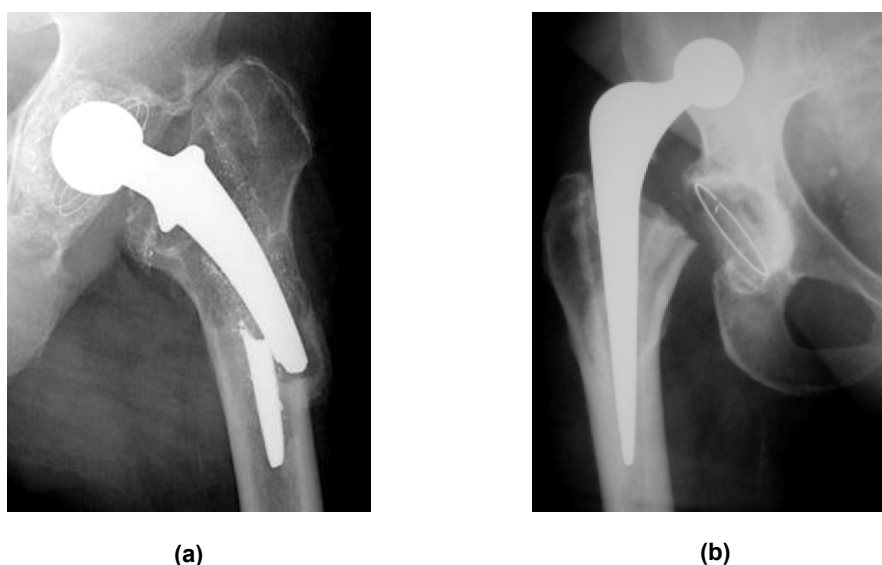


**Figure 2.10: Reasons for revision of THR (a) Stem fracture (b) Prosthesis dislocation**

### **2.6.2 Wear debris induced bone resorption**

Although it has not been completely understood, previous investigations with the use of roentgen stereophotogrammetric analysis (RSA) have indicated that aseptic loosening can be primarily attributed to bone resorption, and retrieval studies have demonstrated that failure of cemented THR is always associated with debonding at the stem–cement interface and also cement mantle deficiencies, such as cracks and fractures. This suggests that debonding at the stem–cement interface, as a prelude to aseptic loosening, may promote the failure process of the cement mantle (Verdonschot and Huiskes 1997b). It is now considered that debonding of the femoral stem from the bone cement may be inevitable for almost all stem designs. Once debonding occurs, there will be subsequent generation of wear and corresponding wear debris, including both metallic debris and cement debris, due to the micromotion at the stem–cement interface. This is particularly

crucial *in vivo*, not only because the debris could result in third-body wear and accelerate more wear debris to be produced, but also because some wear debris within a certain size range would transport along cement mantle deficiencies to those sites surrounding the bone tissues, where a significant macrophage response would occur, figure 2.11. The immune system in the human body recognises certain debris as foreign material and the defence system is thus activated to isolate this material, during this process the osteoclast cells destroy the bone stock. This leads to bone resorption, or the so called osteolysis, which finally results in aseptic loosening of the femoral component.

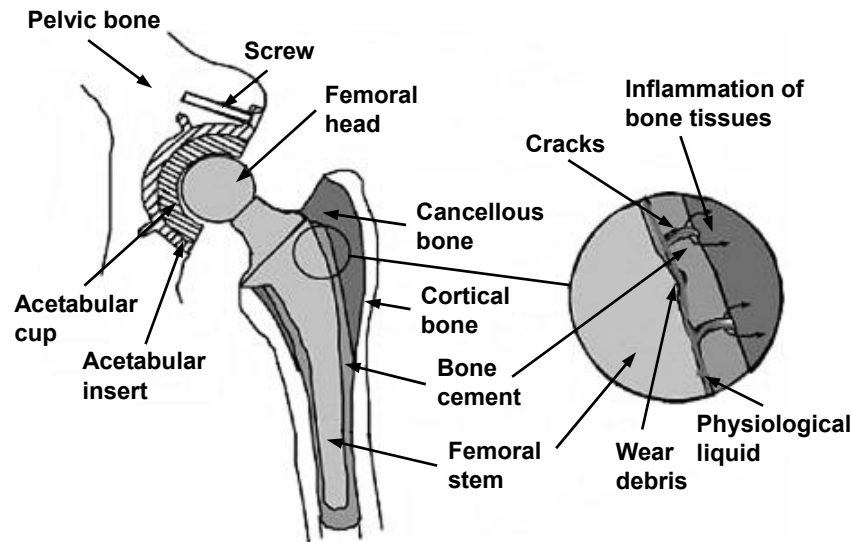


**Figure 2.11: Migration of wear debris to bone tissues through gaps at the stem–cement interface**

The adverse effect of bone cement debris has been reported by several authors (Maloney *et al.* 1990, Shardlow *et al.* 1999). Furthermore, the debris may migrate to the head–cup interface, accelerating generation of more UHMWPE debris. Biological reaction to the UHMWPE debris originating from the acetabular cup has been expatiated by Ingham and Fisher (2000) in detail, and they believe it is the main reason for late aseptic loosening. Historically, wear for the most part is produced at the head–cup interface due to the fact that this articulating interface is designed to allow for mobility. The stem–cement interface, as a potential candidate for generation of wear debris, has been to a certain degree neglected. However, with the renaissance of new hard-on-hard bearing systems with nearly zero friction, wear at the head–cup interface has been greatly reduced. It thus may shift research interest to the stem–cement interface. This current research concentrates mainly on the wear at this interface.

### 2.6.3 Stress shielding

Stress shielding, also called remodelling of the femur, is another reason that has been suggested to lead to bone resorption and subsequent aseptic loosening of the hip implant (Lewis *et al.* 1984). It is a biomechanical phenomenon that causes adaptive changes in bone strength and also stiffness around the metallic implant. It has been observed that bone adapts to the load by increasing or decreasing bone density, which is termed as “Wolfe’s Law of Bone”, i.e. bone grows or remodels in response to the stresses that are placed on it. Ideally, the hip prosthesis would carry stress and distribute it to the underlying bone in a manner identical to the original bone. However, this does

not occur as it is expected. In a hip prosthesis, much of the load applied to the femoral component tends to be transmitted to the bone near its distal tip, thus the force at the proximal femur is highly reduced. Consequently, bone loss will occur right at that site, and the atrophy of bone structures would contribute to the loosening of the femoral component due to lack of support in the proximal area. Figure 2.12 (a) shows a body with no hip implant, the physiological loading of the human body is supported by the bones and the bones adapt to the loading by sustaining the minimum bone density required to handle the stress. Figure 2.12 (b) shows the femur with a hip implant, which carries much of the physiological loading. The load transferred to the bone around the hip implant thus decreases greatly because the bone biologically believes that there is no load to carry. The shielding of the stress to the bone therefore reduces the bone's apparent need to be supportive and dense.

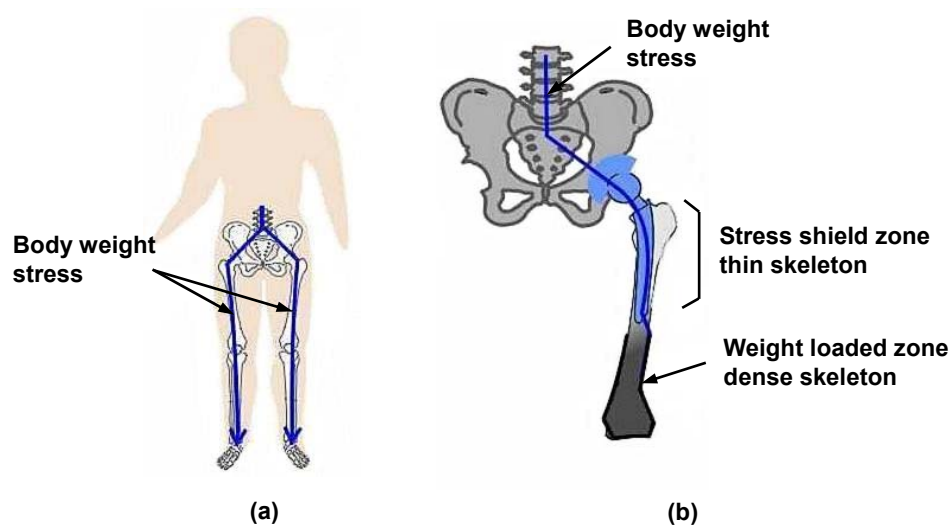


**Figure 2.12: Effect of stress shielding**

Basically, stress shielding is more often associated with uncemented THR than cemented THR, especially in those cases where a larger and stiffer femoral stem is used. Although it is considered that a point of equilibrium between loss of bone and production of bone will be reached, research does demonstrate that this is a potential hazard to the long term success of THR.

## **2.7 Wear at the stem–cement interface**

### **2.7.1 General introduction**

It has been mentioned above that the introduction of acrylic bone cement has brought about three sites that are very easy to compromise, these being the stem–cement interface, the bone cement itself and the cement–bone interface. Previous investigations have come to diverse conclusions with regard to which one acts as the most significant contributor to initiate aseptic loosening of the whole system (Jasty *et al.* 1991, Cardiner and Hozack 1994, Revell *et al.* 1997). Nowadays, more and more retrieval studies are showing evidence of debonding at the stem–cement interface, which has strengthened the importance of this site and has predicted the necessity for further study.

The stem–cement interface has been consistently deemed as a weak link in cemented THR, which forms a junction through mechanical interlock rather than chemical bonding. It is a transitional

zone between the femoral stem and the bone cement, two materials with significantly different stiffness, hardness and elastic modulus. Consequently, the strains at this interface are not perfectly matched under certain loading conditions. From the mechanical point of view, this will lead to a relative motion between the two materials at the interface, and as is known to all, where there is motion there is the potential for wear. This would seem unbelievable at first sight because the occurrence of wear at the stem–cement interface firstly needs debonding of this interface, but for a long time it was generally believed that the stem was well anchored within the cement mantle *in vivo*. Recently, however, there is an increasing body of evidence, e.g. RSA studies, which has shown subsidence of the femoral stem within the cement mantle for almost all hip designs, regardless of stem geometry and surface finish (Kiss *et al.* 1996, Alfaro–Adrián *et al.* 1999). This suggests that debonding at the stem–cement interface may be not only common but also inevitable. Thus there is no wonder as to why wear will generate on the femoral stem, if it is subjected to sufficient loading and a number of loading cycles.

### **2.7.2 Evidence of wear on the stem**

Although to a certain degree it is underestimated, femoral stem wear was recognised early as an intractable problem involved in cemented THR. The original clinical incidence could be traced back to the work published by Willert *et al.* in 1974, in which superficial “polishing” of the shaft of Charnley–Müller hip prosthesis was reported and it was attributed to friction between the femoral metal and the bone cement. Later on in 1983, Dobbs *et al.* presented evidence of “rub marks” on 180 McKee and Stanmore femoral stems, and it was indicated that, for those loose femoral stems, the incidence of “burnishing” appeared to increase with implantation time. From then on, a large amount of literature concerning femoral stem wear has been published, which shed much light on this crucial issue in cemented THR. In 1990, Anthony *et al.* reported “abrasive wear” on matt Exeter femoral stems which were revised due to localised endosteal bone lysis, figure 2.13. It was explicitly demonstrated that the “polishing” evidence was exclusively located on the anterolateral and posteromedial surfaces of the femoral stem, where large rotational forces were expected to occur. In 1991, Witt *et al.* showed “burnishing” evidence on the medial proximal portion of the McKee stems, which were made from Ti alloy and had a shot-blasted surface finish. They further examined the stem surface employing optical microscopy and scanning electron microscope (SEM) and concluded that the damage was caused by repeated “rubbing” of the femoral stem against the bone cement. Likewise in 1992, Buly *et al.* reviewed 71 Ti alloy cemented total hip arthroplasties, in which 71% of the femoral stems with aseptic loosening were abraded from the bone cement. Again in a study carried out by Salvati *et al.* in 1993, it was indicated that when the Ti alloy femoral stem became loosened *in vivo*, it would abrade against the fragmented bone cement and generate metallic as well as cement debris. In 1997, Shardlow *et al.* reported “fretting wear” of Charnley low friction arthroplasties, and they further identified that this wear affected the anterolateral and posteromedial edges of the femoral stems. All of these early studies accentuated the significance of femoral stem wear and contributed to providing useful information for further investigation. However, various terms have been used to describe femoral stem wear in these studies, such as “polishing”, “rub marks”, “burnishing”, “abrasion” and “fretting”, which has made comparison between the wear damage a little confusing.

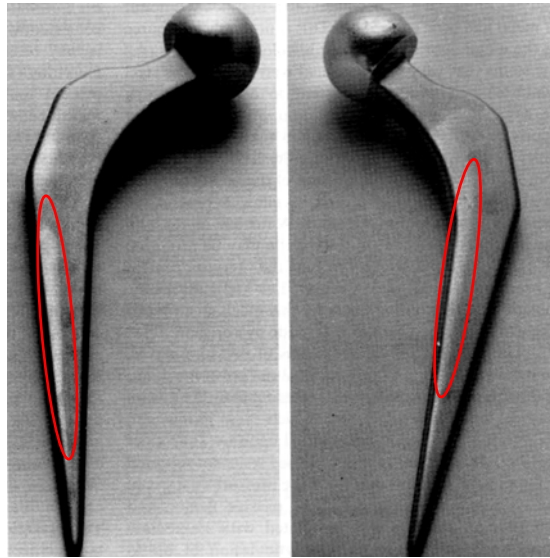


**Figure 2.13: Evidence of abrasive wear present on matt Exeter femoral stems**

### **2.7.3 Wear mechanism at the stem–cement interface**

As wear at the head–cup interface has been greatly reduced with the introduction of cross-linked UHMWPE and hard-on-hard bearing systems, wear at the stem–cement interface is considered to be playing a more and more significant role in the overall wear of cemented THR. Although cemented THR has been previously noticed as a situation that can lead itself to wear, the wear mechanism involved in this whole system, especially at the stem–cement interface, has been little investigated. Initial suggestions attribute the wear on the femoral stem to fretting wear, which is caused by low-amplitude oscillatory movement at the interface. However, even then there is no substantial evidence to support this concept, and other wear patterns have also been reported. It should be specially noted that most of the literature published in the 1990s regarding stem wear have focused on matt femoral stems. There was a dearth of research in this area as to polished femoral stems, and only a few studies have been performed to ascertain the relationship between femoral stem surface finish and femoral stem wear. This issue came to the fore due to the fact that most femoral stem designs experienced much evolution as they developed, with surface finish the one leading to the most intensive controversies (Crowninshield *et al.* 1998). The first attempt to set foot in this area was considered to be the study carried out by Howell *et al.* in 1999. They examined 150 femoral stems and characterised femoral stem wear using contact profilometry, interference profilometry and SEM associated with energy dispersive X–ray (EDX) analysis, from which it was confirmed that a fretting mechanism was responsible for the damage and the damage was influenced by femoral stem alloy and also surface finish. However, a deep insight into the influence of femoral stem surface finish was not gained at that time. Later on numerous reports were published on failed prostheses that exhibited varying surface finishes (Collis and Mohler 2002, Lefevre *et al.* 2004), but none of them has correlated femoral stem surface finish with femoral stem wear.

It is not until recently an intensive study on surface morphology of explanted femoral stems was performed that a better understanding of this issue has been obtained. In the investigation carried

out by Howell *et al.* (2004), it was demonstrated that 92% of the 172 retrieved femoral components showed wear on the stem and the wear mechanism behind polished and matt stems appeared fundamentally different in spite of very similar wear locations. For polished stems, the morphology of the wear produced by cyclical movement of the stem within the cement mantle indicated a fretting mechanism which generated typical fretting pits below the level of the original stem surface and did not damage the bone cement much, figure 2.14. By contrast, matt stems wore against the bone cement by an abrasive mechanism which sacrificed parts of the inner surface of the cement mantle and consequently resulted in destabilisation of the femoral stem and generation of both metallic and cement debris, figure 2.15. Additionally, 74 femoral stems which were found to be absolutely fixed in the cement mantle *in vivo* at the time of revision also showed evidence of wear on the stem surface. This suggested that wear may occur in the absence of obvious loosening of the femoral stem within the cement mantle, even for stable femoral stems. This study indicates that wear on the femoral stem is primarily determined by femoral stem surface finish. Another significant contribution to this area that should be particularly mentioned was ascribed to Brown (2006), who developed a semi-quantitative method to calculate volume loss during wear of matt femoral stems. By comparing this result with that calculated from a mathematical truncation model, it was confirmed that the wear mechanism for matt femoral stems was abrasive wear rather than classic fretting wear, at least until a fully polished surface was attained by which point it was considered that classic fretting wear would subsequently predominate, figure 2.16. However, there is no persuasive *in vitro* evidence of successful reproduction of fretting wear on polished femoral stems as well as the influence of stem geometry, stem surface finish and bone cement brand on it. Furthermore, there is relatively little perception that has been gained with regard to initiation and propagation of femoral stem wear, and this issue has not been fully understood as yet.

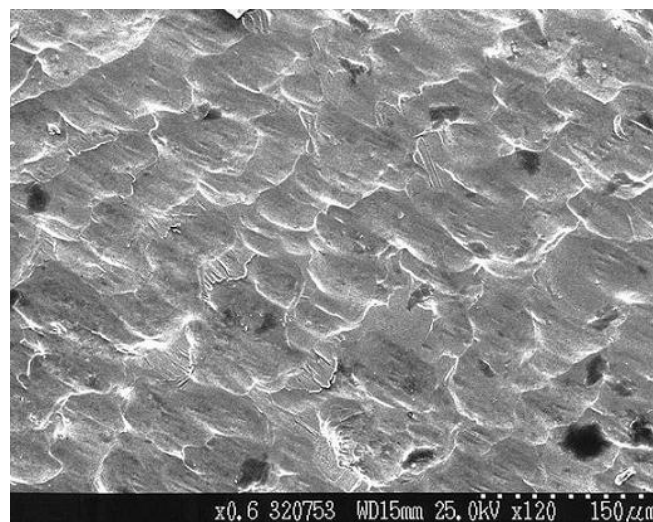
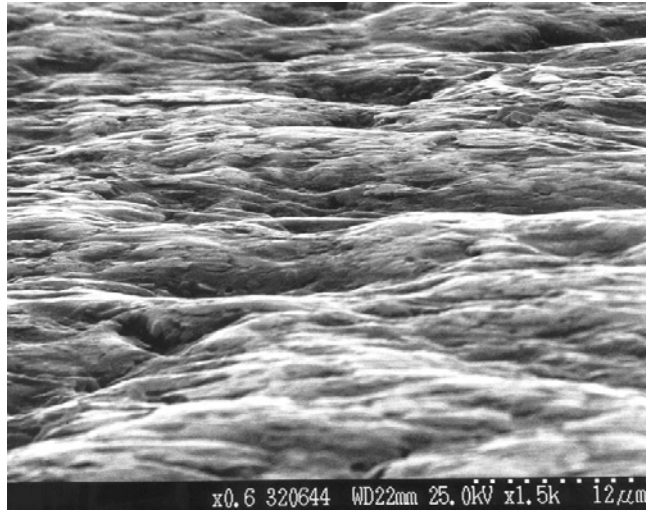
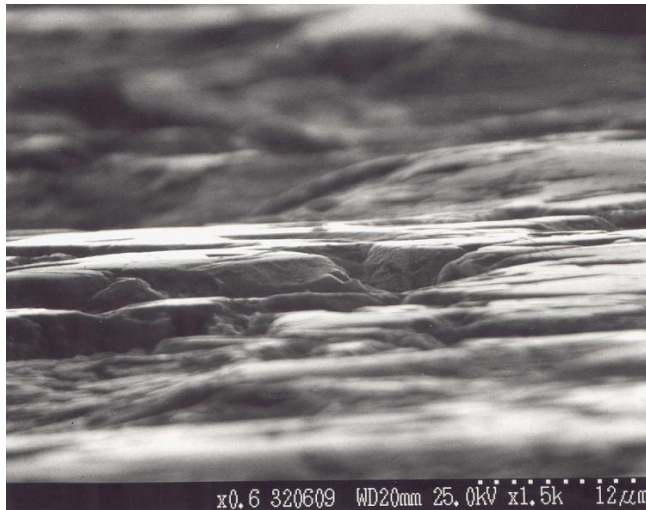


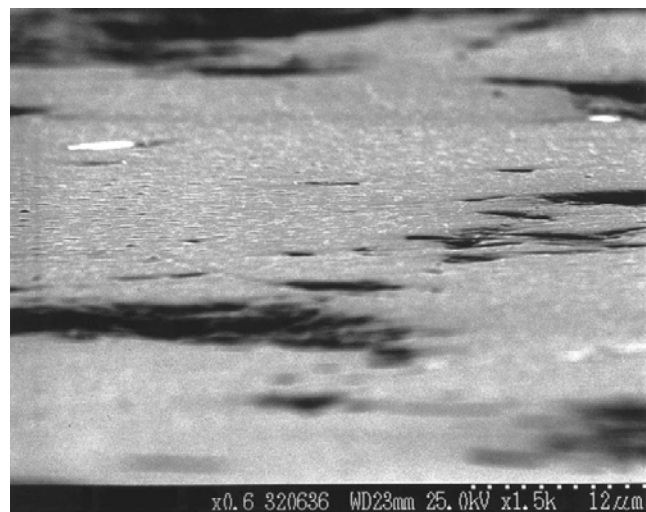
**Figure 2.14: Fretting wear on an explanted polished Exeter femoral stem measured by SEM**



(a)



(b)



(c)

**Figure 2.15: Grazing incidence SEM images showing increasing degrees of polishing wear on matt-surfaced stems (a) An unworn area (b) An area of slight polishing wear (c) An area of marked polishing wear (Howell *et al.* 2004)**

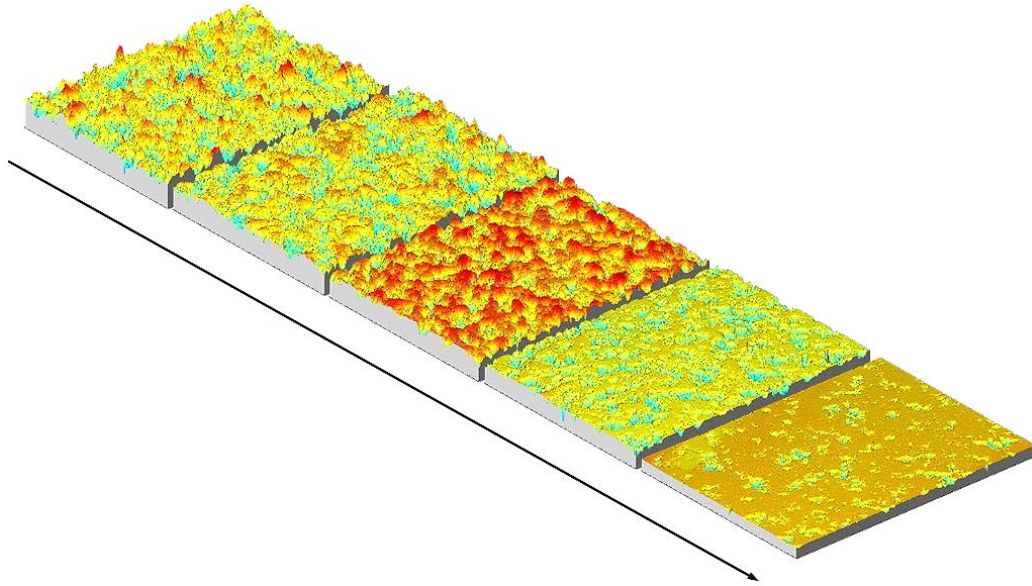


**Figure 2.16: The axonometric plots showing progressive stages of abrasive wear on an Exeter matt-surfaced stem, the asperities present on the unworn surface are removed during the wear process (Brown 2006)**

## 2.8 Fretting wear and *in vitro* simulation

### 2.8.1 Fretting wear

Fretting wear is suggested to be the wear mechanism between polished femoral stem and bone cement. By definition, the term fretting wear denotes a surface degradation process in which removal of materials is induced by low-amplitude oscillatory movement between two contacting components. The amplitude of relative motion is usually less than  $25\mu\text{m}$  and certainly not greater than  $130\mu\text{m}$  (Waterhouse 1972). This is considered to be the most distinctive characteristic that differentiates fretting wear from other forms of sliding wear. The typical features of fretting wear are evident, which are summarised by Engel and Klingele (1981) as follows: (a) Grey staining—the formation of matt surface due to micropitting; (b) Undulations—in parts metallically smooth; (c) Pitting formation—due to the localised piling up of debris; (d) Roughening—in the form of uniform corrugations, sometimes with the amassing of loose, powdered debris; (e) Tower like growth—a few highly strengthened contact points built-up from debris. The schematic diagram of these features is shown in figure 2.17.

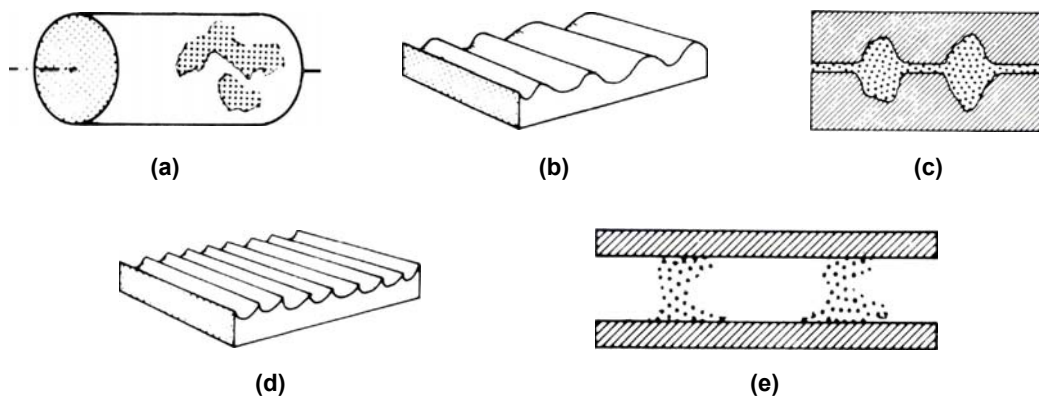


**Figure 2.17: The schematic appearance of fretting damage on metal surfaces**

The most noticeable characteristic of fretting in addition to the formation of debris, suggested by Waterhouse (1972), is local pitting on the surface.

As a result of the great efforts made by both orthopaedic surgeons and researchers in performing implant retrieval studies and tissue analysis, fretting wear has early been identified as a potential degradation mechanism in orthopaedics, especially with regard to the modular implant design (Hoeppner and Chandrasekaran 1994). However, investigations with regard to fretting damage on hip prosthesis, in particular on the femoral stem, are exceedingly scarce. Taking into consideration the special environment of the human body, corrosion may occur during the fretting process due to chemical reaction, and this is termed as fretting corrosion. The problem is raised due to the fact that those implantable metals owe their corrosion resistance to a thin passive oxide film, whilst wear of femoral stem against hard bone cement especially where radiopaque BaSO<sub>4</sub> or ZrO<sub>2</sub> has been added could result in disruption of this protective passive film, and therefore the unoxidised subsurface metal is exposed to further damage. Some retrieval studies have shown evidence of severe corrosive damage on the stainless steel femoral stems. In 1996, Musolino *et al.* reported corrosion under the collar of 18 stainless steel T-28 femoral stems, which illustrated a multi-layered and multi-textured nature under SEM. Later on in 1998, Walczak *et al.* investigated the morphology and composition of the corrosion product presented on 11 Charnley and Müller stainless steel femoral stems, using SEM associated with EDX analysis. They found that some areas on the stem surface had discoloured into a black compound and a chromium-rich (Cr) plaque was detected in these sites. This appears to indicate a repeated removal and subsequent formation of oxide films in the process of fretting corrosion. Recently in 2004, Thomas *et al.* reviewed severe corrosion of 12 cemented Ti Furlong straight stems which was typical of crevice corrosion. It is considered that a crevice-like sheltered region exists between the femoral stem and the bone cement following debonding of the stem–cement interface. This promotes the development of an acidic environment that accelerates dissolution of metal ions from the bulk implant. In this region, a combination of fretting corrosion and crevice corrosion is considered to occur. All these studies have indicated that no efforts should be spared to reduce femoral stem wear in order to protect the substrate of the femoral stem from being corroded.

### **2.8.2 *In vitro* simulation of fretting wear**

*In vitro* wear simulation is generally accepted as an effective method to evaluate the performance of a newly designed hip prosthesis prior to being introduced for clinical use. Wear simulation at the head–cup interface has been comprehensively carried out, with significant reduction of wear when using hard-on-hard bearing systems. However, research to date has indicated that simulation of wear at the stem–cement interface has seldom been tried. This is in part due to the fact that it is extremely difficult to exactly simulate the *in vivo* human conditions. Additionally, no standardised testing methods in accordance with ISO or BS standards have been described concerning *in vitro* wear simulation of cemented femoral stems. The present standards available only refer to testing methods which aim primarily at static and fatigue mechanical testing of hip implant strength or endurance (BS ISO 7206–4 2002). Therefore, most wear tests just employ a simple pin-on-plate or pin-on-disk model, figure 2.18, in which a bone cement or bone pin wears against a metal disk in terms of displacement control (Geringer *et al.* 2005). Consequently, the influence of functional

aspects of stem design such as geometry and surface finish and bone cement brand on generation of fretting wear has rarely been investigated.

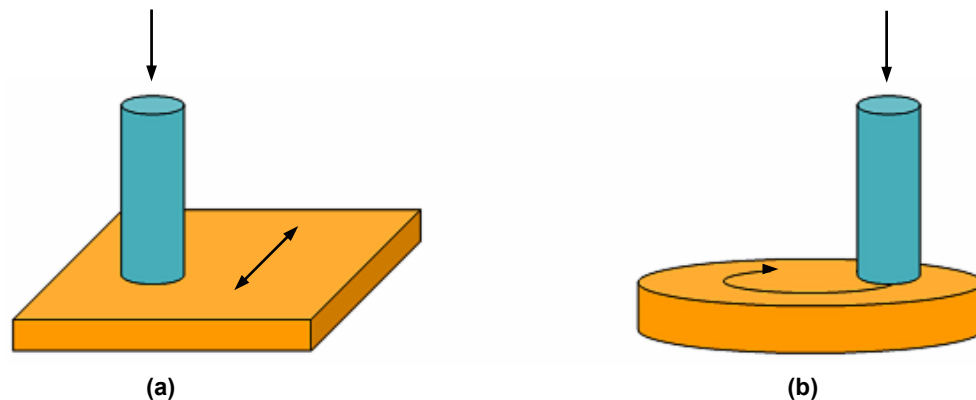


**Figure 2.18: (a) The model of simplified pin-on-plate device, the arrows show axial force on the pin and sliding motion of the plate (b) The model of simplified pin-on-disk device, the arrows show axial force on the pin and rotating motion of the disk**

The initial attempt to reproduce fretting wear on femoral stems through *in vitro* wear simulation was performed by Cook (1998). Although a useful insight has been gained from her unremitting endeavour, it is considered that by then the results were rather limited. However, it inspires more and more researchers to pay special attention to this area. In 2003, Cristofolini *et al.* developed a protocol to carry out *in vitro* wear testing of femoral stems under force control rather than displacement control. Force control is considered to be more clinically relevant as it simulates physiological loading that the femoral stem experiences in the human body. They reported in detail the generation of cracks and micro-damage in the cement mantle. However, as to femoral stem wear, they only mentioned that the surface roughness of the femoral stem increased at the end of the test and it was considered to be caused by a fretting process against the bone cement. In 2004, Bader *et al.* established a “novel” test method to analyse the abrasive wear behaviour of cemented Ti alloy and CoCr alloy CAP–M femoral stems (Peter Brehm Chirurgiemechnik, Weisendorf, Germany), which showed a wide polished surface at the loaded areas, associated with a noticeable decrease in surface roughness. However, they had disconnected the femoral stem from the cement mantle before the test and applied displacement control to initiate the wear process, therefore the universality of this study was compromised. In 2005, Ebramzadeh *et al.* carried out a pin-on-disk test using cortical bone pins and titanium alloy disks in terms of displacement control and static compressive loading. It was demonstrated in this study that greater wear of bone was produced against the rougher plasma-sprayed surface in comparison with the fibre-mesh surface. These previous studies provided a basic as well as considerable knowledge for the researchers who would pursue to conduct *in vitro* wear simulation of cemented femoral stems. However, it is still considered that no great success has been gained through these investigations and thus extensive research on this issue is highly required.

## **Chapter 3 Metrology strategy**

### **3.1 Chapter summary**

THR probably represents the most significant advance in orthopaedic surgery in the latter half of the 20<sup>th</sup> century. Along with alleviation of pain and allowing for mobility for a number of patients crippled with hip osteoarthritis, the increased prevalence of THR has been unhappily subjected to premature failure. It has been demonstrated that failure of THR is highly correlated with wear of the components and the accompanying wear debris. Information regarding wear of hip prosthesis could be readily obtained from implant wear assessment in a range from simple visual observation to utilisation of sophisticated instruments, including stylus instruments, optical interferometers, and electron microscopy. In this regard, measurement and characterisation of the implant surface plays a key role.

In this chapter, it is firstly indicated that surface metrology in hip orthopaedic industry is currently confronted with a great challenge in that, either for the articulating head–cup interface or for the stem–cement interface, traditional methods for wear assessment adopted by international standard is no longer entirely applicable. This could be mainly attributed to the improvement of material selection and manufacturing technology. As the development of new techniques to evaluate wear of hip implant to a certain degree needs appropriate instrumentation with sufficient measurement range and resolution, a summary of the 3D instruments employed throughout the research of the project is presented in detail in the following sections. Finally, the superiority of 3D surface characterisation technology is discussed, based on the introduction of the limitations of 2D surface measurement and characterisation.

### **3.2 The challenge for metrology in hip orthopaedic industry**

The analyses of hip retrieval studies and tissue engineering indicate that aseptic loosening is the most prolific reason for failure of THR, and it is directly caused by periprosthetic bone resorption, which could be further attributed to an immune system response to particulate debris generated by wear of the hip prosthesis. Therefore, the amount of wear that the hip joint incurs is regarded as a good indicator of the performance of THR, with the higher wear rate typically leading to reduced function and premature failure. Consequently, measurement and assessment of wear are extremely crucial.

The orthopaedic industry, especially exemplified by the hip sector, continuously invests enormous amounts of time and money into researching methods to improve design of replacement joints and to enhance tribological properties of the components, because the nature of the bearing surfaces as a whole requires minimisation of friction and maximisation of lubrication conditions. The overall aim is to reduce the production of wear debris, which may arise from all the interfaces of the hip prosthesis, including the head–cup interface, the head–taper interface, the stem–cement interface, and the cement–bone interface, as there will be inevitably some movement between these surfaces.

#### **3.2.1 The head–cup interface**

Traditionally, a metal femoral head would articulate with a UHMWPE cup, and it is considered that the head–cup interface functions as the main source for generation of wear debris, associated with the presence of other foreign materials such as cement particles or HA particles from coatings

on uncemented implants. For a long time, the standard strategy for wear measurement has been the utilisation of a gravimetric method (BS ISO 14242–2 2000). However, the effectiveness of this method, whilst well established and standardised, can be somewhat limited in certain situations when measuring simulated wear in total joint replacements. This is highlighted when significant errors in the measured wear volume are caused by material transfer from the metal component to the plastic component or when trying to consider the effects of fluid uptake into the UHMWPE counterface. Additionally, recent development has seen a great reduction of wear at the head–cup interface, with the advent of cross-linked UHMWPE (Wroblewski *et al.* 1996) and hard-on-hard bearing systems (Firkins *et al.* 2001, Hatton *et al.* 2002). In these circumstances, the volume of material removed as a result of wear is extremely small compared to the mass of the component and consequently it is difficult to evaluate small mass changes against large component masses as affordable equipment sensitive enough to discern between materials is not currently available. In the case of explanted bearings, the use of a gravimetric method is not feasible at all due to there being no pre-wear data. It provides a great challenge for researchers to develop new techniques to evaluate such wear. One great contribution that should be noted in this area is attributed to Bills *et al.* (2007), who developed a method for more accurately determining clinical wear of explanted hip joints through geometrical assessment of the bearing surfaces using CMM, and it is considered as a very important tool in ascertaining long term wear of THR. Undoubtedly, the advance in manufacturing technology and material selection, and also the great need to accurately analyse explanted bearings for true clinical wear are pushing traditional wear assessment methods to their limits. Novel metrology solutions are required to evaluate wear of hip joints following *in vivo* and *in vitro* use.

### **3.2.2 The stem–cement interface**

The reduction of wear at the articulating head–cup interface has facilitated further research interest on wear assessment to other interfaces that are subjected to movement, primarily the stem–cement interface. The issues with regard to wear and the resulting wear debris around the femoral stem and its subsequent effects on aseptic loosening in particular are now showing an increasing significance in failure of THR. The wear mechanism, as has been previously discussed, is largely dependent on surface finish of the femoral stem, with abrasive wear for matt stem and fretting wear for polished stem. However, it is not clear as to the exact surface finish level that produces abrasive wear or fretting wear. Therefore, assessment of the stem surface finish, which is mainly focused on measurement of surface texture in the nanometer scale, is in great demand. In order to ensure that THR performs to an optimum, large numbers of studies have been carried out to investigate wear at the stem–cement interface, and it is indicated that increased surface roughness of hip implants would increase the propensity for this wear, associated with higher loosening rates. However, the wear damage is very difficult to quantify and define due to the mixed mechanisms of wear involved. Additionally, just as the situation that is present for the head–cup interface, the formation of oxide debris at the stem–cement interface, and also the possibility of material transfer from the bone cement to the femoral stem do not promote the possibility of simple gravimetric assessment. New techniques are to be developed to quantitatively evaluate femoral stem wear and to gain an insight into its characteristics and potential indicators.

### 3.2.3 Summary

The relatively slow process of reviewing and publishing standards to ensure comprehension and accuracy has made it difficult to update them in line with the fast moving development in industry. The growing replacement of traditional metal or ceramic-on-UHMWPE configurations by modern hard-on-hard bearing systems has considerably reduced the production of wear, and what could once be easily assessed by the gravimetric method is nowadays out of the scope of detection with feasibly affordable instrumentation. It has been further accentuated where materials transfer between the components would happen either at the head–cup interface or at the stem–cement interface, resulting in great incorrectness through utilisation of the gravimetric method. As a consequence, it is essential that alternative means of evaluating wear and function of the hip prosthesis should be developed.

### 3.3 Instrumentation employed throughout the research of the project

There are several types of 3D surface measurement instrumentation, which can be classified into contacting method and non-contacting method based on different physical principles. The stylus instruments are typically a contacting method, and the optical interferometer uses a non-contacting method. Scanning microscopy covers both contacting and non-contacting techniques. As with all kinds of instruments there are potential advantages and disadvantages, the measurement range and resolution are considered to be an initial criterion for selection of the appropriate method. An amplitude–wavelength plot for the common methods is given in figure 3.1, in which the two axes represent the range (away from the origin of the axes) and the resolution (towards the origin of the axes) of the instruments both in vertical and horizontal directions, and each block indicates the working area of an instrument (Blunt and Jiang 2000).

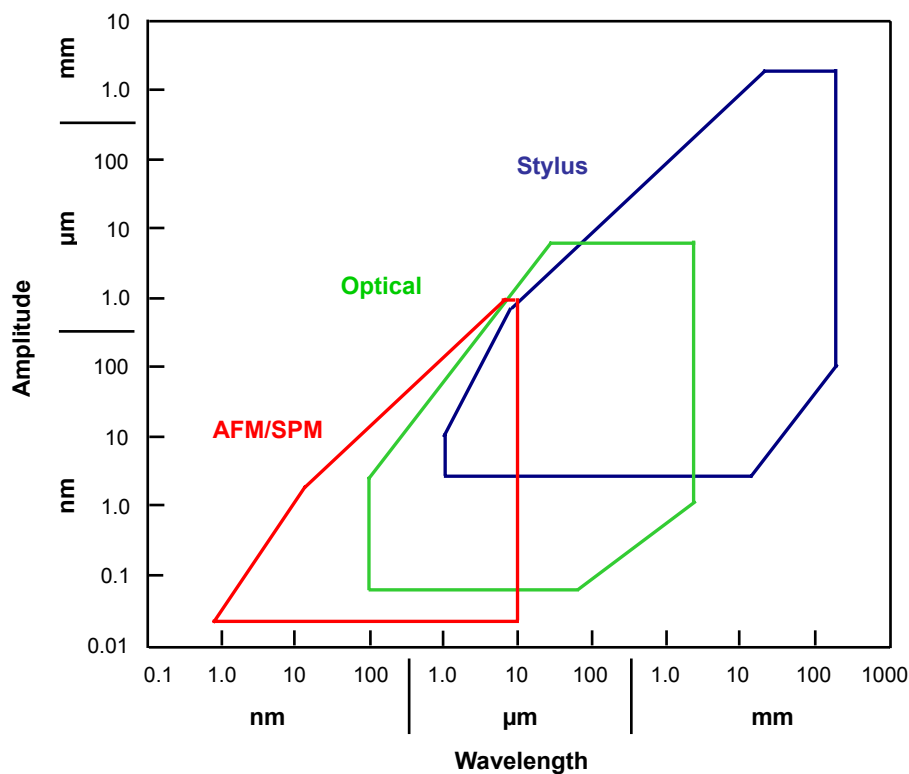
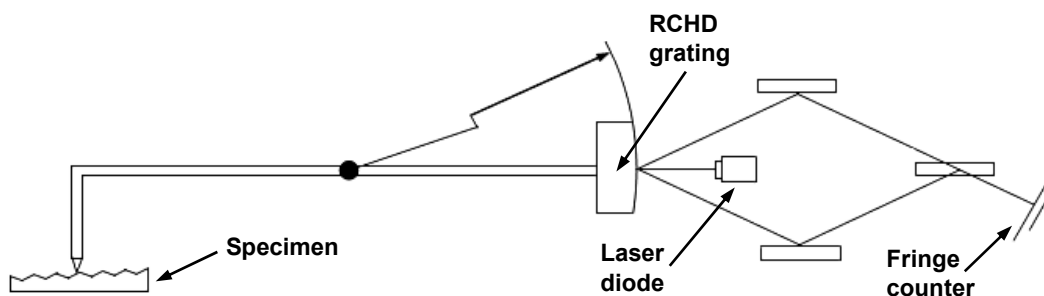


Figure 3.1: The plot showing range and resolution for the available measurement techniques

### 3.3.1 Contacting stylus measurement—Talysurf PGI Series 2

The stylus method refers to those instruments that use a mechanical probe via a transducer, such as an inductive transformer or an optical interferometer, to measure the vertical displacement of the stylus as it moves across the surface. This information is converted into an electric signal and then amplified before being transformed into a digital signal through analogue-to-digital converter. The digital signal is subsequently fed into a computer where different forms of numerical analysis will take place. Traditionally, the inductive transformer has been preferred as it possesses a very simple structure and a good stability, but it cannot attain a high precision over a large measuring range. Although the optical interferometer method can solve this problem, some other issues, such as complicated sensor structure and very expensive stable laser system, become noticeable. A far superior method has been recently developed based on the Doppler principle of the laser, which utilises a reflective cylindrical holographic diffraction (RCHD) grating, figure 3.2. The vertical displacement of the stylus is measured precisely by detecting the beat frequency fringe signal of the phase changes of the RCHD grating. The grating constant of a RCHD acts as the standard reference, and the width of the fringe pattern produced by the grating interference equals half of the grating constant. The fringe signal is fed into specially designed hardware for fringe counting. Similarly, an analogue-to-digital converter is employed to ensure fine division of the signal with a nanometer precision. As the grating interferometer is illuminated by using a relatively cheap and lower power semiconductor laser, this method not only gives a high ratio of signal to noise, but also provides a compact configuration, a low cost, and great resistance to vibration.



**Figure 3.2: The schematic diagram showing the principle of RCHD grating transducer**

However, the nature of the stylus method has proved to be its major drawback in that the loaded diamond stylus may scratch or damage the surface, this is especially critical when softer material is measured. Additionally, a further problem associated with stylus instruments for measurement of orthopaedic joint prosthesis is that the physical size of the stylus prevents it from penetrating small sharp pits on the surface and convolution effects can occur where sharp steps on a specimen surface tend to be smoothed. In such a situation, the stylus functions as a low pass filter because very high frequency features will not be recorded whilst low frequency features are. Furthermore, wear of the stylus due to mishandling or long time utilisation could also influence the result, and therefore it is recommended to regularly check the stylus for wear or damage.

The Talysurf PGI (Phase Grating Interferometer) Series 2 (Taylor Hobson Ltd., Leicester, UK) has been utilised in the present research, which is based on the RCHD grating method, figure 3.3. It is designed to mainly meet the varied and changing requirement of industry. A choice of transverse

units, software and other accessories allow high precision surface finish and form measurement to be made on small or large components. The excellent resolution throughout its gauge range makes it almost the most powerful gauging system currently available on any form and surface texture stylus instrument. Its typical specifications are summarised in table 3.1.

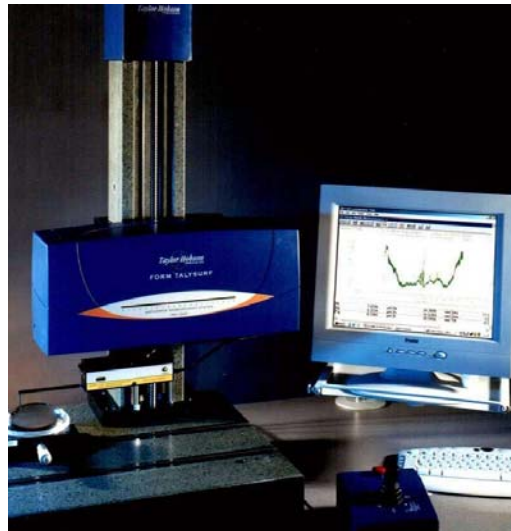


**Figure 3.3: The contacting stylus measurement instrument—Talysurf PGI**

**Table 3.1: The typical specifications of Talysurf PGI Series 2**

Talysurf PGI Series 2	Specifications
Vertical resolution	12.8nm
Lateral resolution	0.25 $\mu$ m
Vertical range	10mm
Lateral range	120mm
Traverse speed	0.5mm/s or 1.0mm/s
Stylus force	1mN

### 3.3.2 Non-contacting optical measurement—Talysurf CCI 3000

Optical measurement typically includes focus detection instruments and optical interferometers, with the latter being able to measure a surface in the nanometer scale. These systems work on the principle of interference of two beams of light where one is reflected from the surface of the specimen, and the other from a reference mirror. Deviations in the fringe pattern relate with deviations in height on the specimen surface. There are two types of interferometry which are incorporated in many commercially available optical interferometers, phase shift interferometry (PSI) and vertical scanning interferometry (VSI). In the case of measuring relatively smooth surfaces, PSI mode is commonly utilised, associated with a high degree of resolution and also the speed at which measurements can be taken. The limitation of this method is that the vertical range is generally restricted to around 650nm. In the case of measuring rougher surfaces, VSI mode is more preferred. Although the resolution is not as high as that of the PSI system, the vertical range extends to 600 $\mu$ m or more, therefore allowing for surfaces with greater roughness to be measured.

The primary drawback of interferometric measurement is that it is limited to those surfaces with a reasonable reflectivity. The maximum range is usually limited to a few hundred microns, and rapid slope changes on the surface are sometimes very difficult to measure. Additionally, a high degree of vibration isolation is typically required during operation as the optical interference technique is much susceptible to environmental noise and vibration.

Talysurf CCI (Coherence Correlation Interferometer) 3000 (Taylor Hobson Ltd., Leicester, UK) has been used in the present research. The general configuration is shown in figure 3.4. It is one of the most advanced interferometers for areal measurement. It uses a patented correlation algorithm to find the coherence peak and phase position of an interference pattern produced by a light source with selectable bandwidth. Basically, the upper beam splitter directs the light from the light source towards the objective lens, and the lower beam splitter splits the light into two separate beams. Each beam travels following its own optical path, one onto a reference surface on the underside of the objective lens, and the other onto the sample surface. The two beams then recombine resulting in an interference pattern being formed, which is collected by the area CCD system, figure 3.5. As a broad band light source is used, interference is only observed when the two optical paths are of closely matched length. By moving the objective lens unit vertically, the point at which maximum interference occurs can be detected for each pixel of the CCD system, based on the coherence correlation algorithm. During this process, the position of the objective lens can be tracked and a 3D topography of the surface is obtained.

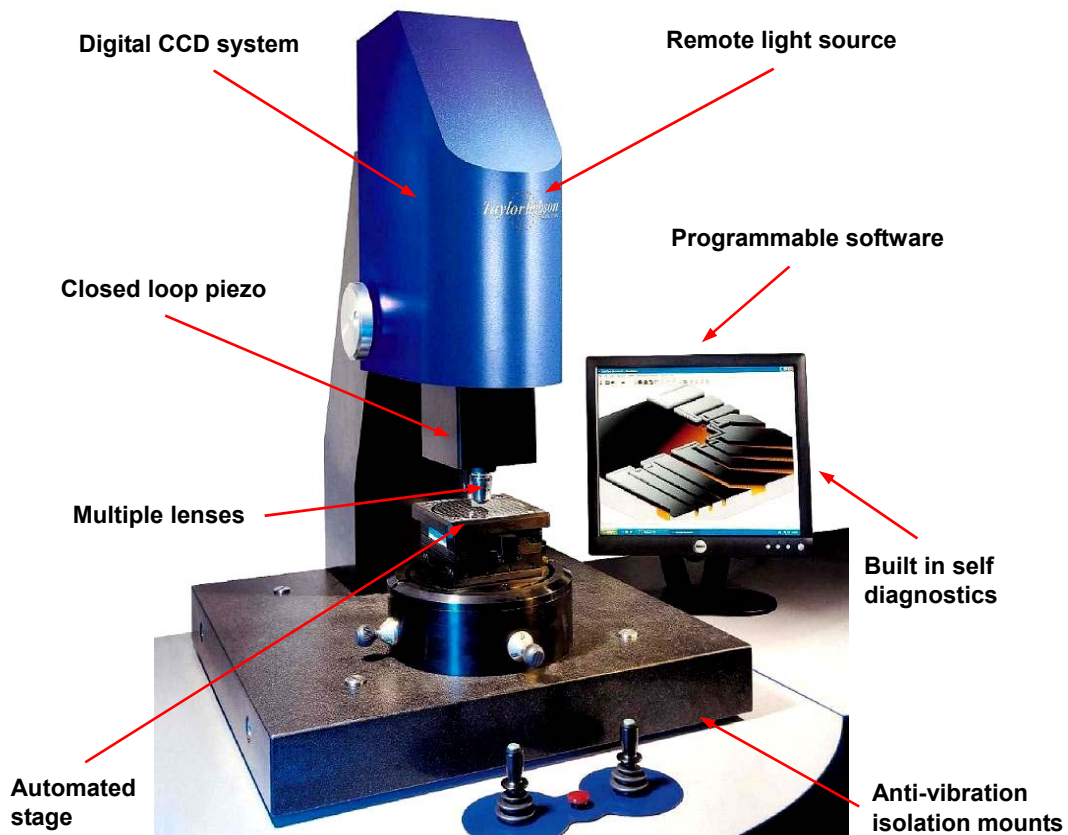
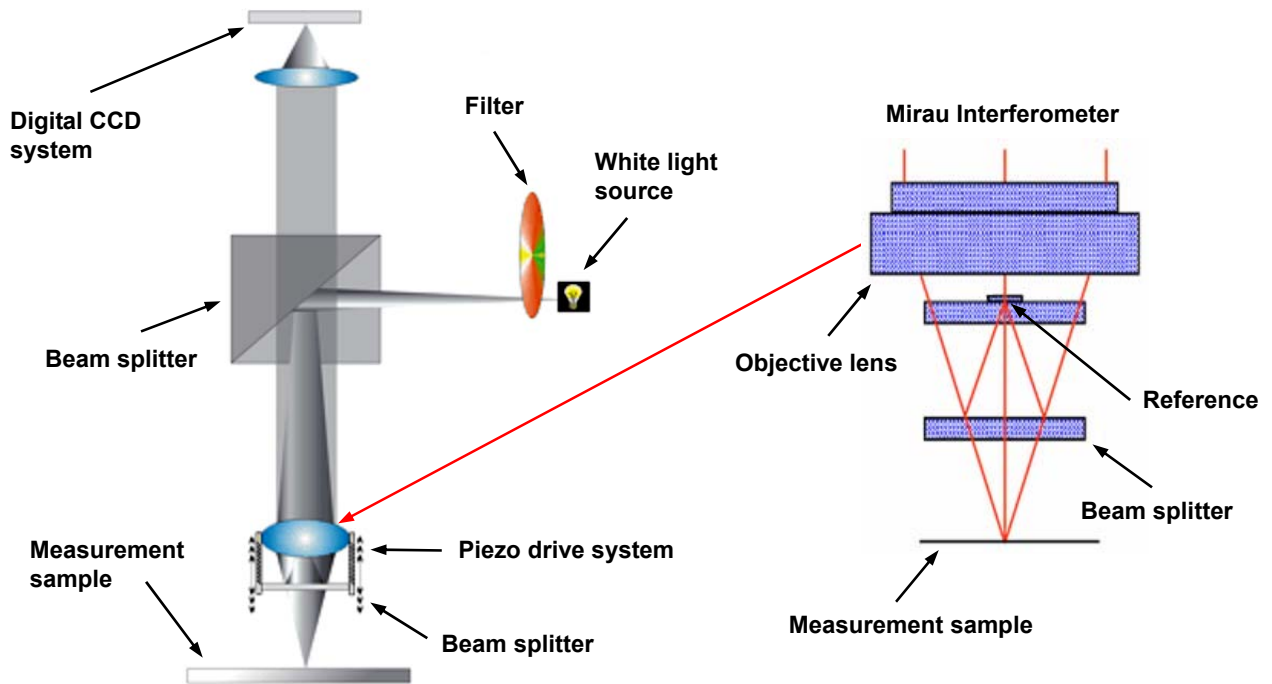


Figure 3.4: The non-contacting optical measurement instrument—Talysurf CCI 3000



**Figure 3.5: The basic principle showing how Talysurf CCI 3000 works**

Talysurf CCI 3000 brings an unparalleled level of performance to the non-contact 3D optical measurement with high resolution and excellent sensitivity to the reflective light. Almost all material types including glass, metal, and polymer with a reflectivity between 0.3% and 100% can be measured. Additionally, it provides three configurations of an anti-vibration system and various automated stages, and the measurement result can be obtained in seconds. Its typical specifications are summarised in table 3.2.

**Table 3.2: The typical specifications of Talysurf CCI 3000**

Talysurf CCI 3000	Specifications
Vertical resolution	0.01nm
Maximum lateral resolution	0.36 $\mu$ m
Vertical range	100 $\mu$ m
Maximum measurement area	7.2x7.2mm <sup>2</sup>
Data points	1024x1024 pixel array
Root mean square repeatability	3pm
Typical measurement time	10–20 seconds

### 3.3.3 Scanning electron microscope—JEOL JSM-6060

Scanning microscopy generally includes SEM, scanning probe microscope (SPM), and scanning tunnelling microscope (STM). As SEM is the one that is frequently employed in this research, an introduction to SEM is herein provided. It is much like an optical microscope in that one of its main purposes is to “see” the detail in samples. However, since it uses electrons as the source of illumination rather than light, far superior resolutions are obtainable.

Due to its unparalleled resolution, SEM is a premiere instrument to study the surface, near surface, and the microstructure of bulk specimens. Since it was invented in the early 1950s, SEM has developed extensive areas of application in both the medical sciences and the physical sciences. It utilises a fine beam of electrons passing through a vacuum to scan the surface of a sample and to build a topographical image, figure 3.6. Basically, the electron beam produced by an electron gun is accelerated to an energy of between 1keV and 30keV. It is then demagnified by a combination of condenser lenses and apertures until, as it hits the sample, it may have a diameter of around 2–10nm. When the energetically-focused electron beam bombard the sample, the interaction between them generates a variety of signals, including secondary electrons, backscattered electrons, X-rays, and transmitted electrons that are given off from each point of the surface, figure 3.7. The position of the electron beam is controlled by scan coils which allow the beam to be rastered over the surface of the sample. This enables information about a defined area on the sample to be collected, whilst certain detectors will view the electron signals. At the same time, the spot of a cathode ray tube (CRT) is scanned across the screen in a rectangular set of straight lines known as a raster, and the brightness of the spot is modulated by the amplified current which is translated through a photomultiplier tube. Gradually the image of the sample is created on the CRT screen.

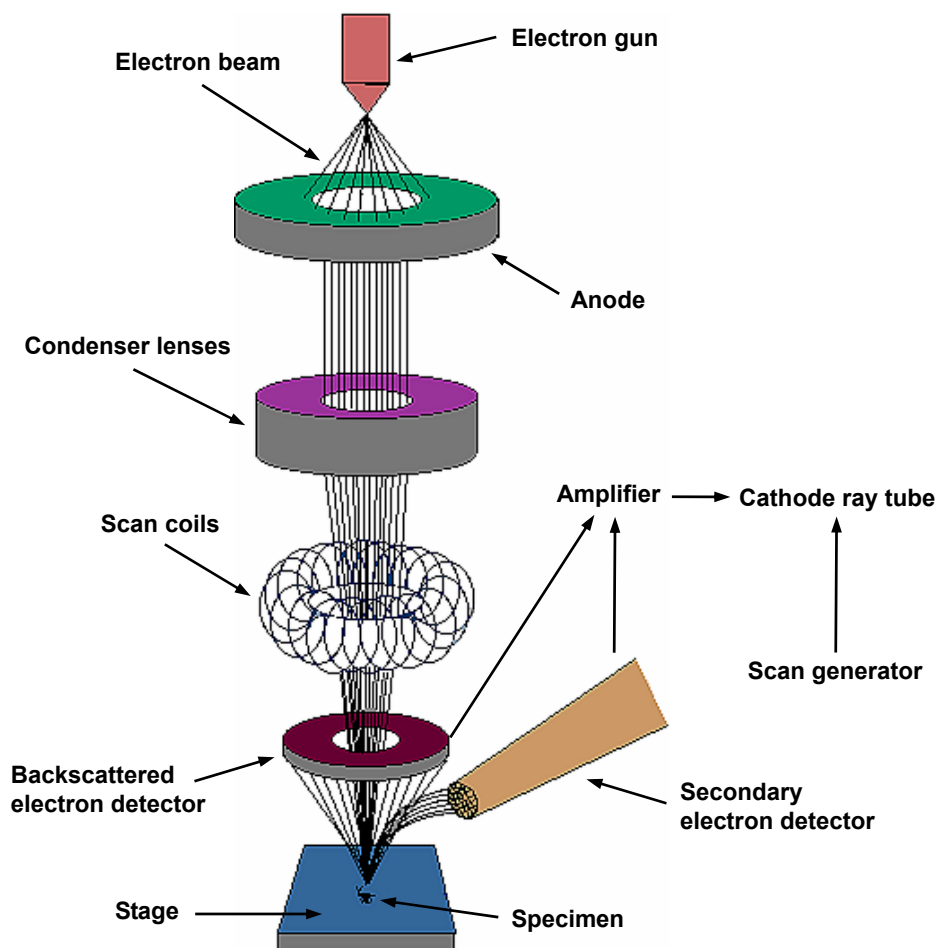
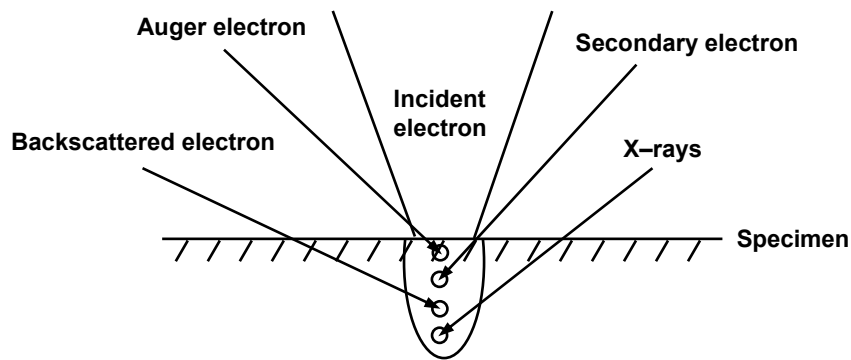


Figure 3.6: The schematic diagram showing the main components of a scanning electron microscope



**Figure 3.7: Various signals generated by the interaction between the electron beam and the specimen**

Secondary electron image (SEI) and backscattered electron image (BEI) are two primary imaging methods that depend on collection of secondary electrons or backscattered electrons. Secondary electrons are excited secondarily by incident electrons on the specimen, with a much lower kinetic energy. Since the generation region is as shallow as approximately 10nm, the diffusion of incident electrons within the specimen has little influence on the resultant image, therefore allowing high magnifications as well as high resolutions to be obtained. In addition, after incident electrons are scattered within the specimen, some of them will be backscattered whilst keeping a relatively high energy and are emitted again from the specimen surface, these are called backscattered electrons. BEI is extremely useful for locating areas of interest with concentrations of heavy elements that are not necessarily visible to the naked eye or to SEI. A gold-coating or carbon-coating technique is usually applied to those materials that are not electrically conductive for effective viewing of the surface morphology.

SEM not only allows outstanding micrographs to be generated, it also provides the X-ray analyser which could match an element to its signature peak. The high-energy electrons can penetrate into the sample and interact with the atoms of the material, producing characteristic X-rays which are fingerprints of the individual atoms encountered. These X-rays can penetrate through the material, allowing them to escape and to be viewed by the detector. Quantitative elemental analysis of the sample can be obtained with the aid of a powerful computer and software capabilities.

JEOL JSM-6060 (Oxford Instruments, Abingdon, UK) has been employed in this present research, figure 3.8. It is a conventional SEM with high performance and a low cost. The intuitive computer interface and standard automated features, such as auto-focus, auto-gun alignment, and automatic contrast and brightness, allow the instrument to be very easily operated. In addition, the specimen chamber can accommodate a sample of up to 32mm in diameter. Its typical specifications are summarised in table 3.3.



**Figure 3.8: The scanning electron microscope—JEOL JSM–6060**

**Table 3.3: The typical specifications of JEOL JSM–6060**

JEOL JSM–6060	Specifications
Resolution	3.5nm guaranteed
Magnification	8x to 300,000x
Probe current	1pA to 0.3 $\mu$ A
Accelerating voltage	0.5 to 30kV
Stage movement	10x20mm

### 3.4 Characterisation technology

#### 3.4.1 The limitations of 2D surface characterisation

Following measurement of a surface through the utilisation of the instruments, it is necessary to quantitatively characterise the surface for further comparison. In this regard, the international standards again fail to be efficiently updated because the current standards for measurement of orthopaedic joint prosthesis assume that traditional 2D profile techniques are used (BS 7251–4 1997). Accordingly, the surface roughness obtained in terms of these standards only addresses a part of the 3D surface topographical information of the bearing surface, whilst the other functional features such as peaks, pits, and scratches, could not be clearly identified and separated. The measurement and analysis of the 2D profile or section, even if properly controlled, could only give an incomplete description of the real surface topography. For example, the 2D surface parameter for specifying surface finish is Ra, which simply represents the average surface roughness in its most primitive form. It is possible that surfaces with different features and consequently different functional properties may have the same Ra value, figure 3.9 (Mummery 1990). On the other hand, with only 2D profile of the surface available, it is often difficult to recognise the exact nature of a topographic feature. For instance, figure 3.10 displays a 2D trace taken from an areal surface measurement. Just from the 2D profile it is impossible to determine whether the surface features are pits or scratches.

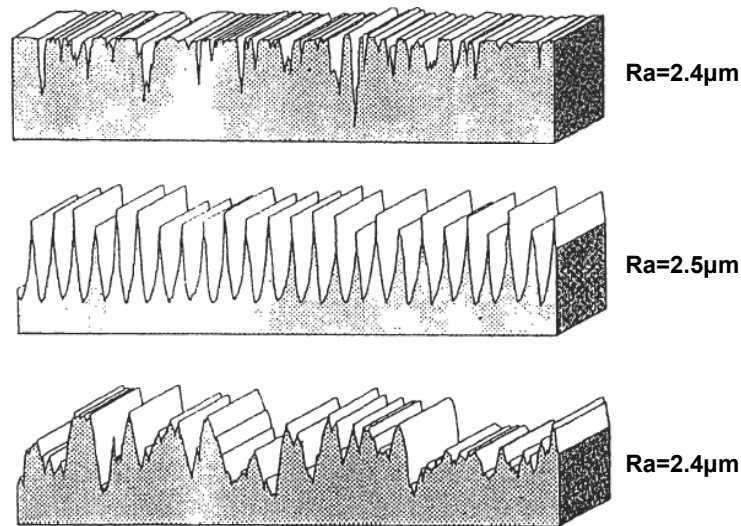


Figure 3.9: Three surfaces with evidently different height distributions but the same Ra

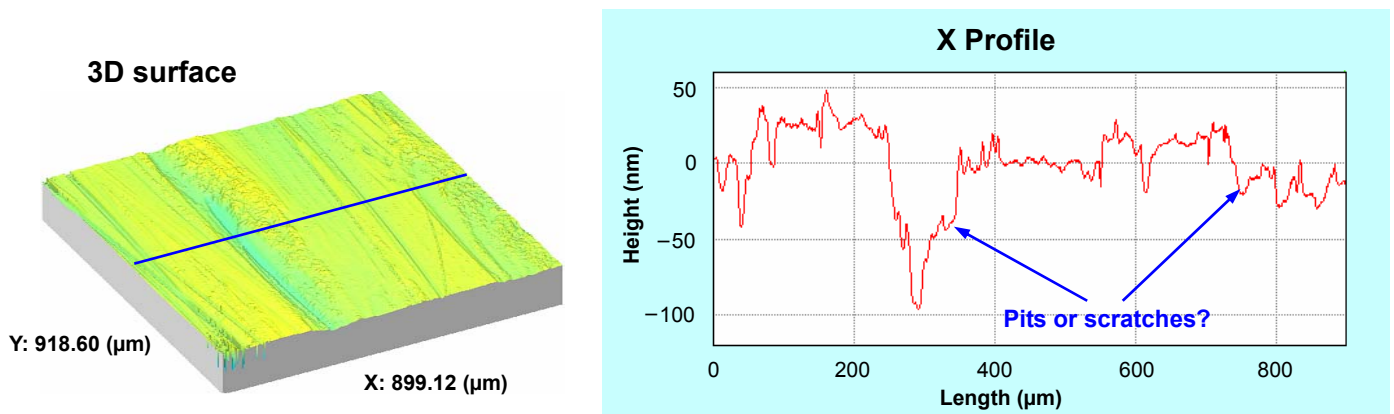
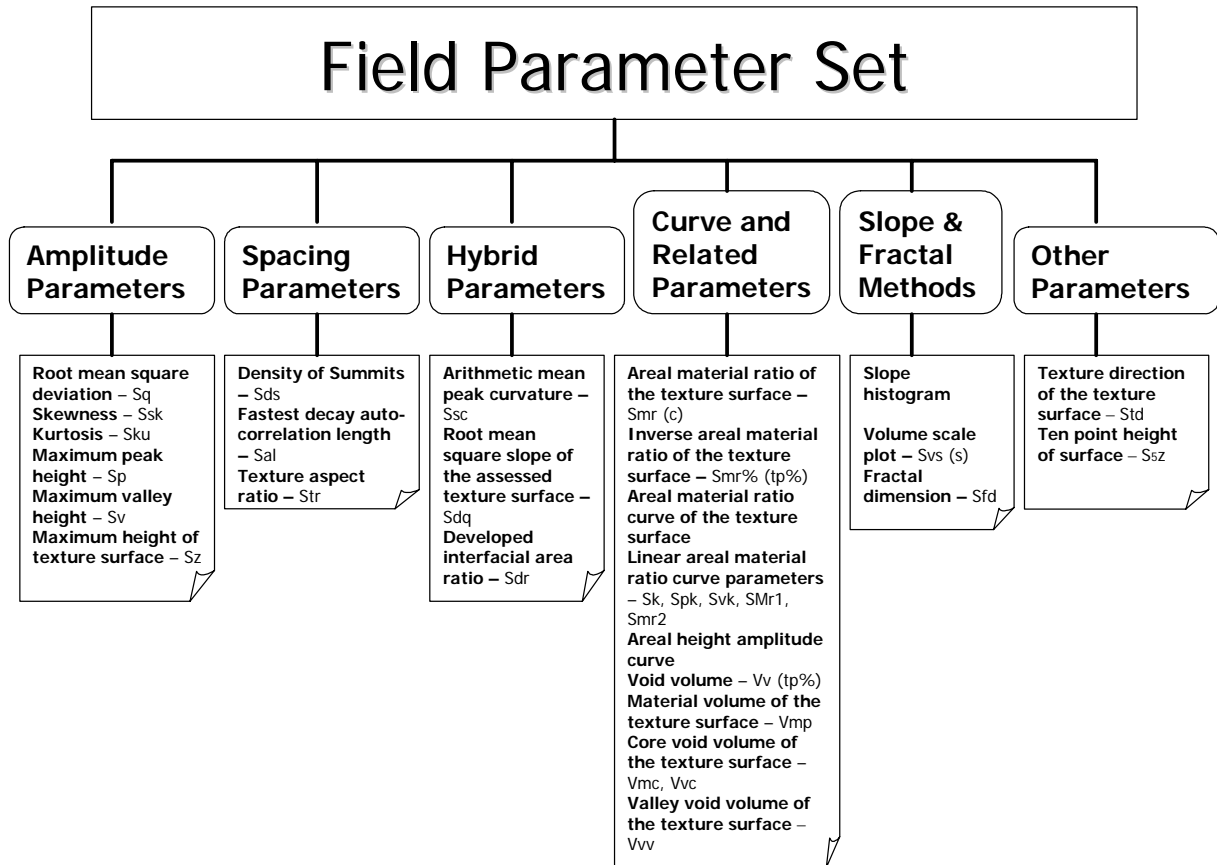


Figure 3.10: A 2D trace taken from an areal surface measurement shows the ambiguity of 2D surface characterisation

Following the development of Ra, there has been a proliferation of 2D parameters with overlap in definition. It is indicated that more than 150 parameters have been introduced. This is termed as “Parameter Rash” and it caused much confusion and expense (Whitehouse 1982). Therefore, it is necessary to end expansion of 2D surface parameters, and to develop 3D surface characterisation to gain a better insight into the functional properties of a surface.

### 3.4.2 3D surface characterisation

The emergence of the 3D surface characterisation is largely due to the limitations of 2D surface analysis, and also as a result of the development of modern powerful computers. Comprehensive research has been initiated with the aim of developing a new fundamental, international standard for 3D surface measurement. A European Union (EU) funded project named “Surfstand” based at the University of Huddersfield sought to develop a suite of parameters that could more effectively characterise a surface. Through standardising filtering and characterisation techniques, a 3D field parameter set was devised, covering the majority of functional aspects of a surface and allowing a holistic picture of the surface to be numerically determined for comparison, figure 3.11. A detailed description of the parameters will be given for those that are utilised in further research.



**Figure 3.11: The 3D field parameter set to describe functional performance of a surface**

With the application of 3D surface measurement as an invaluable tool in advanced manufacturing engineering, tribology and material science, etc, the development of 3D characterisation just acts as a favourable momentum. The introduction of 3D surface measurement into the field of the joint replacement systems has meant that it has undergone further expansion. The key to the expansion is that the measurements can be carried out using non-contacting instruments with adequate range and resolution. These instruments can reduce the levels of surface contamination, eliminate the possibility of surface contact damage, and allow relatively soft materials to be measured with a high accuracy. This leads to a better understanding of the functional performance of surfaces.

## Chapter 4 The stem–cement interfacial strength

### 4.1 Chapter summary

As the term “fretting” describes a small oscillatory movement between two contacting surfaces, the generation of fretting wear on the stem theoretically requires debonding at the stem–cement interface, enabling a relative micromotion to occur at this interface. Additionally, transportation of the wear debris, associated with synovial fluid that is pumped into the stem–cement interface, also needs loss of integrity of this interface. It has been suggested that bone cement may shrink away from the prosthetic stem following polymerisation *in vivo*. This may create a gap around the hip prosthesis at the stem–cement interface. However, some other studies indicated that an excellent bonding between the stem and the cement could be obtained, especially using “modern cementing techniques”, but it is not very clear whether this interface could remain stable under physiological loading during the *in vivo* service. In order to ascertain whether debonding would occur at the stem–cement interface, an interfacial gap test associated with a series of pull out tests were carried out to investigate the shear strength at the stem–cement interface.

The first test investigated the so called stem–cement interfacial gap in terms of fluid flow along this interface. It was demonstrated that the blue ink could not penetrate through the stem–cement interface for a period of up to two months for all the specimens studied, which confirmed the presence of a good mechanical bonding at the interface. The second test compared the static shear strength between polished femoral stem and commercial available bone cements. The influence of bone cement brand, cement viscosity, and cement mantle thickness on the results was investigated employing a three-way analysis of variance (ANOVA), and the effect of tobramycin additive to Simplex P bone cement on the interfacial strength was studied using an unpaired student t-test. In addition, bone cement transfer films were found on the stem surface following the test, which are considered to contribute significantly to the interaction between polished stem and bone cement. The third test investigated the influence of stem surface finish on the interfacial static shear strength, where a general increase of the strength with the rise of surface roughness was identified. 3D surface parameters were employed to quantitatively assess the stem and cement surfaces. Two different failure modes were typically observed for the femoral stems with four kinds of surface finish, indicating two different interactions at the stem–cement interface. Following the test, the femoral stems and the bone cements interfaced with them showed different surface morphologies, and this was considered to correlate with the pull out process. Finally, the pull out forces and the typical physiological loadings at the hip joint were found to be comparable, thus it was concluded that debonding at the stem–cement interface was inevitable.

### 4.2 The stem–cement interfacial gap

#### 4.2.1 Background and aims

The mechanical properties of the stem–cement interface are considered essential in understanding the mechanism leading to failure of total hip joint system and it is nowadays still far from being well documented. It has been demonstrated from retrieval studies that failed prostheses are always associated with debonding at the stem–cement interface, which is identified as a radiolucent line around the hip prosthesis on the radiograph. In spite of unanimous support for this concept, one

important issue has not been fully addressed, i.e. whether debonding at the stem–cement interface is produced under cyclical physiological loading during the *in vivo* service of the hip prosthesis or by other reasons. It was indicated in literature (Müller and Schürmann 1999) that a gap at this interface would form due to shrinkage of the bone cement following polymerisation just shortly after implantation of the stem. Additionally, the formation and distribution of this interfacial gap may be influenced by stem surface finish (Race *et al.* 2002). This gap to a certain degree could jeopardise integrity of the stem–cement interface and contribute to the final debonding at this interface. However, no sufficient evidence is available to prove this and few studies have been performed to provide similar results. This present study therefore aims to test the integrity of the stem–cement interface by investigating the fluid flow along this interface.

#### 4.2.2 Materials and methods

Four stainless steel rods with polished, glass bead-blasted, shot-blasted, and grit-blasted surface finishes were manufactured. The polishing and blasting media will be discussed in detail later in section 4.3.2 and 4.4.2 respectively. Additionally, four steel blocks with a through hole in the middle and four steel caps to ensure centralisation of the rods in the steel blocks were fabricated. The procedure to prepare the experimental specimens was explained below: (1) An adhesive was obtained by thoroughly mixing Araldite resin and Araldite hardener into a compound. (2) The four steel blocks were stabilised by this adhesive upon curing on a clean glass plate. (3) Simplex P bone cement was mixed by hand and injected into the steel blocks to a predetermined height. (4) The cylindrical rods with the custom-made steel caps around were implanted to the steel blocks and the bone cement cured *in situ*. (5) The caps were gently removed from the rods and a cement cavity was produced. (6) Blue ink was injected into the cavity and the specimens were fixated on the glass plate again by the adhesive. A schematic diagram is given to clearly describe these steps, figure 4.1, and the experimental specimen is shown in figure 4.2.

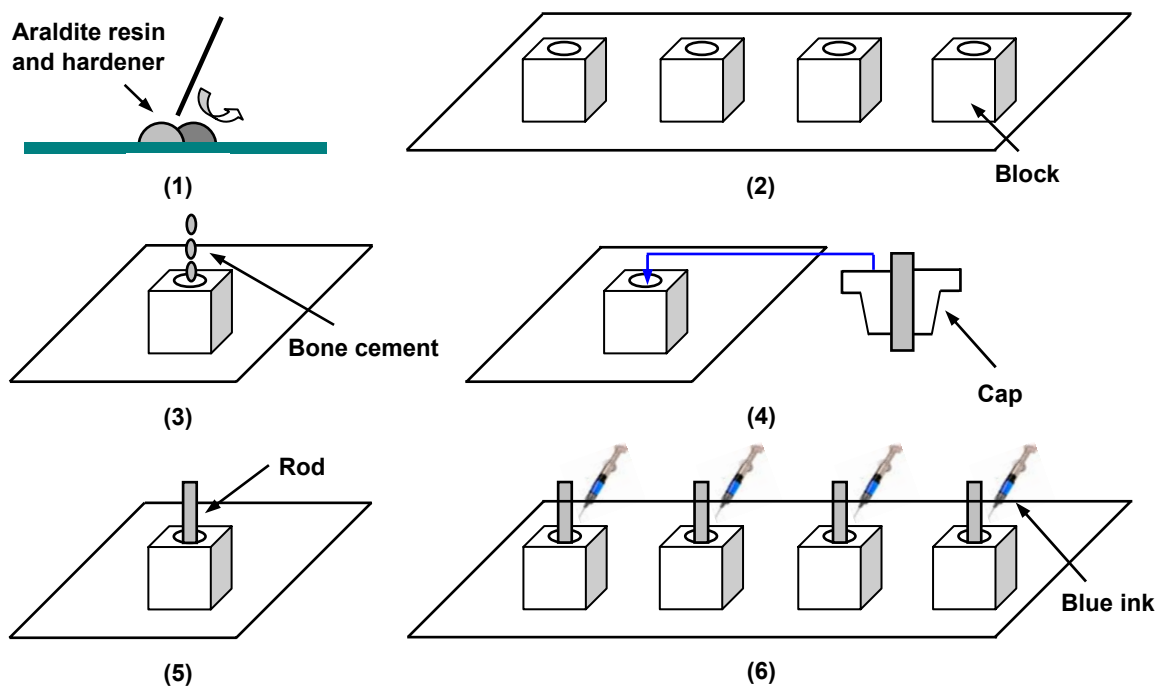
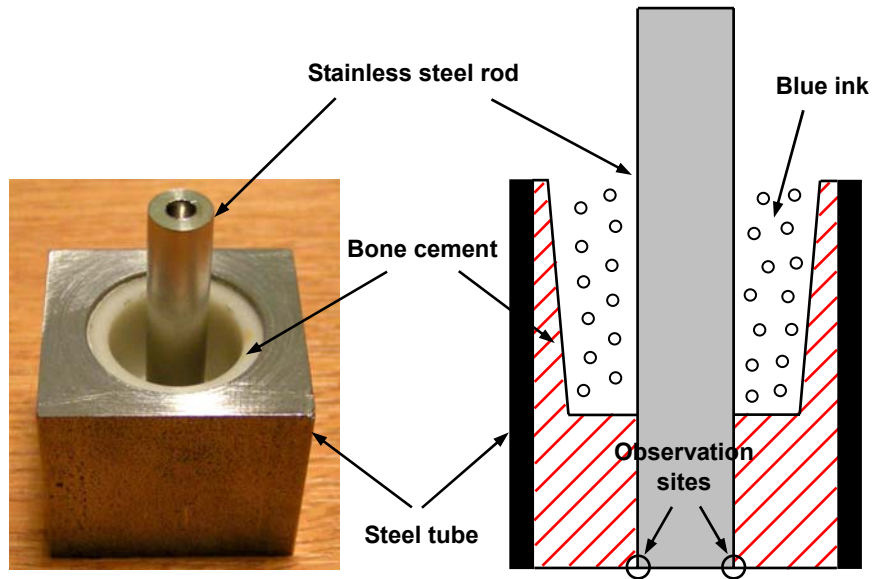


Figure 4.1: The schematic diagram to describe the steps to prepare the experimental specimen



**Figure 4.2: The experimental specimen to test fluid flow along the stem–cement interface**

The penetration of the blue ink through the rod–cement interface to the bottom of the stainless steel rod was recorded up to a period of two months.

#### 4.2.3 Results and discussion

It was demonstrated that after two months there was no evidence of penetration of the blue ink to the bottom of the stainless steel rod through the rod–cement interface. This result was consistent for all the specimens with different surface finishes, it therefore indicated that a good mechanical bonding was present at the interface. Subsequently, the stainless steel rods were all debonded from the cement mantle through application of a vertical loading on the top, and then the blue ink was injected to the cement cavity to test penetration. After 48 hours the blue ink was observed at the bottom of all the stainless steel rods. Figure 4.3 shows the result for the shot-blasted rod.

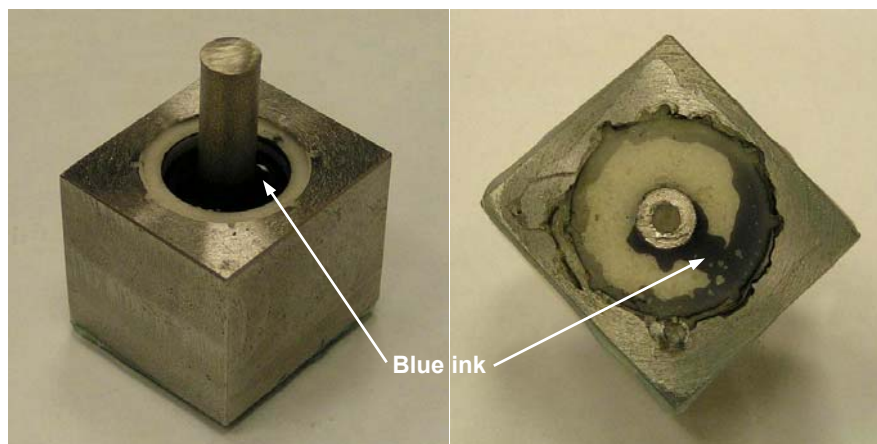


**Figure 4.3: Observation of the blue ink at the bottom of the shot-blasted stainless steel rod**

A similar study was previously carried out by Crawford *et al.* (1999), and in the study they found that methylene blue penetrated through the stem–cement interface for the matt specimens, whilst for the polished specimens, the interface only showed a tide mark at the border of the bone cement where it was in contact with the fluid. This result to a certain degree conflicted with the present

study with regard to the non-debonded matt specimens, and it was attributed to a gap that was produced at the stem–cement interface due to poor interdigitation of the cement into the asperities of the matt specimens or caused by shrinkage of the cement following polymerisation. The curing process of bone cement is a complex solidification phenomenon, and *in vivo* polymerisation starts at the warmer cement–bone interface and therefore induces a gap at the stem–cement interface by shrinking the cement away from the stem. The occurrence of this interfacial gap was further confirmed by Wang *et al.* (1999) who performed a study to section the stem–cement interface and evaluated the gap through a computerised video digital system. This gap was considered to be significant as it may contribute to debonding of the femoral stem from the cement mantle, and it has been suggested to explain the poor results of a certain bone cement (Race *et al.* 2005).

However, it was not clear whether or not such a gap was formed at the rod–cement interface in the present study as shrinkage of the cement away from the stem requires temperature gradient at the interface and in this study, there should be no significant difference in the contact between the rod and the cement and between the cement and the steel block. Additionally, the specimens were not sectioned as suggested by other researchers because it was considered that the common method to achieve this by utilising a circular high-speed saw would potentially compromise the result by loosening the stem–cement interface.

#### **4.2.4 Conclusions**

It was shown from this present study that the blue ink did not penetrate through the stem–cement interface after two months for all the stainless steel rods investigated. This indicated that a good mechanical bonding was available at this interface and loss of integrity was potentially initiated by physiological loadings during the *in vivo* service of the hip prosthesis.

### **4.3 Interfacial strength between polished stem and bone cements**

#### **4.3.1 Background and aims**

It has been mentioned above that there are numerous brands of acrylic bone cement on the market, most of them are similar in composition but have inherently different characteristics during and following polymerisation, such as viscosity, creep, and mechanical properties. Many studies have concentrated on how to enhance the bond strength at the stem–cement–bone interfaces, in which some influencing factors are investigated, e.g. employing a matt surface finish stem (Vail *et al.* 2003), pre-coating the stem with a fine layer of bone cement (Davies *et al.* 1992), and utilising “modern cementing techniques” to reduce porosity in the cement mantle (Jasty *et al.* 1990). The most commonly used method to test bond strength is a pull/push out test, where a metallic rod is often employed to represent the femoral stem (Chen *et al.* 1998, Wang *et al.* 2003). Finite element analysis (FEA) has also been used to simulate the physical conditions at the stem–cement interface, from which it was demonstrated that debonding at this interface is primarily dominated by shear failure (Verdonschot and Huiskes 1997b). To date, however, very few comprehensive studies have been performed to establish comparative data across a range of commercially available bone cements. Therefore, such a study would be particularly useful if it determined the shear strength at the stem–cement interface, taking into consideration its contribution to debonding at this interface, and by extension to the survivorship of cemented THR. Additionally, in contrast to the general

acceptance that matt femoral stems can form a better interfacial strength with bone cement due to enhanced cement integration, a cascade of retrieval studies have shown a relative superiority in terms of survivorship for polished stems, e.g. the Exeter stem, where matt stems are proved to be less clinically successful (Rockborn and Olsson1993, Howie *et al.* 1998). It has been suggested that polished femoral stems with double taper design can achieve stabilisation through mechanical interlocking of the stem within the cement mantle, but the contact mechanism between polished femoral stem and bone cement has seldom been studied, especially in terms of shear strength. Therefore, this current study aims to comprehensively investigate the static shear strength at the polished femoral stem–bone cement interface, and to gain an insight into the interaction between these two materials through a pull out test.

### 4.3.2 Materials and methods

#### 4.3.2.1 Preparation of test specimen

In the present study, seven brands of commercially available bone cement were collected, and the details of these cements are displayed in table 4.1. Stainless steel (type: 316L; composition: C—0.02%, Cr—17.9%, Ni—12.9%, Mo—2.55%, Si—0.8%, Mn—0.1%, Fe—balance; Mechanical properties: hardness—HB140, Young’s modulus—197GPa, 0.2% yield strength—310MPa, ultimate tensile strength—635MPa) rod was utilised to simply represent the femoral stem.

**Table 4.1: Relative viscosity and composition of the seven commercial PMMA bone cements**

Bone cements	Viscosity	Powder (w/w)	Liquid (w/w)	Suppliers
Cemfix 3	Low	PMMA—87.6; BPO—2.4; BaSO <sub>4</sub> —10	MMA—84.4; DMPT—2.4; BMA—13.2; HQ—20ppm	Teknimed S.A., France
Coriplast 3	Low	PMMA—45; PMMA/MA—45; BaSO <sub>4</sub> —10	MMA—98; DMPT—2; HQ—45ppm	Corin Medical Ltd., UK
Simplex P	Medium	PMMA—15; PMMA/ST—75; BaSO <sub>4</sub> —10	MMA—97.4; DMPT—2.6; HQ—60ppm	Howmedica International Inc., Ireland
Simplex P–T	Medium	PMMA—15; PMMA/ST—75; BaSO <sub>4</sub> —7.5; T—2.5	MMA—97.4; DMPT—2.6; HQ—60ppm	Howmedica International Inc., Ireland
CMW 3	Medium	PMMA—88; BPO—2; BaSO <sub>4</sub> —10	MMA—97.5; DMPT—2.5; HQ—25ppm	DePuy International Ltd., UK
CMW 1	High	PMMA—88.85; BPO—2.05; BaSO <sub>4</sub> —9.1	MMA—99.18; DMPT—0.82; HQ—25ppm	DePuy International Ltd., UK
Palacos R	High	PMMA/MA—84.25 ; BPO—0.75; ZrO <sub>2</sub> —15; C—200ppm	MMA—97.87; DMPT—2.13; HQ—64ppm; C—267ppm	Biomet Merck Ltd., UK

Note: PMMA/MA—Polymethylmethacrylate/methylacrylate; PMMA/ST—Polymethylmethacrylate/styrene; BMA—Butylmethacrylate; T—Tobramycin; C—Chlorophyll.

For each bone cement brand, two kinds of stainless steel rods were manufactured, enabling two different cement mantle thicknesses to be tested, figure 4.4 (a). The stainless steel rods were sequentially polished with the use of 45µm, 15µm, 6µm and 1µm diamond pastes to achieve a surface roughness value of Sq about 10nm, measured by the optical interferometer Talysurf CCI 3000 at x50 magnification, this roughness being directly comparable to the commercial polished femoral stems. Additionally, a cylindrical holder made of mild steel was fabricated for the bone cements to be poured into, resulting in a nominal cement mantle thickness of 7mm and 9mm,

corresponding to the two kinds of stainless steel rods (diameters 12mm and 8mm respectively), figure 4.4 (b). Before cementing, the stainless steel rod was cleaned with alcohol and then fixated using a milling machine chuck, which could ensure accurate axial alignment of the rod within the cement mantle. All the bone cements were hand mixed at room temperature, according to the manufactures' instructions. A metallic ring was connected to the cylindrical holder by screws in order to apply pressure on the cement during the polymerisation process and to make sure that the interfacial failure will not occur between the bone cement and the cylindrical holder. Following polymerisation, the stainless steel rod was held into position vertically in a blind hole in the cement mantle, figure 4.5.

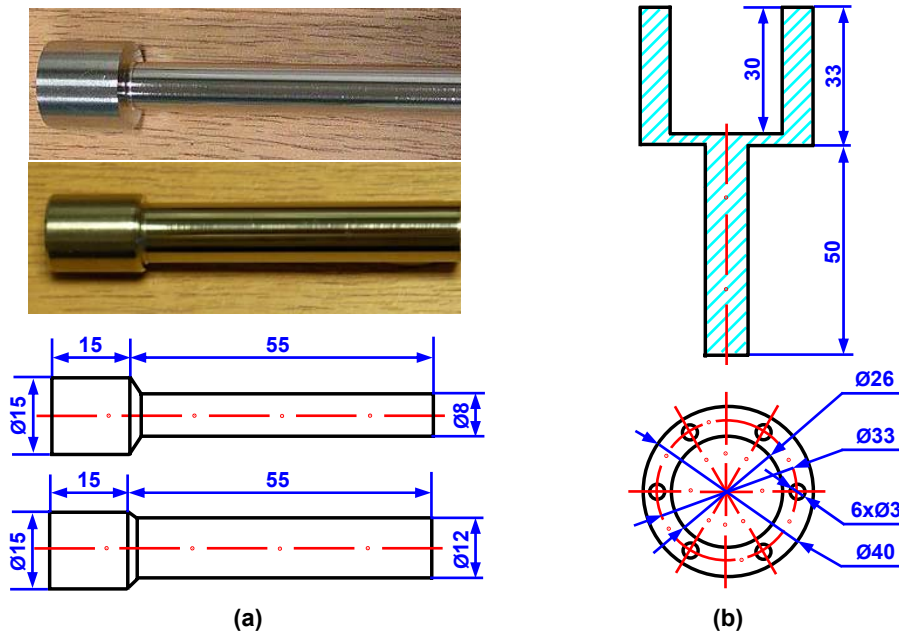
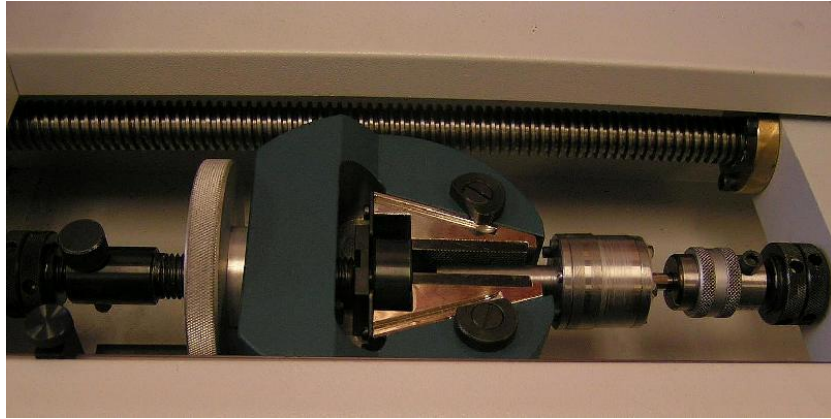


Figure 4.4: (a) Dimension of the stainless steel rods (b) Design of the steel holder



Figure 4.5: Preparation of specimen using a milling machine chuck to ensure axial positioning

The specimen was laid aside for 24 hours to fully cure before being tested employing a Hounsfield Test Machine H20K-W (Hounsfield Test Equipment Ltd., Surrey, UK), figure 4.6. A load-displacement plot for the pull out test was then recorded. All the tests were performed at a constant speed of 2mm/min by displacement control. Repeated tests were carried out five times for each cement brand and each cement mantle thickness to provide statistical viability.



**Figure 4.6: Set up of pull out test on a Hounsfield Test Machine H20K-W**

#### **4.3.2.2 Analysis of test specimen**

Following each pull out test, the stainless steel rod was re-polished to ensure identical surface roughness grade, and the cement was cautiously extracted from the mild steel holder and cut longitudinally into two equal parts. The inner surface of the cement was cleaned by alcohol and stained using red dye to facilitate observation of porosity with a Leica optical stereomicroscope (MZ6, Leica Microsystems Ltd., Wetzlar, Germany), figure 4.7. Totally 10 images were taken arbitrarily on the cement surface at x10 magnification, with each image area being  $4\text{mm}^2$ . All the images were processed using Matlab software 6.5 and the micropores were recognised based on grey scale threshold, figure 4.8. For each image, the porosity was determined by the ratio of the area of micropores to the area of whole cement surface. The number of micropores on the image was counted and the mean area of one micropore was determined. Subsequently, the micropore size was calculated as the diameter of one micropore, assuming it to be a perfect circle. Finally, the mean value of porosity and micropore size were obtained on the basis of the 10 images for each test.



**Figure 4.7: The Leica optical stereomicroscope**

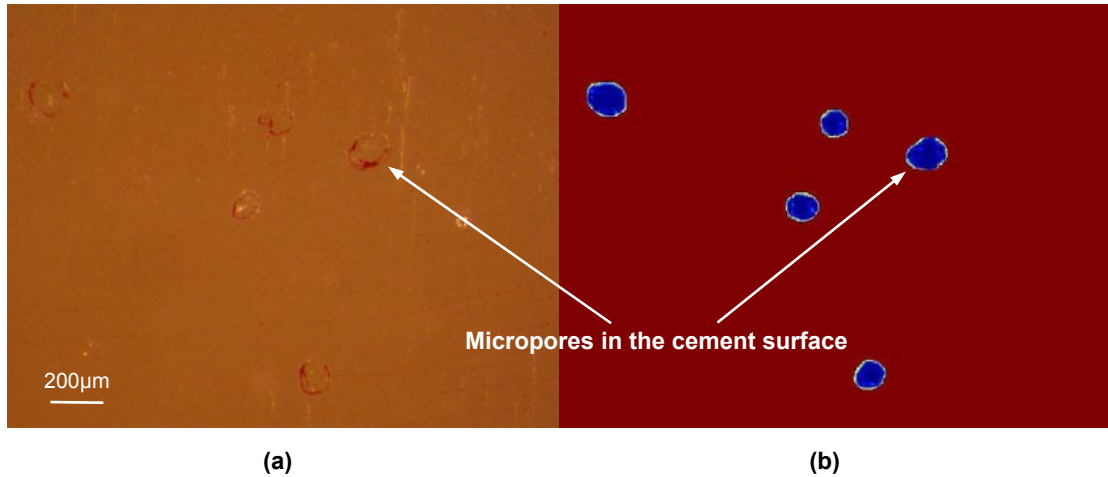


**Figure 4.8: Micropores detection based on grey scale threshold (a) Original image (b) Detected image**

#### 4.3.2.3 Calculation of static shear strength and statistical analysis

The static shear strength ( $\sigma$ ) was determined through the following equation, utilising the initial debonding force, i.e. the peak force during the pull out process, divided by the real surface contact area.

$$\sigma = \frac{F}{\pi DL(1-\eta)} \quad (4.1)$$

$F$  is the initial debonding force (N), which can be obtained from the load–displacement plot.  $D$  is the rod diameter (m), and  $L$  is the internal length of rod within the cement mantle (m), the exact values of these two parameters were measured utilising a vernier caliper.  $\eta$  is the porosity of the cement surface (%) as described above. The final static shear strength of each cement brand and each cement mantle thickness was calculated as the mean value of the five tests carried out.

As for Cemfix 3, Coriplast 3, Simplex P, CMW 3, CMW 1 and Palacos R bone cements, a three-way ANOVA was performed to investigate the factors, e.g. cement mantle thickness, cement viscosity and cement brand, which would potentially influence the static shear strength, interfacial porosity and micropore size. The model of the three-way ANOVA is shown in figure 4.9. With regard to Simplex P and Simplex P with Tobramycin (Simplex P–T) bone cements, an unpaired student t-test was carried out to establish the effect of the antibiotic additive on the results. The software used is SPSS 12.0 for windows.

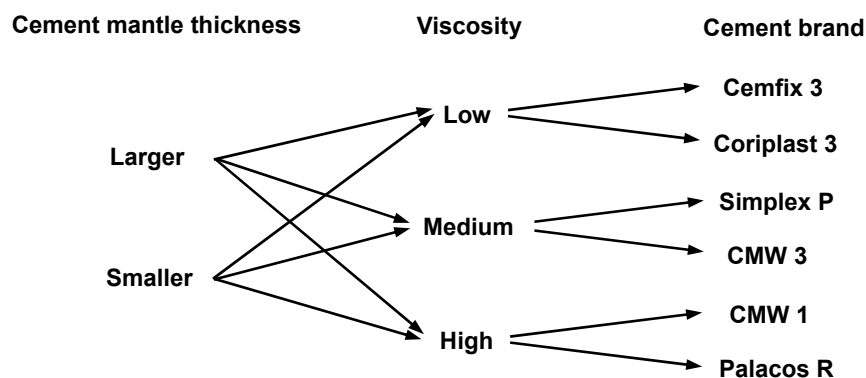


**Figure 4.9: The model of three-way analysis of variance**

### 4.3.3 Results

#### 4.3.3.1 Static shear strength, interfacial porosity, and micropore size

The static shear strength, interfacial porosity, and micropore size (mean value and range) for each cement brand and each cement mantle thickness are shown in figures 4.10–4.15. It is evident to see from these figures that there is no direct relationship between the static shear strength and cement viscosity. It is, however, more dependent on cement brand, i.e. cement composition. In addition, the interfacial porosity shows much lower values for the cements with low viscosity possibly because of greater facilitation for the air bubbles to escape from the bulk matrix, but there seems to be no significant difference in terms of interfacial porosity for the cements with medium and high viscosity. The micropores size also appears to be determined by cement brand.

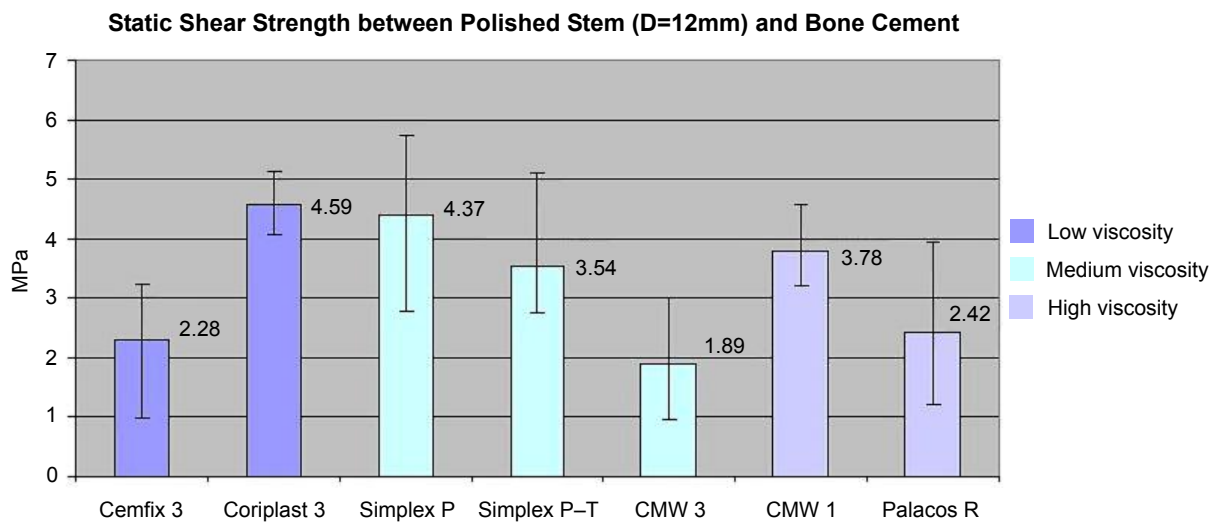


**Figure 4.10: Static shear strength for the 12mm diameter stainless steel rod**

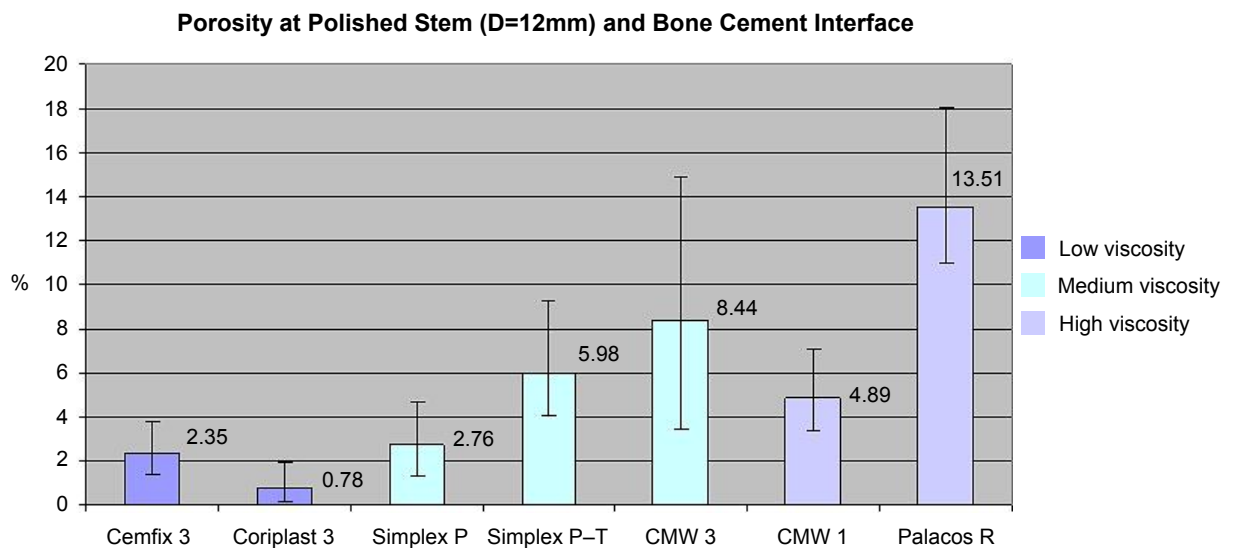


**Figure 4.11: Interfacial porosity for the 12mm diameter stainless steel rod**

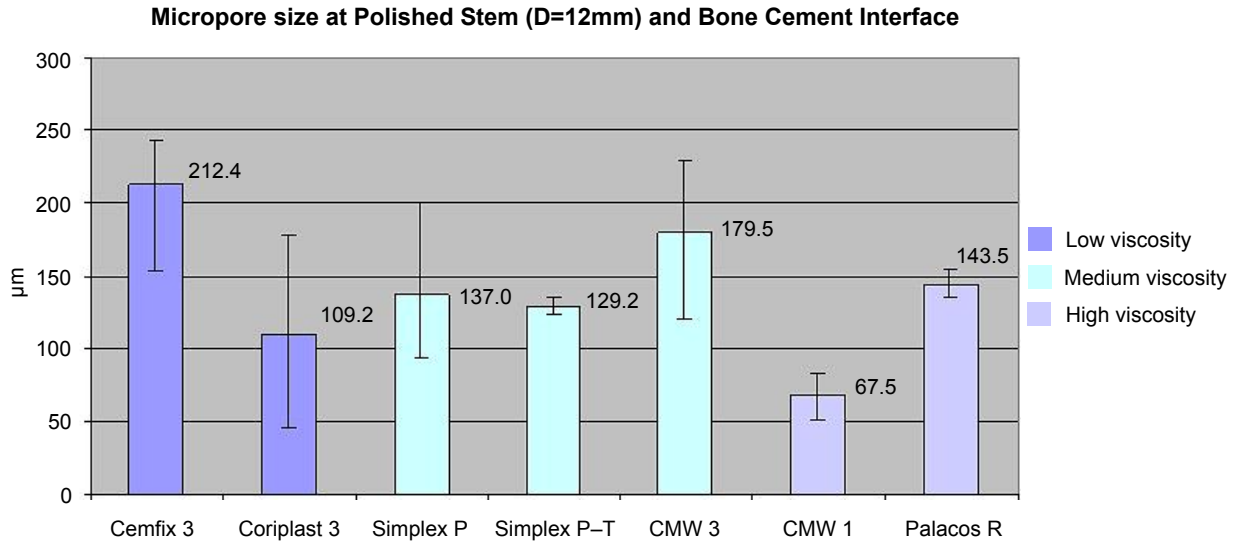


**Figure 4.12: Micropore size at the interface for the 12mm diameter stainless steel rod**

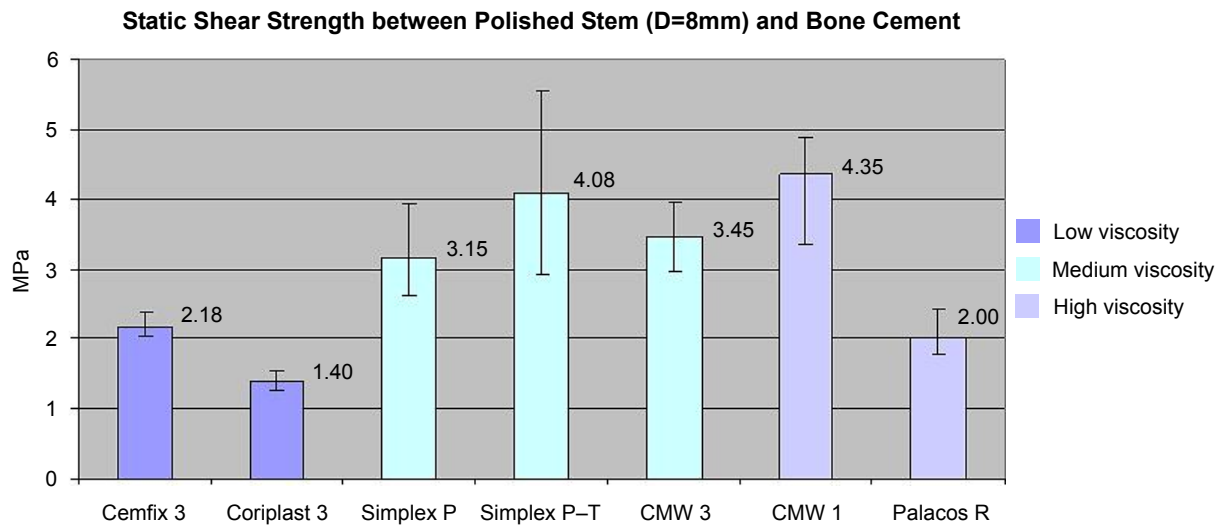


**Figure 4.13: Static shear strength for the 8mm diameter stainless steel rod**

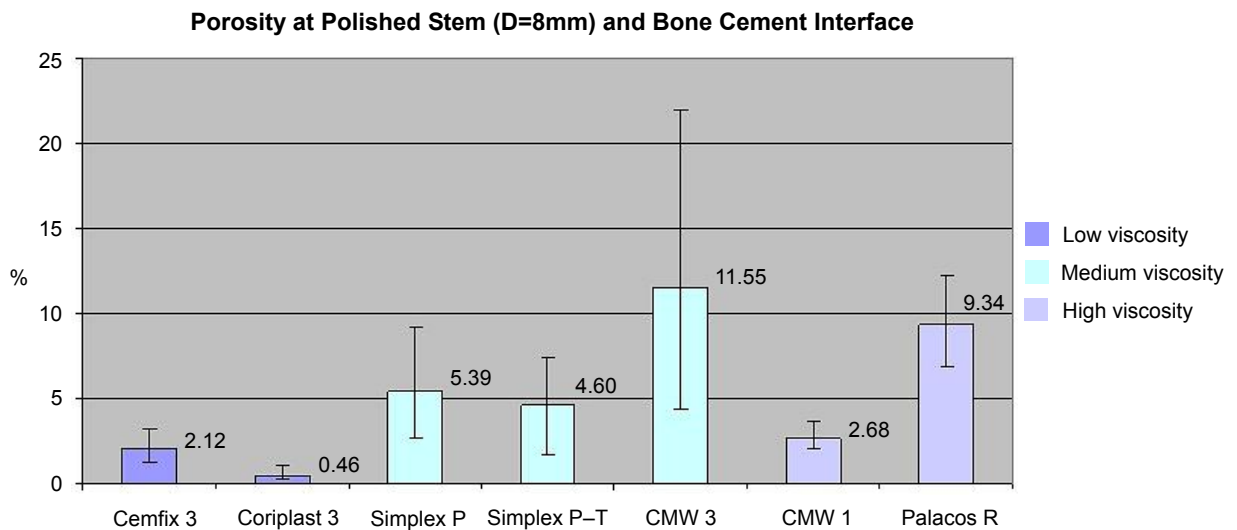


**Figure 4.14: Interfacial porosity for the 8mm diameter stainless steel rod**

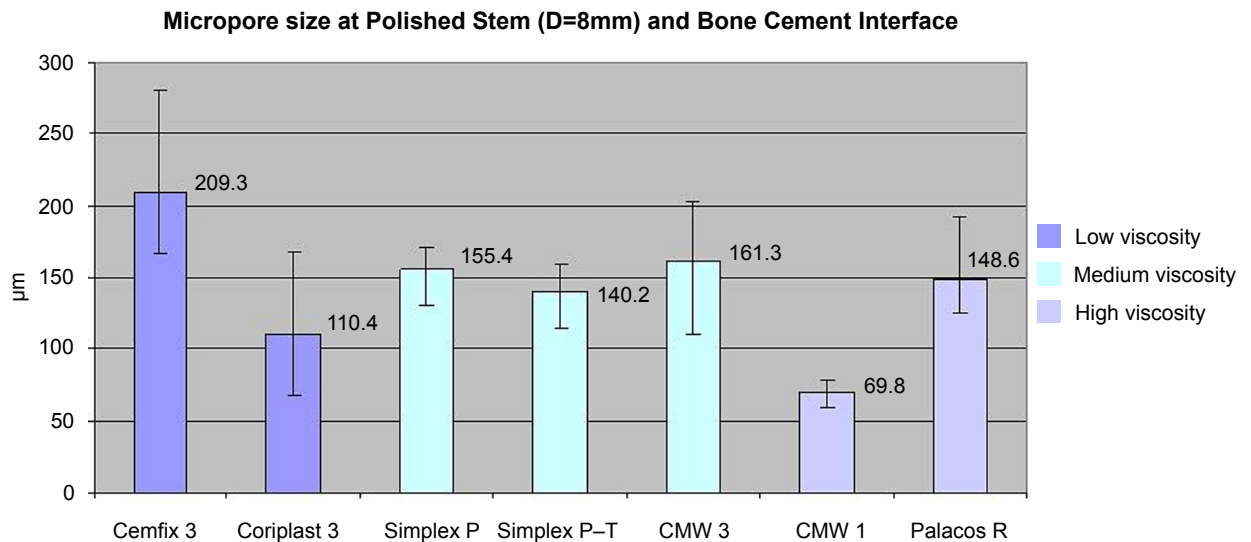


**Figure 4.15: Micropore size at the interface for the 8mm diameter stainless steel rod**

It was further demonstrated from the three-way ANOVA that the static shear strength was not significantly influenced by cement mantle thickness and cement viscosity ( $P>0.01$ ), whereas there was significant difference across various cement brands ( $P<0.01$ ). For porosity and micropore size, cement mantle thickness again was not a crucial factor ( $P>0.01$ ), while they were significantly influenced by cement viscosity and cement brand ( $P<0.01$ ), see Appendix I. The unpaired student t-test demonstrated that there was no significant difference as to the static shear strength, porosity, and micropore size between Simplex P and Simplex P-T cements ( $P>0.01$ ), which indicated that an addition of tobramycin to the cement composition was not a contributory factor to the results, see Appendix II. The final mean static shear strength, porosity and micropore size for each cement brand are shown in table 4.2, from which it is clear that CMW 1 bone cement gives the highest interfacial strength value, followed by Simplex P-T and Simplex P bone cements.

**Table 4.2: Static shear strength, porosity, and micropore size for each cement brand (mean±std)**

Bone cements	Static shear strength (MPa)	Porosity (%)	Micropore size (µm)
Cemfix 3	2.23±0.65	2.22±0.92	210.7±40.5
Coriplast 3	2.99±1.12	0.43±0.28	109.8±46.1
Simplex P	3.76±1.08	4.08±2.80	146.2±30.7
Simplex P-T	3.84±0.99	5.22±2.18	135.3±14.7
CMW 3	2.67±1.04	8.67±4.77	170.4±42.3
CMW 1	4.06±0.78	3.79±1.83	68.7±12.2
Palacos R	2.18±0.81	11.19±3.25	146.3±25.2

#### 4.3.3.2 Typical load–displacement plot and potential explanation

A representative test result obtained from the Hounsfield Test Machine H20K–W displaying the load–displacement plot is exhibited in figure 4.16. The plot shows an initial linear increase of load with incremental displacement until a peak force value is reached. This point is defined as the initial debonding force. The force then drops to a lower value before cycling around 1.4kN until the rod is fully pulled out from the cement mantle where the force returns to zero.

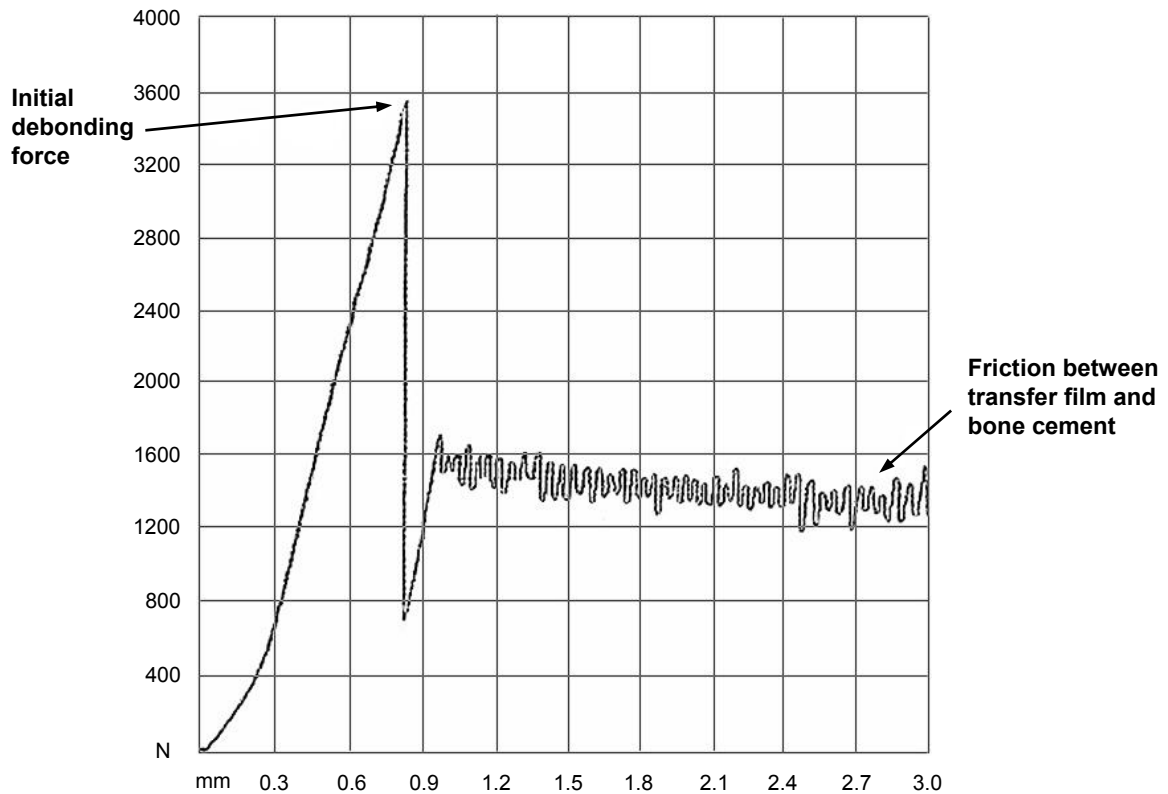
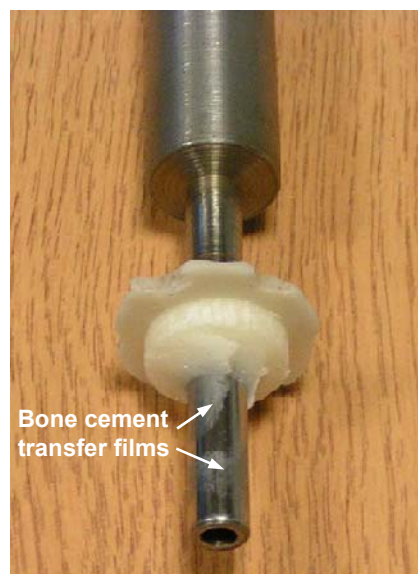


**Figure 4.16: A typical load–displacement plot for the pull out test**

The cyclical force was considered to be unusual and an additional test using CMW 3 bone cement was repeated on an Instron Test Machine 1273 (Instron Ltd., High Wycombe, UK) in order to discount machine error. The experimental conditions were the same as previous pull out tests, figure 4.17 (a). This test again showed a similar result, i.e. an initial high debonding force followed by a cyclical force around a significantly lower value. Large areas of bone cement transfer films were detected on the rod surface, which were considered to be involved in the cyclical force reading, figure 4.17 (b).



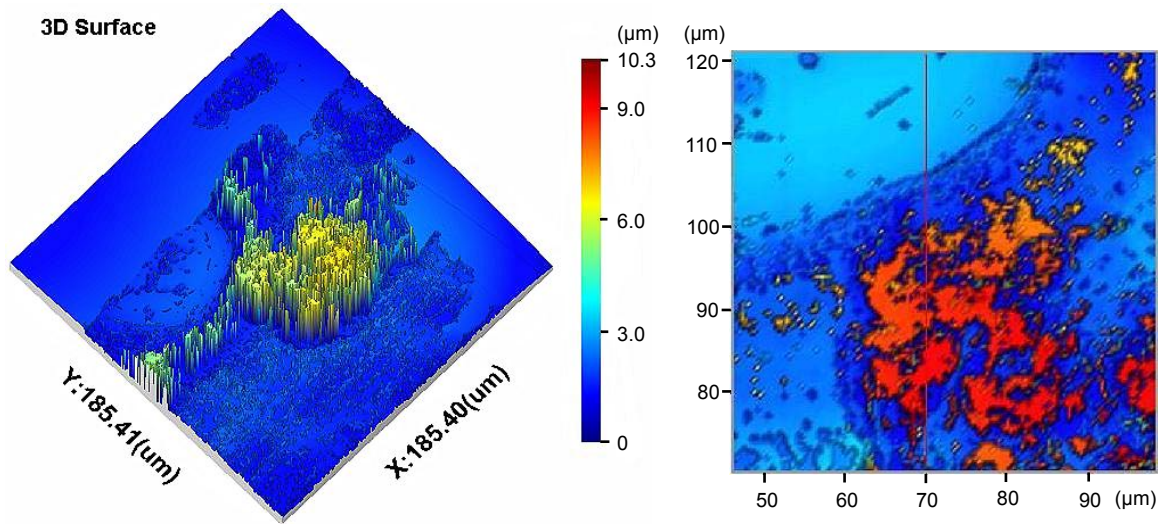
**(a)**



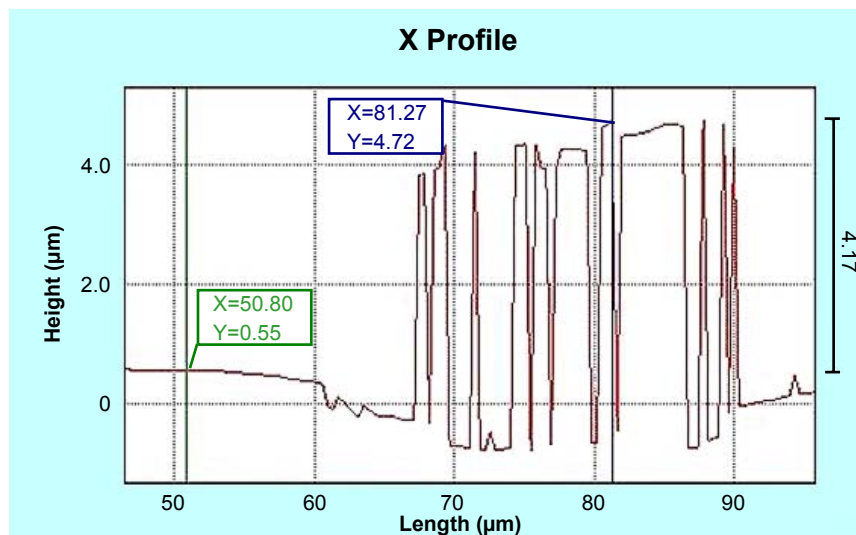
**(b)**

**Figure 4.17: (a) Pull out test performed on Instron Test Machine (b) Transfer films on the rod surface**

The stainless steel rod was further measured utilising the Talysurf CCI interferometer. Figure 4.18 shows the 3D and 2D topography of the cement transfer films, the height of which was about 4 $\mu\text{m}$ . It was thought that the cyclical force was a result of either frictional force between the debonded rod and the bone cement or internal shear within the bone cement. It was also considered to be important to investigate this phenomenon because it could have a bearing on stem movement in debonded hip prosthesis and in such stem designs where the stem subsidence is common, e.g. the polished Exeter stem.



(a)



(b)

**Figure 4.18: (a) Transfer films detected for CMW 3 bone cement in the pull out test by Instron (b) 2D profile showing height of transfer films for CMW 3 bone cement in a pull out test by Instron**

It is stated by Hutchings (1992) that many polymers (including acrylic bone cement) sliding against hard surfaces (e.g. metals, especially with smooth surface) transfer detectable films onto the counterfaces. These transfer films play an important part in the friction and wear of the polymers. Once these transfer films have formed, subsequent interaction occurs between the

polymer and this layer of similar material, irrespective of the composition of the substrate. On further sliding the polymer may continue to wear by adding new materials to the transfer films, since the interfacial bond to the counterface is often stronger than that within the bulk of the polymer itself. However, these transfer films whose thickness is of the order of several microns are usually removed subsequently as wear debris. This wear mechanism is also elucidated by Ludema (1996). Based on this theory, it was assumed that in the present study the frictional force build up began with the “clean” rod trying to move against the cement surface. This interface was strong and the force increased until interfacial failure occurred within the cement mantle, thus giving a pseudo debonding. Following this, transfer films formed and bone cement flowed over the cement transfer films, causing a drop in the measured force. It was further considered that the cyclical force was the result of subsequent breakdown of the interface due to shear of the transfer films followed by reforming and successive breakdown of new transfer films or frictional force between the bone cement and the transfer films. However, the total contact area between the rod and the bone cement was diminished gradually, resulting in a decrease of the cyclical force until the rod was completely pulled out. The failure process was accompanied by an audible sound. A flow diagram was given to describe the pull out process of the polished stainless steel rods from the cement mantle, figure 4.19.

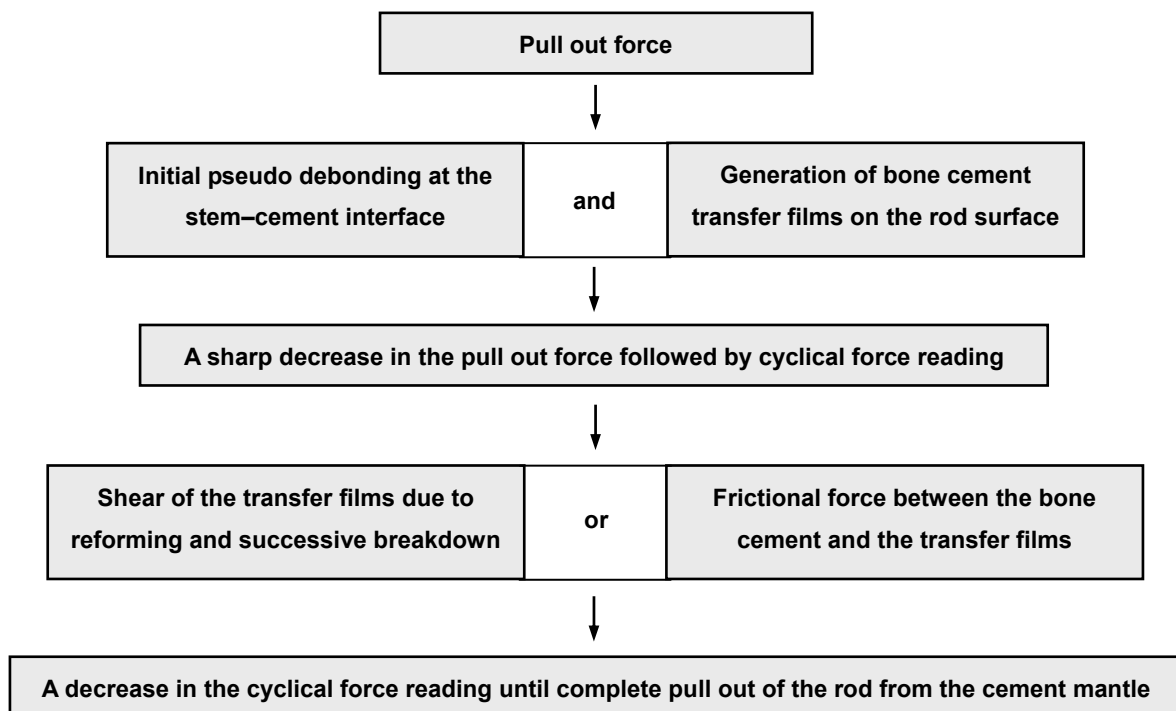


**Figure 4.19: The flow diagram showing the pull out process of the rod from the cement mantle**

A very similar load–displacement plot was noted by Hull (1981) during pull out of a cylindrical fibre from a resin disk, in which the cyclical element of the debonding curve was attributed to frictional forces caused by residual stresses and differential thermal contraction, figure 4.20. The evidence of the transfer films was also detectable on the stainless steel rod surface tested on the Hounsfield Test Machine. Figure 4.21 shows the 3D and 2D topography of the cement transfer films, measured by the Talysurf CCI interferometer at x50 magnification. The height of these transfer films was calculated to be about 10µm, using a Surfstand software V3.3.

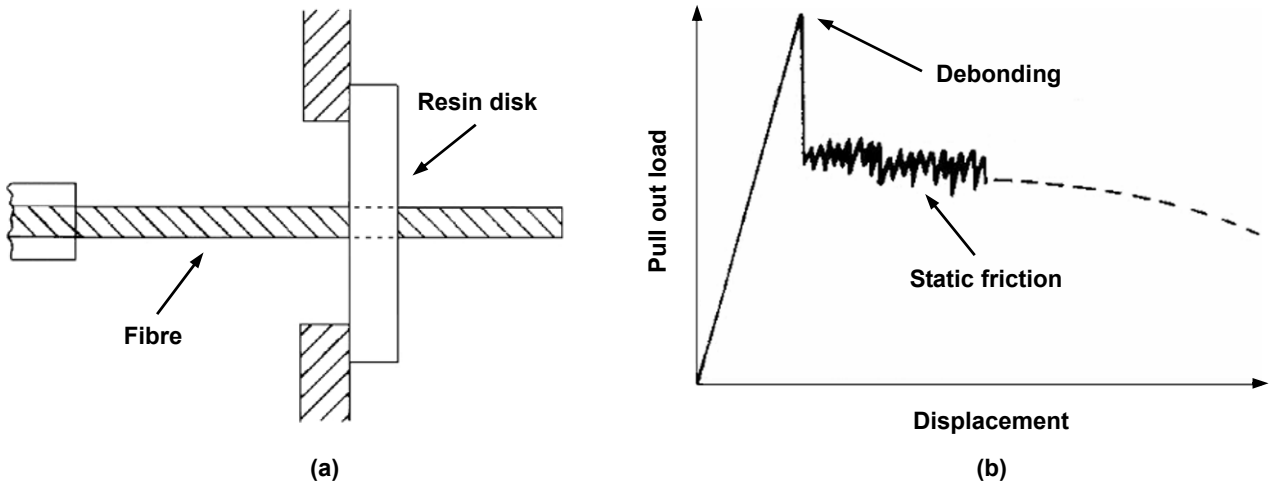
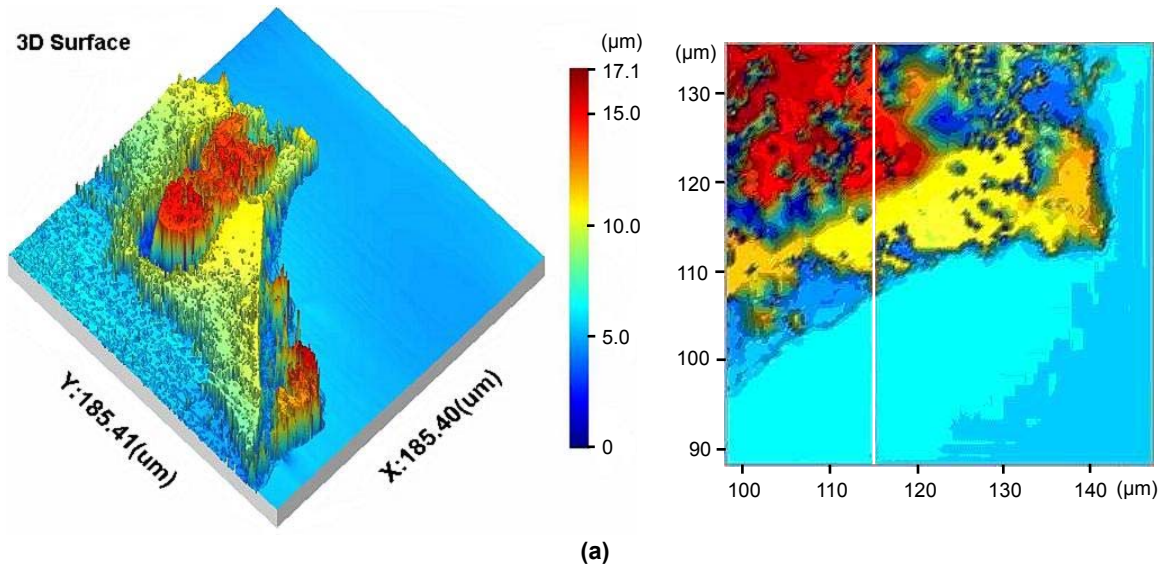
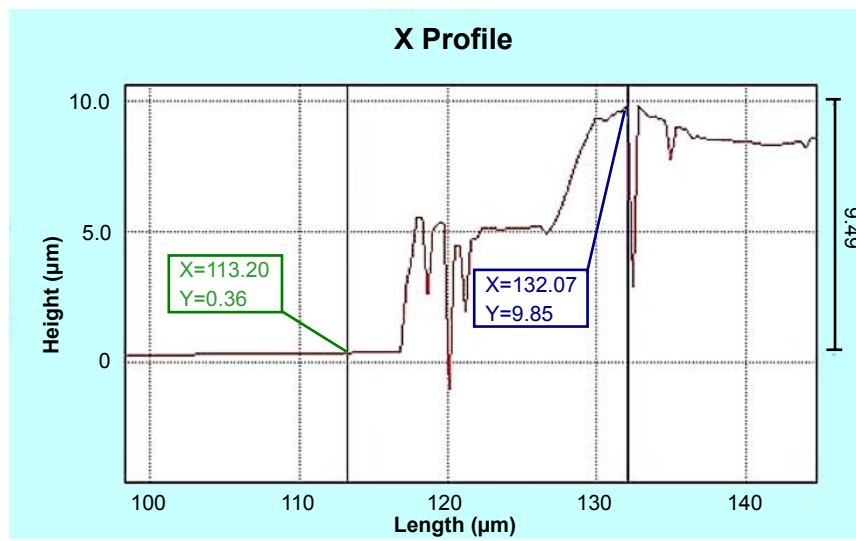


Figure 4.20: Pull out test of a cylindrical fibre from a resin disk (a) The fibre embedded in the resin disk (b) Typical load–displacement curve



(a)



(b)

Figure 4.21: (a) Transfer films detected for CMW 3 bone cement in a pull out test by Hounsfield (b) 2D profile showing height of transfer films for CMW 3 bone cement in a pull out test by Hounsfield

#### 4.3.4 Discussion

In the present study, the static shear strength between polished femoral stem and seven bone cements were investigated through a series of pull out tests. Porosity and micropore size were also calculated based on image processing. The results indicated that the static shear strength was more dependent on cement brand than cement viscosity and cement mantle thickness. This compared well with the studies of other researchers (Lewis 2000), who drew the conclusion that effort should focus less on manipulating cement viscosity and more on making compositional changes. However, it was indicated in the present study that cement viscosity did have an influence on interfacial porosity and micropore size. Previous laboratory tests have shown superiority of strength for low viscosity bone cements (Hansen and Steen 1992), but when they are applied for clinical use, those cements are more easily displaced from the irregularities in the bone by blood, thus providing lower shear strength at the cement–bone interface. This is considered to be one reason why an increased revision rate has been found for those femoral components implanted with low viscosity bone cements. Clinically, it is considered desirable to inject and pressurise low viscosity bone cements into the medullary canal in order to achieve optimal flow and mechanical interdigitation into cancellous bone. The optimal thickness of bone cement has been recommended to be approximately 3–4mm (Ramaniraka *et al.* 2000). Any thickness lower than this value was considered to be prone to micromovement at the stem–cement–bone interfaces, whilst a thickness higher than 5mm was believed to cause more serious thermal necrosis to the bone. The present study has, however, suggested that the heat generated during cement polymerisation is not highly detrimental to the static shear strength at the stem–cement interface. Clinical studies based on the data of the Norwegian Arthroplasty Register demonstrated that there were significantly increased rates of failure for Charnley hip prosthesis inserted with CMW 1 and CMW 3 bone cements (Espehaug *et al.* 2002), whereas the static shear strength for these two bone cements did not show the lowest value, indicating that there must be other factors influencing the failure mode of cemented THR. In addition, the femoral stem insertion rate, which could not be consistent for all the pull out tests in this study, potentially had some influence on porosity and distribution of micropore. However, a previous study carried out by Baleani *et al.* has shown that there was no significant difference concerning porosity at the stem–cement interface for different insertion rates of femoral stems (Baleani *et al.* 2003).

Surprisingly, the static shear strength was much larger in this study than the results of previous research which employed a similar test but in a push out mode. Wang *et al.* (2003) reported that the static shear strength at the stem–cement interface was 0.53MPa for Palacos R bone cement using “modern mixing techniques”, whereas in the present study the strength was calculated to be 2.4MPa and 2.0MPa respectively for the two cement mantle thicknesses. It seemed that Wang *et al.* (2003) did not make area modification in their study, and this lack of “correction” could in part have accounted for their lower value of static shear strength. Additionally, both the porosity and micropore size of the bone cements calculated in this study, ranging from 0.5% to 13.5% and from 70µm to 210µm respectively, were much lower, although the cements were all mixed by hand. It was demonstrated by FEA studies that the interfacial conditions at the loading fixture played an important part in interface stress (Harrigan *et al.* 1990), which implied that the differences involved in test specimen preparation and experimental conditions would potentially contribute to the significantly different results. Furthermore, Geiger *et al.* (2001) concluded in their study that

vacuum-mixed bone cements did not appear to reduce porosity at the stem–cement interface or to improve mechanical properties for all bone cements. The static shear strength obtained in this study varied from 1.4MPa to 4.6MPa, which, in spite of its higher value, was still lower than the typical mean shear stress at the stem–cement interface, approximately 5MPa (Chang *et al.* 1998). Thus, debonding at this interface was considered to occur inevitably during the *in vivo* service of the prosthesis. It was further revealed from the present study that, for bone cements with similar viscosity, larger static shear strength was always obtained where lower porosity was generated at the stem–cement interface. This was consistent with the results of another study, in which Iesaka *et al.* (2005) made a conclusion that increased porosity correlated with a reduction in shear strength after immersion in saline. Indeed, the effect of porosity should not be overlooked because the micropores not optically visible but present immediately below the cement surface could affect the interfacial shear strength. Porosity was also a significant factor that was considered detrimental to the mechanical properties of bone cement as well as the bond strength at the stem–cement–bone interfaces. Thus any porosity reduction both in the bulk cement and at the interfaces has been regarded as clinically beneficial.

Antibiotics such as gentamicin and tobramycin have been added to PMMA bone cement in order to prevent or treat infection and clinically better results have been reported. Despite their clinical benefit, it is generally accepted that mechanical properties of bone cement will be modified with additions of antibiotics, exemplified by alteration in density, bending strength, and an increase in viscosity. In the present study, however, it was indicated from the unpaired student t-test that an addition of tobramycin to Simplex P bone cement did not result in significant differences to the static shear strength and porosity at the stem–cement interface nor did it influence micropore size greatly.

Bone cement transfer films were detected in the present pull out tests. These transfer films were considered to contribute significantly to the cyclical force reading following the initial debonding at stem–cement interface, where interaction occurred between bone cement and the transfer films. It was speculated that there might remain a large bond strength between the bone cement and the transfer films, resulting in the cyclical force after debonding as evident on the load–displacement plots. Cement transfer films have been previously observed on retrieved femoral stems, and they were deemed to play a role in friction and wear at the stem–cement interface (Cook 1998).

#### **4.3.5 Conclusions**

The following conclusions could be drawn from the pull out test:

- The static shear strength between polished stainless steel rod and bone cement appears more dependent on cement brand than on cement viscosity and cement mantle thickness. With regard to the bone cements with similar viscosity, a larger static shear strength is obtained in the case of a lower porosity at the interface, with an accompanying lower value of micropore size.
- The highest mean static shear strength at the stem–cement interface for all the bone cements studied is obtained for CMW 1, followed by Simplex P with tobramycin and Simplex P bone cements.
- The porosity and micropore size of bone cement are significantly influenced by cement brand

and viscosity, while cement mantle thickness is not an influencing factor.

- The static shear strength measured in the present study is much larger in comparison with that of previous research, whilst the porosity and micropores shows much smaller values, although all the bone cements are mixed by hand.
- There is no significant difference between Simplex P and Simplex P with tobramycin bone cements in terms of static shear strength, porosity and micropore size, which indicates that the antibiotic additive is not a contributory factor to the results.
- Bone cement transfer films are detected on the polished rod surface after the pull out test, and they are considered to contribute significantly to the interaction at the interface. The height of the transfer films are calculated to be about 4–10µm.

#### **4.4 Influence of stem surface finish on stem–cement interfacial strength**

##### **4.4.1 Background and aims**

The optimal surface finish for the hip prosthesis has been debated for many years. Since 1997, however, it seems that the controversy has intensified as reports have been published on failed prostheses that exhibit varying amounts of surface roughness or surface coating. Although it is generally accepted that a femoral stem with matt surface finish would promote a greater bond strength at the stem–cement interface and it has been well documented that matt stems do give satisfactory results even at 10–20 years follow up (Sanchez–Sotelo *et al.* 2002), there is a body of evidence which suggests that the long term survival of femoral stems with roughened surface is clinically compromised. Until now, it still hangs in doubt as to whether matt stems can accomplish a permanent stabilisation during their *in vivo* service as diverse conclusions have been drawn from previous studies. Therefore, this present pull out test was performed with the aim of investigating the influence of stem surface finish on the static shear strength at the stem–cement interface, and getting a better understanding of the interaction between bone cement and femoral stems with different surface finishes.

##### **4.4.2 Materials and methods**

###### **4.4.2.1 Preparation of test specimen**

In this study, Simplex P bone cement was selected to be tested due to its superior clinical outcome and prevalence. In addition to the polished stainless steel rods used in the previous pull out test, another three kinds of stainless steel rods with different surface finishes were fabricated, which are glass bead-blasted (with the use of glass beads, size range: 0.15mm–0.25mm), shot-blasted (with the use of carbon steel balls, nominal size: 0.5mm) and grit-blasted (with the use of non-spherical carbon steel, size range: 0.3mm–0.7mm). For each kind of surface finish, totally four rods were manufactured with a diameter about 8mm. The polished rods were measured using the Talysurf CCI interferometer with an area of 0.34 x 0.34 mm<sup>2</sup>, and the other rods were measured utilising the Form Talysurf PGI Series 2 with an area of 2x2 mm<sup>2</sup>. Note that the differing area size is not considered important in this case. Due to the potential table error that may occur when employing contacting stylus instrument to measure super-polished samples, it is more appropriate to measure them using non-contacting optical instrument. The measurements obtained are shown in figure 4.22. Three measurements were carried out on each rod surface. The mean values of some selected

3D surface parameters—Sq, Sz, Sdq, and Sdr were calculated through the Surfstand software V3.3. These parameters are further expatiated in table 4.3, and they are considered to give a relatively full description of the surface in height deviation, which correlate with the static shear strength at the interface.

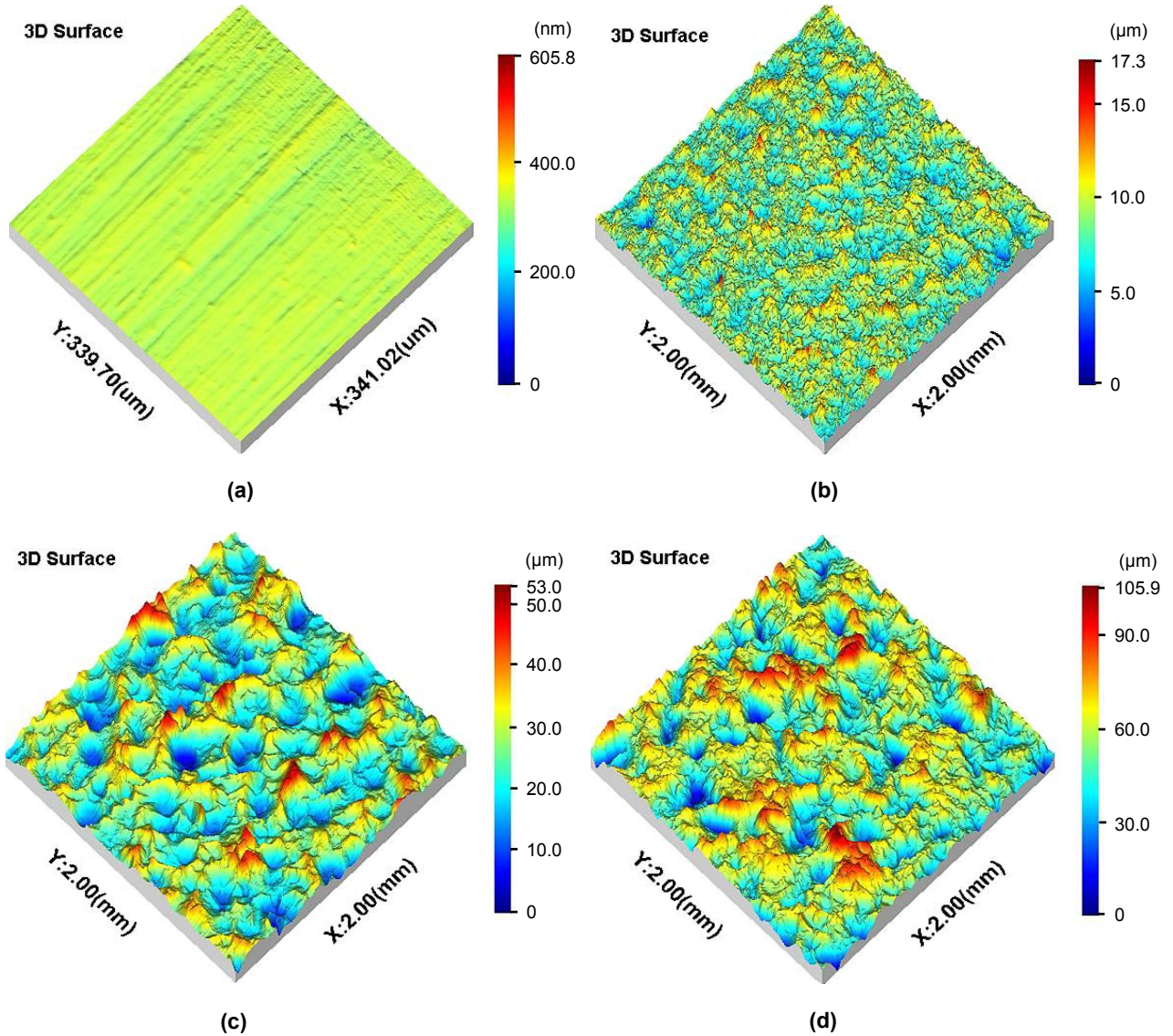


Figure 4.22: 3D surface topography of stainless steel rods before pull out test (a) Polished (b) Glass bead-blasted (c) Shot-blasted (d) Grit-blasted

Table 4.3: Expatiation of 3D surface parameters to assess a surface in height deviation

Parameter	Abbreviation	Explanation
Root mean square deviation of the surface	Sq	A more stable expression of average surface roughness
Maximum height of the surface	Sz	Height between the tallest peak and the deepest valley
Root mean square slope of the surface	Sdq	Root mean square value of surface slope within the assessed area
Developed interface area ratio	Sdr	Ratio of the increment of the interfacial area of a surface over the sampling area, tends to zero for smooth surface

A new cylindrical holder made of mild steel was fabricated, with an internal diameter of 18mm, an external diameter of 28mm, and a length of 30mm. This geometry gave a nominal cement mantle thickness of 5mm to resemble the clinical situation. The Simplex P bone cement was again hand mixed at room temperature following the manufacture’s instructions. The preparations of the test specimen and the test conditions were the same as the previous pull out test. The only difference was that the static shear strength ( $\sigma$ ) was calculated using the initial debonding force divided by the apparent contact area, where the definitions of  $F$ ,  $D$ , and  $L$  are the same as equation (4.1), as the porosity corrections were not feasible in this case.

$$\sigma = \frac{F}{\pi DL} \quad (4.2)$$

#### 4.4.2.2 Analysis of test specimen and statistical analysis

After each test, the stainless steel rod was examined using the Leica stereomicroscope to detect any cement debris present on the surface. In addition, the Simplex P bone cement was cautiously extracted from the metallic holder and cut longitudinally into two equal parts. The inner surface of the cement was cleaned with alcohol and measured employing the Form Talysurf PGI Series 2. Likewise, three measurements were carried out on the cement surface, with each area 2x2mm<sup>2</sup>. The mean values of Sq, Sz, Sdq, and Sdr were also calculated using the Surfstand software V3.3. Furthermore, the bone cement which contacted with the polished stainless steel rod was further cut into smaller pieces, enabling observation of the micropores using the SEM JEOL JSM–6060. The same tests were repeated four times for each surface finish rod. The final static shear strength was calculated as the mean value of the four tests performed. Statistically significant difference was investigated to establish the influence of surface roughness on the static shear strength, based on a one-way ANOVA. Additionally, a Tukey–Kramer Post Hoc Test was carried out to determine significant differences among the mean values of the static shear strength. The software utilised is SPSS 12.0 for windows.

### 4.4.3 Results

#### 4.4.3.1 Static shear strength

The selected 3D surface parameters of the four kinds of surface finish rods are listed in table 4.4. It is demonstrated clearly from these parameters that the grit-blasted rods generate the roughest surface, followed by shot-blasted, glass bead-blasted and polished rods. The mean value of the static shear strength is shown in figure 4.23, from which it is evident that the strength in general increases with the rise of surface roughness.

**Table 4.4: 3D surface parameters of stainless steel rods with differing surface finishes (mean±std)**

Stainless steel rods	Sq (µm)	Sz (µm)	Sdq	Sdr (%)
Polished	0.01±0.0002	0.61±0.05	0.01±0.0007	0.0075±0.0007
Glass bead-blasted	2.44±0.11	17.91±0.84	0.30±0.02	4.30±0.58
Shot-blasted	11.68±0.57	54.45±2.15	0.44±0.06	8.42±1.15
Grit-blasted	19.20±4.65	102.71±4.55	0.78±0.01	25.25±0.52

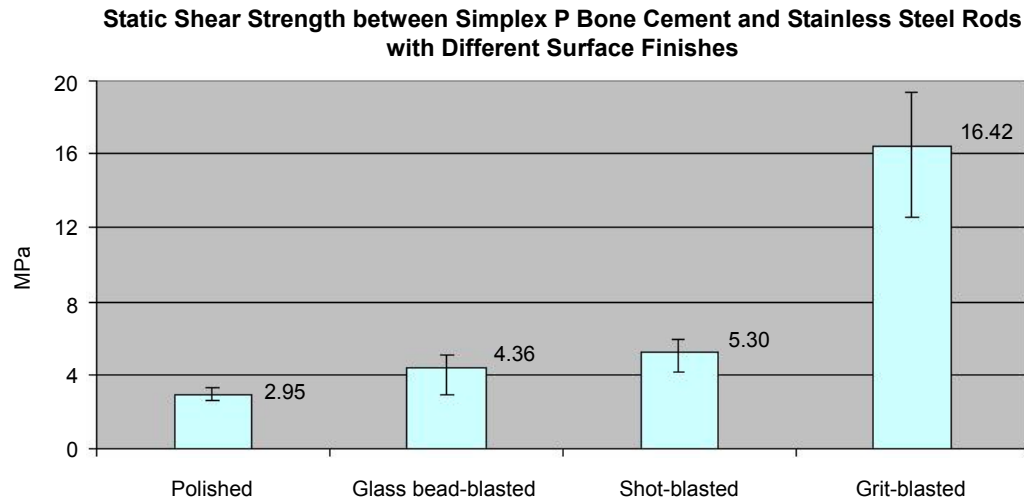


**Figure 4.23: Interfacial strength between Simplex P bone cement and different surface finish rods**

It was further revealed from the one-way ANOVA that the static shear strength was significantly influenced by surface roughness ( $P < 0.01$ ), although there was no great increase from the polished rods to the glass bead-blasted rods, and from the glass bead-blasted rods to the shot-blasted rods. In addition, the Tukey–Kramer Post Hoc Test indicated that the static shear strength using the grit-blasted rods was significantly different from that using other surface finish rods ( $P < 0.01$ ), i.e. the grit-blasted rods were markedly higher in terms of the static shear strength, see Appendix III.

#### 4.4.3.2 Typical load–displacement plot

Figure 4.24–4.26 displays the typical load–displacement plots for the glass bead-blasted stainless steel rods, the shot-blasted stainless steel rods, and the grit-blasted stainless steel rods respectively. The plot for the polished stainless steel rods was almost the same as what was obtained in the previous pull out test. Generally speaking, the failure modes can be classified into two categories, which indicated that the interactions between bone cement and stainless steel rods with various surface finishes were inherently different. The polished and glass bead-blasted rods illustrate a slip-stick-slip failure during the pull out process whereas the shot-blasted and grit-blasted rods display gross interface breakdown. The potential reason for the slip-stick-slip failure mode has been discussed in the previous section. With reference to the shot-blasted and grit-blasted rods, it was considered that the bone cement had penetrated into the deep valleys of the surface micro-topography and formed a high mechanical interlocking. It is evident from table 4.4 that the shot-blasted and grit-blasted rods present a much larger  $S_z$  and  $S_{dq}$ , which would promote a more intimate contact with the bone cement. This therefore caused gross failure of the interface within the cement mantle.

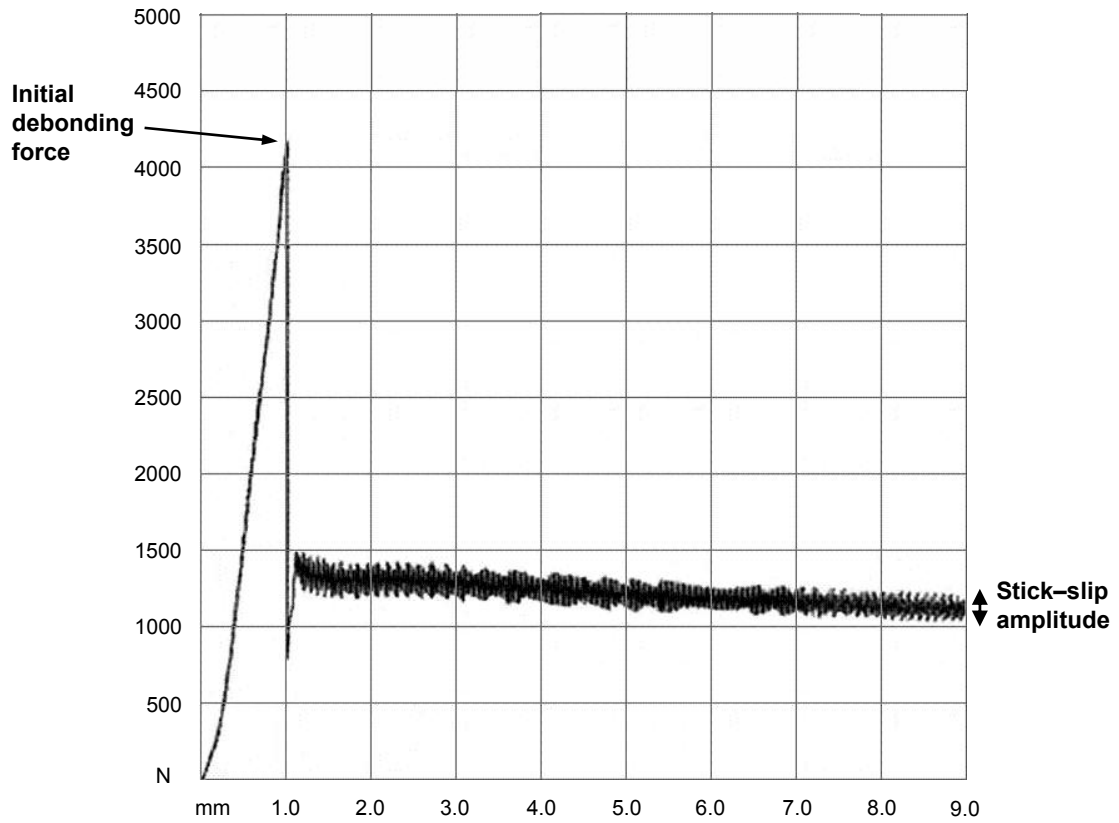


Figure 4.24: Typical load–displacement plot for pull out test of glass bead-blasted stainless steel rods

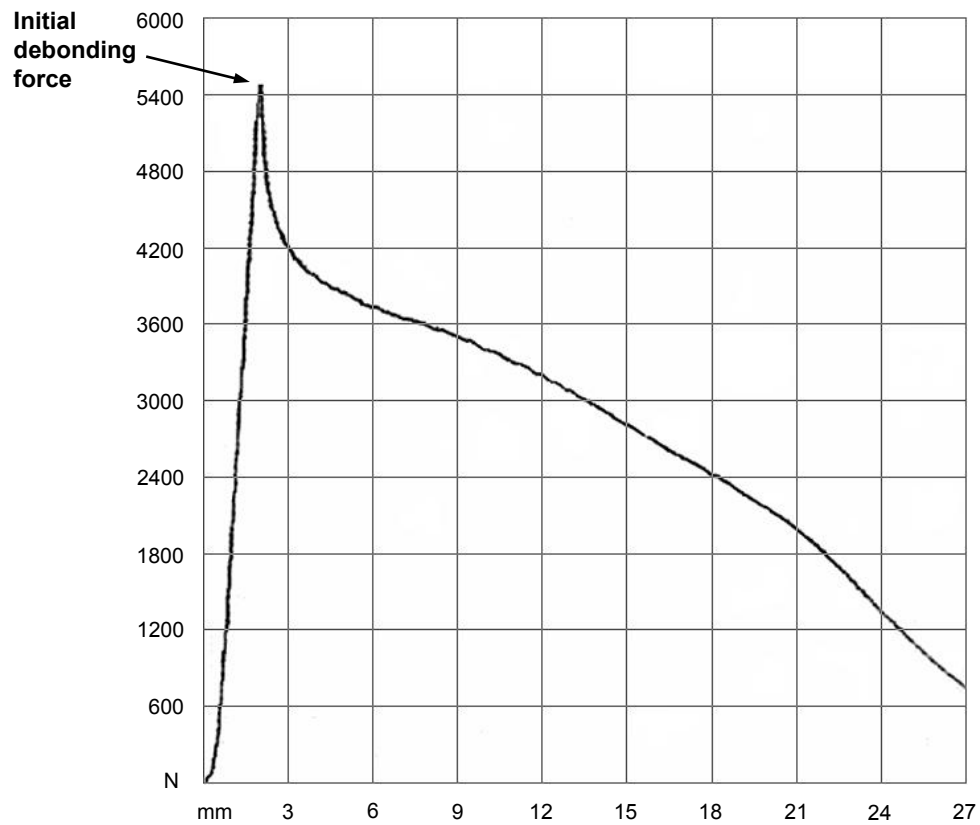
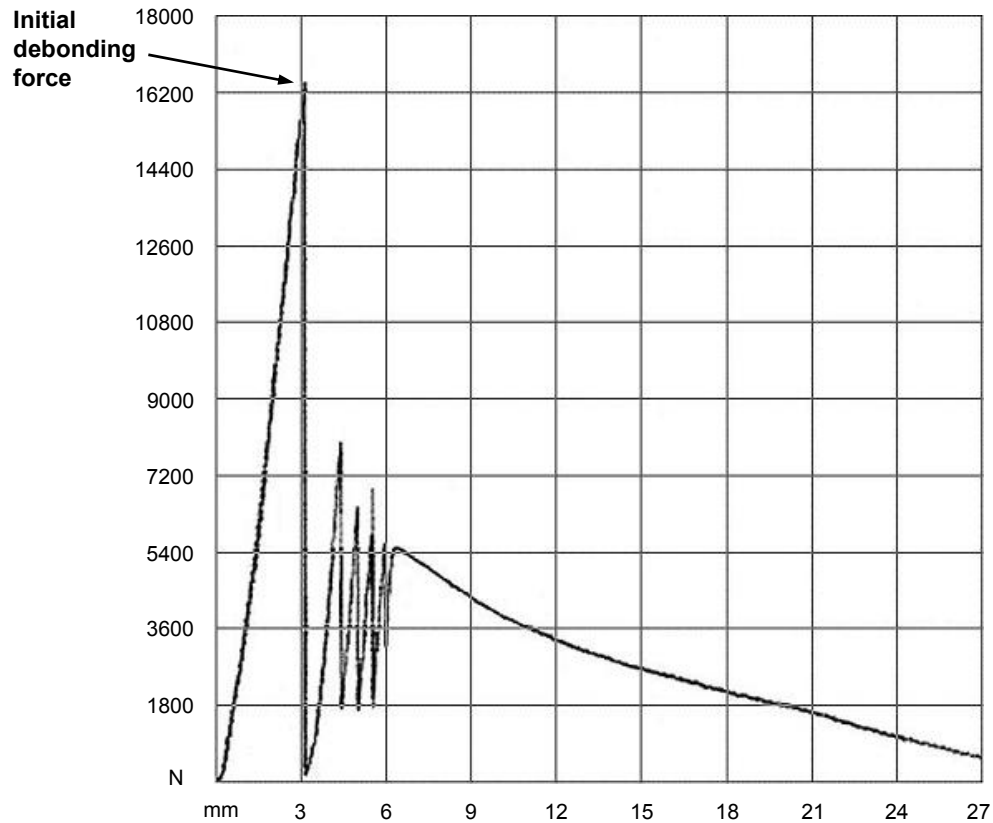


Figure 4.25: Typical load–displacement plot for pull out test of shot-blasted stainless steel rods



**Figure 4.26: Typical load–displacement plot for pull out test of grit-blasted stainless steel rods**

#### **4.4.3.3 Characterisation of the rod and cement surface**

The optical micrographs of the rod surfaces following the pull out test are shown in figure 4.27. As reported in the previous pull out test, the polished rods show presence of cement transfer films. Additionally, there is clear evidence of cement debris adhered to the surface of the grit-blasted rods. However, there seems to be no cement present either on the glass bead-blasted rods or on the shot-blasted rods. The reason why bone cement transfer films were not detected on the glass bead-blasted rods following the test was probably due to their accompanying removal as cement debris by the asperities on the rod surface, as the glass bead-blasted rods are in nature much rougher than the polished rods. The relatively low static shear strength for the shot-blasted rods and lack of cement debris present on the rod surface following the pull out test indicated a weak mechanical interlocking with the bone cement, compared with the grit-blasted rods.

An SEM micrograph of the bone cement in contact with the polished stainless steel rods shows that abundant micropores are prevalent in the surface, typically 120µm in diameter, figure 4.28. The other areas are smooth and appear undamaged, figure 4.29 (a). However, the cement surface interfaced with the glass bead-blasted rods shows slight scratches along the pull out path (in the Y direction), figure 4.29 (b), and the cement surface in contact with the shot-blasted and grit-blasted rods are greatly damaged, figure 4.29 (c) and (d). Deep scratches and scores dominate the surface feature, which are considered to be caused by sliding of the metal asperities against the cement surface.

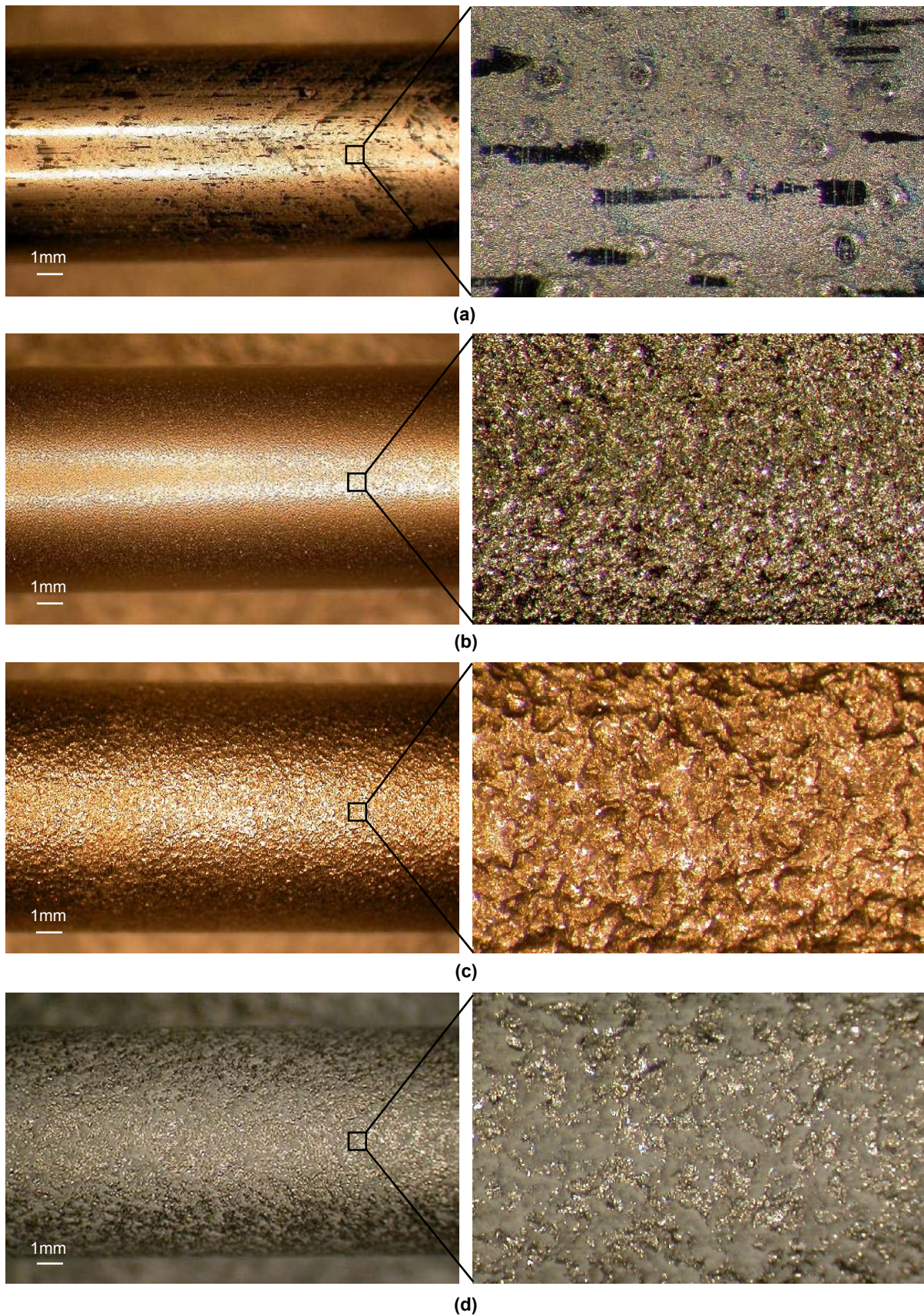


**Figure 4.27: Stainless steel rod surface after pull out test (a) Polished rod, the black substrate is the polished rod, and the lighter areas are the transfer films (b) Glass bead-blasted rod, no cement is present on the surface (c) Shot-blasted rod, no cement is present on the surface (d) Grit-blasted rod, the shiny substrate is the grit-blasted rod, and the grey covering is cement debris**

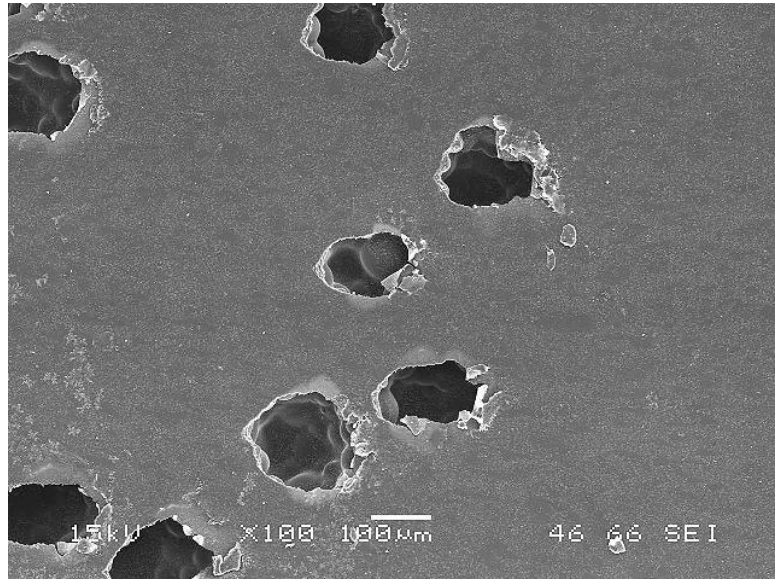


Figure 4.28: Micropores formed in the cement surface interfaced with polished rods

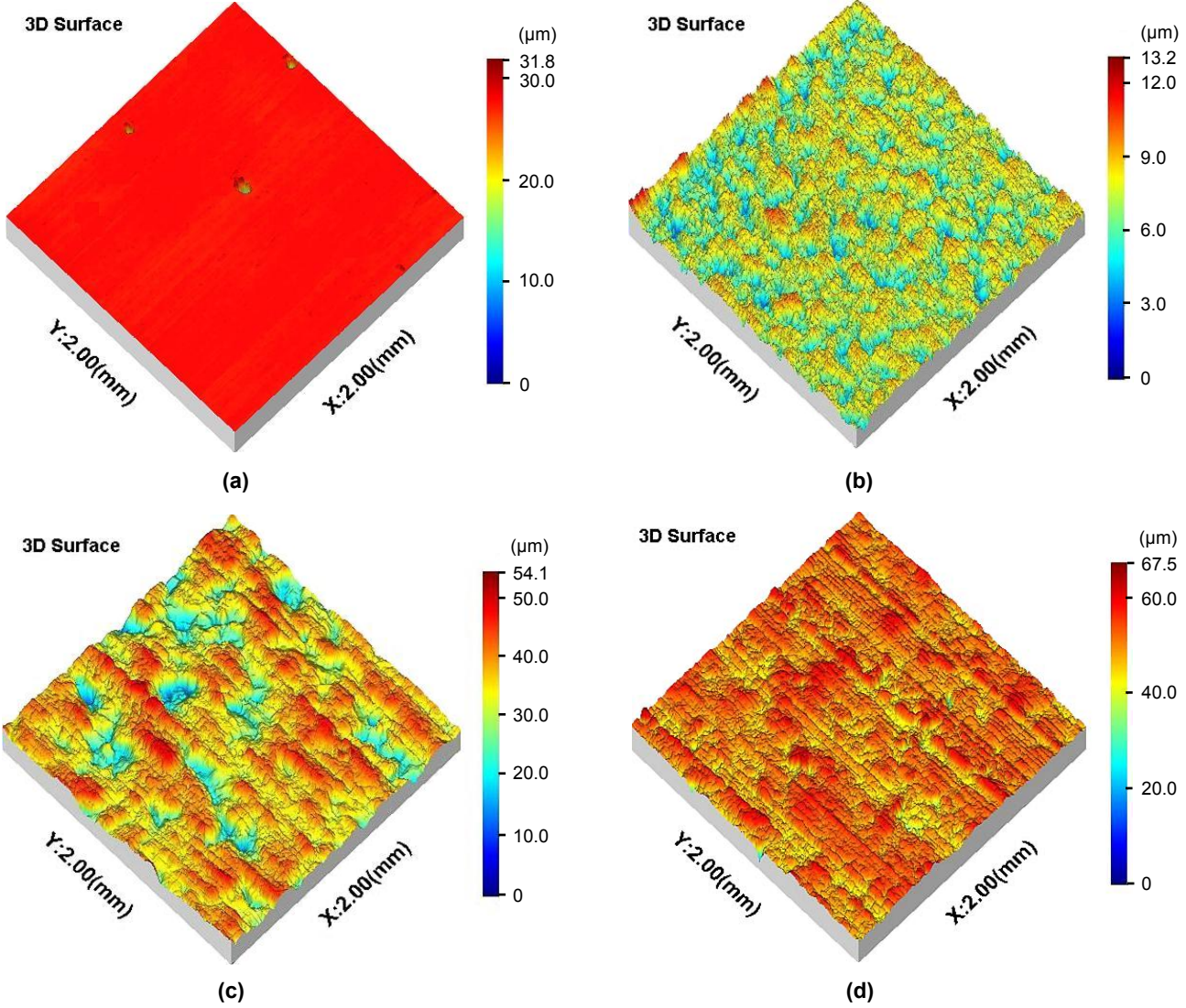


Figure 4.29: 3D surface topography of bone cement interfaced with stainless steel rods (a) Polished (b) Glass bead-blasted (c) Shot-blasted (d) Grit-blasted

The selected 3D surface parameters of bone cement interfaced with these stainless steel rods are calculated following the measurements, which are shown in table 4.5. From the table we can see that the cement surface in contact with the grit-blasted rods shows a lower value of Sq than that of the shot-blasted rods. The reason for this abnormality could be attributed to cement fracture that occurs in the cement mantle interfaced with the grit-blasted rods due to the presence of a higher interfacial strength, thus leaving cement debris in the pits of the rod surface and making the bone cement surface relatively smooth. Additionally, the Sz parameter of the cement surface interfaced with the polished rod is larger than that in contact with the glass bead-blasted rod owing to the presence of micropores in the surface, which results in a big increase of the deepest surface valley and consequently an increase of the maximum height of the topographic surface.

**Table 4.5: 3D surface parameters of bone cement interfaced with the four kinds of surface finish rod (mean±std)**

Cement surface interfaced with—	Sq (μm)	Sz (μm)	Sdq	Sdr (%)
Polished rods	0.565±0.013	32.066±0.412	0.0745±0.0007	0.307±0.006
Glass bead-blasted rods	1.33±0.11	10.52±0.48	0.215±0.01	2.536±0.24
Shot-blasted rods	7.58±0.56	47.94±5.59	0.35±0.015	5.93±0.47
Grit-blasted rods	5.21±0.71	84.50±15.9	0.47±0.036	9.95±1.03

Furthermore, an optical micrograph shows that metallic debris embeds within the cement mantle originating from the tests of the grit-blasted rods, figure 4.30. This indicates a great mechanical interlocking at the interface which has dislodged relatively loose metallic blast debris during the pull out process.

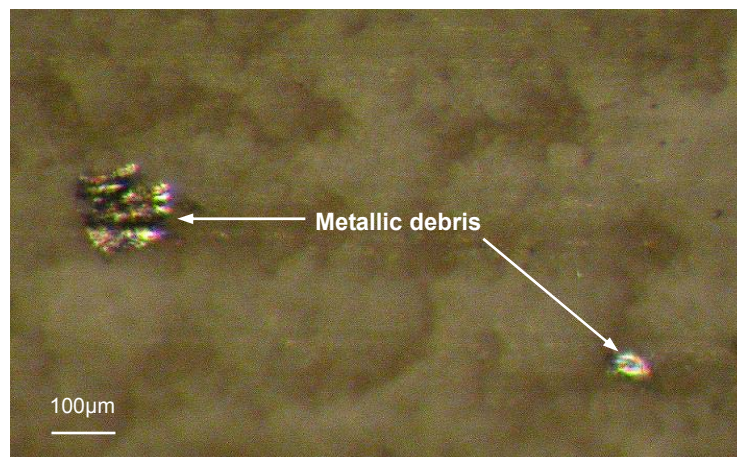


**Figure 4.30: Metallic debris embedding within the cement mantle originating from the grit-blasted rod pull out test**

#### 4.4.4 Discussion

In the present study, the static shear strength at the stem–cement interface was investigated through a series of pull out tests, using Simplex P bone cement and stainless steel rods with four kinds of surface finish. There was a general tendency that the strength increased with the rise of surface roughness. However, the strength did not go up significantly from the polished rods to the shot-blasted rods, in spite of a great increase from the shot-blasted rods to the grit-blasted rods.

This result compared well with the conclusion of another study, in which Wang *et al.* (2003) reported a significant increase from the bead-blasted rods to the grit-blasted rods but no significant difference between the polished rods and the bead-blasted rods, or between the grit-blasted rods and the plasma-sprayed rods. However, the static shear strength they obtained (0.53MPa, 2.00MPa, and 9.85MPa for the polished, glass bead-blasted, and grit-blasted specimens respectively) was a lot lower in comparison with the results of the present study (2.95MPa, 4.36MPa, and 16.42MPa for the polished, glass bead-blasted, and grit-blasted specimens respectively), in spite of utilising the same equation. It was worth noting that they used Palacos R bone cement in their study and no details concerning the polishing and blasting media were given. Also they investigated the static shear strength of the stem–cement interface in a push out mode, and the rod samples protruded through the cylindrical cement mantle. These may result in the significant difference between the two studies. Additionally, Bundy and Penn (1987) reported a greater interfacial strength for the coarsest surface finish (grit-blasted and porous coated) and also the finest surface finish (highly polished using 1 $\mu$ m diamond paste) specimens, as compared with the intermediate surface finish (polished using 6 $\mu$ m and 15 $\mu$ m diamond pastes) specimens. They considered that the stem–cement adherence depended upon superposition of mechanical interlocking and atomic interaction effects, with the former predominating for the coarse surface finishes and the latter responsible for the fine surface finishes. One debate involved in their study was that the interfacial strength of the highly polished specimen was even higher than that of the grit-blasted specimen, which was in great contradiction to the results of the present research. It was further indicated in another study carried out by Chen *et al.* (1999) that the stem–cement interfacial strength increased monotonically with the rise of Rdq (2D surface parameter, root mean square slope of the surface) rather than Ra (2D surface parameter, average surface roughness of the surface). In a sense, however, there is certain limitation with the use of 2D surface parameters to evaluate an areal surface. This could be attributed to the insufficient information these parameters contain based on the restricted surface data they have collected. In the present study, the selected 3D surface parameter—Sdq (root mean square slope of the surface) also increased with the rise of surface roughness—Sq (3D surface parameter, root mean square deviation of the surface), with the grit-blasted rods having the largest value. We can therefore draw the conclusion that the static shear strength increases with the rise of surface roughness as well as surface slope, and this would be consistent with a better mechanical interlocking. Furthermore, the grit-blasted rods possess the highest Sdr, which is an indication of a larger contact area with bone cement. This may further explain why the grit-blasted rods generated the largest apparent static shear strength, i.e. a better mechanical interlocking and a greater surface contact area may facilitate increased molecular bonding.

The typical load–displacement plots of the pull out tests displayed in figure 4.24–4.26 showed two types of failure modes for the test specimens, i.e. a slip-stick-slip failure for the polished and glass bead-blasted rods and a gross interface failure for the shot-blasted and grit-blasted rods. Stone *et al.* (1989) also reported a slip-stick-slip failure mode in their study, using PMMA pre-coated rods. They finally drew the conclusion that the PMMA coating may act as a lubricant between the rod and the cement, which to a certain degree was of similar function as the transfer films detected on the polished rods in the present study. An amount of micropores were present in the cement surface interfaced with the polished rods. However, the micropores were not easily observed on the other cement surfaces, where the surface features were dominated by slight or deep scratches

along the pull out path. These scratches were considered to be caused by sliding of the metal asperities against the cement surface. In addition, metallic debris was observed embedding within the cement mantle originating from the tests of the grit-blasted rods. The dislodgment of metallic blast debris supported the theory of strong mechanical interlocking between the bone cement and the grit-blasted rods.

It should be mentioned that “modern cementing techniques” have been widely employed when mixing bone cement and implanting femoral stems in surgery, with the aim of reducing porosity at the interfaces as well as in the cement matrix, and enhancing interlock between bone cement and bone. These techniques were not utilised in this study, therefore it demonstrated the worst case scenario. However, it is considered that the validity of the results obtained in this study should not be significantly compromised as it mainly focused on the interfacial shear strength. The present research indicated that roughened surfaces were superior to smooth surfaces in terms of static shear strength. However, there is a body of evidence which suggests that the long term survival of femoral stems with roughened surface was not that satisfactory, especially in those designs where the femoral stem is expected to subside, e.g. the polished Exeter stem. Consequently, the present work would seem to be most applicable only to those stem designs where mechanical interlocking of the stem in the initial fixed position was essential. We should bear in mind, however, that if the forces applied on the femoral stem exceed the pull out force for the grit-blasted samples, it then will have severe implications for those matt stems incorporated with collarless design.

#### **4.4.5 Conclusions**

The following conclusions could be drawn from this work:

- The static shear strength between Simplex P bone cement and four kinds of surface finish rods has been established. The interfacial strength generally increases with the rise of surface roughness, and it is much larger in comparison with that of previous research.
- The failure modes for the test specimens are classified into two categories, and this indicates that the interaction between bone cement and stainless steel rods with various surface finishes is essentially different.
- Following the pull out tests, the stainless steel rods show change in surface characteristics and the bone cement surface also demonstrates varying severities of damage depending on the surface roughness of the rod. It is originally attributed to the different surface finishes of the stainless steel rods and correlates with the pull out process.
- 3D surface parameters are introduced to assess stainless steel rod and bone cement surfaces in terms of surface roughness, and they are considered to be more useful than the use of 2D surface parameters.

#### **4.5 Summary**

In this chapter, a stem–cement interfacial gap test and the two series of pull out tests were carried out. From the results of these studies, the static shear strength between polished stainless steel rod and commercially available bone cements were established, and the influence of stem surface finish on the interfacial shear strength was investigated, which combined together to give a better understanding of the characteristics of the stem–cement interface. With regard to the pull out forces, it is considered that they are comparable to the physiological loading applied on the hip

joint during human normal activities. If coupled with torsional effect of the physiological loading, it is reasonable to conclude that the stem–cement interface is critical for debonding *in vivo*, which would promote relative micromotion and subsequent generation of fretting wear at this interface.

One potential shortcoming involved in the pull out test is that the interfacial strength was tested in a pull out mode, whilst in fact for the most part it is cyclical compressive loading that applies on the hip joint. However, as the pull out tests performed primarily aims to establish the interfacial strength between simulated femoral stem and bone cements, the results of these tests should not be greatly compromised.

## Chapter 5 Reproduction of fretting wear on the femoral stem

### 5.1 Chapter summary

Generally, there are two effective methods that are commonly utilised to investigate femoral stem wear; they are *in vivo* retrieval study and *in vitro* wear simulation. Whilst retrieval studies on stem wear have been reported by many researchers, there are relatively few studies with regard to *in vitro* wear simulation of femoral stems. One potential reason for this is due to the fact that the loading mechanism of the hip joint in the clinical situation is so complicated that it makes *in vitro* simulation of the real *in vivo* conditions in the human body extremely difficult or to a certain degree currently impossible to accomplish. Most previous studies concerning wear simulation of the femoral stem simplified this by carrying out pin-on-disk tests, and research in this area to date has gained only very limited achievements in spite of the great efforts made by many researchers. Consequently, there is pressing demand to propose a creative new method or to modify those techniques which already exist to successfully reproduce fretting wear on the femoral stem.

In this chapter, a new methodology was developed through modifications of standardised fatigue testing of the femoral stem at typical physiological loading. By modifying the method of fixation to incorporate initial stem implantation in a sawbone along with the introduction of saline solution to mimic the *in vivo* conditions, it has been possible to replicate fretting wear seen on polished stems. This was further confirmed by consistently reproducing fretting wear through the proposed method. Following the wear simulations, the femoral stem and the bone cement were collected and examined through optical microscopy, optical interferometry and SEM. Additionally, the surface topography of the femoral stem pre and post simulation was evaluated utilising 3D surface parameters. The initial results gave an insight into the progression of fretting wear and potential wear initiators concerned with polymerisation of bone cement.

From this chapter on until chapter 7, a series of *in vitro* wear simulations will be consecutively carried out, and a summary of these simulations can be found in Appendix IV in order to give a clear overview of the comparison between these wear simulations.

### 5.2 Initial attempt to replicate fretting wear at the stem–cement interface (Simulation I)

#### 5.2.1 Background and aims

Nowadays, wear at the stem–cement interface is showing an increasing significance in the overall wear of cemented THR due to the great progress that has been made in reducing wear at the head–cup interface with the advent of cross-linked UHMWPE (Wroblewski *et al.* 1996) and hard-on-hard bearing systems (Firkins *et al.* 2001, Hatton *et al.* 2002). The accompanying wear debris from the stem–cement interface could migrate through cement mantle deficiencies to reach bone tissue areas, where the biological process of lytic bone resorption and aseptic loosening begins. Since the introduction of cemented THR, the stem–cement interface has been consistently cited as a weak link (Jasty *et al.* 1991) and it is considered to experience fretting wear owing to the low-amplitude oscillatory micromotion under cyclical physiological loading (Howell *et al.* 2004). The previous two pull out tests have demonstrated that the stem–cement interfacial strength is critical for initiating debonding at the interface, and debonding is considered to be a prerequisite for the generation of fretting wear. Although there is a body of clinical evidence of fretting wear on

polished femoral stems, *in vitro* simulation to reproduce this wear has seldom been attempted. Cook (1998) was considered to be the first to set foot in this area, but even then only limited success was achieved. Previous studies which employed pin-on-disk tests in terms of displacement control and static compressive loading cannot represent the *in vivo* environmental conditions in the human body. In addition, the potential influence of bone cement brand, femoral stem geometry, and surface finish on generation of fretting wear has not yet been established. Taking into account the considerable varieties of femoral stem designs and bone cement brands available on the market (Murray *et al.* 1995, Lewis 2002), an investigation of the influence of these contributory factors would clearly be desirable. Accordingly, the present study aims to address this issue by carrying out *in vitro* fretting wear simulations, through which an insight into the wear mechanism and the influencing factors would hopefully be established.

## 5.2.2 Materials and methods

### 5.2.2.1 Preparation of test specimen

A polished Exeter V40™ femoral stem (stainless steel, Stryker Howmedica Osteonics, Newbury, UK) and Simplex P bone cement were used in the present simulation, both of which have shown excellent clinical track records. The bone cement was hand mixed according to the manufacture's instructions, and transferred into a reamed sawbone (3<sup>rd</sup> generation composite femur, Sawbones, Malmö, Sweden) in a retrograde fashion utilising a cement delivery system. Whilst it is recognised that vacuum mixing is the usual practice, hand mixing was chosen in this case in an attempt to accentuate the deleterious effect of experimental conditions. The femoral stem was then implanted and the cement cured as instructed to mimic surgical techniques. Acrylite resin (Rubert & Co Ltd., Cheadle, UK) was employed to stabilise the stem–cement–sawbone system in a steel tube, figure 5.1. A custom-made fixture was designed to enable fretting wear simulation employing an Instron test machine 1273 (Instron Ltd., High Wycombe, UK).

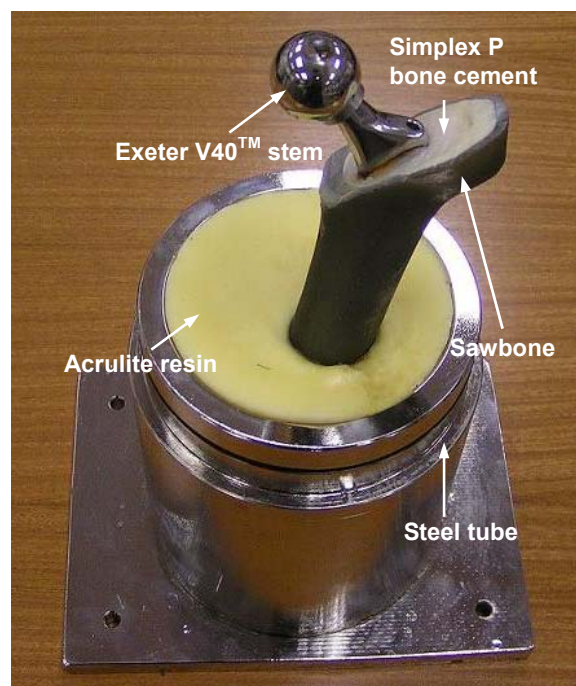


Figure 5.1: Preparation of specimen for fretting wear simulation

### 5.2.2.2 The regime of wear simulation

The simulation was performed in part with reference to the specifications for endurance of hip prosthesis instructed by BS ISO standard 7206–4, the femoral stem–bone cement–sawbone system was fixated at a position of 10° in adduction and 9° in flexion to the stem axis. The load was applied vertically to the femoral head in compression between 0.3kN and 2.3kN in the form of a sine wave to simulate the hip joint force during walking, the peak value of which is about 3BW (Bergmann *et al.* 1993), supposing that the average weight of a person is 75kg, figure 5.2. The wear simulation was performed at 3Hz for 5 millions cycles uninterruptedly, corresponding to approximately 5 years' *in vivo* wear of the femoral stem. Additionally, 9g/l saline solution was utilised to represent the environmental conditions in the human body, and a cylindrical plastic tube was attached close to the top of the steel tube in order to contain the saline solution, in which the stem–bone cement–sawbone system was immersed.

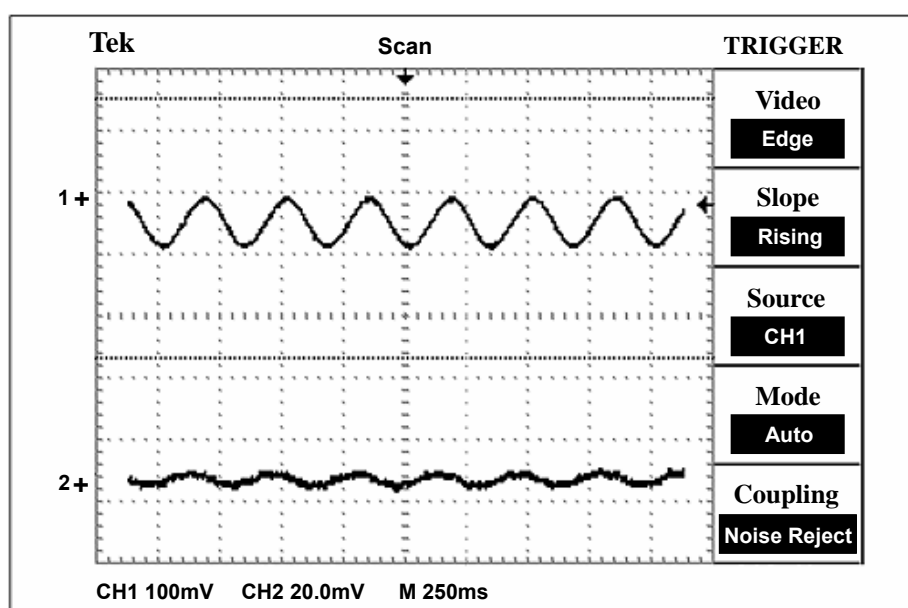


Figure 5.2: Oscilloscope displaying the sine wave force applied to femoral head (Channel 1) and the corresponding displacement of the experimental specimen (Channel 2) of Instron test machine

### 5.2.2.3 Analysis of test specimen before and after simulation

Quantification and analysis of fretting wear on the stem were conducted before and after wear simulation to detect any evidence of surface change, employing the Talysurf CCI interferometer at x20 magnification. Locations of surface measurement were determined through the utilisation of modified Gruen zones, as originally described by Gruen *et al.* (1979) for detailed review of anteroposterior radiograph of cemented femoral component. The definition of modified Gruen zones is shown in detail in figure 5.3, and it is a very useful tool to segregate the femoral stem into specific areas. Some selected 3D surface parameters—Sq, Sz, Sdq, and Sdr were calculated by the Surfstand software V3.3. A detailed explanation for these parameters is shown in table 4.3 and they were used to quantitatively assess fretting wear on the stem surface.

In addition to the measurements performed in each Gruen zone of the stem surface, some extra measurements were carried out with the assistance of a grid coordinate system, which could

relocate the position on the stem surface and enable comparison of the measurements pre and post simulation, figure 5.4. Firstly, the femoral stem was placed on a graph paper which was previously attached to the automated stage of the Talysurf CCI interferometer, and the contour of the stem was drawn along the perimeter of the stem. Then the measurement was performed on an area of interest on the stem surface, and the two coordinates of the position were recorded. After the simulation, the stem was placed back to the graph paper, matching as closely as possible to the contour that was drawn before. This enables a rough relocation of the femoral stem after wear simulation. A further fine relocation was achieved by precisely moving the automated stage to the coordinates recorded. The efficiency of this relocation system was validated by figure 5.5, which shows two measurements taken on the stem surface at different time using this system.

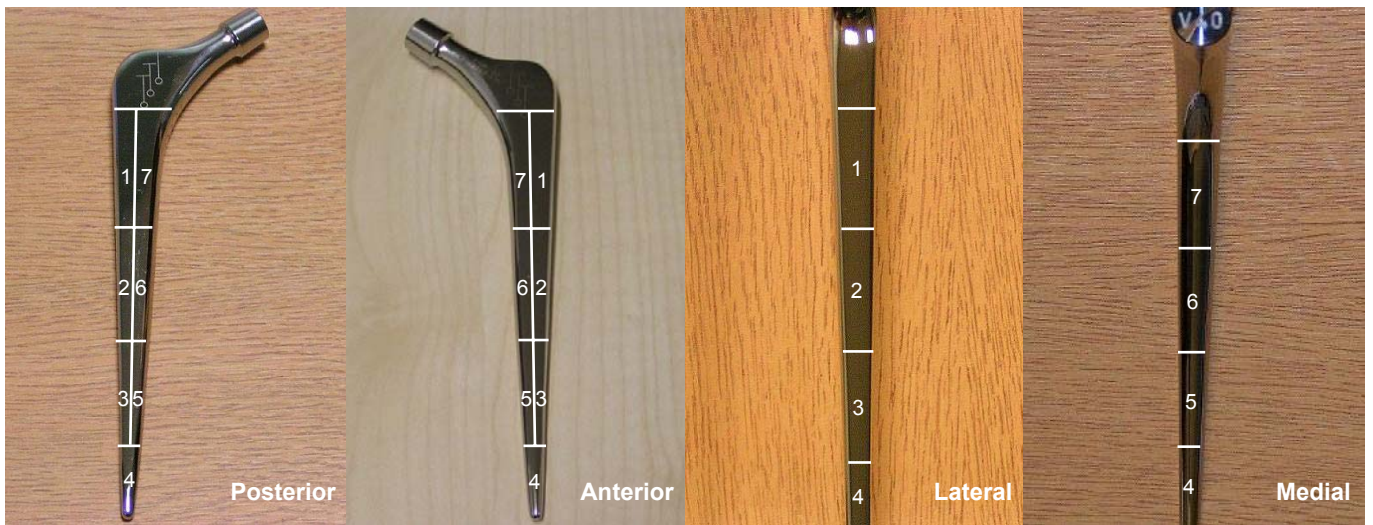


**Figure 5.3: Definition of Gruen zones of the stem surface**

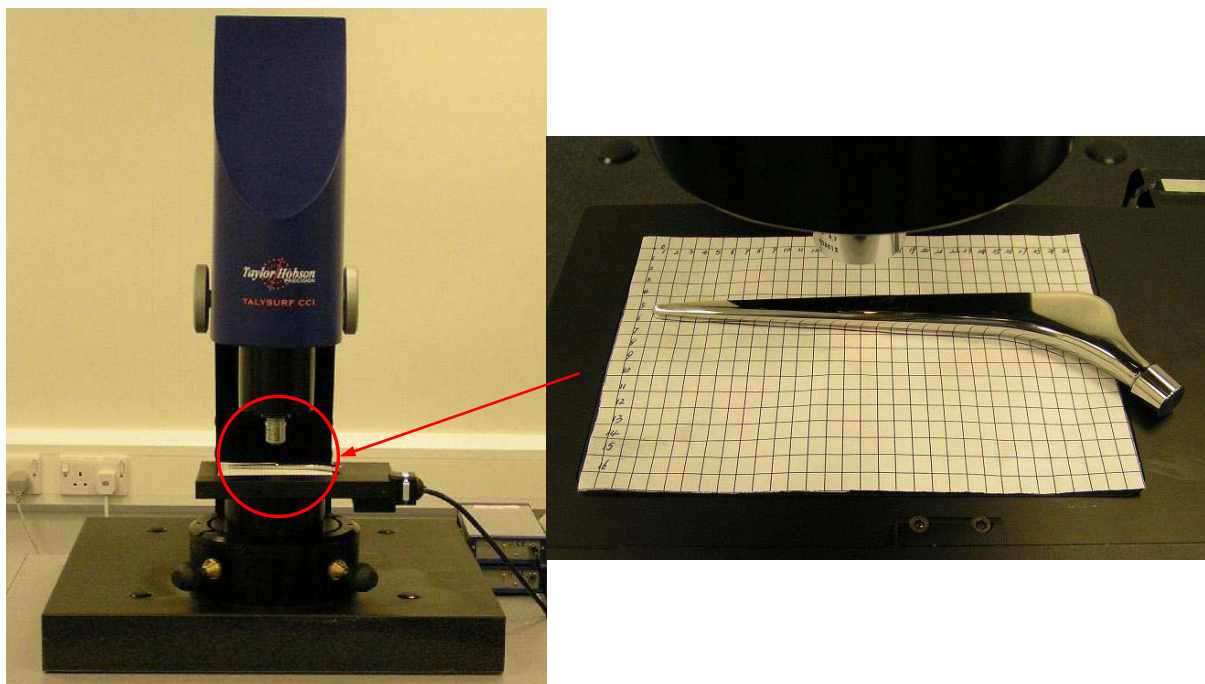


**Figure 5.4: The grid coordinate system to relocate the position of femoral stem**

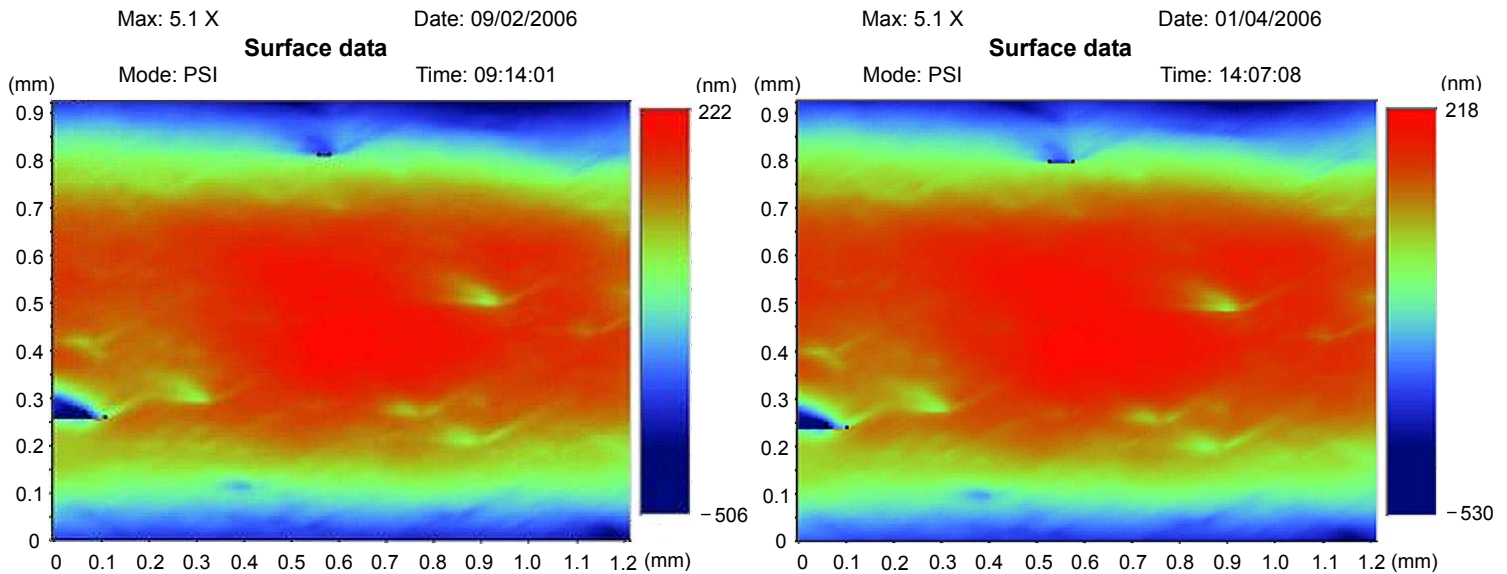


**Figure 5.5: Validation of the relocation system by two measurements taken at different time**

After the simulation, the femoral stem was cut into small pieces using a slitting wheel to facilitate observation of stem surface morphology employing the SEM JEOL JSM–6060. Additionally, the sawbone was sawn longitudinally into two equal parts to enable investigation of the bone cement surface, using the Talysurf CCI interferometer. Care was taken throughout all these procedures to ensure that the results would not be compromised. Subsequently, the bone cement was sectioned and gold-sputtered to facilitate an SEM study associated with an EDX analysis to detect any wear debris on the surface. Furthermore, both the femoral stem and the bone cement were investigated using the Leica optical microscope. This enabled a much larger area on the surface to be evaluated, which consequently may allow an insight into initiation and propagation of fretting wear on the stem to be gained. A summary of the instruments utilised in this study was given in table 5.1.

**Table 5.1: A summary of the instruments used to analyse femoral stem wear**

Instruments	Measurement area	Feature of interest
Talysurf CCI interferometer	0.9x0.9 mm <sup>2</sup>	Surface evaluation of femoral stem, with quantitative 3D surface parameters
SEM & EDX	0.35x0.3 mm <sup>2</sup>	Characteristics of fretting wear on the stem, and composition of wear debris
Optical microscope	6.5x4.5 mm <sup>2</sup>	Fretting wear areas on the stem and corresponding zones on the cement

### 5.2.3 Results

#### 5.2.3.1 Femoral stem

##### (1) Visual examination

The polished Exeter V40<sup>TM</sup> femoral stem was found to be firmly fixated in the cement mantle after simulation. Following cautious extraction from the cement mantle and cleaning with alcohol, the stem showed convincing evidence of worn areas on all the surfaces, figure 5.6. Generally, the worn areas were primarily concentrated on anterolateral, posteromedial, and under-neck zones of

the stem surface, which compared well with the results of retrieval studies (Cook 1998). The other areas were relatively smooth and appeared undamaged. These figures were then processed using Matlab software 6.5, and a programme was developed to identify the wear damage based on grey scale threshold, figure 5.7. The coverage of the worn areas in each Gruen zone was calculated as the ratio of the worn area to the area of each Gruen zone, and this was summarised in table 5.2. A similar method has been used previously to recognise micropores in the cement surface and to calculate porosity.

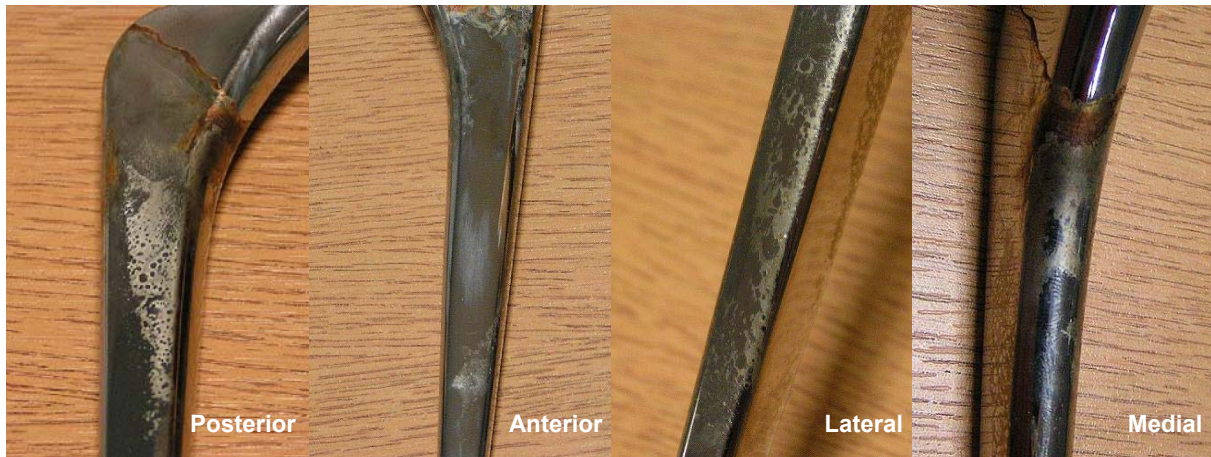


**Figure 5.6: Fretting wear generated on the femoral stem surface (Simulation I, use Simplex P cement)**

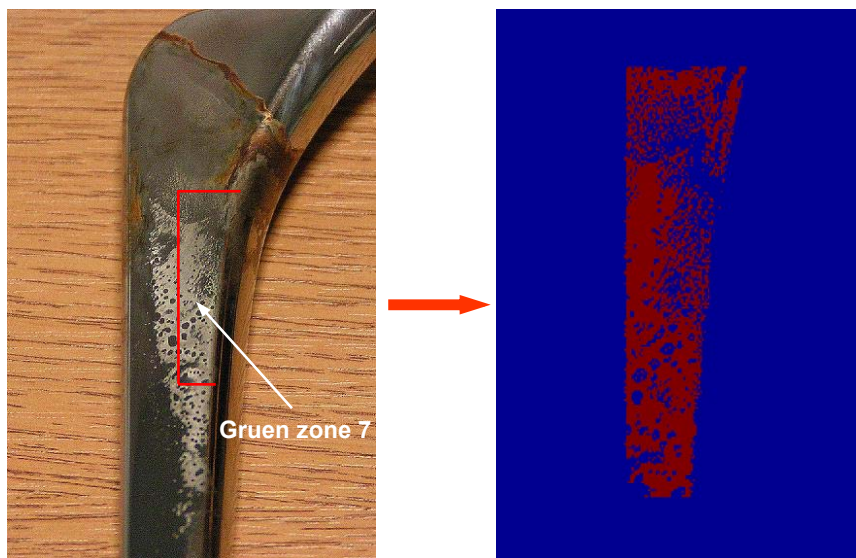


**Figure 5.7: Detection of worn areas on the stem surface based on grey scale threshold**

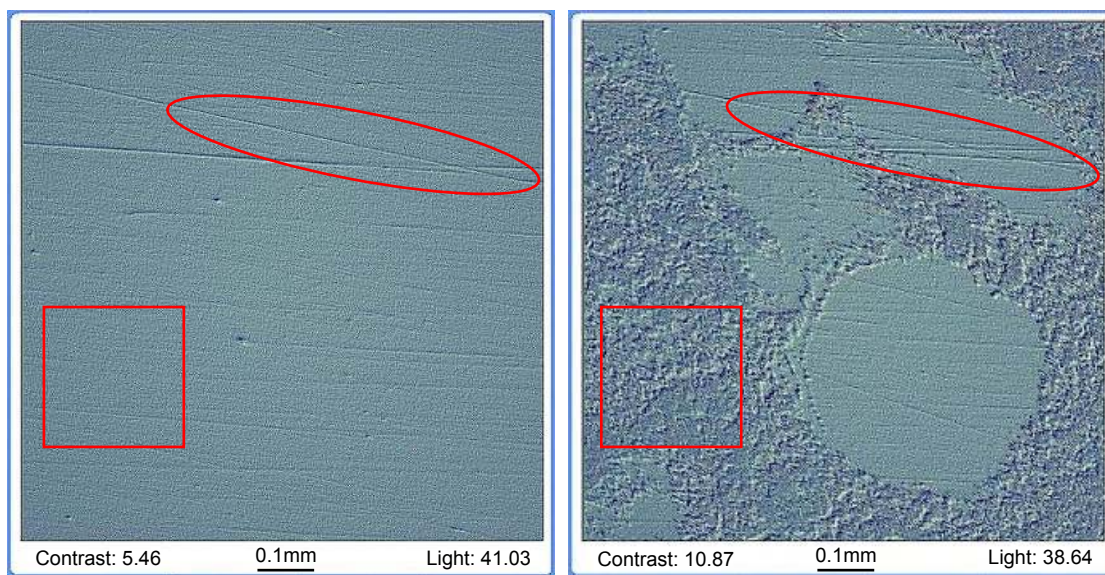
In addition, there was no evidence of formation of bone cement transfer films on the stem surface, although these transfer films were detected on the polished stainless steel rods in the previous pull out tests. It was considered that the transfer films would potentially be further removed as wear debris by the cyclical relative micromotion at the stem–cement interface even if they had been generated in the course of the wear simulation. Another reason could be attributed to the potential removal of the transfer films during the cleaning procedure of the stem. However, it was visually confirmed that there was no evidence of transfer films on the stem surface even before cleaning of the stem was performed.

**Table 5.2: Coverage of fretting wear area in each Gruen zone on the stem surface (%)—Simulation I, use Simplex P cement**

Stem surface	Posterior	Anterior	Lateral	Medial
Zone 1	60	0	10	
Zone 2	20	20	90	
Zone 3	0	30	10	
Zone 4	0	0	0	0
Zone 5	10	10		0
Zone 6	80	30		10
Zone 7	90	10		80

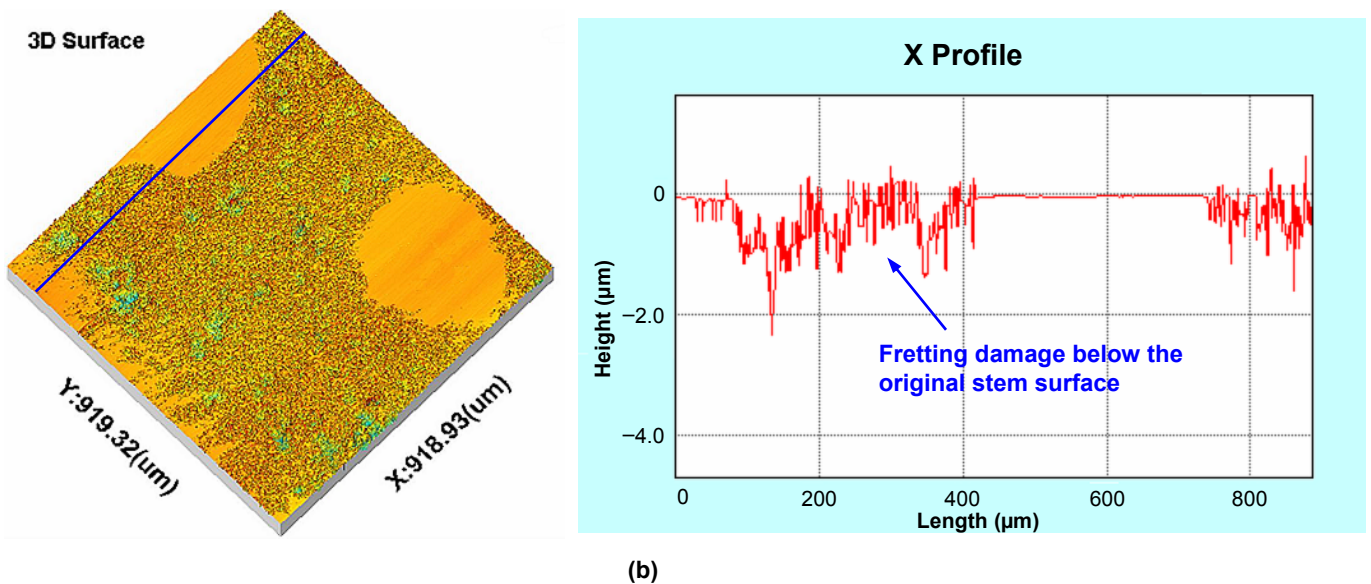
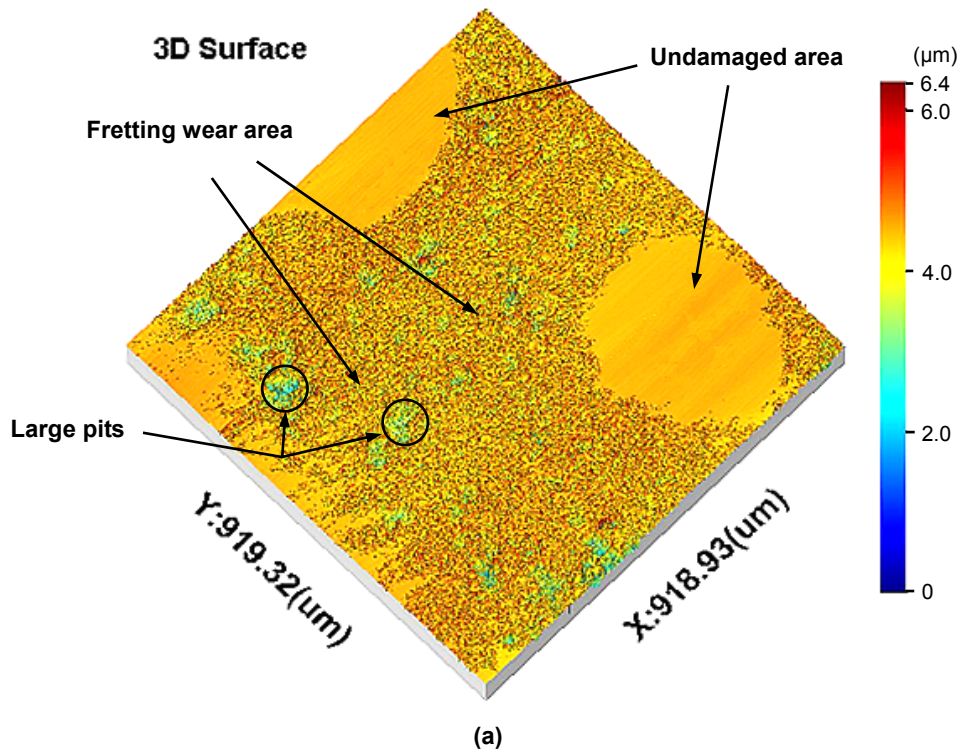
**(2) Optical interferometer evaluation**

Figure 5.8 shows the comparison of one position on the stem surface using the relocation system pre and post simulation, from which it is clear that some areas (shown in red square) are severely roughened by the fretting process at the stem–cement interface, whereas the other areas remained relatively unchanged (shown in red ellipse).



**Figure 5.8: Change of stem surface at the same position pre and post simulation (Simulation I, use Simplex P cement)**

As can be clearly seen from table 5.2, Gruen zone 6 and Gruen zone 7 on the posterior surface of the femoral stem illustrate evidence of the most severe of wear damage. Therefore, a total of 20 measurements were carried out for each of these two Gruen zones, utilising the Talysurf CCI interferometer. Figure 5.9 (a) shows one typical measurement performed in Gruen zone 6, which demonstrates clearly the comparison of surface topography between the worn area and the undamaged area. The worn area shows the formation of a number of relatively large pits in the stem surface, which is one typical characteristic of fretting wear. Figure 5.9 (b) demonstrates the 2D surface topography of the worn area, from which it can be confirmed that the wear damage occurred below the original stem surface, and this is another typical characteristic of fretting wear. Four more examples of surface measurement of the stem are provided in Appendix V.



**Figure 5.9: (a) Comparison of fretting wear area and undamaged area on the femoral stem (b) 2D surface topography of the worn areas (Simulation I, use Simplex P cement)**

Before calculating the selected 3D surface parameters of the worn areas, a thresholding process was applied to the raw data to remove some of the peaks above the baseline of the profile, which are considered to be potential particulate debris on the stem surface or measurement artefact in the form of spikes, figure 5.10. As stated by Engel and Klingele (1981), owing to the oscillatory micromotion of fretting wear, the particles generated are unable to escape from between the contacting surfaces and they may finally impress into the surface. The presence of these peaks may compromise evaluation of fretting wear as fretting wear actually occurs below the original stem surface, and in this case it was the fretting wear which was of explicit interest. The mean values of the 3D surface parameters are illustrated in figures 5.11–5.14, from which it can be seen

that the stem surface has changed greatly. The significant increase of  $S_q$ ,  $S_z$ ,  $S_dq$ , and  $S_{dr}$  all demonstrated that the femoral stem was much rougher after simulation.

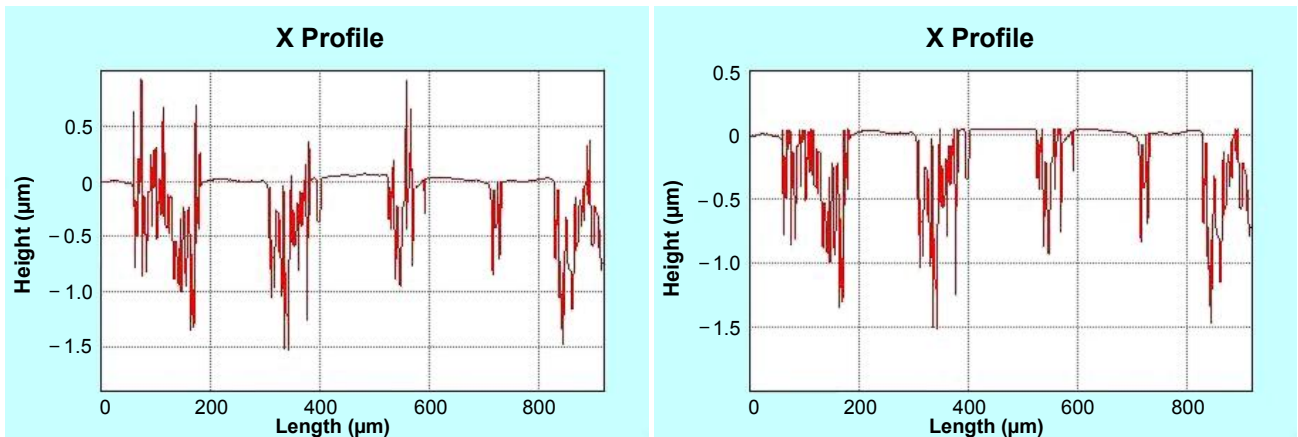


Figure 5.10: The thresholding process to remove potential wear debris above the original stem surface

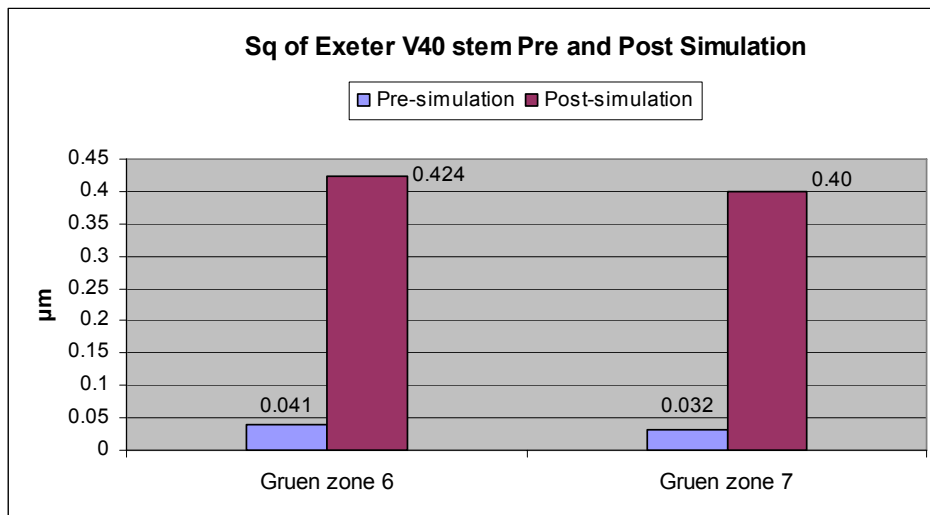


Figure 5.11: Histogram showing change of  $S_q$  pre and post simulation of selected area on the stem

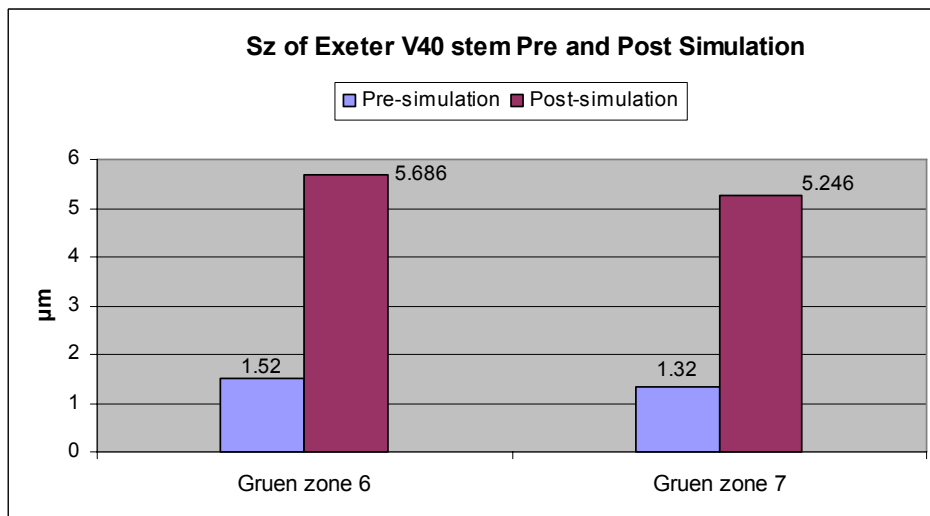


Figure 5.12: Histogram showing change of  $S_z$  pre and post simulation of selected area on the stem

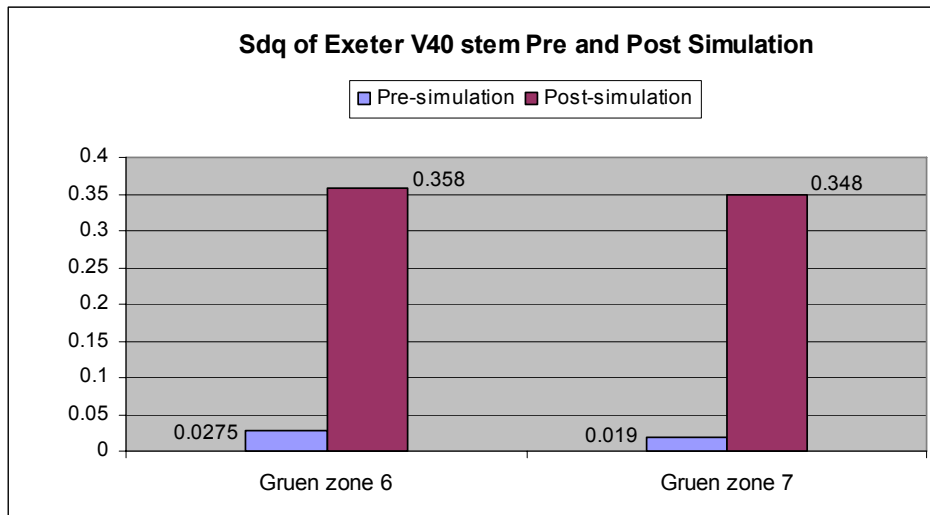


Figure 5.13: Histogram showing change of Sdq pre and post simulation of selected area on the stem

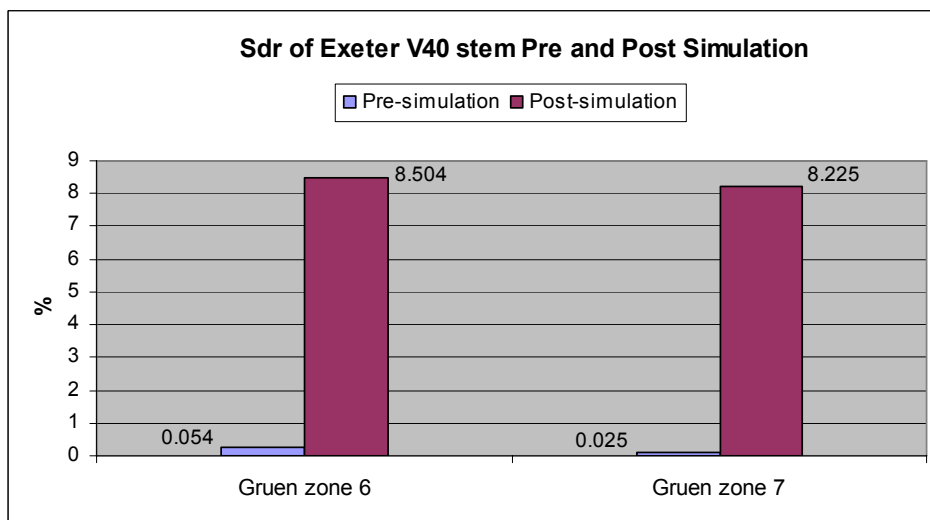
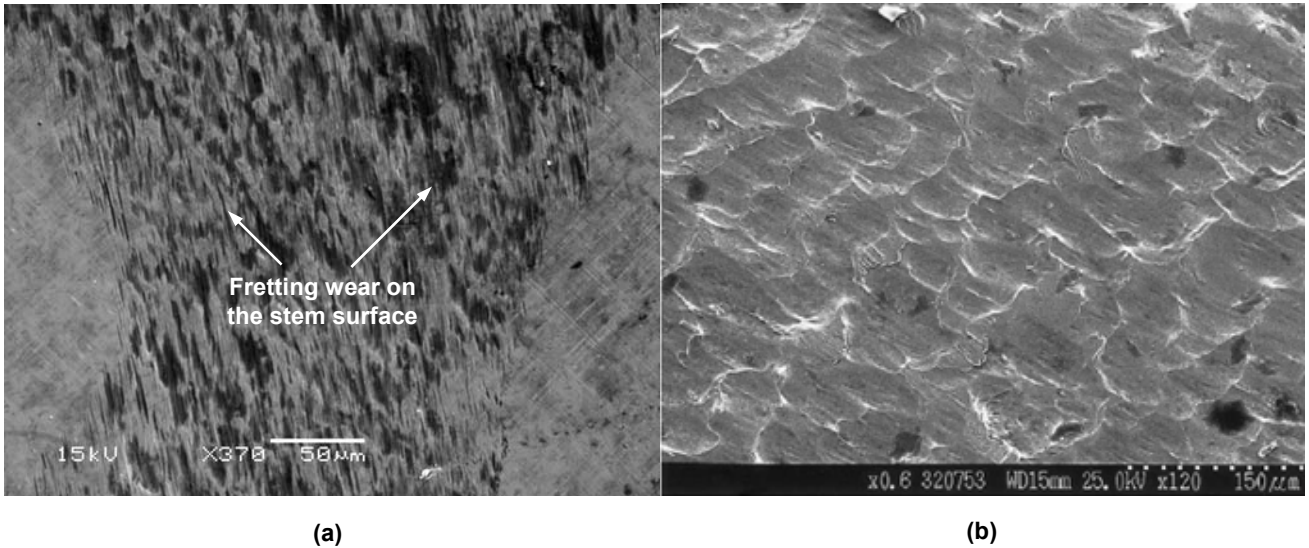


Figure 5.14: Histogram showing change of Sdr pre and post simulation of selected area on the stem

### (3) SEM assessment

Figure 5.15 displays the surface topography of the fretting zones on the femoral stem from the wear simulation and on an explanted Exeter stem derived from a retrieval study (Howell *et al.* 2004), both of which were measured using SEM. Note that these two micrographs are at optimal magnification of their own to show fretting effects. The similar pitting and crater features again confirmed that the wear reproduced on the femoral stem in the present simulation was fretting wear. Further evidence of SEM measurement can be found in Appendix VI.

The optical microscope examination of the femoral stem was given in the next section together with the bone cement.



**Figure 5.15: Comparison of fretting zones between (a) Simulated Exeter femoral stem and (b) Explanted Exeter femoral stem (Simulation I, use Simplex P cement)**

### **5.2.3.2 Bone cement**

#### **(1) Visual examination and optical interferometer evaluation**

It was shown from gross visual inspection of the bone cement that there were many micropores present in the cement surface, especially in the areas in contact with the fretting zones on the stem surface, and these areas seemed much rougher than the other areas, i.e. the cement surface also displayed differing wear severities, figure 5.16. Thus, a total of 20 measurements were performed on the “worn” and “unworn” areas, using the Talysurf CCI interferometer. The mean Sq values for these two areas were 0.21µm and 0.04µm respectively, which indicated that the “worn” areas were severely damaged during the fretting process.

#### **(2) SEM and EDX assessment**

The investigation of the cement surface using SEM demonstrated that there was an amount of fretting debris located in the micropores, figure 5.17 (a). From the corresponding EDX analysis, as shown in figure 5.17 (b), it was noted that neither an iron-rich (Fe) plaque nor a Cr-rich plaque was detected. This suggested that the debris was just cement particles rather than metal particles. This debris was potentially dislodged from the cement surface and then retained in the micropores during the simulation. Additionally, there were no fatigue cracks visible in the cement mantle.

#### **(3) Optical microscope examination**

In order to gain a better insight into initiation and propagation of fretting wear, the Exeter V40™ femoral stem and the Simplex P bone cement were further investigated utilising the Leica optical microscope. It was shown on the stem surface that some “undamaged islands” were surrounded by worn areas, which was in agreement with the result of the study performed by Cook (1998), figure 5.18 (a). Interestingly, these “undamaged islands” were found to correspond pretty well to the micropores in the cement surface, figure 5.18 (b). This indicated that these micropores might contribute to initiation and propagation of fretting wear on the stem surface. It is considered that

the differential stress distribution across the differing thicknesses adjacent to the edge of the micropores would facilitate interfacial micromotion of the bone cement relative to the femoral stem under physiological loading. This is essential to the generation of fretting wear on the stem surface.

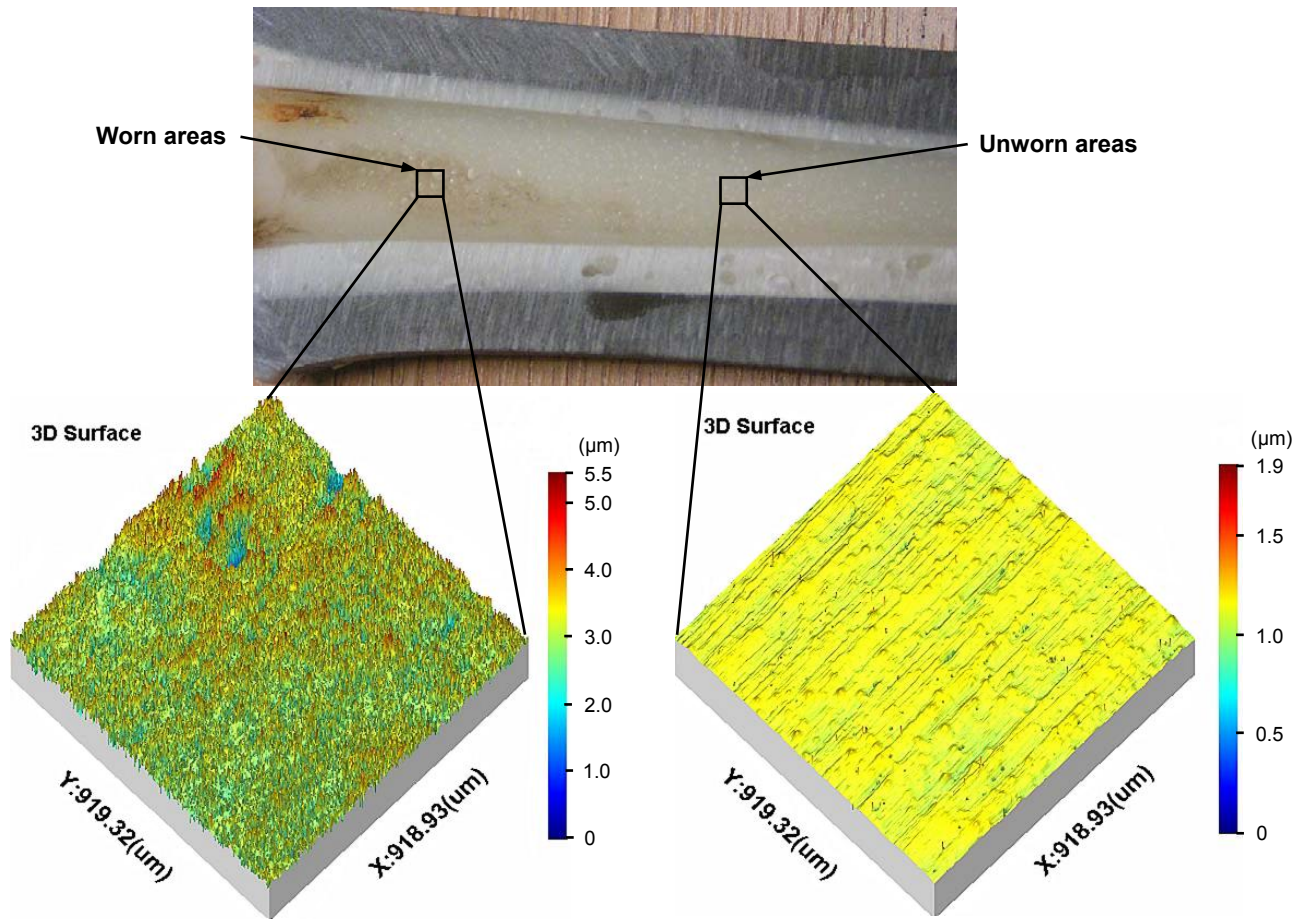


Figure 5.16: Comparison of worn and unworn areas on the Simplex P cement surface (Simulation I)

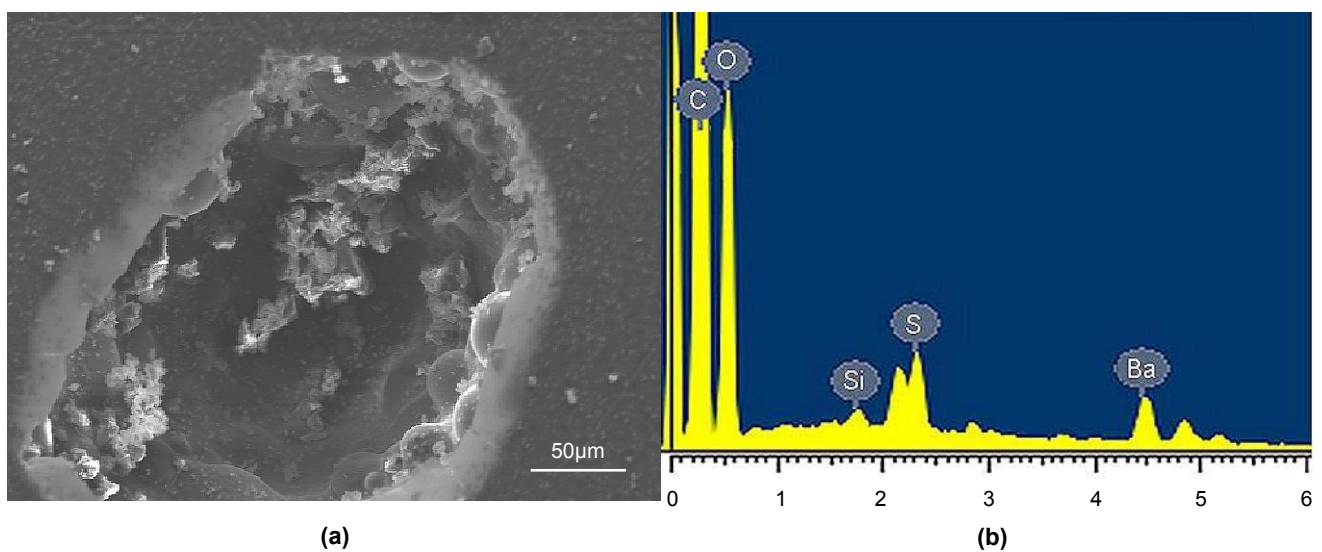
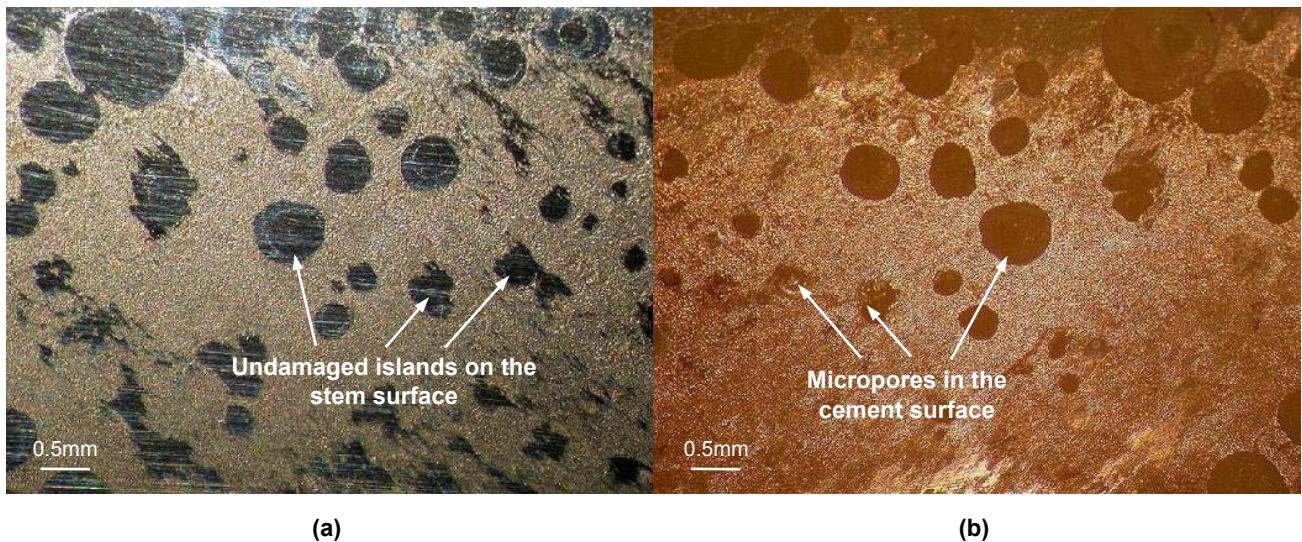


Figure 5.17: (a) SEM micrograph showing fretting debris located in the micropores (b) Corresponding EDX analysis (Simulation I, use Simplex P cement)



**Figure 5.18: (a) Optical micrograph showing “undamaged islands” on the stem surface and (b) Corresponding micropores in the cement surface (Simulation I, use Simplex P cement)**

#### 5.2.4 Discussion

In this study, fretting wear has been successfully reproduced at the stem–cement interface through an *in vitro* wear simulation, this was confirmed by the measurements performed using the Talysurf CCI interferometer and the SEM. The wear locations matched well with the results of retrieval studies, which also corresponded to the sites where the largest stress is considered to occur under physiological loading. Additionally, there were many micropores present in the cement surface. These micropores, which have been previously detected in the clinical situation, were considered to be formed during cement mixing, delivery and stem implantation process. They may lead to a decrease of the stem–cement interfacial bond strength, and act as stress concentrators to result in generation of fatigue cracks in the cement mantle. However, no fatigue cracks were observed in the present simulation. This to a certain degree was in contradiction to the results of retrieval studies, in which the formation of fatigue cracks in the cement mantle was detectable (Jasty *et al.* 1991, Maloney *et al.* 2002). This could be attributed to the relatively limited loading cycles carried out in the present simulation, and fatigue cracks may have occurred if the simulation had been continued. Furthermore, these cracks were regarded to act as potential channels to transport wear debris to the sites surrounding bone tissues, causing a macrophage response and subsequent aseptic loosening of the femoral component. Although the micropore-induced fatigue cracks were not detected in this study, these micropores in the cement surface were found to potentially contribute to initiation and propagation of fretting wear on the stem surface. It was considered that the stress distribution across those areas adjacent to the edge of the micropores was differential. This therefore would facilitate interfacial micromotion of the cement relative to the stem under physiological loading, which was a prerequisite for fretting wear. Taking this into consideration, the application of “modern cementing techniques”, typically vacuum mixing and centrifugation, could not only theoretically promote a larger bond strength at the stem–cement interface, but also retard initiation of fretting wear due to a significant reduction of porosity.

The cement surface was severely damaged in those areas in contact with the fretting zones on the stem surface, with retention of cement debris located in the micropores. However, it was indicated

in retrieval studies that metallic debris was embedded within the cement mantle, and the EDX analysis demonstrated a similar Cr-rich and Fe-rich plaque on the cement surface as was found on the stem surface (Walczak *et al.* 1998, Jones *et al.* 2005). The reason why no metallic debris was detected in the present study was probably due to the fact that the femoral stem utilised in this simulation is highly polished. Fretting wear for polished stems, unlike abrasive wear for matt stems, tended to result in less generation of metallic wear debris. This was suggested to be one rationale behind the success of polished stem design. In fact, the optimal surface finish of femoral stem has been debated for many years. There are many studies showing excellent long term results of cemented femoral stems using roughened femoral components (Sanchez-Sotelo *et al.* 2002, Meneghini *et al.* 2003). Conversely, the Exeter femoral stem incorporating a double tapered, collarless geometry with a polished surface which is designed to subside within the cement mantle to acquire re-stabilisation also demonstrated excellent long term survivorship (Williams *et al.* 2002). Although clinical studies have indicated that wear on the stem was mainly dependent on stem surface finish, there is no convincing *in vitro* evidence that has been gained to date to support it, and this therefore needs further study. Additionally, metallic debris may have been detected if the simulation had been running over a longer period.

It should be noted that the frequency was set at 3Hz in the present study to reduce test duration, whereas a frequency as high as 5Hz and as low as 0.75Hz has been utilised in previous studies (Maher *et al.* 2002, Cristofolini *et al.* 2003, Bader *et al.* 2004). High frequency is criticised as contributing to frictional heating at the stem–cement interface. This is not a crucial issue in the present study as the stem–cement–bone system was immersed in saline solution. However, the frequency of the simulation could have some effect on the results by influencing the re-passivation process of the stem surface. The stem–cement interface should experience a more severe fretting wear at a very high frequency due to the fact that there is not enough time for the stem surface to be re-passivated and consequently more unoxidised subsurface metal will be exposed to further fretting wear. However, it is considered that this influence is not significant in the present study, and the results are not greatly compromised.

There are several other limitations involved in this study. Firstly, the simulation was carried out without any rest period, as a result of which creep and stress relaxation in the cement mantle was to a certain degree prevented. Secondly, there was no temperature control during the simulation, whereas it has been reported that temperature has some effect on the creep performance of bone cement with a higher creep rate observed at body temperature (Liu *et al.* 2002). Thirdly, the distal centraliser was not used in this study, whilst it has been clinically employed when implanting an Exeter femoral stem to allow for subsidence and to accommodate creep. All of these limitations seem to correlate with the creep behaviour of bone cement, which may have some influence on the results. In general, creep of bone cement can result in relaxation of cement stresses and decelerates damage accumulation in the cement mantle. If creep and stress relaxation of bone cement is to some extent constrained, there will be more stress concentrations (probably around the micropores) in the cement mantle which would promote fretting wear at the stem–cement interface.

### **5.2.5 Conclusions**

The following conclusions could be drawn from this work:

- Fretting wear is successfully reproduced using a polished Exeter V40<sup>TM</sup> femoral stem and Simplex P bone cement, the wear locations compares well with the result of retrieval studies.
- There is no evidence of bone cement transfer films on the stem surface and no fatigue cracks in the cement mantle after simulation. However, there are prevalent micropores in the cement surface.
- The cement surface is severely damaged in those areas in contact with the fretting zones on the stem surface, with retention of cement debris located in the micropores.
- The micropores in the cement surface, which correspond to the “undamaged islands” on the stem surface, are considered to potentially contribute to initiation and propagation of fretting wear.

### **5.3 Consistent reproduction of fretting wear at the stem–cement interface (Simulation II)**

#### **5.3.1 Background and methods**

The initial wear simulation to replicate fretting wear at the stem–cement interface was considered successful. In order to validate the new test methodology proposed and to consistently reproduce fretting wear, another simulation was performed, utilising the same type of femoral stem and bone cement and under the same experimental conditions.

#### **5.3.2 Results**

##### **5.3.2.1 Visual and optical microscope examination**

In comparison with the previous simulation, the result showed similar wear locations on the stem surface but significantly different wear coverage. There were fewer worn areas generated in this new simulation, see the examples in Appendix VII. Although the stem surface was also dominated by plenty of “undamaged islands” with fretting zones circling around, these fretting zones did not form an entire worn area as seen in figure 5.18. Instead, the fretting zones seemed to be just initiated and only slight wear was apparent, figure 5.19 (a). No bone cement transfer films were observed on the femoral stem and no fatigue cracks were present across the cement mantle. Again, many micropores distributed along the cement surface and the edges of these micropores were found to match very well to the initial worn area generated on the stem surface, figure 5.19 (b).

Figure 5.20 gives another evidence to show the relationship between the micropore and the initial worn area, which further indicated the potential contribution of the micropores to initiate fretting wear on the stem surface. Figure 5.21 provided a third worn area with higher magnification, in which the initial damage on the stem surface appeared to be starting to propagate and form a larger worn area. As a consequence, this area was measured using the Talysurf CCI interferometer. The interferometric micrograph displayed the propagation of fretting wear more clearly, figure 5.22 (a). Note that the interference fringes around the “undamaged islands” indicated height deviations in these areas. In addition, the measurement was further processed by the Surfstand software V3.3, and its 2D surface topography indicated that those smooth areas with little variation in amplitude were the “undamaged islands”, connected by fretting zones occurring below the original femoral stem surface, figure 5.22 (b).

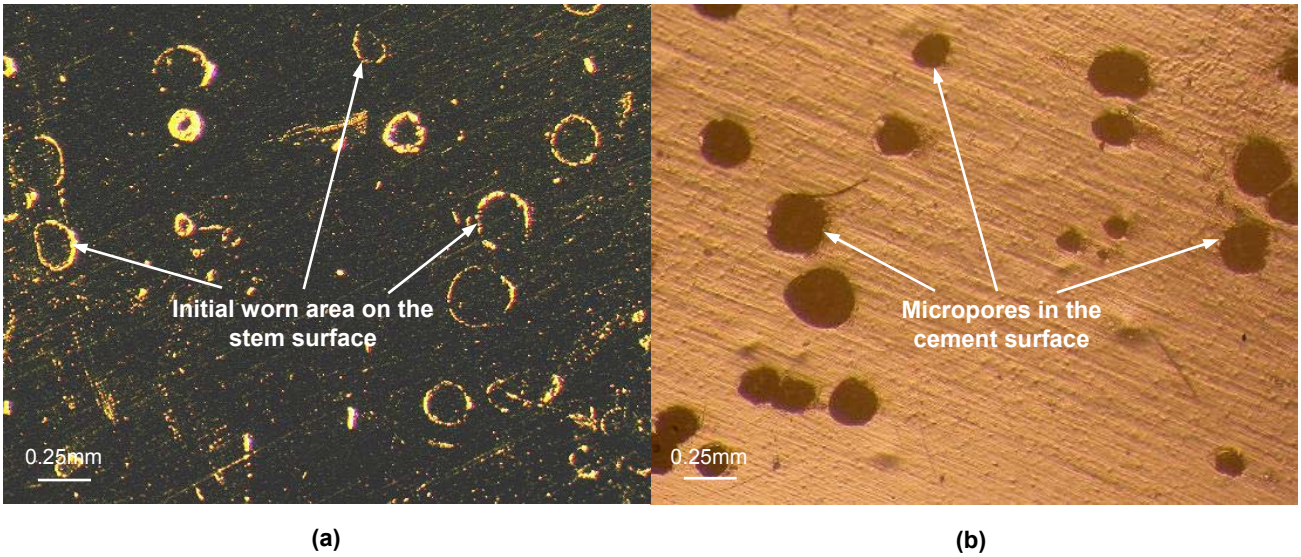


**Figure 5.19: Initiation of fretting wear on the stem surface and micropores in the cement surface (Simulation II, use Simplex P cement)**

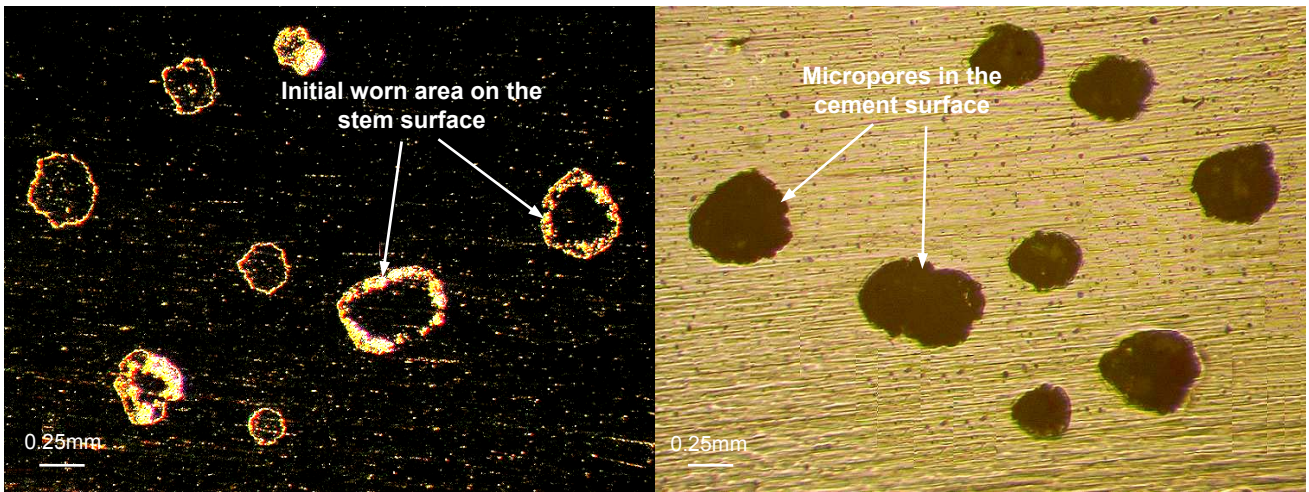


**Figure 5.20: Initiation of fretting wear on the stem surface and micropores in the cement surface (Simulation II, use Simplex P cement)**

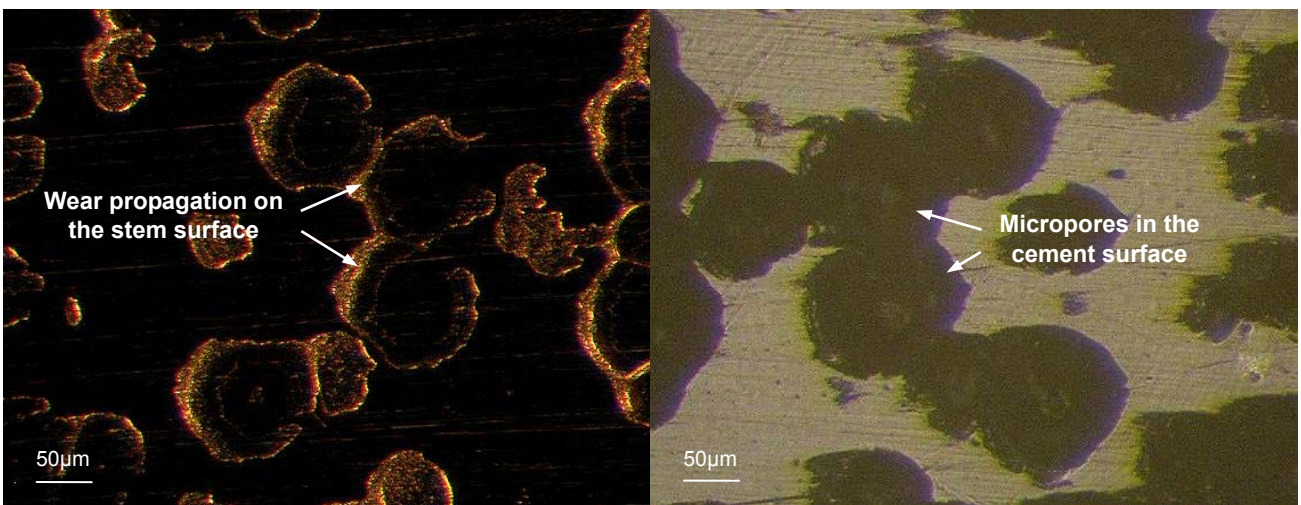
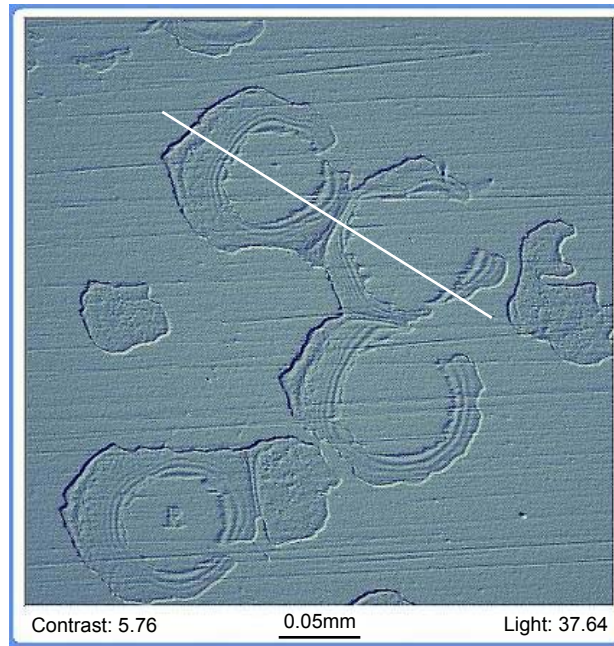
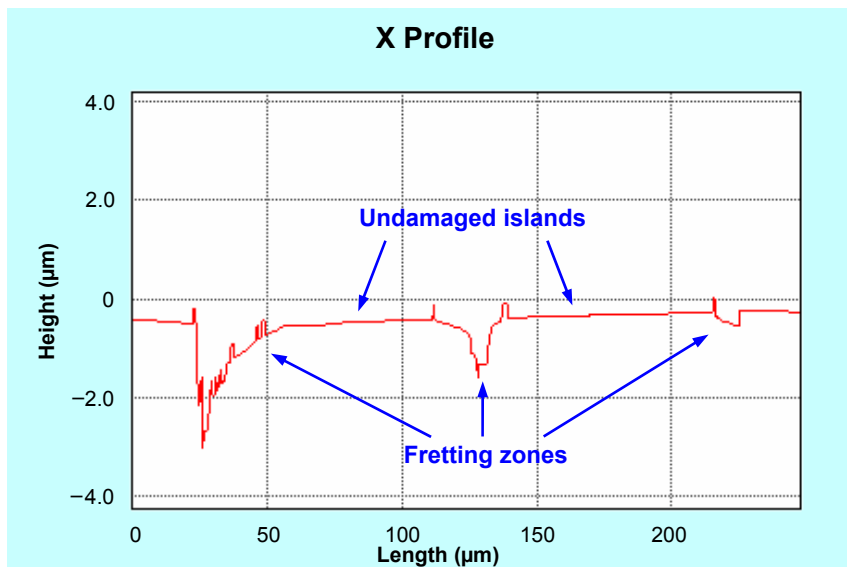


**Figure 5.21: Propagation of fretting wear on the stem surface and micropores in the cement surface (Simulation II, use Simplex P cement)**



(a)



(b)

**Figure 5.22: (a) Interferometric micrograph of the worn areas showing propagation of fretting wear on the stem surface (b) 2D surface topography of the worn areas (Simulation II, use Simplex P cement)**

All this evidence together indicated that fretting wear on the stem surface was probably initiated at those areas where the femoral stem was in contact with the edges of the micropores in the cement surface. The initial wear damage then propagated and coalesced with each other due to the relative micromotion at the stem–cement interface, and finally formed an entire worn area surrounding the “undamaged islands”. It was also noted that where the cement mantle contained large zones of pore-free contact, no wear was evident on the stem surface.

### 5.3.2.2 Position output of the experimental specimen

The maximum and minimum positions of the experimental specimen were recorded from the display of the front panel during the simulation and they are shown in table 5.3. From the table it is clear that although the values of the maximum and minimum positions varied with the number of loading cycle, the difference between them remained consistent, i.e. around 170 $\mu$ m.

**Table 5.3: The maximum and minimum positions of the experimental specimen—Simulation II, use Simplex P cement**

Loading cycle	Maximum position (mm)	Minimum position (mm)	Maximum–Minimum ( $\mu$ m)
16200	97.99	97.82	170
32000	98.28	98.12	160
45343	98.52	98.35	170
61555	98.70	98.53	170
75218	98.77	98.60	170
104145	98.79	98.62	170
259024	98.33	98.16	170
276090	98.30	98.14	160
294820	98.16	97.99	170
307652	98.10	97.93	170
326500	98.11	97.94	170
341770	98.11	97.94	170
360409	98.11	97.94	170
377230	98.10	97.92	180
514365	98.56	98.39	170
558548	98.53	98.37	160
592000	98.51	98.34	170
1250900	98.34	98.18	160
1280000	98.55	98.39	160
1328630	98.77	98.60	170

However, this difference was considered as neither the relative micromotion at the stem–cement interface nor the movement between the bone cement and the specimen fixture, or a combination of these two factors. Actually, it was just the elastic deformation of the experimental system under the applied compressive loading. These data were further illustrated in figure 5.23, from which it can be seen that the maximum and minimum positions demonstrated some periodical tendency as the loading cycle increased. This was potentially caused by the change of temperature of the experimental environment as well as the accumulative heat released by the Instron machine during the wear simulation. This change was detected by the sensor and further influenced the output of the position. Although the invariable difference between the maximum and minimum positions of the experimental specimen was to some extent insignificant, it could confirm that the experimental specimen was well stabilised by the acrilite resin otherwise the difference would become larger and larger with the increase of loading cycle, e.g. the stem–cement–sawbone system subsides within acrilite resin.

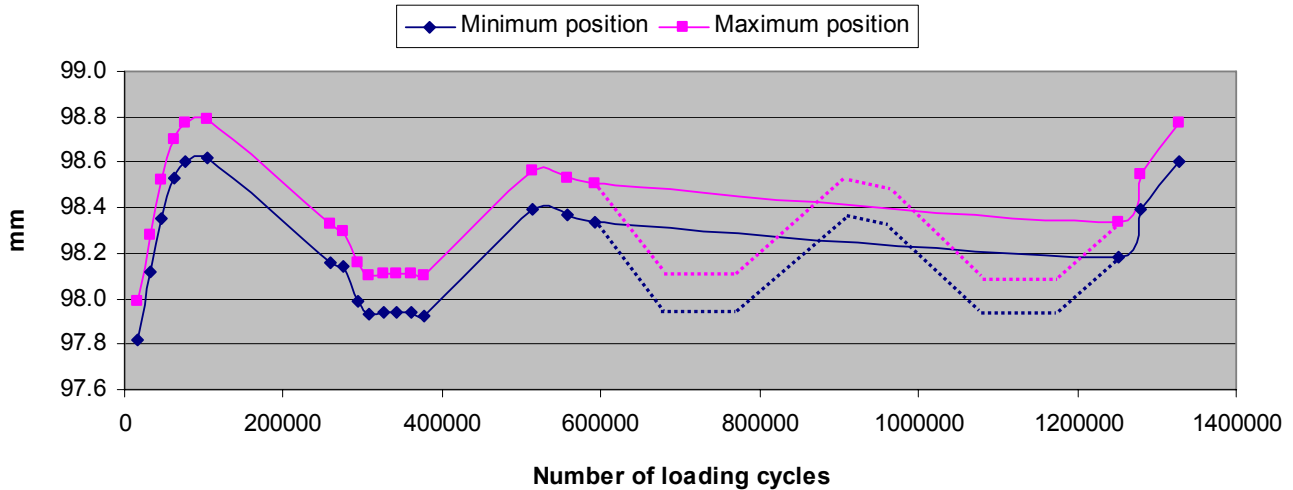


**Figure 5.23:** The maximum and minimum positions of the experimental specimen, note that the dashed line is fitted according to the tendency of the data (Simulation II, use Simplex P cement)

### 5.3.3 Discussion

Extensive porosity at the stem–cement interface was firstly reported by James *et al.* (1993) based on a study of a multiplicity of *in vivo* and *in vitro* specimens, and later on its presence was further confirmed in retrieval studies (Eliades *et al.* 2003). Although Hernigou *et al.* (1999) concluded from their investigation on survivorship of a series of cemented femoral components that porosity only made a minor contribution to the durability of bone cement mantle, vacuum mixing and centrifugation have been widely employed in surgery when mixing bone cement, with the aim of reducing porosity at the stem–cement interface. It has been demonstrated that a marked reduction in the rate of aseptic loosening of femoral component has been achieved by utilising improved cementing techniques (Mulroy and Harris 1990, Barrack *et al.* 1992), typically distal plugging and retrograde filling, etc. However, these techniques could not necessarily result in porosity reduction, and consequently the better clinical outcome probably might not be correlated with reduction of interfacial porosity.

In this study, the micropores in the cement surface were indicated to contribute significantly to initiation and propagation of fretting wear on the stem surface. These micropores, in combination with the regime of physiological loading during patient normal activities, may fundamentally determine the wear locations and wear severities. This is considered the first time that evidence has been provided to highlight the importance of micropores in the cement surface to contribute to femoral stem wear. As a matter of fact, femoral stem wear is a crucial issue and it has not been completely understood until now with regard to how this wear is initiated. It has been previously postulated that shrinkage bumps on the cement surface may act as potential participant to promote femoral stem wear (Brown *et al.* 2001). These bumps, about 50 $\mu\text{m}$  in width and 1–2.5 $\mu\text{m}$  in height, are formed due to shrinkage of bone cement following polymerisation, figure 5.24. Therefore, the stress distribution along the stem–cement interface under physiological loading would be mainly concentrated at these areas. However, it was indicated from this study that the function of the shrinkage bumps was insignificant in comparison with the micropores.

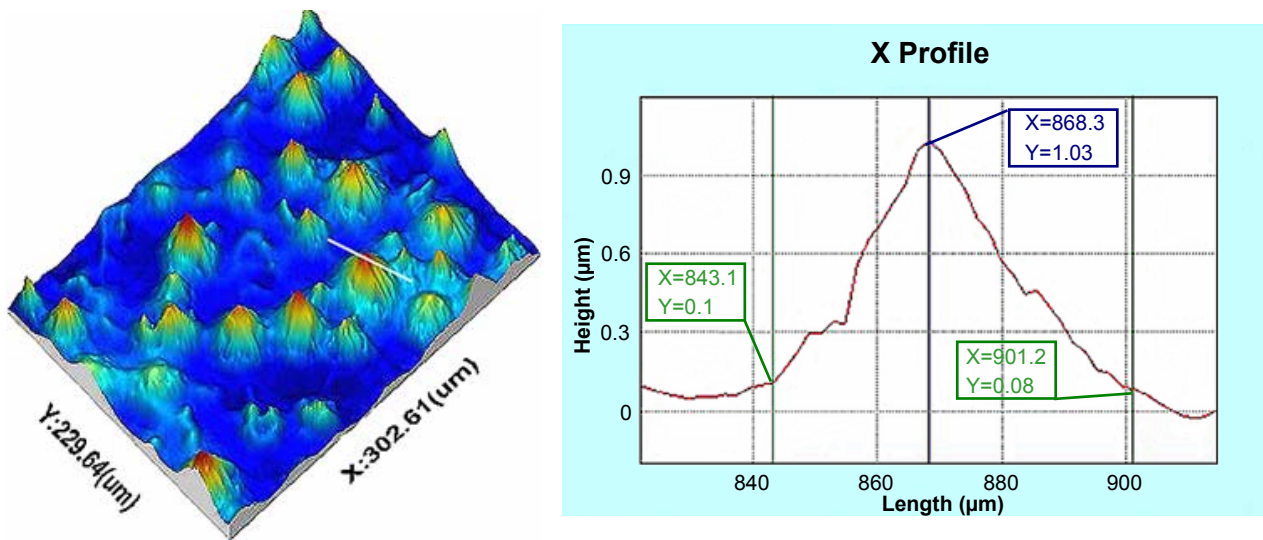


**Figure 5.24: Shrinkage bumps on the cement surface following polymerisation and its 2D profile**

It has to be mentioned that the wear severities of the two simulations were significantly different. Generally, the test materials and experimental conditions were the same, with the only difference being that the Simplex P bone cement used in the first simulation was almost expired with a long storage time whilst the one used in the second simulation was brand new. It is considered that variations in physicochemical stability of bone cement may develop over time during storage, and this potentially influences its long term performance which further modifies the characteristics at the stem–cement interface and results in different wear severities on the stem surface.

**5.4 Summary of the *in vitro* wear simulations**

Fretting wear at the stem–cement interface has been successfully and consistently reproduced through *in vitro* wear simulations, utilising polished Exeter V40<sup>TM</sup> femoral stems and Simplex P bone cement. It has shown great progress in comparison with previous investigations. Therefore, this gives scope for further comparative studies of the influence of stem geometry, stem surface finish, and bone cement brand on generation of fretting wear, which is considered to be significant and essential to evaluate various femoral stem designs and bone cement brands on the market. Additionally, the micropores in the cement surface were suggested to play an important part in initiating and propagating fretting wear on the femoral stem, which contributes to gaining a deep insight into the development of fretting wear at the stem–cement interface.

## Chapter 6 Relative micromotion at the stem–cement interface

### 6.1 Chapter summary

As it has been demonstrated that debonding at the stem–cement interface was inevitable, a low-amplitude relative micromotion would therefore occur at this interface upon physiological loading. This is considered as the prerequisite for the generation of fretting wear. Theoretically, the term “fretting” denotes a small oscillatory movement between two solid surfaces in contact, in a range typically from 1µm to 100µm (Hutchings 1992). Although fretting wear has been successfully and consistently reproduced on polished Exeter femoral stems through *in vitro* wear simulations, the value of the relative micromotion at the stem–cement interface and whether it is within the typical range of movement for fretting are unclear. Consequently, this chapter aims to gain an insight into this issue through a further simulation and the parallel development of a new sensor to measure migration of the femoral stem within the cement mantle.

It was demonstrated that migration of the polished Exeter femoral stem within Simplex P bone cement generally went up as the number of loading cycle increased, with a gradual decrease of migration rate. This is considered to be consistent with clinical situations. A total migration of about 50µm was obtained at the end of the simulation. Additionally, following examination of the femoral stem and the bone cement using both optical microscopy and optical interferometry, the potential significance of the micropores in the cement surface in generation of fretting wear on the stem surface was again confirmed. This was further highlighted by the fact that no damage was observed on the femoral stem where the areas were in contact with the pore-free zones on the bone cement. This present *in vitro* simulation has gained an insight into the migration behaviour of the polished Exeter femoral stem within the cement mantle.

### 6.2 Investigation of relative micromotion at the stem–cement interface (Simulation III)

#### 6.2.1 Background and aims

The rationale of cemented THR is to transfer physiological loading of the human body through the hip prosthesis to the femur with preferable stabilisation. However, migration of cemented femoral stem has been extensively reported in clinical studies (Kiss *et al.* 1996, Alfaro–Adrián *et al.* 1999), and it was indicated to correlate with aseptic loosening of the femoral component and early failure of the whole joint system (Walker *et al.* 1995). It is considered that migration of the stem within the cement mantle is the long term accumulation of the relative micromotion at the stem–cement interface, which results in generation of fretting wear on the stem surface. It is therefore a valuable parameter to gain an insight into the wear mechanism at the interface.

Clinically, RSA has been comprehensively utilised to measure migration of the femoral stem with an accuracy of a few tenths of a millimetre, and it was demonstrated that the stem migrated very rapidly in the early stage after operation (Alfaro–Adrián *et al.* 2001). Using this method, however, the data obtained is relatively limited, i.e. the data is sequentially recorded with an interval of several months. Accordingly, an alternative method, i.e. *in vitro* testing, has been attempted by other researchers, in which an extensometer or a linear variable differential transformer (LVDT) is usually employed to give instant output (Burke *et al.* 1991, Maher *et al.* 2001, Cristofolini *et al.* 2003). It is considered that several million cycles of loading is generally required to evaluate the

stem performance utilising the *in vitro* testing method. However, the tests in these studies either used static loading or were completed at relatively limited cycles. Additionally, the experimental materials and testing methodology were totally different from what was proposed in Chapter 5. Therefore, it is worth a venture to investigate migration of the polished Exeter femoral stem within the cement mantle, based on the *in vitro* wear simulation previously developed.

## 6.2.2 Materials and methods

### 6.2.2.1 Development of a new custom-made sensor

In the present study, a new custom-made sensor was developed to measure migration of a polished Exeter V40™ femoral stem within Simplex P bone cement mantle. The basic configuration of the sensor includes a strain gauge, and a stainless steel frame which was fabricated through electrical discharge machining (EDM), figure 6.1 (a). The frame has two legs, and they will be connected to the stem and the cement respectively. One surface of the frame was cleaned for attachment of the strain gauge utilising M-Bond 200, which is an adhesive certified for use in bonding strain gauge. Enough long wires were soldered to the strain gauge for output in a Model P3 strain indicator and recorder.

The rationale for the new sensor to measure relative micromotion at the stem–cement interface is based on deformation of the strain gauge, as shown in figure 6.1 (b). The leg of the stainless steel frame connected to the cement remains stable, and when debonding at the stem–cement interface occurs under the compressive loading, the stem will subside within the cement mantle. The shape of the frame therefore changes and the strain gauge deforms, resulting in the change of output in the strain indicator and recorder. Consequently, the output correlates with migration of the femoral stem.

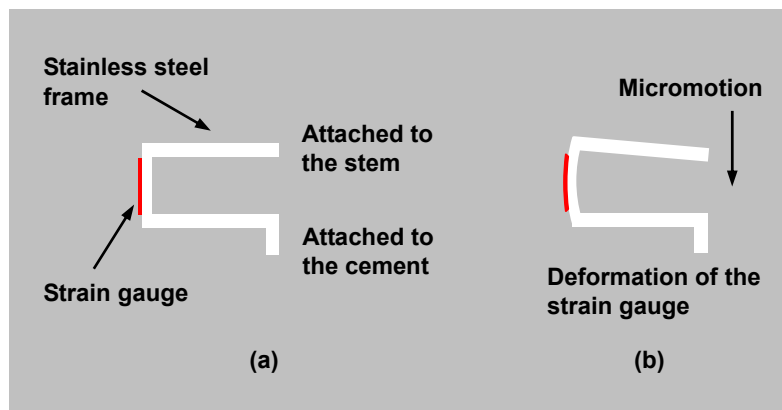


Figure 6.1: The schematic diagram showing the principle of the micromotion sensor

### 6.2.2.2 Calibration of the new custom-made sensor

The new micromotion sensor was calibrated using an extensometer before being connected to the stem and the cement, figure 6.2. The extensometer has a resolution of  $4\mu\text{m}$ . The strain indicator and recorder was firstly balanced to zero when there is no deformation for the stainless steel frame. Then an incremental micromotion of  $4\mu\text{m}$  was applied to the upper leg of the frame until a total micromotion of  $400\mu\text{m}$  was reached. The output of the strain indicator and recorder was recorded,

see Appendix VIII, and the data obtained was fitted into a curve using linear least squares analysis, figure 6.3.

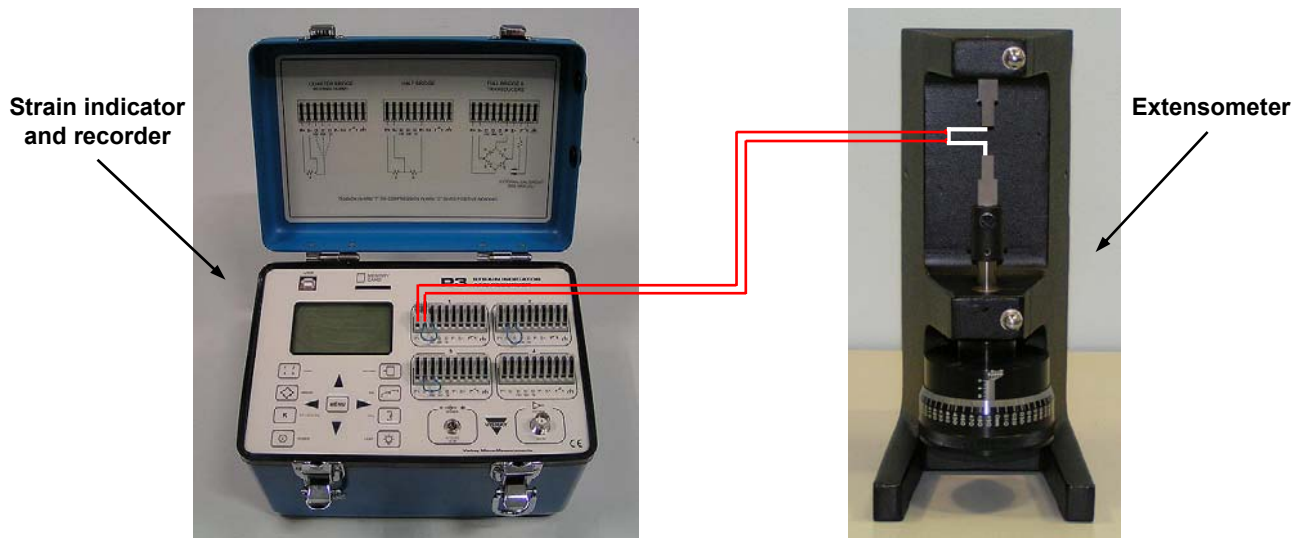


Figure 6.2: Calibration of the micromotion sensor using the extensometer

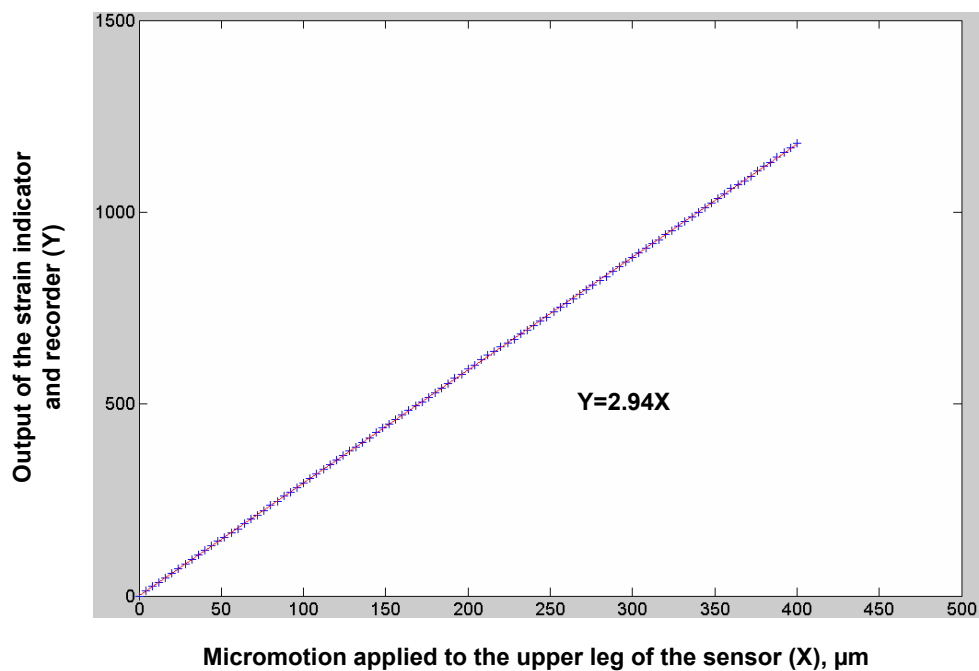


Figure 6.3: The curve (shown in red line) fitted using least squares analysis based on the recorded data (shown in blue +)

### 6.2.2.3 Experimental setup

Employing a polished Exeter V40<sup>TM</sup> femoral stem and Simplex P bone cement (brand new), a new simulation was performed under the same experimental conditions as described in detail in Chapter 5. The only difference was that a slot was made at the neck of the stem to connect with the upper leg of the micromotion sensor using super glue. Additionally, another groove was cut in the bone cement to connect with the lower leg of the micromotion sensor. This was followed by

application of another small dose of Simplex P bone cement to fill up the interspaces between the groove and the lower leg of the sensor, ensuring that the lower leg keeps stable in the cement mantle during the simulation. The experimental specimen is shown in figure 6.4.

In order to make sure the strain gauge works properly in saline solution, a circuit board lacquer was daubed on the surface of the strain gauge for several courses to prevent potential corrosion. It was also applied to the slot at the neck of the femoral stem. The strain indicator and recorder was balanced again before the simulation was started at 3Hz for a duration of 5 million cycles.

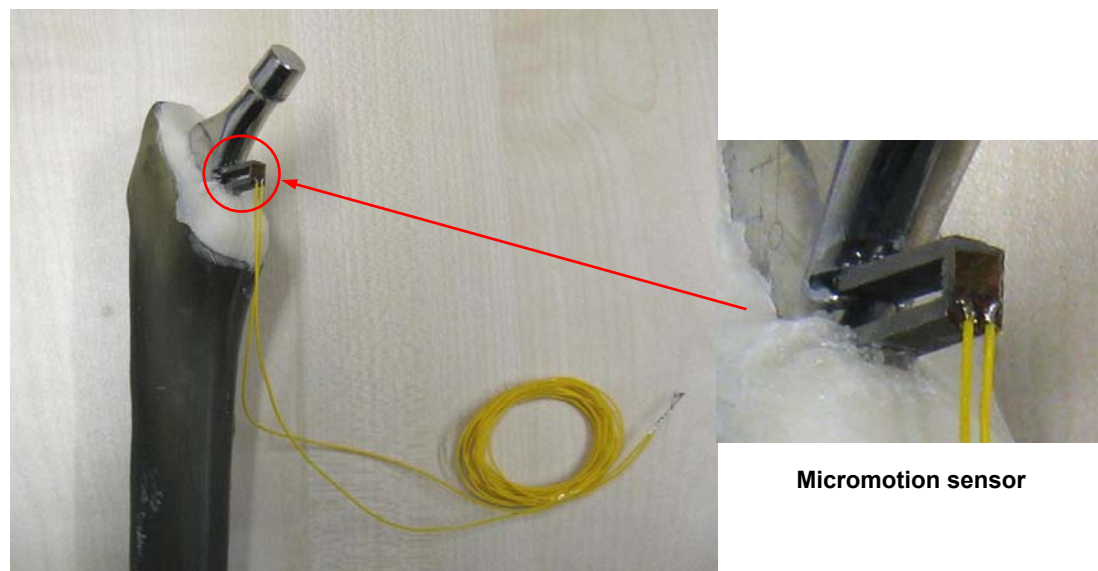


**Figure 6.4: The experimental specimen prepared for the present simulation**

## **6.2.3 Results**

### **6.2.3.1 Migration of the polished Exeter stem within the cement mantle**

According to the features of the strain indicator and recorder, the display update rate is 2Hz, i.e. 2 readings per second. Because the simulation is performed at 3Hz, the first reading from the strain indicator and recorder thus corresponds to the maximum value (2.3kN) of the compressive loading, and the second reading represents the minimum value (0.3kN) of the compressive loading of the next cycle. As a consequence, the display of the strain indicator and recorder shows a high output and then a low output alternately.

All of the maximum value readings and the minimum value readings were recorded with the increase of loading cycle. The femoral stem was preloaded at 0.3kN and 2.3kN respectively prior to the simulation, and the corresponding output were subtracted from the maximum and minimum readings of the strain indicator and recorder recorded during the simulation as it is considered that the preload reading was caused by the bending effect of the stem but not due to subsidence. The strain output was subsequently converted to micromotion based on the calibration result of the sensor. The simulation was somehow stopped at 3.4 million cycles, and it was restarted after a short period until another 1.6 million cycles of loading were completed continuously.

Migration of the polished Exeter stem within the cement mantle is displayed in figure 6.5. It was demonstrated from the figure that the curves corresponding to the maximum and the minimum

compressive loadings show a similar tendency, i.e. migration of the stem generally went up with the increase of loading cycle. A peak value of about  $48\mu\text{m}$  was achieved before the simulation was stopped indeliberately at 3.4 million cycles, and the migration value to some extent decreased after the simulation was restarted. One potential reason for this could be due to the creep behaviour of bone cement. It is considered that the femoral stem tends to move upwards a little following creep of bone cement and this therefore results in a pseudo small decrease of the output of the strain indicator and recorder. Additionally, the influence of environment temperature on the output of the strain indicator and recorder could also contribute to this decrease in the figure. However, the migration value increased again until a second peak value of about  $52\mu\text{m}$  was obtained when the simulation was completed at 5 million cycles. Furthermore, it was noted that the migration rate decreased with the increase of loading cycle.

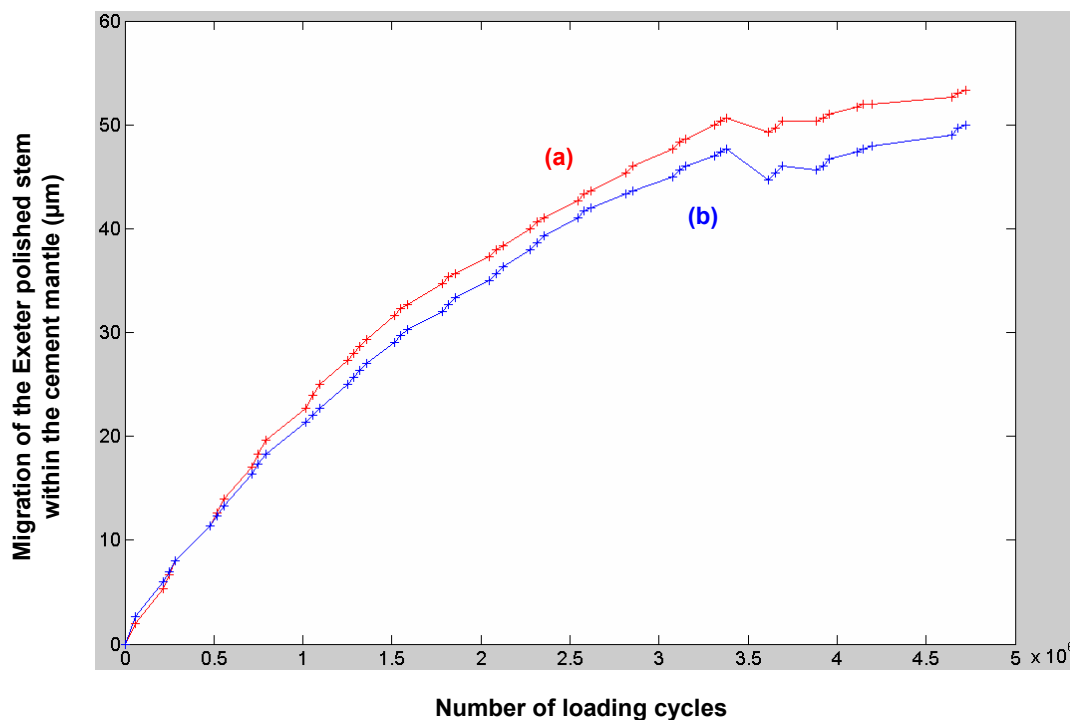


**Figure 6.5:** Migration of the polished Exeter stem within the cement mantle, the curves (a) and (b) correspond to the maximum and minimum values of the compressive loading respectively

### 6.2.3.2 Assessment of the femoral stem and the bone cement

The polished Exeter femoral stem was extracted from the cement mantle after 5 million cycles loading was completed, and the sawbone was sawn into two parts to enable investigation of the cement surface. The results were quite similar to that of simulation II. There was clear evidence of generation of fretting wear on the stem surface, with similar wear locations and wear severity, i.e. fretting wear seemed to be just initiated and did not form an entire worn area. Figure 6.6 shows the wear scars with fretting pits about  $4.6\mu\text{m}$  in depth, measured by the Talysurf CCI interferometer. In addition, no bone cement transfer films were observed on the stem surface.

An amount of micropores were present in the cement surface, and the potential significance of these micropores in initiation of fretting wear on the femoral stem was further identified. The edges of the micropores matched quite well to the initial fretting damage on the stem, figure 6.7.

The cement surface with the presence of micropores appeared very rough, corresponding to the worn areas of the stem surface. The other areas were smooth and no damage was detected. The femoral stem in contact with these areas also displayed a smooth surface with no occurrence of fretting damage, figure 6.8. Note that blue ink was daubed across the cement surface to obtain a picture with more contrast. This indicated that fretting wear on the stem surface could be greatly reduced or even eliminated through an effective control of porosity at the stem–cement interface. Furthermore, there was no generation of fatigue cracks across the cement surface.

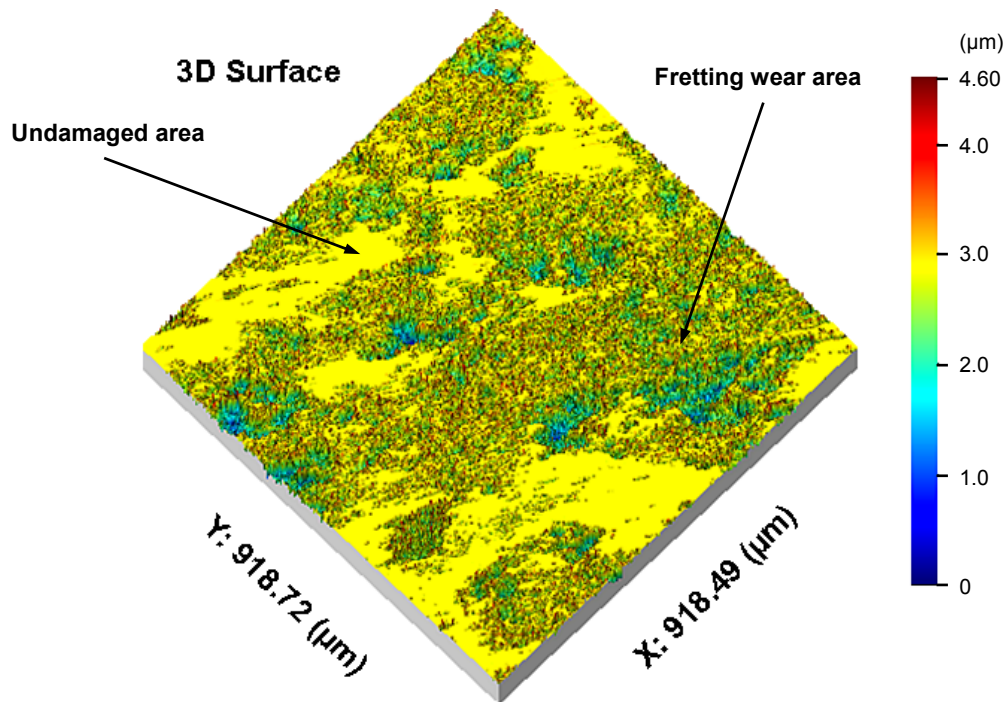


Figure 6.6: Generation of typical fretting pits on the femoral stem surface (Simulation III)

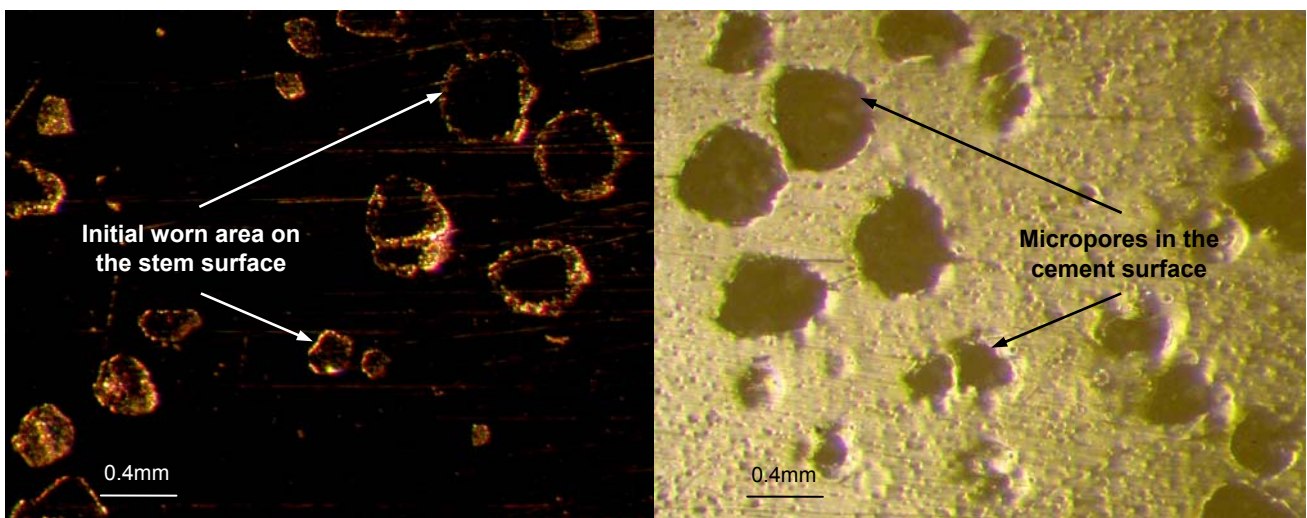
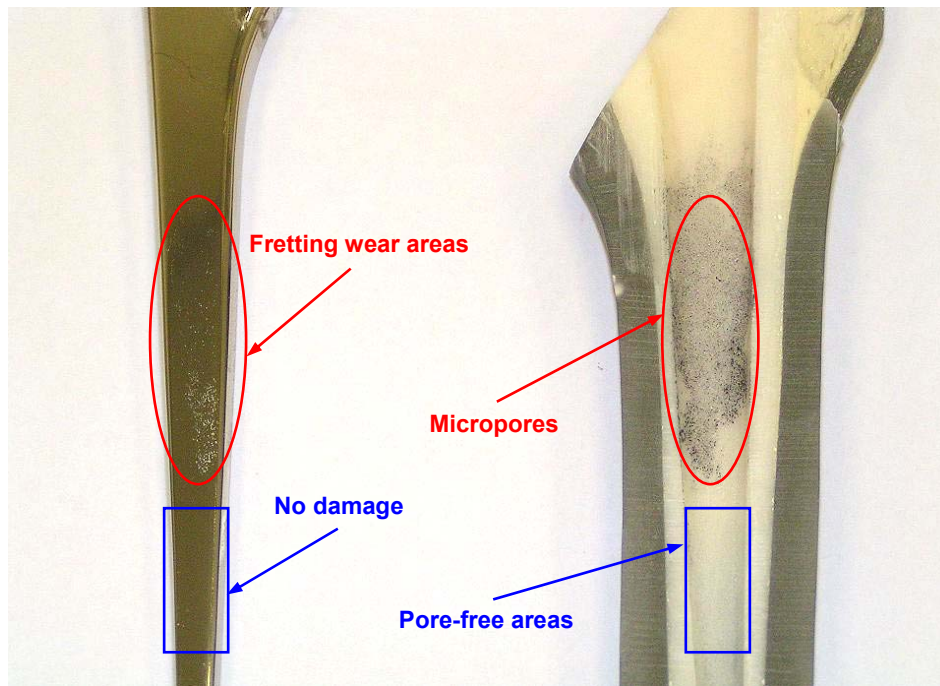


Figure 6.7: Initiation of fretting wear on the stem surface and micropores in the cement surface (Simulation III)



**Figure 6.8: The femoral stem and bone cement surfaces after simulation demonstrating an evident relationship between fretting wear damage and unworn areas on the stem surface and corresponding contact areas on the cement surface (Simulation III)**

#### 6.2.4 Discussion

It has been demonstrated from both *in vivo* clinical studies and *in vitro* experimental simulations that debonding at the stem–cement interface may be inevitable, regardless of stem geometry and surface finish (Jasty *et al.* 1991, Wang *et al.* 2003). As a consequence, a low-amplitude oscillatory micromotion is supposed to occur at this interface, which acts as a prerequisite for generation of fretting wear on the stem surface. As nowadays femoral stem wear is showing an increasing significance in the overall wear of cemented THR (Zhang *et al.* 2008), it is considered useful to gain an insight into the relative micromotion between the femoral stem and the bone cement. The long term effect of relative micromotion at this interface is shown in terms of migration of the stem within the cement mantle, and clinically there is a body of RSA studies available reporting the migration of cemented femoral component (Walker *et al.* 1995, Alfaro–Adrián *et al.* 1999). However, very few experimental studies have been performed, largely owing to the great difficulty of simulating physiological loadings *in vitro*, and also the problems of detecting minute movements. Employing electrical displacement transducers, Burke *et al.* in 1991 evaluated the initial stability of seven cemented femoral stems within the femoral canals of cadaver femurs during simulated single limb stance and stair climbing. The micromotion between the prosthesis and the bone was reported to be about 42 $\mu$ m and 76 $\mu$ m respectively for these two cases. However, the value of the micromotion at the stem–cement interface is unknown. As they used collared femoral components which are “force closed design”, it seemed reasonable to assume that the micromotion primarily occurred at the cement–bone interface. Additionally, Maher *et al.* in 2001 designed a micromotion device to measure migration of cemented Lubinus SP II femoral stem (Waldemar Link, Hamburg, Germany) relative to the composite femur. They applied cyclical sinusoidal loads (0.2–1.8kN) at a frequency of 10Hz for two million cycles, and observed a rapid

initial migration, followed by a period of steady-state migration. A distal migration up to 100 $\mu$ m was reported at the end of the test, but again it was not clear as to the micromotion between the femoral stem and the bone cement. In 2003, Cristofolini *et al.* investigated the micromotion at the stem–cement interface employing the LVDT. A compressive loading between 275N and 1683N was applied on the stem at 0.75Hz for one million cycles. They reported in their study markedly different migration curves for two stem designs, with the maximum migrations being 43 $\mu$ m for Lubinus SP II stem and 172 $\mu$ m for Muller curved stem (Sulzer, Winterthur, Switzerland). However, the results in these studies were to some extent compromised as either only static loading was applied or the test was completed at relatively limited cycles. Additionally, different results were expected because various types of femoral stem and testing methodology were utilised.

In the present study, a new micromotion sensor was developed based on deformation of the strain gauge, and it was demonstrated that migration of the polished Exeter femoral stem within the cement mantle went up with the increase of loading cycle. It showed a relatively higher migration rate in the first one million cycles, and then it decreased to some extent in the rest of the loading cycles. This finding is consistent with the clinical observations, from which it was demonstrated through the use of RSA that the femoral stem migrated rapidly at the early stage after implantation (Kiss *et al.* 1996, Alfaro–Adrián *et al.* 2001). However, these studies also reported migration of the stem relative to the bone. Kiss *et al.* evaluated cemented Hinek components (Corin Medical, Cirencester, UK) with a series of ridges in the metaphyseal region in their study. Considering the design of the stem is to prevent movement at the stem–cement interface, they assumed that the rapid early stem migration (up to 0.94mm in the first year) mainly occurred at the cement–bone interface, and they attributed it to resorption of the bone layer injured by surgical trauma and the heat generated during polymerisation of bone cement. In addition, Alfaro–Adrián *et al.* in 2001 investigated the migration behaviour of cemented Charnley Elite stem (DePuy International Ltd., Leeds, UK) and Exeter stem (Howmedica International Ltd., London, UK). They concluded that with the Charnley Elite stem there was migration at both the stem–cement interface and at the cement–bone interface, whereas with the Exeter stem migration occurred at the stem–cement interface (up to 1mm in the first year). In this present study, migration of the polished Exeter stem was found to be about 50 $\mu$ m when the simulation was completed at 5 million cycles. This value is a lot less than that obtained from clinical studies, and there are several potential reasons for this. One could be due to the relatively reduced loading level, which primarily represents walking activity but does not include other activities where much higher loadings are involved, e.g. stair climbing and running. Secondly, migration of the stem is suggested to be facilitated with the presence of stem–cement interfacial porosity, incomplete cement mantles, and cement fractures (Verdonschot and Huiskes 1997a). These were very common in clinical situations, but in the present study only an amount of micropores were detected in the cement surface, which may not greatly facilitate migration of the stem. Additionally, the 5 million compressive loading cycles were almost applied continuously, whereas normally patients have alternative periods of activity and rest. In the rest period, stress relaxation of bone cement can occur, reducing the constraining capacity of the cement mantle and allowing for further migration of the stem once the stem is re-loaded. However, it was surprising to note that the migration value decreased to a certain degree after restart of the simulation due to indeliberate interruption. This is considered to be potentially caused by creep of bone cement, which promoted a small movement of the femoral stem in the

upward direction and consequently the output of the strain indicator and recorder still decreased when the simulation was restarted.

One thing that needs to be mentioned is migration of the polished Exeter femoral stem within the cement mantle occurred at an early stage of the simulation, and it suggested that the stem–cement interface debonded shortly after the beginning of the simulation. Furthermore, the micropores in the cement surface were again found to potentially promote initiation of fretting wear on the stem surface. This was further confirmed by the fact that where the stem surface was in contact with pore-free areas on the cement surface, no evidence of fretting damage was detected. Consequently, in order to control generation of fretting wear on polished femoral stem, methods can be attempted to reduce porosity at the stem–cement interface, e.g. vacuum-mixing the cement, centrifugation, pre-heating the stem, etc.

### **6.2.5 Conclusions**

The following conclusions could be drawn from this work:

- A new micromotion sensor based on deformation of strain gauge is developed to investigate the relative micromotion at the stem–cement interface.
- Migration of the polished Exeter femoral stem within Simplex P bone cement mantle goes up as the number of loading cycle increases, with a gradual decrease of migration rate. This is considered to conform to clinical studies.
- The femoral stem migrates up to 50µm after 5 million cycles of compressive loading, and it seems that the increasing tendency of migration with the rise of loading cycle still continues.
- The micropores in the cement surface potentially promote generation of fretting wear on the stem surface.

### **6.3 Summary**

In this chapter, migration of a polished Exeter femoral stem within Simplex P bone cement mantle was investigated through the use of a micromotion sensor newly developed based on deformation of strain gauge. The results demonstrated a general increase of migration with the rise of loading cycle, in spite of a gradually decreasing migration rate. After the completion of 5 million cycles of compressive loading, a total migration value of approximately 50µm was obtained at the stem–cement interface. Although this value is far less than that reported in RSA studies, it is considered that the current experimental setup could more realistically mimic clinical situations, and it further validates the effectivity of the wear simulation.

## Chapter 7 Factors influencing fretting wear on the femoral stem

### 7.1 Chapter summary

The new test methodology showed great success in reproducing fretting wear on polished femoral stems, it therefore allowed for comparative studies to be performed to investigate the contributory factors to generation of fretting wear. It is considered that many participants are involved in this critical issue, e.g. femoral stem geometry, femoral stem surface finish, the duration of hip implant in the human body, and bone cement brand, etc. However, there are many stem designs currently available on the market, and consequently it is extremely difficult to test them one by one. Also, much work needs to be performed before the exact surface level that differentiates fretting wear and abrasive wear can be determined. Accordingly, these two factors will be investigated in future studies and in this chapter the duration of hip implant in the human body and bone cement brand were studied.

Firstly, the influence of the duration of *in vivo* service of the hip prosthesis was investigated. This was accomplished by extending the wear simulation to 10 million loading cycles whilst keeping other experimental conditions unchanged. Again, fretting wear was successfully replicated on the stem surface, and it was further noted that metallic wear debris was dislodged from the femoral stem, congregating around the micropores in the cement surface. Additionally, the initiation of micro-cracks was detected at the edge of the micropores. These findings were not observed in the previous simulations with 5 million cycles.

In the second part, the influence of bone cement brand was investigated utilising two more bone cements in addition to Simplex P, i.e. CMW 3 and Palacos R. The potential contribution of the micropores in the cement surface to generation of fretting wear on the stem surface was further identified through these simulations. In addition, the presence of metallic wear debris was detected around the micropores for these two bone cements, although all of the simulations were completed at 5 million loading cycles. Furthermore, the Vickers microhardness (HV) of the bone cements was measured, and it seemed that this factor did not correlate with generation of wear debris at the stem–cement interface.

### 7.2 Influence of the duration of *in vivo* service of the hip prosthesis on generation of fretting wear (Simulation IV)

#### 7.2.1 Background and methods

Previously, it is generally accepted that one million cycles of *in vitro* wear simulation simply represent one year's *in vivo* wear of the femoral stem (Zahiri *et al.* 1998). However, this number has been suggested to be underestimated as nowadays cemented THR is also performed on many younger and more active patients, as a result the hip joint is expected to experience excessive loading due to the increased activity level. According to a study carried out by Silva *et al.* (2002), the average walking activity of patients with a well-functioning THR approached closely to about 2 million cycles per year. Obviously, the duration of *in vivo* service of the hip prosthesis has an effect on the survivorship of cemented THR, and a lower survivorship has been reported for long term follow up of Charnley stems in comparison with short term and median follow up (Vázquez *et al.* 2006). However, few studies have been performed to date to investigate the influence of the

duration of *in vivo* service of the hip prosthesis on generation of fretting wear on polished femoral stem. Therefore, this present study aims to gain an insight into this issue by performing a further *in vitro* wear simulation with 10 million loading cycles whilst keeping the other test conditions unchanged. The Simplex P bone cement used in this study was also brand new.

## 7.2.2 Results and discussion

### 7.2.2.1 Femoral stem (visual and optical interferometer examination)

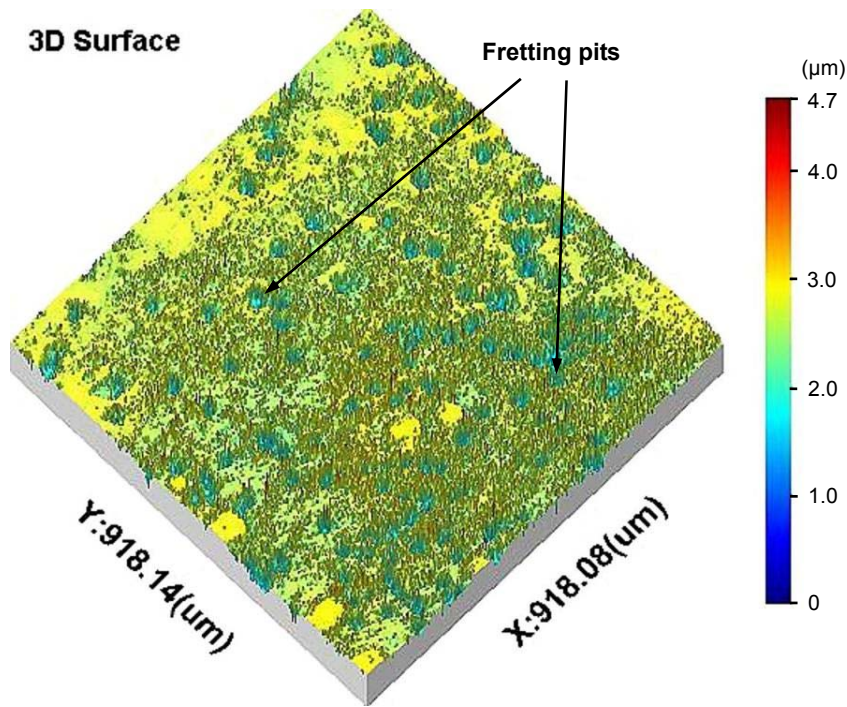
Again, the Exeter V40™ femoral stem demonstrated evidence of fretting wear on all the surfaces and the wear locations compared well with the results of retrieval studies, figure 7.1. Similarly, the coverage of fretting wear in each Gruen zone was calculated on the basis of grey scale threshold, using the same method as described in Section 5.2.3, table 7.1. The fretting wear was much more severe in terms of coverage area than that of both simulation II and III, but still less than that of simulation I. Figure 7.2 shows one typical measurement of the worn area on the stem using the Talysurf CCI interferometer, which clearly delineates the presence of some fretting pits on the surface. These fretting pits may potentially be caused by fretting corrosion or crevice corrosion due to development of an acidic environment at the stem–cement interface, which would facilitate the corrosion process.



Figure 7.1: Fretting wear generated on the femoral stem surface (Simulation IV, use Simplex P cement)

Table 7.1: Coverage of fretting wear area in each Gruen zone on the stem surface (%)—Simulation IV, use Simplex P cement

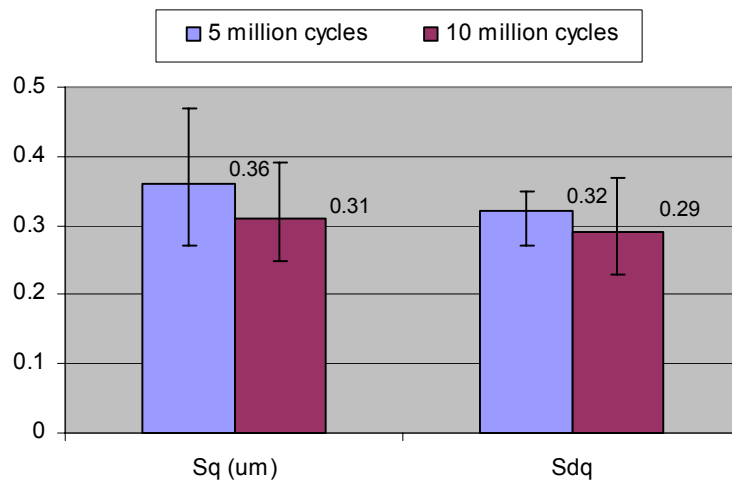
Stem surface	Posterior	Anterior	Lateral	Medial
Zone 1	20	40	30	
Zone 2	0	0	0	
Zone 3	10	0	0	
Zone 4	0	0	0	0
Zone 5	10	0		0
Zone 6	20	0		0
Zone 7	80	20		30



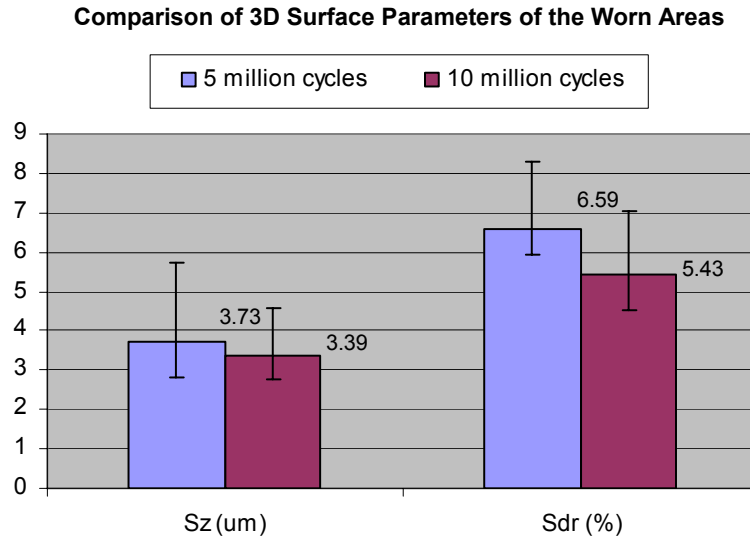
**Figure 7.2: Talysurf CCI measurement of worn areas on the stem surface (Simulation IV, use Simplex P cement)**

A total of 10 measurements were performed at the fretting wear area, and selected 3D surface parameters—Sq, Sz, Sdq, and Sdr were calculated by Surfstand software V3.3. The mean values of these parameters were compared with that of the worn areas from simulation I showing similar fretting damage, figure 7.3. A one-way ANOVA was carried out, and it was indicated that there was no significant difference between these two groups of 3D surface parameters ( $P > 0.01$ ), see Appendix IX. This suggested that the typical fretting damage on the stem surface in these two simulations was alike in terms of characteristics, and the most distinctive difference with regard to wear severity is the wear coverage rather than the damage itself.

**Comparison of 3D Surface Parameters of the Worn Areas**



(a)



(b)

**Figure 7.3: Comparison of 3D surface parameters of the worn areas on the femoral stem between two wear simulations (Simulation I and Simulation IV)**

**7.2.2.2 Bone cement (optical microscope and SEM evaluation)**

Many micropores were present in the cement surface as well as throughout the cement mantle, and these micropores showed a large variety of diversities in both size and shape. In particular, the optical micrograph of the bone cement surface obtained by the Leica stereomicroscope indicated that there were some highly reflective sites around the micropores, which appeared to be metallic wear debris, figure 7.4. This figure also confirmed that the influence of the procedure to extract the femoral stem from the cement mantle on the experimental results was negligible, otherwise this wear debris would not be only concentrated at the perimeter of the micropores.

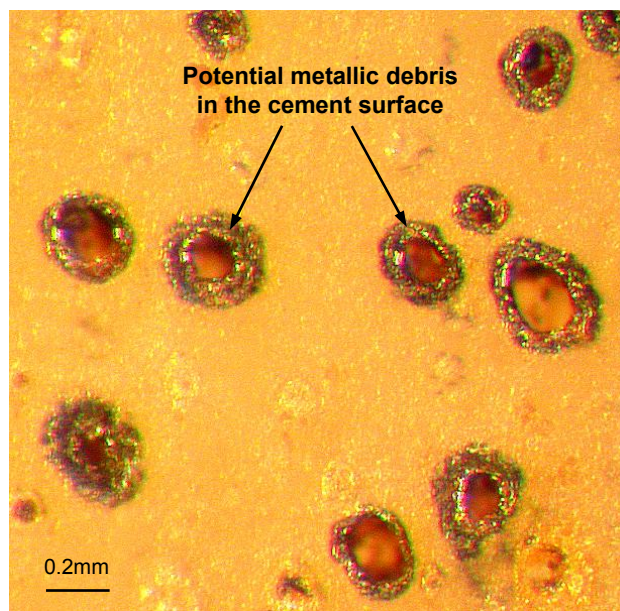


**Figure 7.4: Optical micrograph of cement surface showing the highly reflective sites around the micropores (Simulation IV, use Simplex P cement)**

Accordingly, in order to ascertain the element composition of the wear debris, the bone cement was further sectioned and carbon-sputtered to facilitate an SEM study associated with an EDX analysis. Figure 7.5 demonstrated the SEM micrograph of the cement surface, from which it is shown that the areas around the micropores are severely worn. The corresponding EDX analysis confirmed that these worn areas indeed contained metallic wear debris as both a Fe-rich plaque and a Cr-rich plaque were detected. This metallic wear debris could only come from the stainless steel stem surface, and it was dislodged by fretting wear during the simulation probably due to the application of more loading cycles.

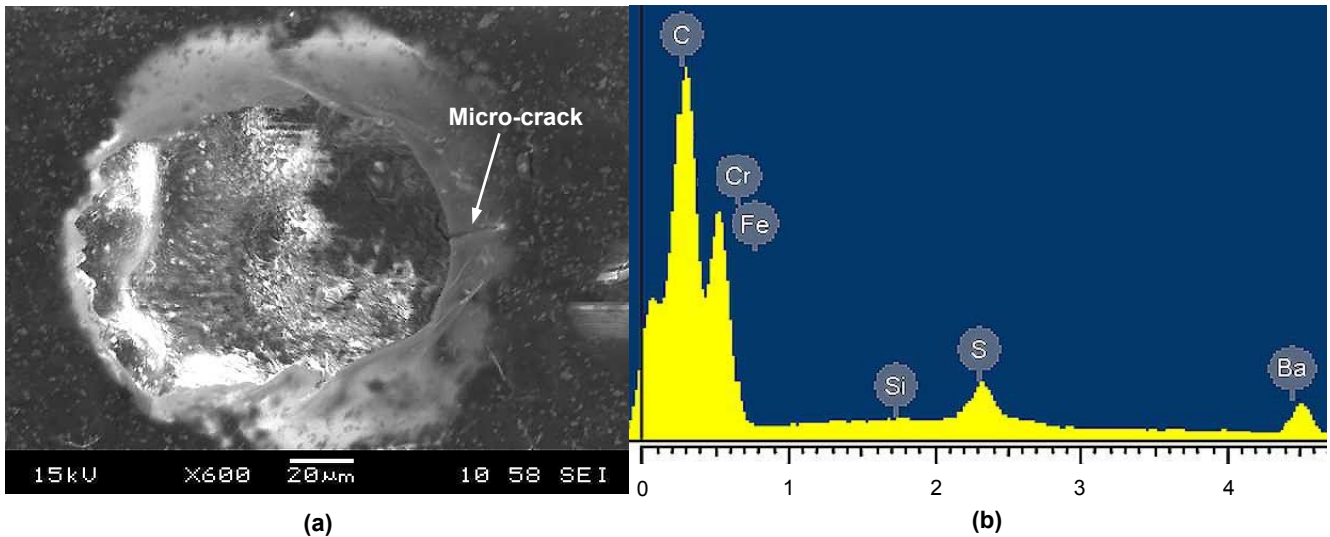


**Figure 7.5: (a) SEM micrograph of the micropores in the cement surface (b) EDX analysis (Simulation IV, use Simplex P cement)**

Interestingly, it was further indicated that for the metallic wear debris, the ratio of the content of Cr to that of Fe was about 9:1, table 7.2. By contrast, as to the original stainless steel stem, the content of Fe is much higher (about 64.5%) than that of Cr, table 7.3 (BS 7252–9 1993). From looking at the composition a fair assumption for this discrepancy could potentially be due to the passive layer which had been previously formed to protect the stem surface. It is considered that it was the passive layer that was initially worn off from the femoral stem by fretting wear and this passive layer was rich in Cr rather than Fe. When the superficial material was damaged, a new passive layer was generated very rapidly as it was very easy for Cr to reform this oxide film. Then the new passive layer was removed and successive re-passivation continued. This was considered the reason why the metallic wear debris around the micropores contained principally Cr.

**Table 7.2: Elemental composition of the wear debris at the edge of the micropores (% , m/m)—Simulation IV, use Simplex P cement**

Elements	Fe	Cr	Ba	Si	S	C
Composition	7.59	63.83	17.54	0.41	6.25	4.38

**Table 7.3: Chemical composition of stainless steel REX 734 specified in BS 7252-9 (% , m/m)**

Elements	Fe	Cr	Ni	Mn	Mo	Nb
Composition	Balance	19–22	9–11	2–4.25	2–3	0.25–0.8
Elements	Cu	N	C	P	S	Si
Composition	<0.25	0.25–0.5	<0.08	<0.025	<0.01	<0.75

Additionally, one SEM micrograph of the cement surface showed the presence of micro-cracks at the edge of the micropores, and these micro-cracks seemed to be initiated from this site and then propagated to its bulk material, figure 7.6 and figure 7.7. This indicated that more bone cement deficiencies will occur with the increase of loading cycle. Furthermore, the significance of the micropores in the cement surface to generation of fretting wear on the stem surface was further validated as these micropores corresponded very well to the “undamaged islands”, figure 7.8.

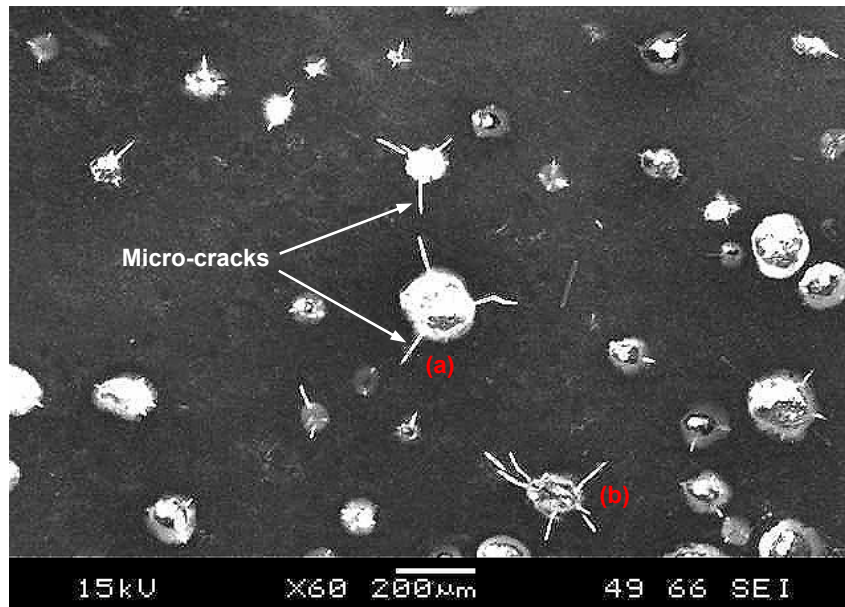


**Figure 7.6: Micro-cracks initiated at the edge of the micropores in the Simplex P cement surface (Simulation IV)**

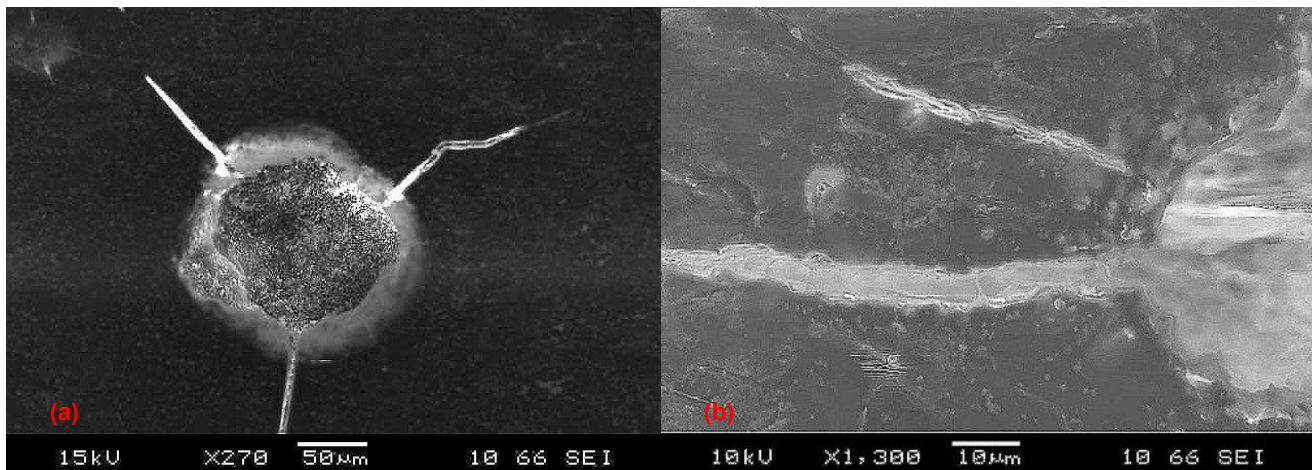


**Figure 7.7: Magnification of the two micro-cracks in figure 7.6**

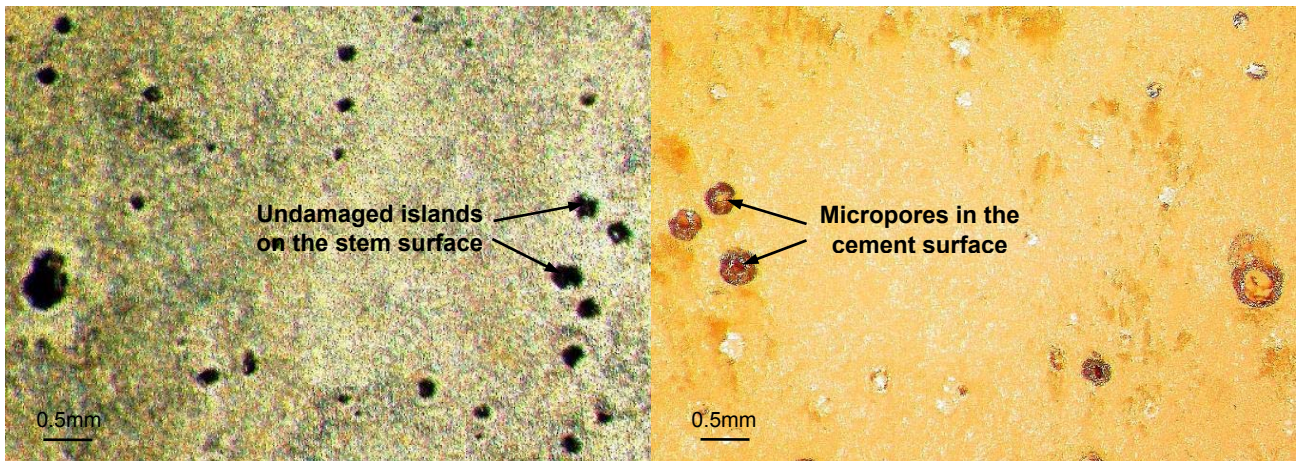


**Figure 7.8: Optical micrograph showing undamaged areas on the stem surface and micropores in the cement surface (Simulation IV, use Simplex P cement)**

### 7.2.3 Conclusions

It was demonstrated in the present study that as the loading cycle increased, metallic debris was liberated from the stem surface, congregating around the micropores in the cement surface. Microcracks also began to initiate from the edge of the micropores and propagated to the bulk material, providing a possible channel to facilitate transportation of the wear debris. This study shed some light on the influence of the duration of *in vivo* service of the hip prosthesis on generation of fretting wear and the accompanying wear debris.

## 7.3 Influence of bone cement brand on generation of fretting wear (Simulation V to VIII)

### 7.3.1 Background and aims

As has been previously mentioned, there are many brands of acrylic bone cement commercially available on the market, with slight variance in composition but inherently different mechanical and physical properties. Generally, Simplex P, CMW 1, CMW 3, and Palacos R are some of the most commonly used bone cements in total joint replacement. It was demonstrated based on the data from the Norwegian Arthroplasty Register that the long term survivorship of cemented THR with the use of different bone cements showed a large discrepancy, with significantly increased rates of failure for the prostheses fixated with CMW 1 and CMW 3 bone cements (Espehaug *et al.* 2002). This phenomenon was further advocated by Wirz *et al.* (2005) as “bone cement does not equal bone cement”. However, the influence of bone cement has been frequently neglected when clinical comparisons are made, and there have been very few studies available as yet correlating bone cement brand with generation of fretting wear on the femoral stem, although such wear has been showing an increasing significance in the overall wear of cemented THR and by extension in aseptic loosening of the whole joint system. Consequently, the following *in vitro* simulations will address this tissue by using polished Exeter V40™ femoral stem and two different bone cements, CMW 3 and Palacos R.

### 7.3.2 Materials and methods

The experimental conditions remained the same as described in detail in section 5.2.2. Totally four

simulations were performed, with two using CMW 3 bone cement and the other two employing Palacos R bone cement. For all these simulations, an initial visual assessment was performed to establish the overall locations of the worn areas. In addition, the coverage of fretting wear in each Gruen zone on the stem surface was calculated using the technique previously developed to detect fretting wear based on grey scale threshold. The femoral stems and the bone cements were then examined utilising the Leica optical microscope to investigate the potential contribution of the micropores in the cement surface to generation of fretting wear on the stem. Furthermore, all the cements were sectioned and carbon-sputtered to facilitate evaluation of the wear debris on the surface through an SEM study associated with an EDX analysis. The Vickers microhardness of the bone cements was measured employing a Micromet 2101 microhardness tester (Buehler Ltd., Illinois, USA) to correlate the microhardness with the generation of the wear debris, figure 7.9. It was calculated by the following equation.

$$HV = 1.8544 \frac{P}{D^2} \quad (7.1)$$

$P$  is the load applied by the diamond pyramid indenter (Kgf), and  $D$  is the mean value of the diagonal length of the indentation on the specimen (mm), i.e.  $D = (d_1 + d_2)/2$ . The load used in this study was 0.3Kgf, and the dwell time was set at around 20 seconds. According to the manual provided by the manufacturer, all the indentations were performed at intervals on the bone cement specimen exceeding four times that of the measured diagonal, and they were far from the edge of the specimens in order not to compromise the results. Totally 10 measurements were made on the cement surface and finally the mean value was calculated.

In addition, the microhardness of Simplex P bone cement (simulation I to IV) was also calculated to enable comparison with that of CMW 3 and Palacos R bone cements.

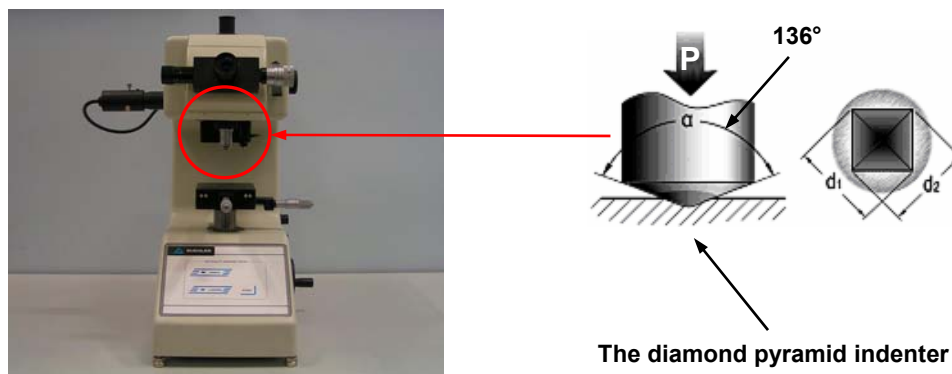


Figure 7.9: The Micromet 2101 microhardness tester

## 7.3.2 Results

### 7.3.2.1 The *in vitro* wear simulations using CMW 3 bone cement (Simulation V and VI)

#### (1) Visual examination

After simulation, the two femoral stems were both firmly fixed in the cement mantle before being cautiously extracted. Typical fretting wear was present on all the surfaces of the stems, figure 7.10 and 7.11, and the wear locations were quite similar to that of previous simulations. The coverage

of fretting wear in each Gruen zone of the stems was shown in table 7.4 and 7.5. It was clear from these two tables that the overall coverage of fretting wear was very similar, with slight decrease for simulation VI in comparison with simulation V. However, there indeed existed certain varieties with regard to the wear distribution. This could be caused by the difference of the initial status of the stem in the cement mantle or any discrepancy between the hand mixed CMW 3 bone cement, e.g. micropore distribution, and residual stress, etc.

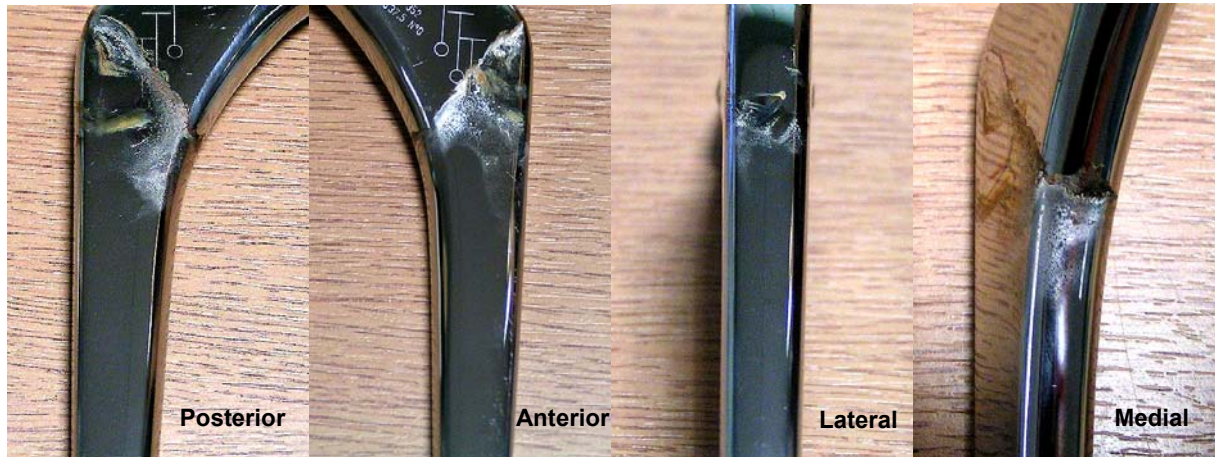


**Figure 7.10: Fretting wear generated on the femoral stem surface (Simulation V, use CMW 3 cement)**

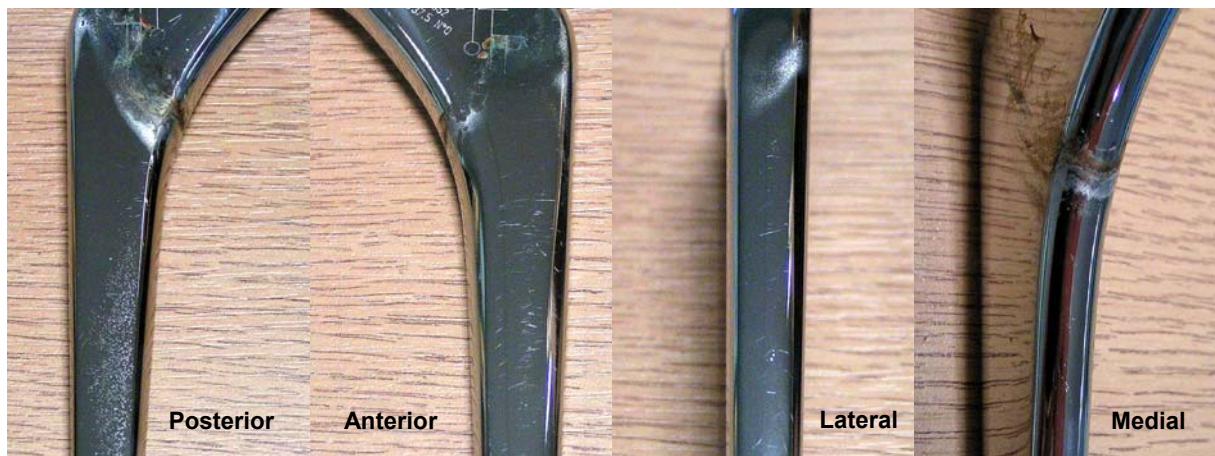


**Figure 7.11: Fretting wear generated on the femoral stem surface (Simulation VI, use CMW 3 cement)**

**Table 7.4: Coverage of fretting wear area in each Gruen zone on the stem surface (%)—Simulation V, use CMW 3 cement**

Stem surface	Posterior	Anterior	Lateral	Medial
Zone 1	10	20	15	
Zone 2	0	0	0	
Zone 3	0	0	0	
Zone 4	0	0	0	0
Zone 5	0	0		0
Zone 6	0	0		0
Zone 7	50	30		25

**Table 7.5: Coverage of fretting wear area in each Gruen zone on the stem surface (%)—Simulation VI, use CMW 3 cement**

Stem surface	Posterior	Anterior	Lateral	Medial
Zone 1	10	5	10	
Zone 2	5	0	0	
Zone 3	5	0	0	
Zone 4	0	0	0	0
Zone 5	5	0		0
Zone 6	10	0		0
Zone 7	20	5		10

**(2) Optical interferometer and optical microscope evaluation**

The most worn areas on the stem surface were measured using the Talysurf CCI interferometer. Figure 7.12 and 7.13 show two typical measurements for these two simulations respectively, from which it was demonstrated that the stem surface was greatly roughened by fretting damage.

The potential significance of the micropores in the cement surface in initiation and propagation of fretting wear on the stem surface was further validated through the optical micrographs obtained using the Leica optical stereomicroscope, figures 7.14–4.17. The good matching between the worn areas on the stem surface and the edges of the micropores in the cement surface indicated that these micropores indeed facilitated generation of fretting wear.

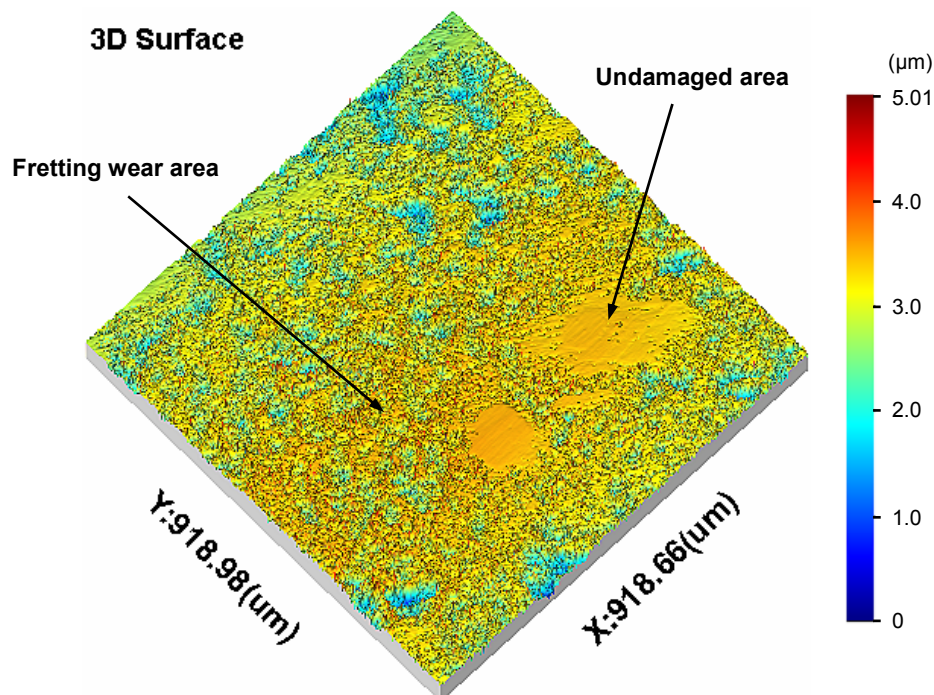


**Figure 7.12: Talysurf CCI measurement of worn areas on the stem surface (Simulation V, use CMW 3 cement)**

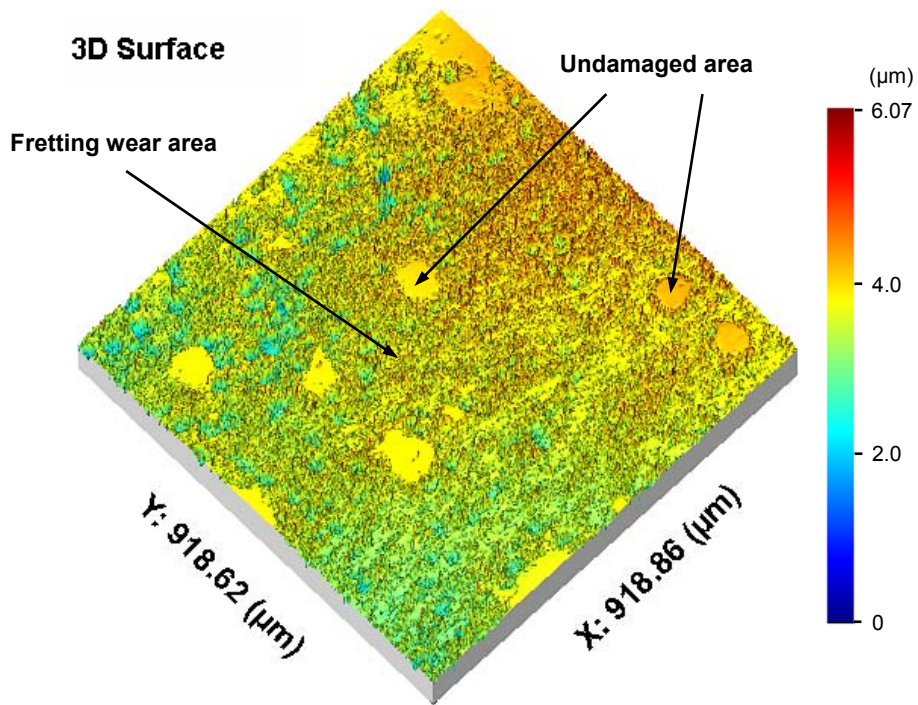


Figure 7.13: Talysurf CCI measurement of worn areas on the stem surface (Simulation VI, use CMW 3 cement)

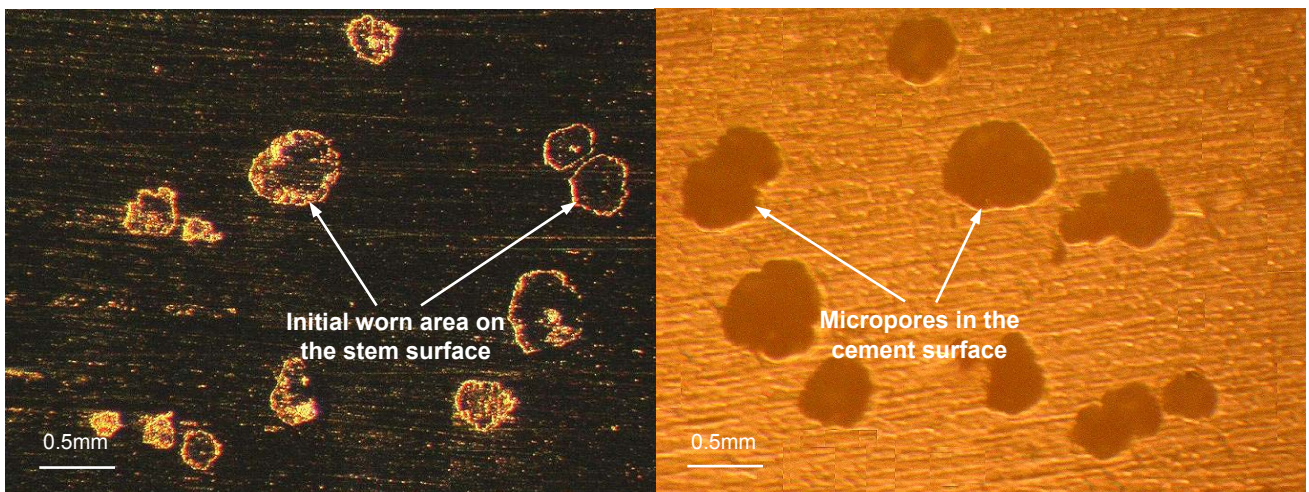
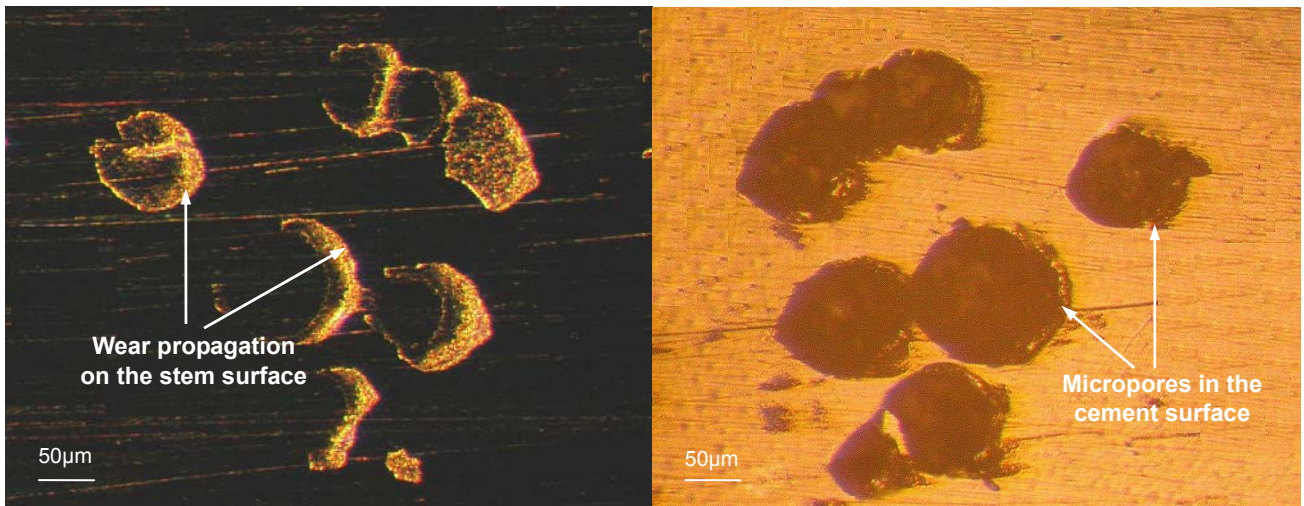
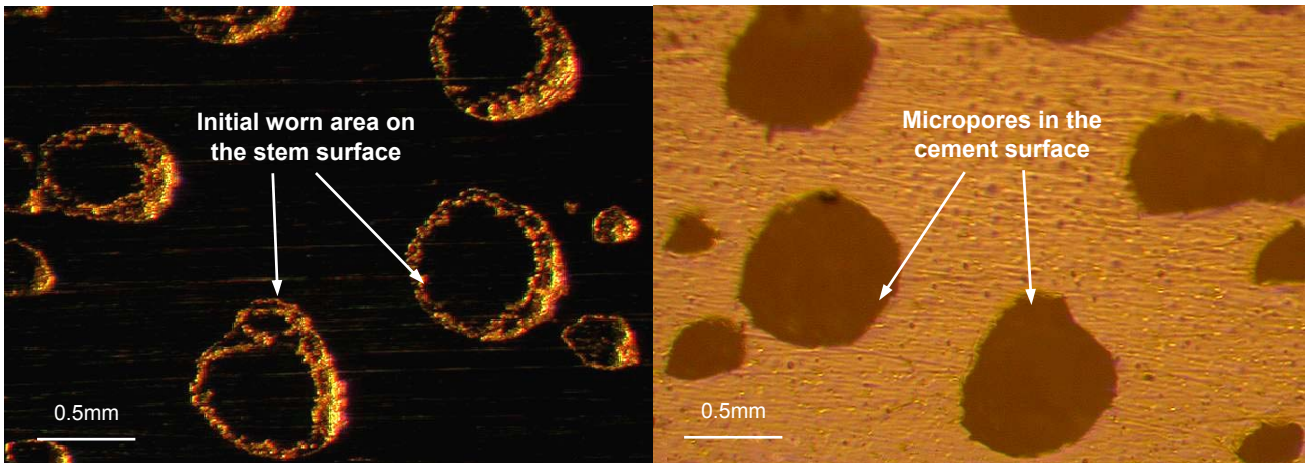


Figure 7.14: Initiation of fretting wear on the stem surface and micropores in the cement surface (Simulation V, use CMW 3 cement)



**Figure 7.15: Propagation of fretting wear on the stem surface and micropores in the cement surface (Simulation V, use CMW 3 cement)**



**Figure 7.16: Initiation of fretting wear on the stem surface and micropores in the cement surface (Simulation VI, use CMW 3 cement)**

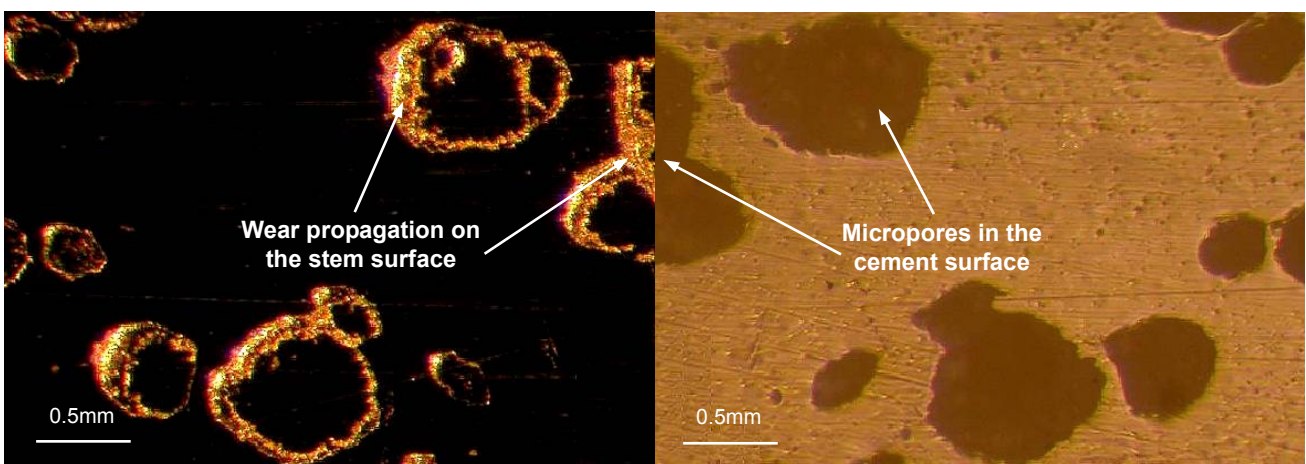


**Figure 7.17: Propagation of fretting wear on the stem surface and micropores in the cement surface (Simulation VI, use CMW 3 cement)**

### (3) SEM and EDX assessment

Furthermore, the optical micrograph of the cement surface showed evidence of potential metallic debris around the micropores for both of these two simulations, and the corresponding SEM study associated with EDX analysis confirmed that these areas certainly contained metallic wear debris owing to the presence of a Fe-rich plaque and also a Cr-rich plaque, figures 7.18–7.21.

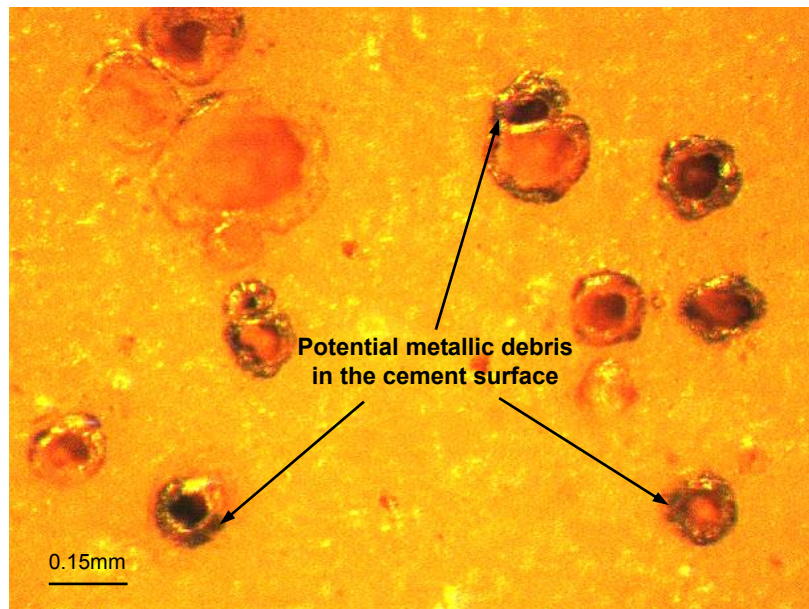


Figure 7.18: Optical micrograph of cement surface showing areas of potential metallic debris around the micropores (Simulation V, use CMW 3 cement)

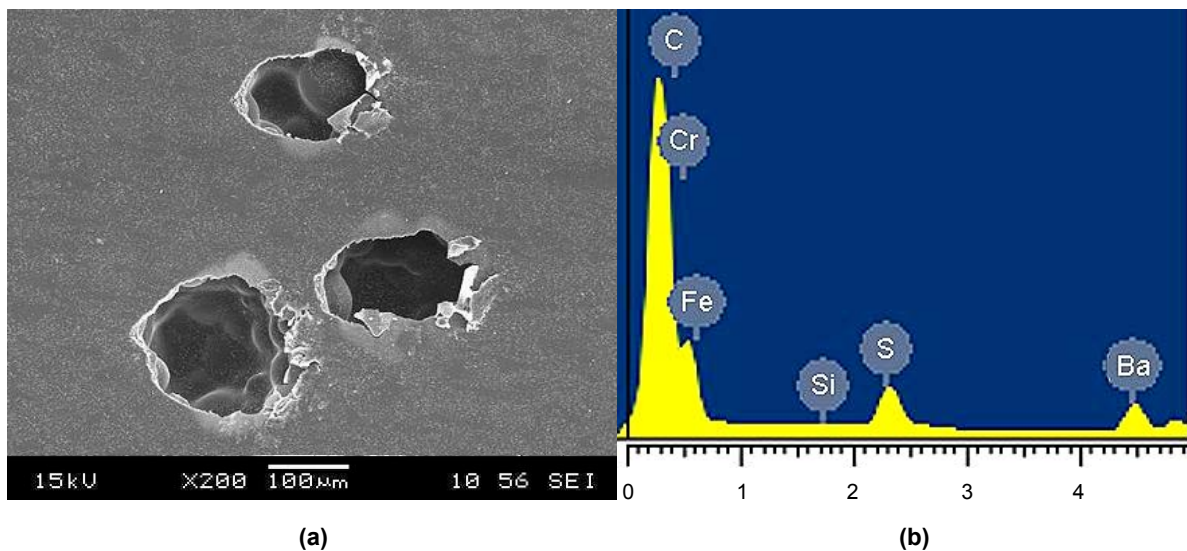


Figure 7.19: (a) SEM micrograph of the micropores in the cement surface (b) EDX analysis (Simulation V, use CMW 3 cement)

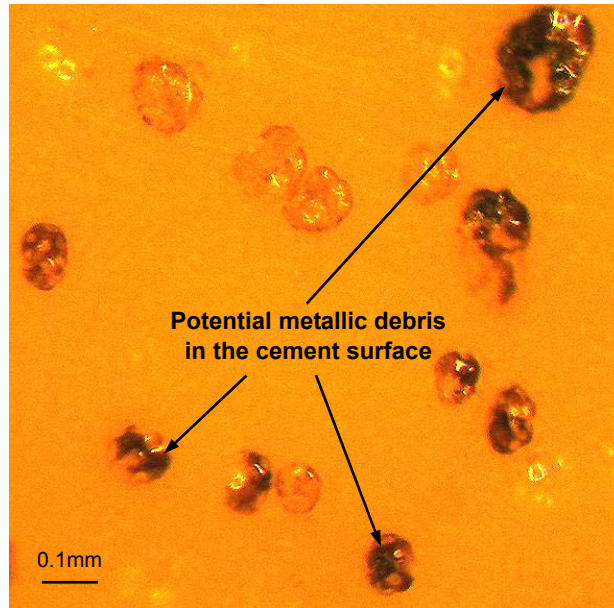


Figure 7.20: Optical micrograph of cement surface showing areas of potential metallic debris around the micropores (Simulation VI, use CMW 3 cement)

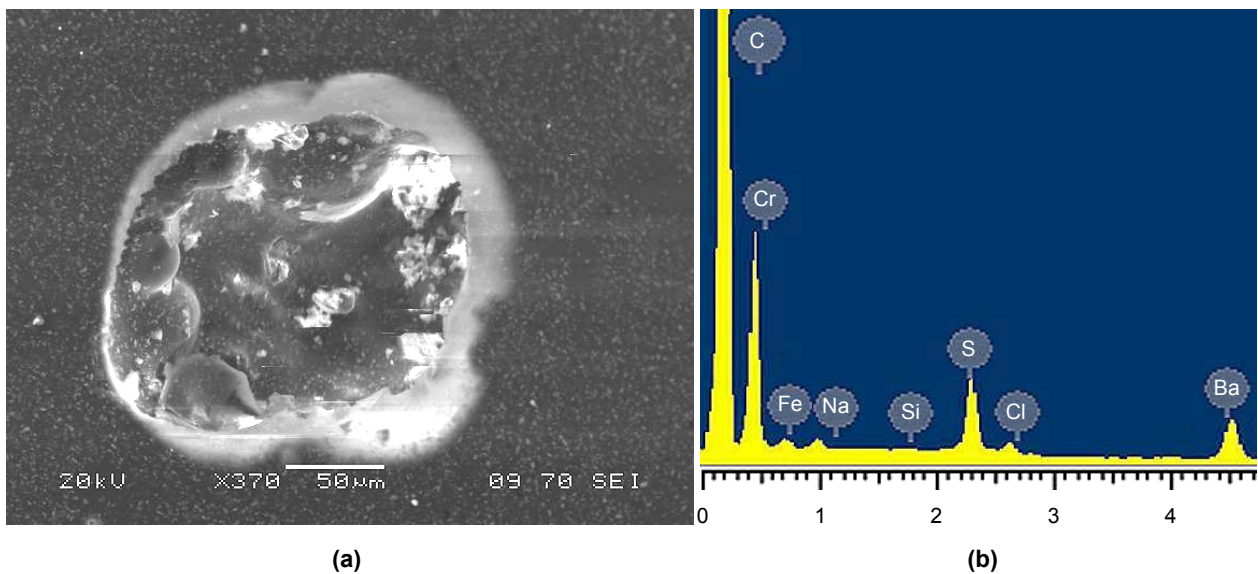


Figure 7.21: (a) SEM micrograph of the micropores in the cement surface (b) EDX analysis (Simulation VI, use CMW 3 cement)

### 7.3.2.2 The *in vitro* wear simulations using Palacos R bone cement (Simulation VII and VIII)

#### (1) Visual examination

Again, the two Exeter V40<sup>TM</sup> femoral stems showed typical fretting wear on the surfaces and they were firmly fixed in the cement mantle prior to extraction, figure 7.22 and 7.23. The coverage of fretting wear in each Gruen zone of the stems was calculated using the same method as described in section 5.2.3, table 7.6 and 7.7. It was indicated from these two tables that the wear coverage in the lateral and medial surfaces of the two stems was similar. However, variation of wear coverage occurred in the posterior and anterior surfaces, and this could be attributed to the discrepancy of

the initial implanting of the femoral stem in the cement mantle. It was further noted that there was increased coverage of fretting wear on the stem surface for these two simulations in comparison with those two using CMW 3 bone cement. This indicated that bone cement brand potentially had an influence on generation of fretting wear on the femoral stem.



**Figure 7.22: Fretting wear generated on the femoral stem surface (Simulation VII, use Palacos R cement)**



**Figure 7.23: Fretting wear generated on the femoral stem surface (Simulation VIII, use Palacos R cement)**

**Table 7.6: Coverage of fretting wear area in each Gruen zone on the stem surface (%)—Simulation VII, use Palacos R cement**

Stem surface	Posterior	Anterior	Lateral	Medial
Zone 1	10	20	20	
Zone 2	0	0	0	
Zone 3	20	0	0	
Zone 4	0	0	0	0
Zone 5	10	10		0
Zone 6	0	0		0
Zone 7	50	5		40

**Table 7.7: Coverage of fretting wear area in each Gruen zone on the stem surface (%)—Simulation VIII, use Palacos R cement**

Stem surface	Posterior	Anterior	Lateral	Medial
Zone 1	50	40	40	
Zone 2	0	5	5	
Zone 3	5	0	0	
Zone 4	0	0	0	0
Zone 5	5	0		0
Zone 6	0	5		0
Zone 7	30	10		30

**(2) Optical interferometer and optical microscope evaluation**

Additionally, the most worn areas on the stem surface were measured employing the Talysurf CCI interferometer. Figure 7.24 and 7.25 showed two typical measurements for these two simulations, from which it was confirmed that the stem surface was severely roughened by fretting damage.

The potential contribution of the micropores in the cement surface to generation of fretting wear on the stem surface was further validated through the optical micrographs of both the femoral stems and the bone cements, obtained utilising the Leica optical stereomicroscope, figure 7.26 and 7.27. The boundaries of the stem worn areas and the edges of the micropores in the cement surface matched quite well with each other.

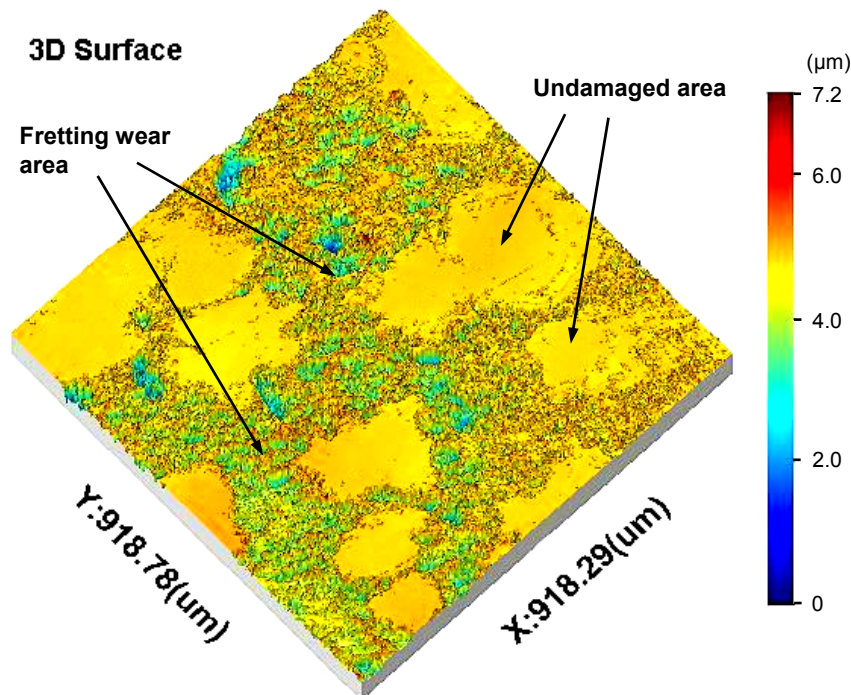


**Figure 7.24: Comparison of fretting wear area and undamaged area on the femoral stem (Simulation VII, use Palacos R cement)**

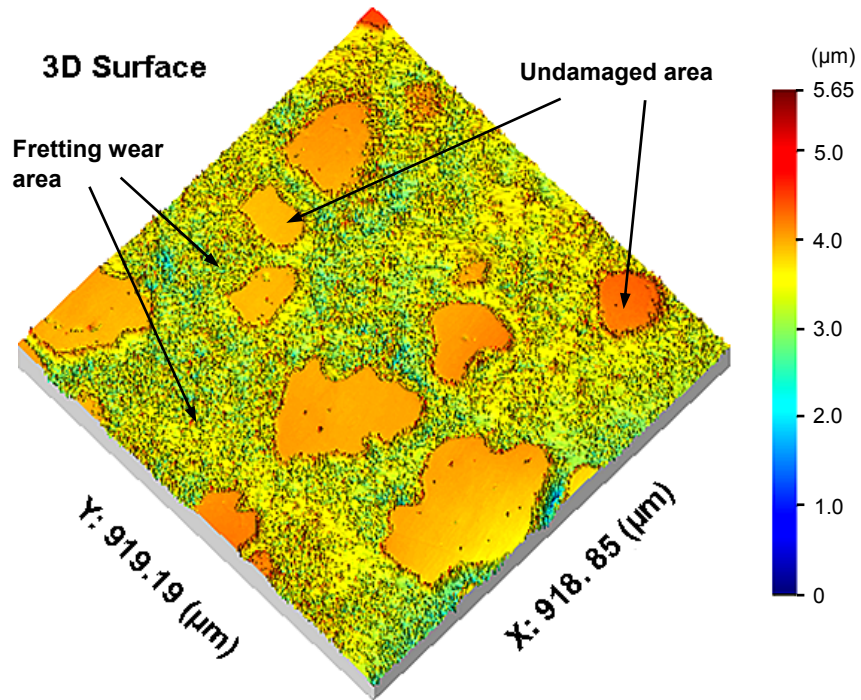


Figure 7.25: Comparison of fretting wear area and undamaged area on the femoral stem (Simulation VIII, use Palacos R cement)

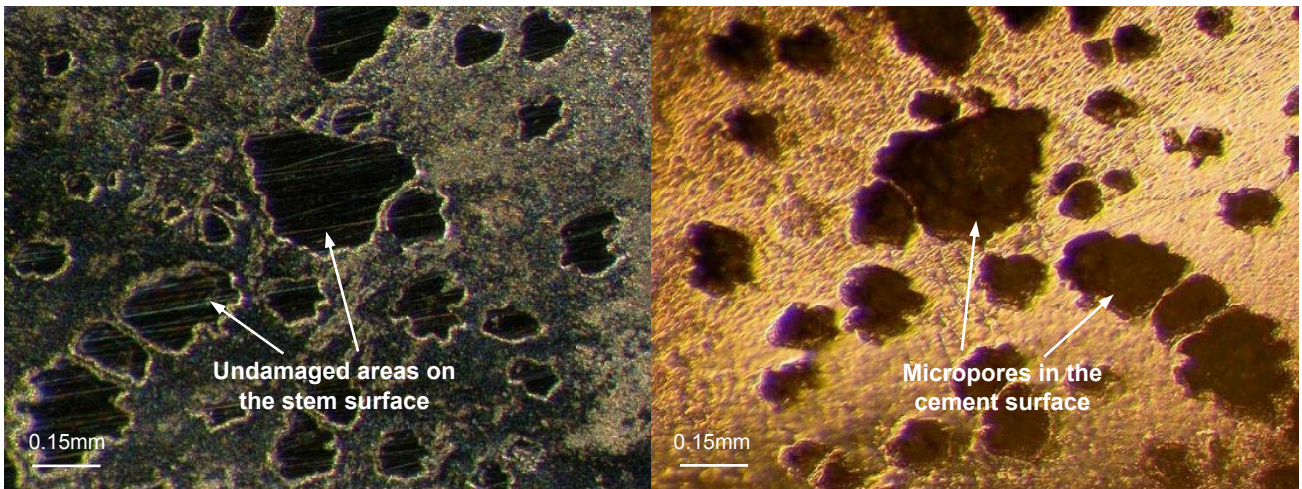
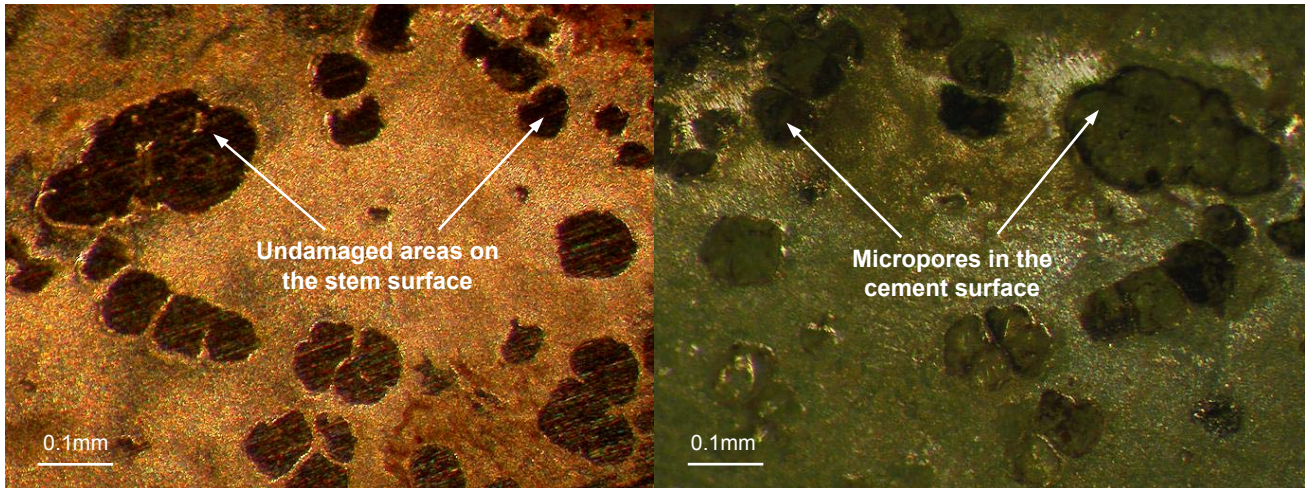


Figure 7.26: Optical micrograph showing undamaged areas on the stem surface and micropores in the cement surface (Simulation VII, use Palacos R cement)



**Figure 7.27: Optical micrograph showing undamaged areas on the stem surface and micropores in the cement surface (Simulation VII, use Palacos R cement)**

**(3) SEM and EDX assessment**

Furthermore, the optical micrograph of the cement surface showed evidence of potential metallic debris around the micropores for both of these two simulations, and the corresponding SEM study associated with EDX analysis confirmed that these areas indeed contained metallic wear debris as a Fe-rich plaque and also a Cr-rich plaque were detected, figures 7.28–7.31.

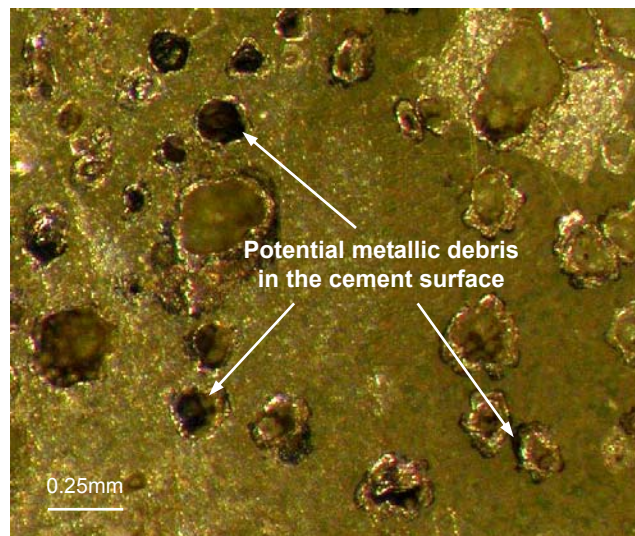


**Figure 7.28: Optical micrograph of cement surface showing areas of potential metallic debris around the micropores (Simulation VII, use Palacos R cement)**

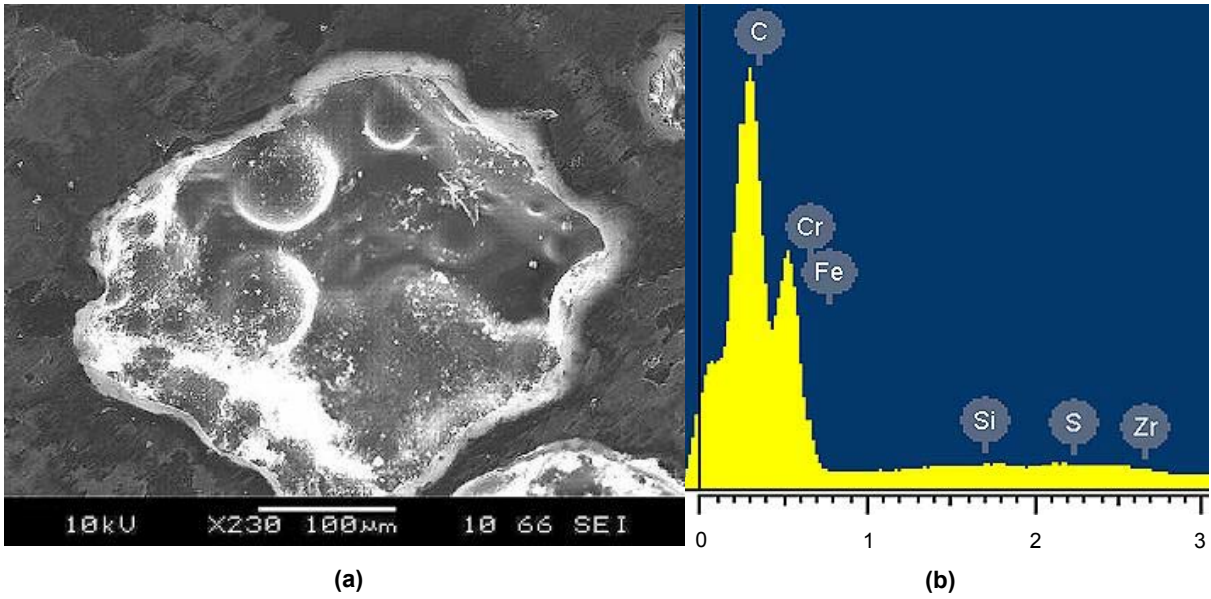


Figure 7.29: (a) SEM micrograph of the micropores in the cement surface (b) EDX analysis (Simulation VII, use Palacos R cement)

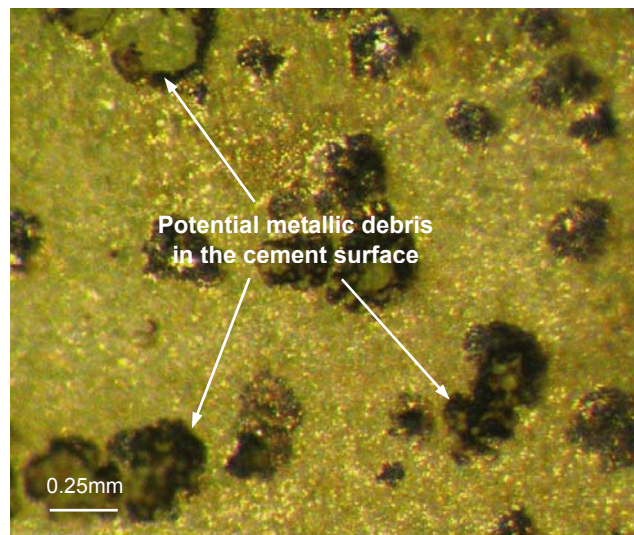


Figure 7.30: Optical micrograph of cement surface showing areas of potential metallic debris around the micropores (Simulation VIII, use Palacos R cement)

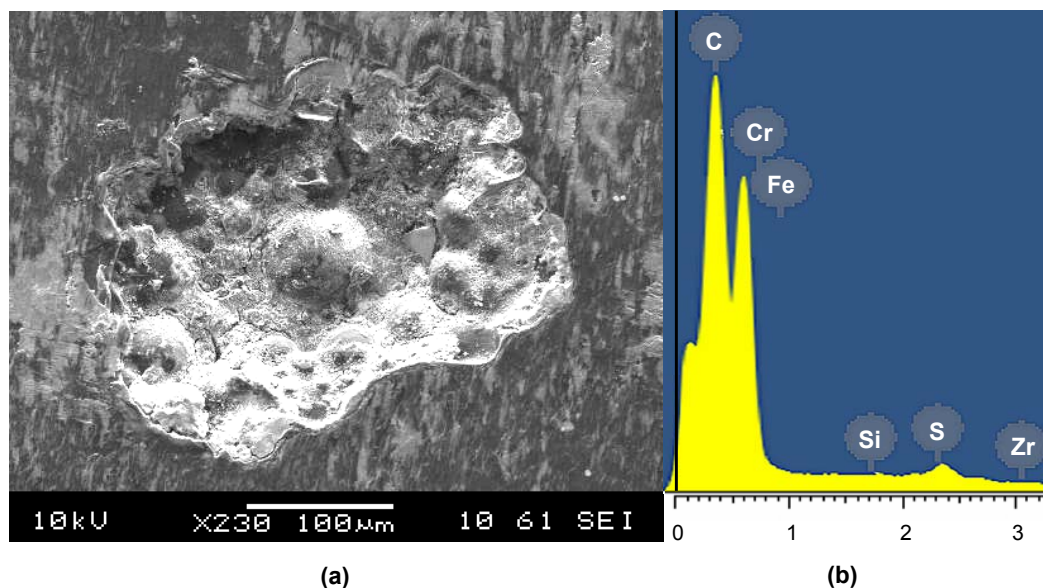


Figure 7.31: (a) SEM micrograph of the micropores in the cement surface (b) EDX analysis (Simulation VIII, use Palacos R cement)

### 7.3.2.3 Vickers microhardness of the bone cements

The Vickers microhardness of the bone cements from all the *in vitro* simulations completed to date is shown in table 7.8. From the table it is clear that there is no significant difference among those values, although Palacos R bone cement does give relatively lower figures, which could be owing to the higher porosity of the cement surface. Therefore, it seemed reasonable to conclude that there was no direct relationship between the microhardness of the bone cement and the generation of wear debris because Palacos R and CMW 3 bone cements did not show a higher microhardness as previously expected.

Table 7.8: Microhardness of the bone cements from the *in vitro* wear simulations

Simulation	Bone cement	Vickers hardness
I	Simplex P	20.30
II	Simplex P	19.88
III	Simplex P	19.78
IV	Simplex P	18.40
V	CMW 3	18.90
VI	CMW 3	17.93
VII	Palacos R	14.70
VIII	Palacos R	15.51

### 7.3.3 Discussion

Numerous bone cements are currently available on the market for the surgeons to choose from, with some of them having unsatisfied long term clinical records. The data from the Swedish and Norwegian hip registry convincingly showed that the revision risk ratio is significantly different among bone cements, and the choice of bone cement may have a greater influence on the outcome of a cemented THR than the prosthesis itself. For example, Simplex P and Palacos R bone cements

are superior to Sulfix 6 and Boneloc bone cements, and the latter two have been withdrawn from the market (Havelin *et al.* 2000). On the other hand, however, Boneloc revealed no difference in results in comparison with other cements when used in combination with the Exeter femoral stem (Thomsen *et al.* 2000). Therefore, in any case, a verdict on cemented THR should never be made without considering the influence of stem geometry, stem material and surface finish, bone cement brand, and cementing technique.

Bone cement may influence the long term survivorship of cemented THR through many means, and one potential possibility can be attributed to the impact on generation of wear debris. However, there are very few reports that have been published to date with regard to the wear characteristic of different bone cements in contact with femoral stem. In addition, the wear debris, as mentioned previously, is believed to be the cause of osteolysis and subsequent aseptic loosening of the hip prosthesis. Little is known, however, about the interaction of different bone cements with different stem surface finishes when fretted. This is considered to be significant as the radiopaque additives with different hardness are added to bone cement to aid in radiological assessment of cemented THR. It might result in generation of different quantities of wear debris, including both metallic and cement particles, thus explaining the variant clinical outcome with one type of prosthesis.

One detailed published data concerning the wear mechanism at the stem–cement interface was ascribed to Wirz *et al.* who performed an *in vitro* study to investigate the wear between matt S-30 stainless steel and different bone cements in a machine designed to replicate multi-directional, i.e. clinically relevant interfacial motion (Wirz *et al.* 2002). A conclusion was drawn from the study that Palacos R had a significantly higher polishing effect associated with the smallest loss of metal weight with fretting, and they attributed it to surface structure resulting from the high molecular weight of Palacos R. However, only matt stainless steel specimens were investigated, and it was considered that actually it was abrasive mechanism between the test specimen and the cement rather than fretting wear. In the present study, the influence of bone cement brand on generation of fretting wear on polished femoral stem was investigated. It was demonstrated that metallic wear debris was liberated from the stem surface for both CMW 3 and Palacos R bone cements, and the debris congregated around the micropores in the cement surface, which could be regarded as additional evidence highlighting the significance of the micropores to initiate fretting wear on the femoral stem. However, this phenomenon was not observed in the simulations using Simplex P bone cement with the same loading cycles, where only cement particles were detected. Therefore, it could be concluded that Simplex P bone cement is superior to CMW 3 and Palacos R bone cements if only their influence on generation of fretting wear on the stem surface is considered, as transportation of the metallic and cement debris to bone tissue areas would stimulate osteolysis and result in further aseptic loosening of the hip prosthesis. Additionally, the coverage of fretting wear on the stem surface using Palacos R bone cement was larger than that utilising CMW 3 bone cement, which indicated that Palacos R bone cement represented the worst case scenario. This to a certain degree conflicted with clinical conclusions that there was significantly increased rate of failure for the hip prosthesis inserted with CMW 1 and CMW 3 bone cements in comparison with Palacos R and Simplex P bone cements (Espehaug *et al.* 2002). As a consequence, it is considered that other mechanisms, in addition to the generation of fretting wear on the stem surface, also contributed to the final failure of cemented THR.

The microhardness of the bone cements did not correlate with the generation of wear debris as although Simplex P bone cement gave relatively higher values of microhardness, metallic debris was not dislodged from the stem surface. However, the presence of metallic debris in the cement surface was observed for the simulations employing CMW 3 and Palacos R bone cements where the microhardness was a bit lower. It is considered that the increased porosity of the high viscosity Palacos R bone cement may contribute to the microhardness measurement as it has been indicated that the hardness near the micropores is reduced than that in other regions due to a more easily deformable characteristic (Liu *et al.* 2001).

#### 7.3.4 Conclusions

The following conclusions could be drawn from this work:

- Bone cement brand shows an influence on generation of fretting wear on polished femoral stem in cemented THR.
- The potential significance of the micropores in the cement surface during the fretting process occurring at the stem–cement interface is well confirmed.
- CMW 3 and Palacos R bone cements both facilitated dislodgment of metallic wear debris from the stem surface and congregation around the micropores in the cement surface.
- There seems no direct relationship between the microhardness of bone cement and generation of metallic wear debris at the stem–cement interface.

#### 7.4 A summary of all the *in vitro* wear simulations completed (from Simulation I to VIII, see Appendix IV)

To date, a total of eight wear simulations have been completed, employing polished Exeter V40™ femoral stem and three brands of bone cement, i.e. Simplex P, CMW 3, and Palacos R. The initial simulation showed great success in reproduction of fretting wear on the stem surface, based on the new test methodology discussed in detail in Section 5.2, and its effectiveness was further validated through simulation II. In simulation III, migration of the femoral stem within the cement mantle was investigated utilising a newly developed micromotion sensor, and it was considered that the setup of the wear simulation could more realistically mimic clinical situation. The influence of the duration of *in vivo* service of the hip prosthesis on generation of fretting wear and wear debris was studied in simulation IV, in which the loading cycle was extended to 10 million whilst the other experimental conditions were kept the same. It was found that metallic debris was liberated from the stem surface and congregated around the micropores in the cement surface. In addition, micro-cracks began to initiate from the edge of the micropores and propagate to its bulk material. From simulation V to simulation VIII, the effect of bone cement brand on generation of fretting wear on the stem surface was investigated, and it was demonstrated that CMW 3 and Palacos R promoted dislodgment of metallic wear debris from the femoral stem surface. In each simulation, evidence was provided showing the potential contribution of the micropores located in the cement surface to initiation and propagation of fretting wear on the stem surface, which experimentally confirmed the significance of the micropores. However, a reduced coverage of fretting wear was obtained for the simulations from II to VIII, which was considered to be caused by the storage conditions of the bone cements.

## **Chapter 8 Initiation and propagation of fretting wear on the femoral stem**

### **8.1 Chapter summary**

As fretting wear on polished femoral stems is showing a more and more significant role in the overall wear of cemented THR associated with generation of both metallic and cement wear debris, it is considered greatly necessary to reduce this wear in order to further improve the long term survivorship of this procedure. As a consequence, it is essential for the researchers to address one crucial issue, i.e. how fretting wear is initiated and propagated at the stem–cement interface.

According to the results of previous *in vitro* simulations to reproduce fretting wear on the femoral stem, it was indicated that the micropores in the cement surface contributed significantly to the progression of fretting wear. Additionally, it has been shown that shrinkage bumps are present in the cement surface upon polymerisation, and these bumps could also act as potential participant in resulting in fretting wear on polished femoral stem. Consequently, the relative contribution of the shrinkage bumps and the micropores to fretting wear should be compared to determine which one is the more important factor, in order to finally develop a model to describe fretting wear.

In this chapter, a 2D finite element model was established to represent the contact between the femoral stem and the bone cement, and a local analysis was performed to investigate the relative contribution of the shrinkage bumps and the micropores through the comparison of one dominant parameter, namely relative micromotion along the stem–cement interface. In addition, the contact pressure normal to the bone cement surface was also investigated. The results indicated that the functionality of the shrinkage bumps was incidental in comparison with the micropores, which confirmed that the micropores did play a role in initiation and propagation of fretting wear on the femoral stem.

### **8.2 Finite element analysis of the stem–cement interface**

#### **8.2.1 Background and aims**

Fretting wear on polished femoral stems has been reported in clinical studies and nowadays it is becoming more and more significant in cemented THR as a source of generation of wear debris. This is especially crucial with the great reduction of wear at the articulating head–cup interface through the use of cross-linked UHMWPE (Wroblewski *et al.* 1996) and the renaissance of hard-on-hard bearing systems (Firkins *et al.* 2001, Hatton *et al.* 2002). Although historically the stem–cement interface received relatively little concern, research to date has gained an insight into the influence of stem surface finish on the wear mechanism at this interface (Howell *et al.* 2004). However, the initiation and propagation of fretting wear has not been fully investigated, and it is considered that a better understanding of this process is necessary to reduce fretting wear, and to further improve the survivorship of cemented THR.

It has been postulated that the shrinkage bumps on the bone cement surface could contribute to generation of fretting wear on polished stems as the stress distribution along the stem–cement interface under physiological loading would be concentrated at these areas, and as a consequence fretting wear would initiate in those sites where the stem is in contact with the shrinkage bumps. The bumps, about 50µm in width and 1–2.5µm in height, are formed due to shrinkage of the bone cement following polymerisation. Figure 8.1 shows these bumps on some common bone cement

surfaces, and more examples are given in Appendix XI. Additionally, it was indicated in Chapter 7 in which a comprehensive investigation on surface morphology of the femoral stem and the bone cement was performed that the micropores in the cement surface also play an important part in the wear process. These studies have shed some useful light on the progression of fretting wear, but it is still not clear which one is the more significant factor. This present study consequently aims to address this issue by comparing these two factors using a finite element analysis, through which an effective method could potentially be obtained to reduce or eliminate fretting wear on polished femoral stems.

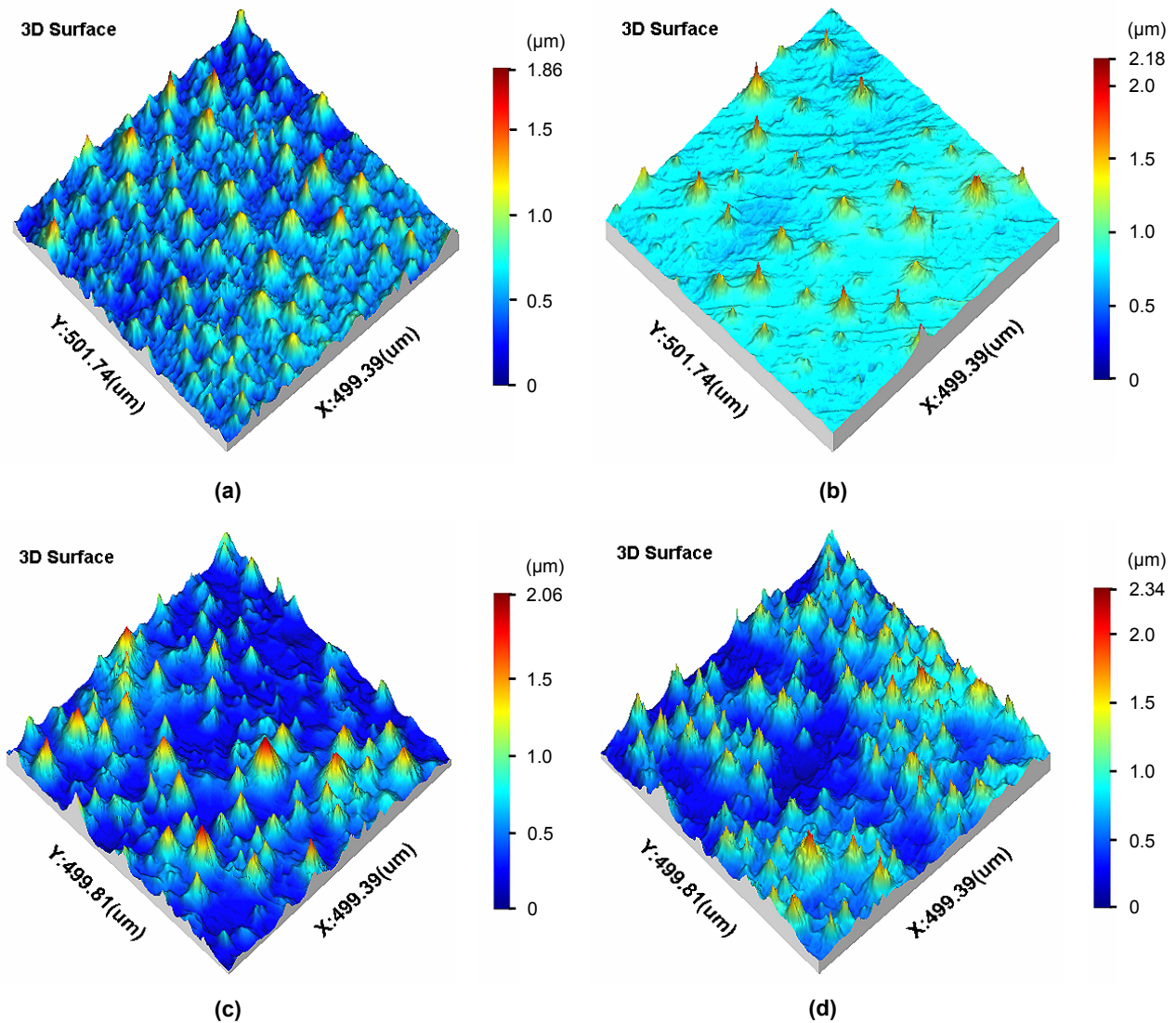


**Figure 8.1: Shrinkage bumps present on the common bone cement surfaces following polymerisation (a) Simplex P with tobramycin (b) Palacos R (c) CMW 1 (d) CMW 3**

### 8.2.2 Methods

By breaking down a structure into a smaller mesh of simple geometrical elements, such as rods, plates, and blocks that are connected at shared nodes, the finite element method is able to calculate stresses and strains at every finite point even within a complicated 3D geometry. Calculations for each element are solved iteratively until agreement is reached between the adjacent elements and

forces and displacements are globally compatible with stresses and strains. Therefore, it is a very suitable tool in orthopaedics taking into consideration the anatomical shape and material property of the components.

### 8.2.2.1 Establishment of the finite element models

In this present study, a 2D finite element model was created utilising ABAQUS software 6.6 to represent the stem–cement interface, which is considered to be easier to incorporate with the optimisation algorithm and much more economical in terms of computational effort than a 3D model. In order to compare the relative contribution of the shrinkage bumps and the micropores in the cement surface on generation of fretting wear, two configurations were established. Figure 8.2 illustrates the model simulating the interaction between the femoral stem and the shrinkage bumps, and figure 8.3 displays the model simulating the interaction between the femoral stem and the micropores. The mesh for the two configurations was finest at the stem–bump contact area and the stem–micropore contact area respectively. Taking into account the size of the shrinkage bumps and the micropores, a local FEA encompassing three studies was performed.

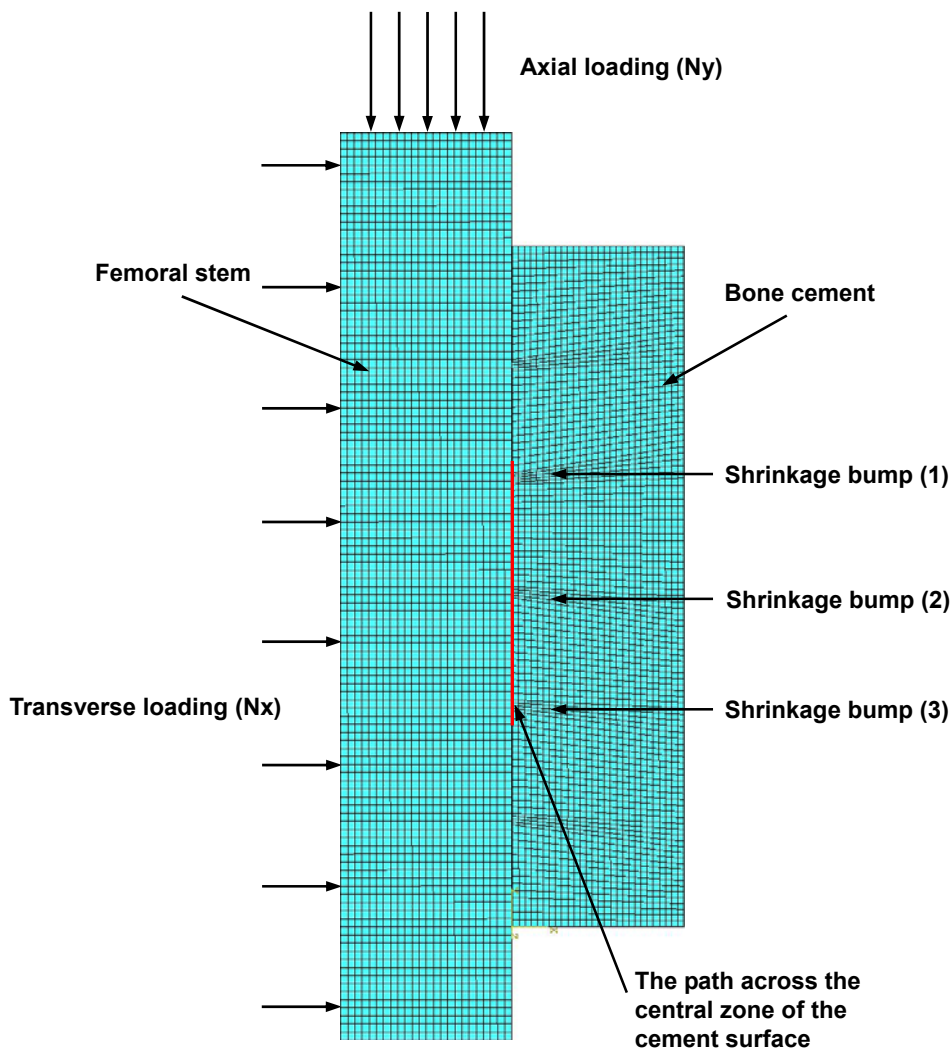
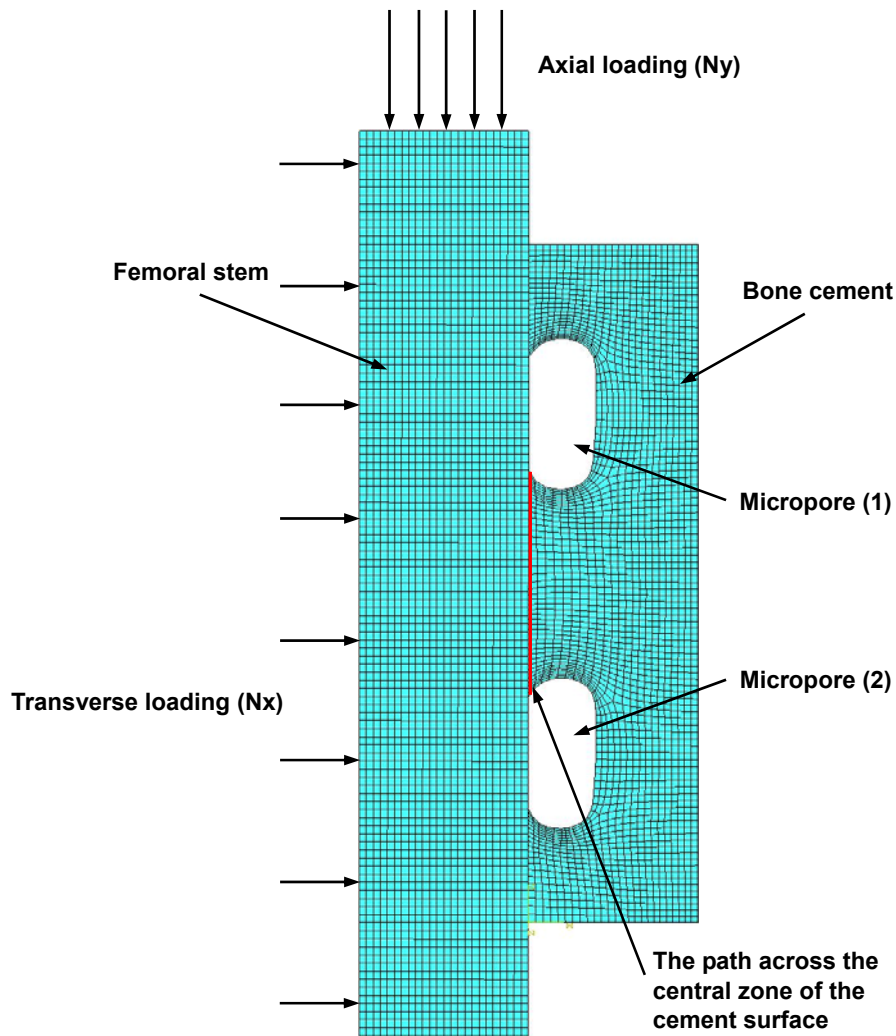


Figure 8.2: 2D finite element model simulating the interaction between the stem and the bumps



**Figure 8.3: 2D finite element model simulating the interaction between the stem and the micropores**

In study I, the relative contribution of the bumps and the micropores on generation of fretting wear was investigated. The polished femoral stem section was 4mm long and 0.75mm wide, and the bone cement mantle was 3mm long and 0.75mm wide. The shrinkage bumps were set as 50 $\mu$ m in width and 2.5 $\mu$ m in height, and the micropores were set as 0.5mm in width and 0.3mm in depth. Such bumps and micropores are very common on the cement surface, especially for those cements mixed by hand (Brown 2006, Jasty *et al.* 1990). Totally five bumps and two micropores were present in these two configurations respectively. The femoral stem was simulated as being made of stainless steel with the Young's modulus of 200GPa, and the Poisson's ratio of 0.3. The Young's modulus and the Poisson's ratio of the bone cement were assigned to be 2GPa and 0.3. Both the stem and the cement were assumed to be linearly isotropic and homogeneous. The element type for these two materials was CPS4R, i.e. four-node bilinear plane stress quadrilateral with reduced integration and enhanced hourglass control. Reduced integration elements can help decrease the analysis time, and enhanced hourglass control reduces the possibility of hourglassing in the model. A combined loading was applied to the femoral stem, with the transverse component (Nx) of 250N and the axial component (Ny) of 3000N. This loading level was comparable with the hip joint force during patient walking activity (Paul 1967). The friction coefficient between the femoral stem and the bone cement was 0.2 because a value around this has been experimentally measured

between polished femoral stem and bone cement (Wheeler *et al.* 1997).

### 8.2.2.2 Output of the finite element models

At the stem–cement interface, the stem acts as the master surface and the cement acts as the slave surface. A path was defined across the central zone of the bone cement surface, and the relative micromotion at the stem–cement interface along this path ( $\Delta M$ ), i.e. the relative tangential motion at the first slip direction, was requested as output. In a 2D finite element simulation, the first slip direction denotes the tangent to the master surface, and the orientation of the tangent is determined by the cross product of the vector into the plane of the model and the normal vector of the master surface. Therefore, the orientation of the first slip direction is just the same as the direction of the axial loading  $N_y$ . A positive magnitude of  $\Delta M$  indicates that the cement surface nodes have moved in the positive first slip direction along the stem surface and vice versa. As a consequence,  $\Delta M$  is calculated through the following equation.

$$\Delta M = M_c - M_s \quad (8.1)$$

$M_c$  and  $M_s$  are the micromotion of the bone cement and the femoral stem along the defined path at the stem–cement interface respectively. This parameter was used to determine which contributes more to generation of fretting wear on polished femoral stems because the relative micromotion is deemed as the prerequisite for fretting wear. In addition, the contact pressure normal to the cement surface was also obtained from the model to provide more information on the characteristic at the stem–cement interface.

Two more FEA were performed to investigate the influence of micropore size and loading level on the generation of fretting wear. In study II, the micropore size was nominated as 0.2mm, 0.3mm, 0.4mm, and 0.5mm in width respectively, and the depth remained as 0.3mm. The transverse and axial components of the loading were 250N and 3000N, and the other simulation conditions were unchanged. The relative micromotion at the stem–cement interface, i.e.  $\Delta M$ , was calculated and compared. In study III, the axial component of the loading was nominated as 2000N, 2500N, 3000N, 3500N, and 4000N respectively, and the transverse component was 250N. The micropore size was 0.5mm in width and 0.3mm in depth, and the other simulation conditions were kept the same. Similarly, the relative micromotion at the stem–cement interface, i.e.  $\Delta M$ , was calculated and compared. In addition, the contact pressure normal to the cement surface in study II and study III was also obtained.

## 8.2.3 Results

### 8.2.3.1 Study I: The relative contribution of the shrinkage bumps and the micropores to generation of fretting wear

A schematic diagram is given to describe the contact between the femoral stem and the shrinkage bumps when pressing the stem to the cement with both a transverse loading and an axial loading, figure 8.4. The figure, which is based on the results of the finite element model, demonstrates schematically that the shrinkage bumps have been badly deformed and skewed in the direction of the axial loading. In addition, there exists a gap at the edge of the bumps at the interface of the two materials before they are in full contact. The leading edge, the peak, and the trailing edge are also defined in this figure to simplify explanation of different areas of the shrinkage bumps.

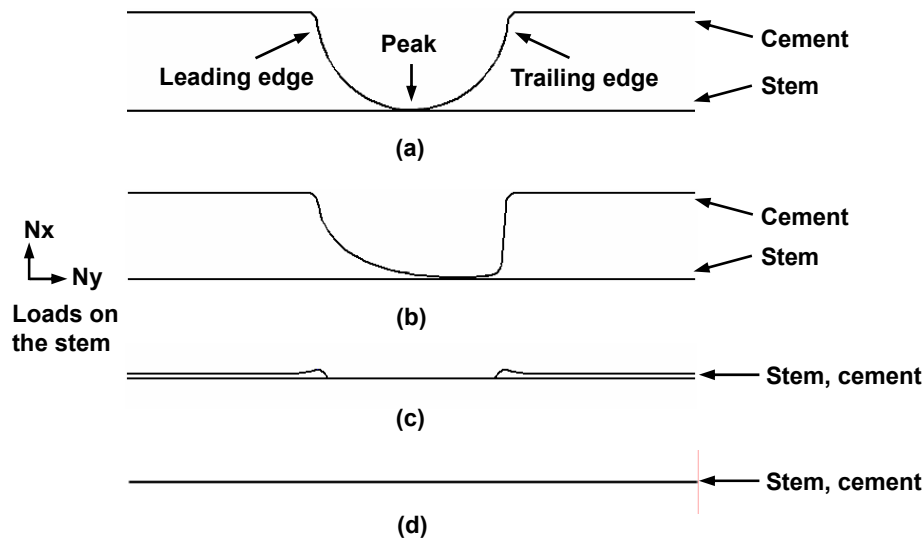


**Figure 8.4: The schematic diagram showing the interaction between the stem and the shrinkage bumps when pressing the stem to the cement (a) The stem and the bumps contact without any deformation (b) The bumps are badly deformed upon loading (c) There exits a gap at the edge of the bumps (d) The stem and the bumps are in full contact**

Figure 8.5 shows the relative micromotion between the femoral stem and the shrinkage bumps along the defined path, and this micromotion is quite small with the maximum value being less than  $0.15\mu\text{m}$  at the peak of bump (2). The micromotion pattern around all of the shrinkage bumps is similar, i.e. it shows an initial low level of micromotion at the leading edge of the bumps as the bump material in this area is moving in the same direction as the stem. The relative micromotion value then increases significantly towards the trailing edge of the deformed bumps after passing the central peak, with the formation of a negative peak in the graph. This is because in these areas the bump material moves much less than that at the leading edge of the bumps. Figure 8.6 shows the contact pressure between the femoral stem and the shrinkage bumps. It is clear that the contact pressure reaches its peak value of  $470\text{Pa}$  at the peak of the bumps, and reduces to the minimum at the leading and trailing edges of the bumps where the interfacial gap was previously located. The contact pressure in the areas between these bumps is about  $310\text{Pa}$ . Although relative micromotion does occur between the femoral stem and the shrinkage bumps, it is considered that it is too small to actually initiate fretting wear on the femoral stem surface as the typical range of movement for fretting is usually from  $1\mu\text{m}$  to  $100\mu\text{m}$ .

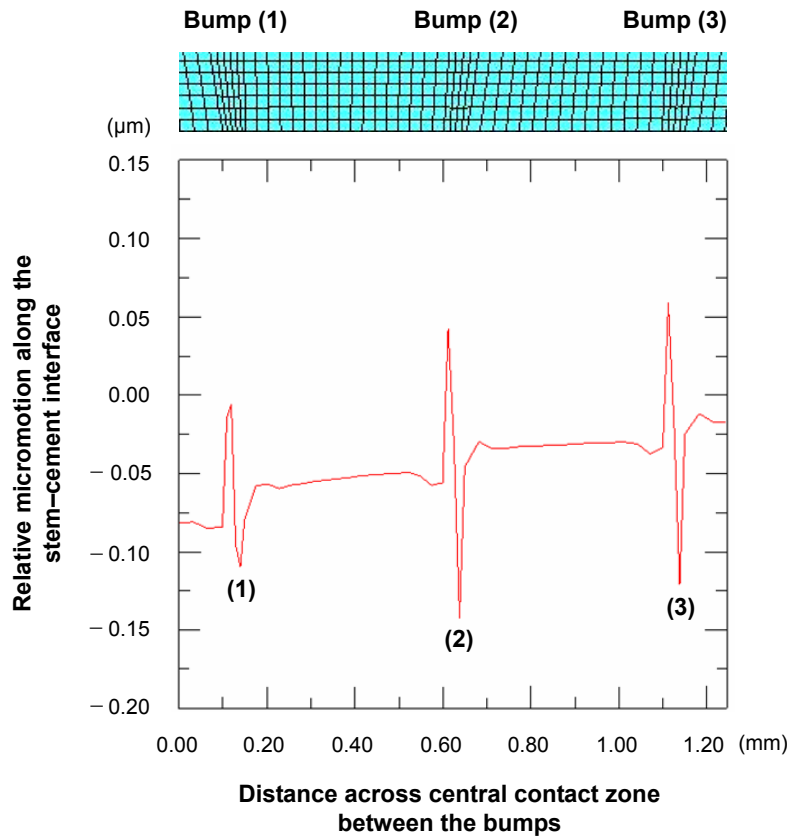


Figure 8.5: The relative micromotion along the stem-cement interface between the stem and the shrinkage bumps

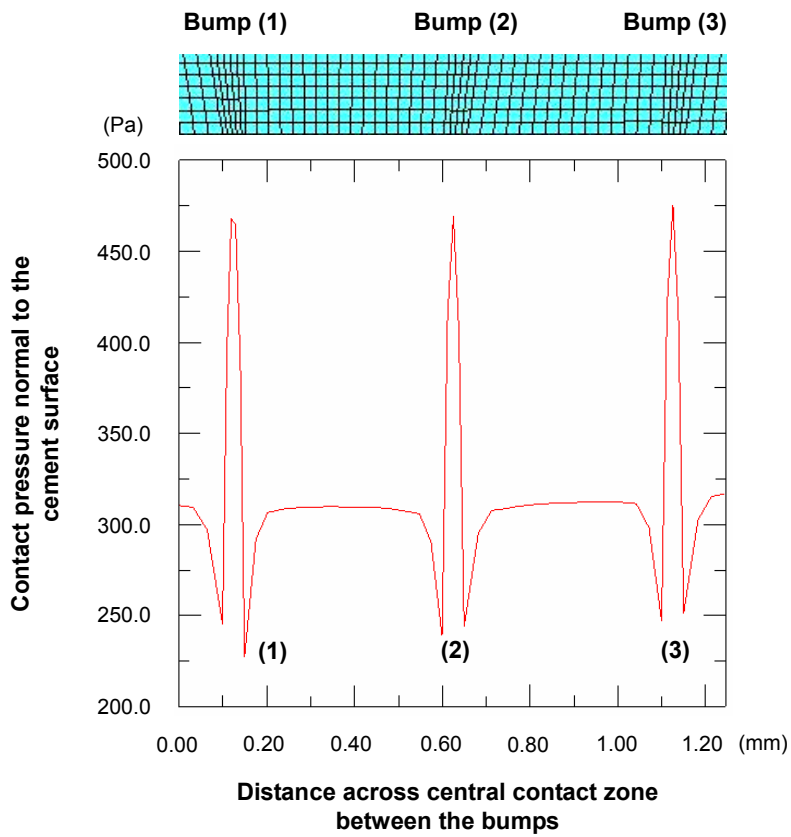
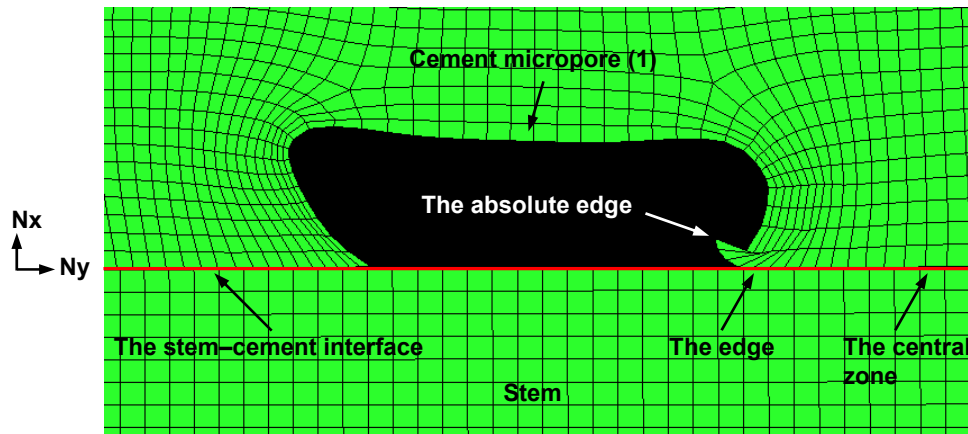


Figure 8.6: The contact pressure normal to the cement surface between the stem and the shrinkage bumps

Figure 8.7 shows a schematic diagram describing the contact between the femoral stem and the micropores when pressing the stem to the cement. From the figure it is evident that the micropores have also been badly deformed, and there is no contact between the femoral stem and the absolute edges of the two micropores. This is caused by the deformation of the micropore edges due to the application of the transverse and axial loading. Additionally, the absolute edge, the edge, and the central zone are defined in this figure to specify different areas of the micropores.



**Figure 8.7: The schematic diagram showing the interaction between the stem and the micropore (1) when pressing the stem to the cement**

The relative micromotion between the femoral stem and the micropores is displayed in figure 8.8, and it is clear that significantly higher relative micromotion (maximum value about  $14\mu\text{m}$ ) occurs around the absolute edges of the micropores, whilst it is almost zero away from these regions. This could be mainly attributed to the larger geometrical deformation at the edges of the micropores. Note that the two peaks in the figure refer to opposite sides of adjacent micropores and would therefore have different values, i.e. the lower side of micropore (1) tends to move in the opposite direction to the femoral stem, with the formation of a negative and high value in the figure, whilst the deformation of the upper side of micropore (2) is in the same direction as the stem, therefore resulting in a positive and relatively smaller value. Figure 8.9 shows the contact pressure between the femoral stem and the micropores. It initially gives zero contact pressure at the absolute edge of micropore (1). The pressure then increases greatly until a peak value of  $680\text{Pa}$  is reached at the edge of micropore (1). This is followed by a small decrease in the central zone between micropore (1) and micropore (2), and then a further increase towards the edge of micropore (2). Finally, it drops off to zero again at the very edge of micropore (2). This is considered to be consistent with the contact properties between the stem and the micropores when they are pressing together.

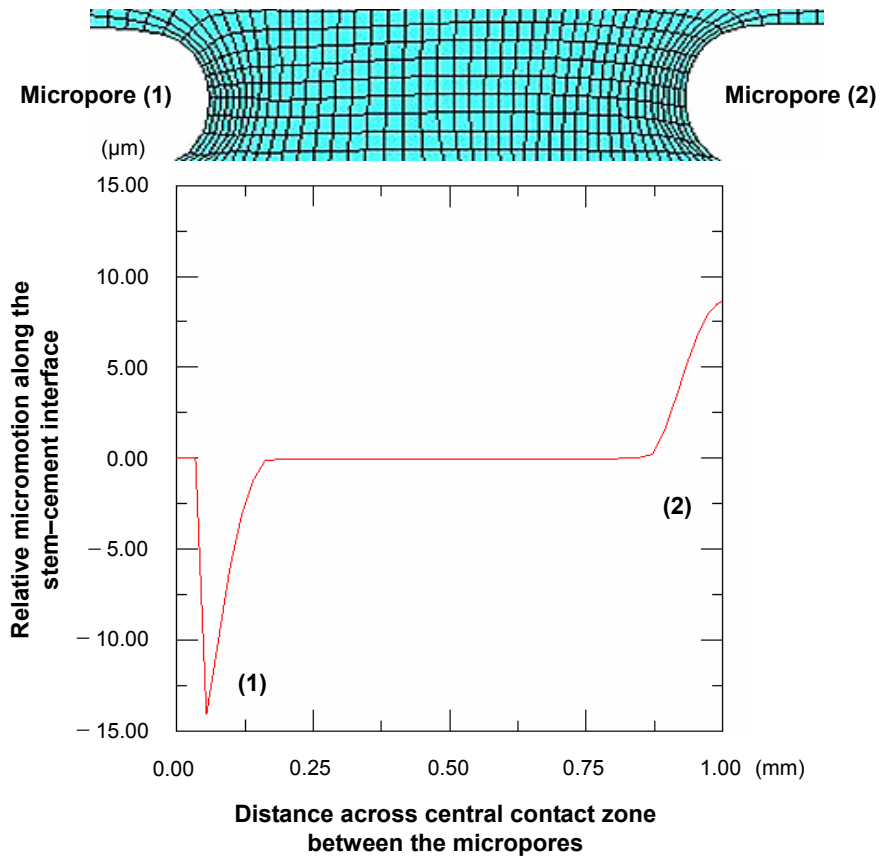


Figure 8.8: The relative micromotion along the stem-cement interface between the stem and the micropores

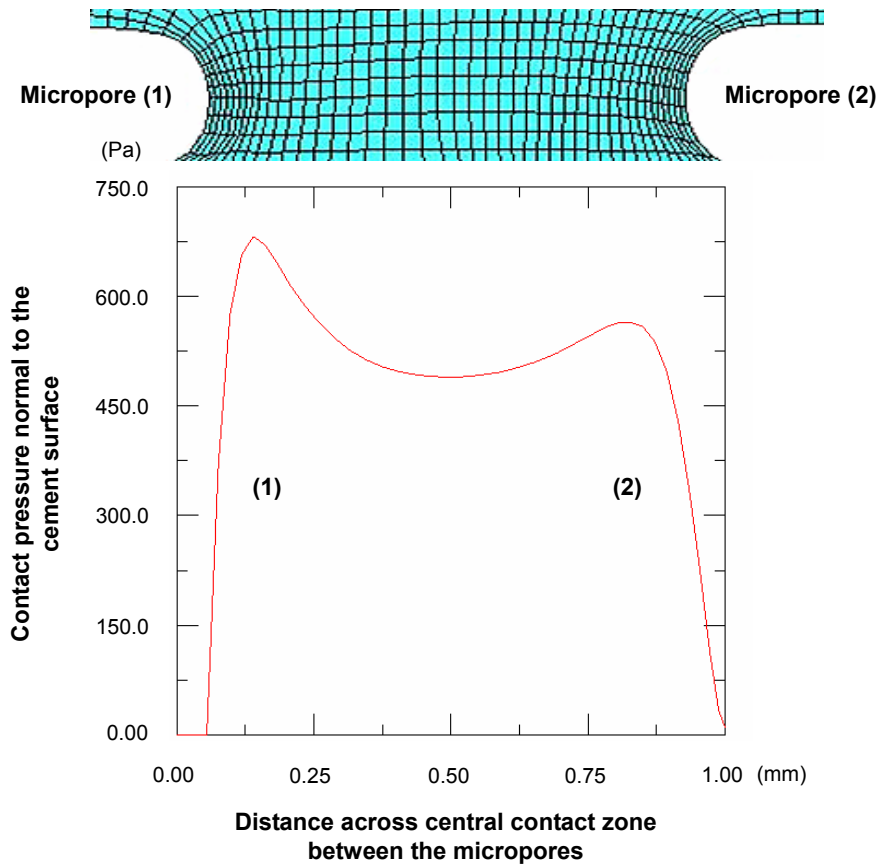
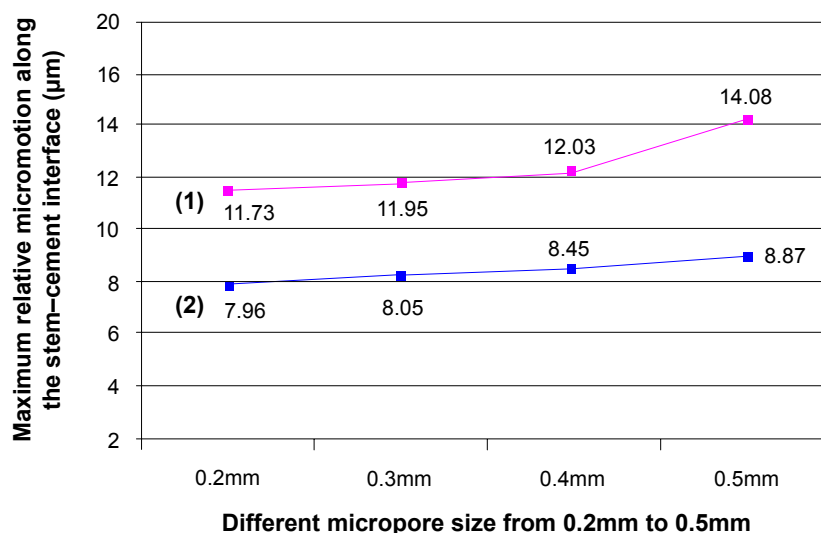


Figure 8.9: The contact pressure normal to the cement surface between the stem and the micropores

From the above it is evident that although there is no significant difference with regard to contact pressure around the shrinkage bumps and the micropores, the relative micromotion adjacent the micropores between the femoral stem and the bone cement was significantly higher, and it is at a level which could initiate fretting wear on polished femoral stems. It should be further noted that the relative micromotion value in other areas away from the micropores along the cement surface was almost zero, i.e. fretting wear could not initiate in these areas. This thus theoretically validated the contribution of the micropores in the cement surface to generation of fretting wear on polished femoral stems.

### 8.2.3.2 Study II: The influence of micropore size on generation of fretting wear

It was demonstrated from study I that the functionality of the shrinkage bumps was incidental in comparison with the micropores on generation of fretting wear on the femoral stem surface. This study investigated the influence of micropore size because it has been previously indicated that the micropores in the cement surface showed a large variety, although it is considered that interfacial porosity has been greatly reduced in terms of size and number with the use of “modern cementing techniques”. Figure 8.10 displays the maximum relative micromotion along the defined path at the stem–cement interface for the two micropores with different sizes. Note that two different levels of micromotion were obtained for the two micropores as explained in section 8.2.3.1. There is a general increase of the relative micromotion value with the rise of micropore size. Accordingly, it is indicated that potentially fretting wear on polished femoral stems would be more severe in the case of larger micropores in the cement surface. As a consequence, in order to retard fretting wear, efforts should be made to reduce both porosity and micropore size at the stem–cement interface, typically through vacuum-mixing the cement, pre-heating the stem, etc.



**Figure 8.10: The maximum relative micromotion along the stem–cement interface between the stem and the micropores with different sizes. The red line shows the tendency for micropore (1) and the blue line shows the tendency for micropore (2)**

Additionally, figure 8.11 illustrates the maximum contact pressure normal to the cement surface with different micropore sizes. It is clear that as the micropore size goes up, the maximum contact pressure increases as well.

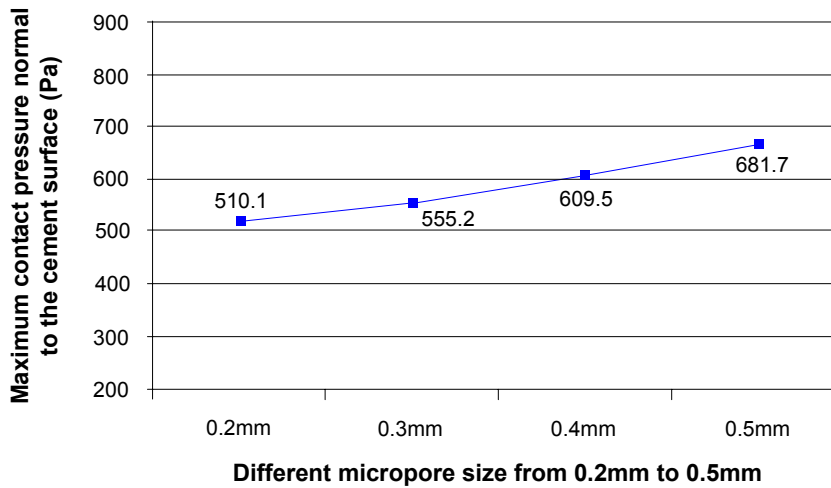


**Figure 8.11:** The maximum contact pressure normal to the cement surface between the stem and the micropores with different sizes

### 8.2.3.3 Study III: The influence of loading level on generation of fretting wear

Although walking is considered to be the most frequent activity during people’s normal life, other activities, such as sitting in a chair, running, and stair climbing in which different physiological loadings are applied to the hip joint also need to be taken into account. This study investigated the influence of loading level on generation of fretting wear. Figure 8.12 shows the maximum relative micromotion along the defined path at the stem–cement interface for the two micropores with different loadings. Again, note that two different levels of micromotion were obtained for the two micropores as explained in section 8.2.3.1. It is evident that although there is no significant difference between these values, the relative micromotion does to a certain degree increase with the rise of the loading level. It is thus indicated that potentially fretting wear present on polished femoral stems would be more severe under higher physiological loadings, and the patients with cemented THR should prevent, as much as possible, the stem from being overloaded excessively.

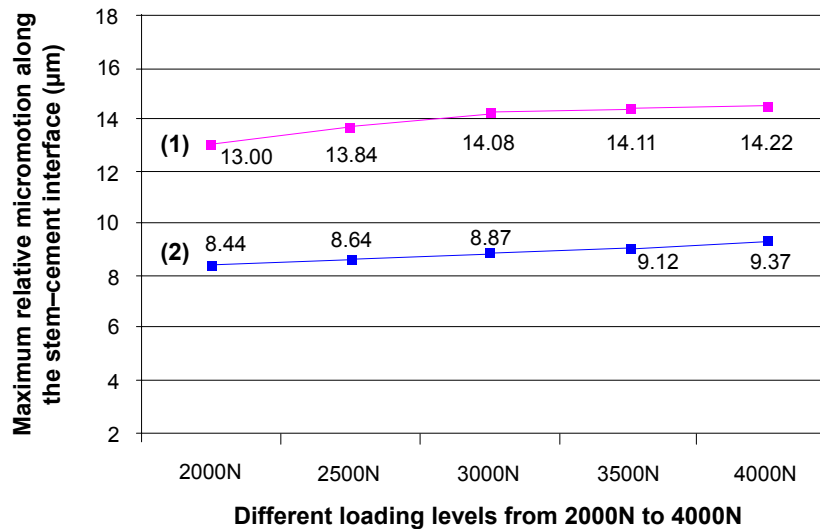


**Figure 8.12:** The maximum relative micromotion along the stem–cement interface between the stem and micropores with different loading levels, the red line shows the tendency for micropore (1) and the blue line shows the tendency for micropore (2)

Additionally, figure 8.13 demonstrates the maximum contact pressure normal to the bone cement surface with different loadings, and it is evident that the contact pressure goes up smoothly as the axial loading increases.

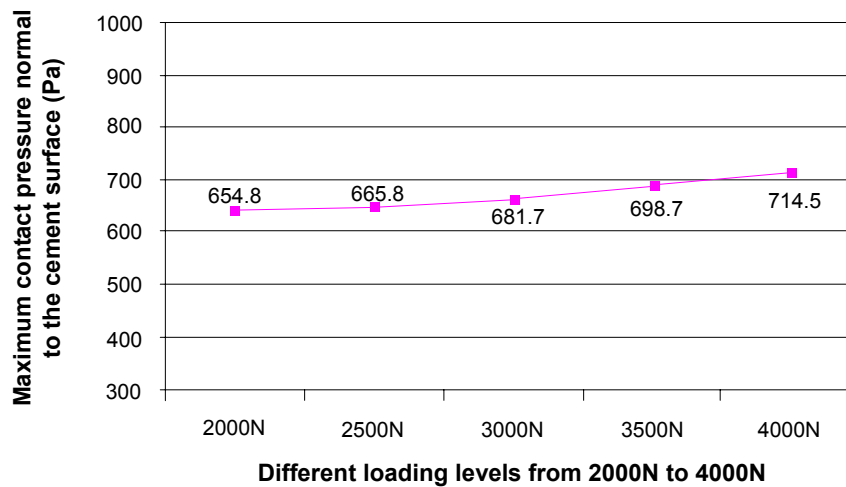


**Figure 8.13: The maximum contact pressure normal to the cement surface between the stem and the micropores with different loading levels**

#### 8.2.4 Discussion

Fretting wear has been clinically detected on polished femoral stems, and it is nowadays showing an increasing significance in the overall wear of cemented THR with generation of both metallic and cement wear debris. However, the initiation and propagation process of fretting wear has not been fully understood as yet. Previous studies have suggested that the shrinkage bumps and the micropores in the cement surface may act as potential participants, but these two factors have not been compared to determine which one contributes more to generation of fretting wear. This is the primary purpose of this study. The presence of shrinkage bumps on the cement surface was firstly reported by Brown *et al.* (2001) using 3D surface analysis to investigate the replication of Simplex P bone cement on stainless steel femoral stems, and later it was indicated that these bumps were present on the surface of many common bone cements following polymerisation. One intractable problem caused by these bumps is that the stress distribution at the stem–cement interface upon physiological loading would be concentrated around these bumps, consequently fretting wear may initiate at those sites where the stem is in close contact with the bumps. Extensive porosity at the stem–cement interface was reported by James et al (1993) based on a study of a multiplicity of *in vivo* and *in vitro* specimens, and it was attributed to the rheological characteristics of the cement. These micropores were further detected in the cement surface in other retrieval studies (Eliades *et al.* 2003), and they were considered to be detrimental as the micropores may decrease the stem–cement interfacial strength and jeopardise the mechanical integrity of the whole cement mantle. Additionally, it was demonstrated through the *in vitro* wear simulations to reproduce fretting wear on the stem surface that the micropores could potentially contribute to generation of fretting wear. By that time, however, only experimental evidence existed and no theoretical confirmation was available. In the present study, the relative contribution of the shrinkage bumps and the micropores was investigated, and it was indicated that the functionality of the shrinkage bumps was incidental because the relative micromotion between the stem and the bumps was significantly lower than

that between the stem and the micropores, which was approximately 14 $\mu$ m. A micromotion of this level at the interface is likely to initiate fretting wear. This is the first time that theoretical evidence has been provided to validate the significance of the micropores on generation of fretting wear on polished femoral stems.

A finite element model has been previously employed to simulate the interaction between two contacting surfaces. As for the stem–cement interface, it is generally accepted that a completely bonded model represents the contact between a matt femoral stem and bone cement, whilst a debonded model simulates the contact between a highly polished femoral stem and bone cement (Norman *et al.* 2001). In the present study, the stem–cement interface was simulated through a debonded model with friction, and the friction coefficient between the femoral stem and the bone cement was assigned to be 0.2. A value around this was generally used in other studies in which an FEA was employed to model the stem–cement interface (Verdonschot and Huiskes 1996, Nuño and Amabili 2002). However, it is considered that the assumption of the stem–cement interface as debonded with friction may not be realistic, which means that there is an absence of adhesion between the stem and the cement. Actually, although no chemical adhesion exists at the interface, a mechanical adhesion of the bone cement to the femoral stem does occur, especially for the matt femoral stems which favour the bone cement to function as an intermediate material assuring implant fixation without reliance on chemical adhesion. The 2D finite element model in this study simulated the contact between a highly polished femoral stem and bone cement. It can be seen from the 2D surface profile of a commercial polished stem that the variation in amplitude is quite small, about 40nm, Figure 8. 14. This could be ignored in comparison with the shrinkage bumps, and consequently it would provide very little mechanical adhesion. Therefore, the model in the present study was considered to be effective. One potential limitation involved in this study was that no non-linear effects such as plastic deformation or creep were introduced. Bone cement is a viscoelastic material and creep occurs when subjected to a constant loading, resulting in relaxation of bone cement stresses and formation of a more favourable stress distribution at the interface. However, it is considered that the creep characteristic of bone cement primarily influences its long term performance, whilst in this study it was the relative micromotion and the contact pressure at the stem–cement interface that was of special interest, therefore the result was not compromised.

“Modern cementing techniques” have been widely employed in surgery when mixing the bone cement and implanting the femoral stem, with the aim of reducing porosity at the stem–cement interface as well as in the cement matrix. In particular, the numbers of macropores (>1mm) was significantly decreased due to the application of vacuum-mixing devices (Wang *et al.* 1996). It was demonstrated in this present study that the maximum relative micromotion increased with the rise of micropore size, which meant that fretting wear could be more severe at the edges of the larger micropores. Therefore, it is considered that the use of vacuum-mixed bone cement is desirable and beneficial in the clinical situation. It was also indicated in the present study that fretting wear was more severe under higher physiological loadings, such as stair climbing, running, etc. Therefore, it is suggested that for a patient with cemented THR, the hip prosthesis should avoid excessive loading wherever possible.

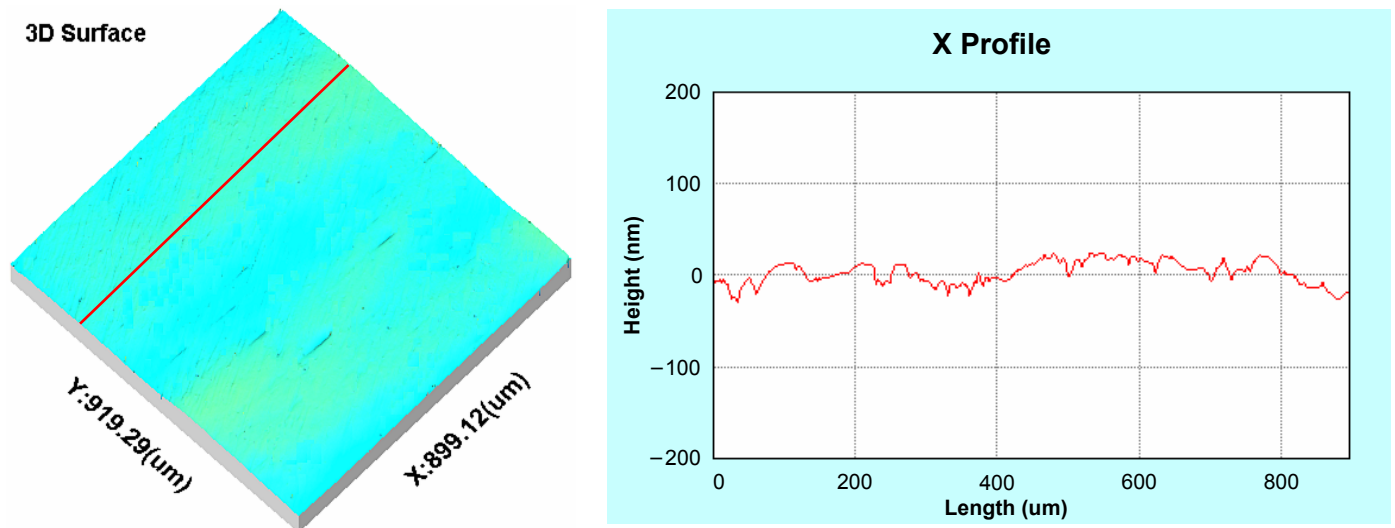


**Figure 8.14: The 2D surface profile of a commercial highly polished femoral stem with the variation in amplitude of about 40nm**

### 8.2.5 Conclusions

In the present study, a local FEA was performed to investigate the relative contribution of the shrinkage bumps and the micropores in the cement surface on generation of fretting wear on polished femoral stems. The influence of micropore size and loading level was also investigated. The following conclusions could be drawn from this work:

- The micropores seem to contribute more to generation of fretting wear in comparison with the shrinkage bumps. Fretting wear would be initiated at those areas where the femoral stem is in contact with the edges of the micropores.
- The relative micromotion increases with the rise of micropore size, indicating that more severe fretting wear would be likely to occur at the edges of the larger micropores.
- The relative micromotion increases with the rise of loading level, indicating that fretting wear is potentially more severe under a higher loading level.
- In order to retard generation of fretting wear on polished femoral stems, it is recommended that an effective method should be performed to reduce porosity and micropore size at the stem–cement interface.

### 8.3 Summary

The FEA reported in this chapter theoretically confirmed the assumption that fretting wear was initiated at those areas where the femoral stem was in contact with the edge of the micropores in the bone cement surface. Incorporating this with the experimental evidence that has been gained in chapter 7, a reasonable conclusion could be drawn to advocate the significance of the micropores in the cement surface in generation of fretting wear on polished femoral stems.

## Chapter 9 Discussion

The introduction of what we now recognise as the modern cemented THR in the 1960s is rightly considered to be one of the major medical breakthroughs in the 20<sup>th</sup> century, especially in the treatment of chronic osteoarthritis. However, it has been reported that very few hip prostheses could survive more than 25 years, associated with a high revision rate of 10% on average. The primary reason for revision continues to be aseptic loosening of the hip prosthesis, either at the acetabular cup or at the femoral stem. It is demonstrated in retrieval studies that wear of the hip prosthesis with the accompanying generation of metallic and non-metallic wear debris contributes significantly to further aseptic loosening by stimulating an adverse macrophage response resulting in periprosthetic bone resorption. Recently, great progress has been made in reducing wear at the articulating head–cup interface with the introduction of cross-linked UHMWPE and hard-on-hard bearing systems. This consequently results in a shift in research interest to another interface which also shows potential contribution to generation of wear debris, namely the stem–cement interface. Fretting wear has been generally accepted as the wear mechanism at this interface due to a low-amplitude micromotion. However, it is indicated that the wear mechanism primarily depends on surface finish of the femoral stem. Whilst previous research has been done with regard to the wear on matt femoral stems (Brown 2006), it is considered essential to further investigate the wear on polished femoral stems, which is the primary aim of the present research project.

According to the theory with reference to the contact between a polished femoral stem and bone cement, the wear at this interface follows a classic fretting mechanism through a low-amplitude oscillatory micromotion. The occurrence of this micromotion initially needs loss of integrity of the stem–cement interface. As a mechanical bonding is present at this interface, studies should firstly address one crucial issue that acts as the prerequisite for fretting wear, i.e. whether debonding at the stem–cement interface would occur under typical physiological loadings. Consequently, the preliminary study of this research concentrated on investigating the bond strength of this interface. By performing a series of pull out tests with the use of simulated polished femoral stem and commercially available bone cements, it is evidently demonstrated that debonding at the stem–cement interface is inevitable, especially for polished femoral stems. Additionally, the detection of bone cement transfer films on the stem surface was observed and considered significant. These transfer films potentially resulted in the slip-stick-slip failure process at the interface. (Chapter 4)

Many matt femoral stems are also currently available on the market, and it is considered that the bond strength between these stems and bone cement is much higher owing to enhanced cement integration. Studies also need to ascertain whether these matt femoral stems would remain stable during their *in vivo* service. Thus, another series of pull out tests was carried out, using simulated femoral stems with polished, glass bead-blasted, shot-blasted, and grit-blasted surface finishes and Simplex P bone cement. Again, it was demonstrated that the pull out forces for these stems were comparable with typical physiological loadings. This finding was further confirmed by a recent study performed by Tevelen *et al.* (2007) in which it was shown that the initial force to release a polished Exeter V40<sup>TM</sup> stem from bone cement was approximately 4kN. Consequently, the stem–cement interface is critical for debonding when the effect of torsional forces is further considered. In this study, 3D surface parameters were introduced to evaluate the stem and the cement surfaces, and they were proved to be a very useful tool in comparison with 2D surface parameters. One

general conclusion was that the static shear strength increased with the rise of surface roughness, which was consistent with previous studies. However, it was shown from the load–displacement plots for the simulated stems that the failure modes could be classified into two categories, with the polished and glass bead-blasted specimens following a slip-stick-slip failure process whilst the shot-blasted and grit-blasted specimens failed by gross interface breakdown. This suggested that the interactions between bone cement and femoral stems with various surface finishes would be essentially different. (Chapter 4)

As debonding at the stem–cement interface has been confirmed through the previous pull out tests, a low-amplitude oscillatory micromotion would therefore likely to occur between the stem and the cement under physiological loadings, and this potentially leads to fretting process at this interface. Whilst fretting wear has been well documented on polished femoral stems in retrieval studies, limited success has been achieved in reproducing this wear through *in vitro* simulation, which is the main purpose of the next part of this research project. In order to fulfill this aim, a new test methodology was proposed through modifications of one current international standard which specifies the conditions for endurance test of hip prosthesis. It showed great success in replicating fretting wear in the initial wear simulation employing a polished Exeter V40<sup>TM</sup> femoral stem and Simplex P bone cement. This was considered the first time that fretting wear has been successfully reproduced *in vitro*. In addition, a technique was developed to detect fretting wear based on grey scale threshold, and then the coverage of the worn area in each Gruen zone on the stem surface could be calculated. Therefore, it has been possible to evaluate the extent of fretting wear and this allows for comparative studies to be carried out in the future. A relocation system was employed to compare surface topography of the femoral stem before and after simulation, and 3D surface parameters were again utilised to evaluate the stem, which quantitatively confirmed that the stem was severely roughened following simulation. Furthermore, a second simulation was performed to consistently reproduce fretting wear under the same experimental conditions, which could validate the effectiveness of the new test methodology. The reduced wear coverage could potentially be attributed to the variety in Simplex P bone cement. Through a scrutiny of the stem and cement surfaces using optical microscope, the contribution of the micropores in the cement surface in initiation and propagation of fretting wear on the stem surface was perceived. This finding was further highlighted by the observation that the stem remained smooth in those pore-free contact areas with bone cement after simulation. (Chapter 5)

Since fretting wear on polished femoral stems has been successfully and consistently reproduced through *in vitro* wear simulations, it is thus useful to gain an insight into the relative micromotion at the stem–cement interface. This was achieved by investigation of migration of a polished Exeter V40<sup>TM</sup> stem within Simplex P cement mantle using the experimental setup previously developed. A new micromotion sensor was manufactured based on deformation of the strain gauge for this purpose. It was demonstrated that the stem migration generally increased with the rise of loading cycle in spite of a gradually decreasing migration rate, and a peak value of 50µm was obtained after 5 million loading cycles. This was considered to be consistent with clinical studies, although the migration value was much less due to certain reasons which were outlined in detail in section 6.2.4. Whilst most RSA studies investigated stem migration relative to the bone rather than the cement and *in vitro* studies usually completed at limited loading cycles, this study has obtained a

better understanding of the relative micromotion at the stem–cement interface, and it also indicates that the setup of the wear simulation could more realistically mimic clinical situations. (Chapter 6)

Obviously there are many participants influencing generation of fretting wear on polished femoral stems, including stem geometry, stem surface finish, the duration of the hip implant *in vivo*, and bone cement brand, etc. The latter two factors were subsequently investigated, considering that it is impossible to test all the stem designs in this research and currently it has not been determined as to the exact surface level that differentiates fretting wear from other wear scenarios. (1) Using a polished Exeter V40™ femoral stem and Simplex P bone cement under the same experimental conditions, the simulation was extended to 10 million loading cycles. An increased coverage of fretting wear was observed on the stem surface, and metallic wear debris was dislodged from the stem and congregated around the micropores in the cement surface. This could act as additional evidence confirming the potential significance of the micropores in generation of fretting wear. In addition, the presence of micro-cracks that initiated from the micropores and propagated to the bulk material was also detected. These micro-cracks may consequently provide a channel enabling transportation of the wear debris. (2) A deep insight into the influence of bone cement brand on generation of fretting wear was gained through performing four more wear simulations, with two utilising CMW 3 bone cement and the other two employing Palacos R bone cement. All these simulations were completed at 5 million loading cycles, and the congregation of the metallic wear debris around the micropores in the cement surface was again identified, although the femoral stems demonstrated similar wear coverage. The microhardness of the bone cements was measured and it was indicated that this parameter did not correlate with generation of metallic wear debris. Additionally, much evidence was given in this study showing the contribution of the micropores in the cement surface in initiation and propagation of fretting wear on the stem surface. (Chapter 7)

Although plenty of experimental evidence with regard to the significance of the micropores was provided in previous studies, no theoretical confirmation was available, and the shrinkage bumps generated on the bone cement following polymerisation may also play a role in the fretting wear process. In order to compare the relative contribution of the shrinkage bumps and the micropores, a 2D finite element analysis was performed. It was indicated that the micropores contributed more to generation of fretting wear as the micromotion around the micropores between the stem and the cement was significantly higher (about 14µm), and it was at a level which could initiate fretting wear on the stem surface. This is considered the first time that the significance of the micropores in generation of fretting wear on polished femoral stems was theoretically validated. Additionally, fretting wear seemed to be more severe with the increase of micropore size and loading level, as a consequence a reduction of porosity and micropores sized at the stem–cement interface is highly advocated and clinically recommended. (Chapter 8)

## Chapter 10 Conclusions

The overall aim of this study is to gain an insight into fretting wear on polished femoral stems and the accompanying generation of wear debris in cemented THR. The following objectives are set out in order to achieve this goal:

- To investigate the stem–cement interfacial bond strength to determine whether debonding at this interface is commonplace.
- To develop a new methodology to reproduce fretting wear on polished femoral stems through *in vitro* wear simulations.
- To design an effective experimental device to study the relative micromotion at the stem–cement interface.
- To analyse the contributory factors on generation of fretting wear, e.g. the duration of *in vivo* service of the hip prosthesis and bone cement brand.
- To obtain a better understanding of the progression of fretting wear and to investigate the potential participants through the use of FEA technique.

In order to fulfil the aims and objectives, a number of experimental studies (including the pull out tests and the *in vitro* wear simulations) associated with theoretical analysis (the development of the finite element model) were performed. The following conclusions can be drawn from the work accomplished in this research project:

- The stem–cement interfacial strength depends primarily on bone cement brand rather than bone cement viscosity and cement mantle thickness.
- The interaction between the femoral stem and the bone cement correlates with stem surface finish, and the interfacial strength increases with the rise of surface roughness.
- Debonding at the stem–cement interface is inevitable under physiological loading, it allows for the occurrence of relative micromotion and subsequent fretting wear at the interface.
- A new test methodology with modifications of standard fatigue testing of the femoral stem is proposed to reproduce fretting wear, and it shows great success in comparison with previous attempts.
- Fretting wear on polished femoral stems is consistently reproduced through *in vitro* wear simulations, which validates the effectiveness of the test methodology.
- Migration of polished stem within the cement mantle goes up as the number of loading cycle increases, with a decreased migration rate.
- The duration of *in vivo* service of the hip prosthesis promotes generation of wear debris and formation of deficiencies in the cement mantle.
- Bone cement brand demonstrates potential influence on generation of fretting wear and also the accompanying wear debris.
- Fretting wear on polished femoral stems initiates in the areas contacting the edges of the micropores in the cement surface, and it propagates and coalesces to form an entire worn zone.
- The contribution of the shrinkage bumps on the cement surface to generation of fretting wear is insignificant in comparison with the micropores.

## Chapter 11 Future studies

The studies completed in this research have gained a deep insight into the interaction between the femoral stem and the bone cement. However, as is often the case it used to be, the work reported here raises as many questions as it answers. There remain an amount of issues that have not been completely elucidated and no conclusive comments have been made. Consequently, these areas warrant further research as they are outlined below. These studies should be performed based on a systematic program of research, concentrating on critical variables under investigation in turn.

### **11.1 Investigation of the influence of storage condition of bone cement on its mechanical properties and long term performance**

It was demonstrated that the initial attempt to reproduce fretting wear on polished femoral stems through *in vitro* wear simulation gave the largest extent of wear on the stem surface. However, the coverage of fretting wear was greatly reduced in the following wear simulations, no matter the same brand of bone cement or different brands of bone cement were used. One potential reason for this discrepancy was attributed to the storage time of the cement. It is considered that variations in physicochemical stability of bone cement may develop over time during storage and this may as a consequence affect its long term performance by modifying the mechanical properties. However, this assumption has not been further confirmed as few studies have investigated the influence of storage condition of bone cement on its mechanical properties and by extension on its long term performance. Therefore, it is considered essential to carry out such a study to gain an insight into this issue. This research primarily involves two steps. The initial step would firstly investigate the mechanical properties of bone cement stored in different conditions, e.g. in air, in saline solution, in bovine serum and with different storage periods. The second step would focus on investigating the potential influence of storage conditions of bone cement on generation of fretting wear by carrying out *in vitro* wear simulations. Through the use of the technique previously developed to detect fretting wear and 3D surface parameters to evaluate fretting wear on the stem surface, a better understanding of this issue would hopefully be obtained. Different brands of bone cement would be collected and studied to ensure universality.

### **11.2 Investigation of the influence of stem geometry and surface finish on generation of fretting wear**

In this research project, the influence of the duration of *in vivo* service of the hip prosthesis and bone cement brand on generation of fretting wear on the stem surface has been studied. However, there are another two factors which may potentially contribute to the fretting process at the stem-cement interface, i.e. femoral stem geometry and surface finish. It has been highlighted in the literature that for a certain femoral stem, it is the design philosophy rather than individual design features that is responsible for the long term survivorship. A matt femoral stem incorporated with a collar and a flange is termed as “shape closed design” which tends to obtain its stability through mechanical interlock between the stem and the cement, and a polished femoral stem associated with a collarless design is termed as “force closed design” which depends on mechanical taper locking of the stem within the cement mantle to achieve self-tightening. In order to differentiate these two factors and investigate their relative contribution to generation of fretting wear, some more *in vitro* wear simulations will be subsequently performed. This again encompasses two steps.

The initial step would firstly study the influence of stem geometry by performing wear simulations employing femoral stems with different geometries but the same surface finish level (e.g. polished Charnley stems and Exeter stems). The second step would then investigate the influence of stem surface finish by collecting and testing certain brand of femoral stems with different surface finishes (e.g. polished and matt Charnley stems or Exeter stems).

### **11.3 Development of a method to evaluate the wear debris at the stem–cement interface**

Wear debris has been implicated in stimulating local inflammatory response which could result in periprosthetic bone loss and subsequently compromise hip implant fixation. As a consequence, the quest for longer survivorship of cemented THR has concentrated on developing new materials and designs which can minimise generation of wear debris. Recently, as great progress has been made in reducing wear at the articulating head–cup interface, the stem–cement interface is showing an increasing significance as another source for generation of wear debris. In this research project, it was indicated from the *in vitro* wear simulations that bone cement brand showed certain influence in terms of generation of wear debris at this interface, with metallic wear debris present around the micropores in the cement surface only for CMW 3 and Palacos R bone cements, and for Simplex P bone cement with increased loading cycles. This is a crucial issue as the metallic wear debris that was dislodged from the femoral stem may contribute to final aseptic loosening of the femoral component. Although it is considered that an initial insight has been gained, further investigations are demanded to develop a method to evaluate this wear debris. It will firstly be extracted from the cement surface and then research would be performed to investigate the composition, weight, and size range, etc. In addition, a comparison of these parameters could also be carried out to look at the diversity between different bone cements.

### **11.4 Further refinement of the simulation rig**

All the *in vitro* wear simulations completed in this research project were performed with reference to modifications of one current standard to test endurance of hip prosthesis, in which a sine wave loading was applied to the femoral stem that was stabilised by acrylic resin in a steel tube at a position of 10° in adduction and 9° in flexion to the stem axis. The initial *in vitro* wear simulation showed great success using this test methodology, and fretting wear was consistently reproduced in the following wear simulations, which can further validate the effectiveness of the proposed methodology. However, it should be noted that the anatomical loading on hip prosthesis is much more complicated during its *in vivo* service, particularly in an aggressive environment of the human body. As the extent of fretting wear on the polished femoral stems was greatly reduced in the following wear simulations, it is therefore considered that there is still feasibility to further refine the simulation rig to reflect anatomical loading. A comprehensive literature review would be performed before a new test methodology is finally determined, and then *in vitro* wear simulations could be carried out to confirm the effectiveness of the new test methodology.

### **11.5 More detailed study of FEA techniques to investigate the stem–cement interface**

FEA has been recognised as a very useful tool when a contact problem between two components is investigated. A 2D finite element model was developed in this research project to represent the stem–cement interface, with the aim of theoretically validating the contribution of the micropores

in the cement surface to the generation of fretting wear on the femoral stem. This preliminary study showed great success in modelling the contact between a polished femoral stem and bone cement. As in the study only the relative micromotion at the stem–cement interface was of interest, no non-linear effects were introduced. However, it is considered to be more realistic to carry out a non-linear analysis when studying the stress distribution in the cement mantle and other long term performances. Additionally, a 3D finite element approach has been nowadays comprehensively employed with the development of modern powerful computers, and it is more preferable in spite of complicated configuration and longer processing time. With the prevalence of FEA techniques to investigate the stem–cement interface, a further research using 3D FEA associated with non-linear effects would be performed to gain a better understanding of the interaction between the femoral stem and the bone cement, such as the damage accumulation in the cement, the influence of stem geometry and surface topography on development of stresses in the cement mantle, etc.

## References

1. Alfaro-Adrián, J., Gill, H.S., Murray, D.W. (1999) Cement migration after THR: a comparison of Charnley and Exeter femoral stems using RSA, *Journal of Bone and Joint Surgery*, 81-B (1), pp. 130–134.
2. Alfaro-Adrián, J., Gill, H.S., Murray, D.W. (2001) Should total hip arthroplasty femoral components be designed to subside, *The Journal of Arthroplasty*, 16 (5), pp. 598–606.
3. Anthony, P.P., Gie, G.A., Howie, C.R., Ling, R.S.M. (1990) Localised endosteal bone lysis in relation to the femoral components of cemented total hip replacements, *Journal of Bone and Joint Surgery*, 72-B (6), pp. 971–979.
4. Armstrong, M.S., Spencer, R.F., Cunningham, J.L., Gheduzzi, S., Miles, A.W., Learmonth, I.D. (2002) Mechanical characteristics of antibiotic-laden bone cement, *Acta Orthopaedica Scandinavica*, 73 (6), pp. 688–690.
5. Bader, R., Steinhauser, E., Holzwarth, U., Schmitt, M., Mittelmeier, W. (2004) A novel test method for evaluation of the abrasive wear behaviour of total hip stems at the interface between implant surface and bone cement, *Proceedings of the Institution of Mechanical Engineers, Part H: Engineering in Medicine*, 218 (4), pp. 223–230.
6. Baleani, M., Fognani, R., Toni, A. (2003) The influence of stem insertion rate on the porosity of the cement mantle of hip joint replacements, *Proceedings of the Institution of Mechanical Engineers, Part H: Engineering in Medicine*, 217 (3), pp. 199–205.
7. Barrack, R.L., Castro, F., Guinn, S. (1996) Cost of implanting a cemented versus cementless femoral stem, *The Journal of Arthroplasty*, 11 (4), pp. 373–376.
8. Barrack, R.L., Mulroy Jr, R.D., Harris, W.H. (1992) Improved cementing techniques and femoral component loosening in young patients with hip arthroplasty: a 12-year radiographic review, *Journal of Bone and Joint Surgery*, 74-B (3), pp. 385–389.
9. Bergmann, G., Graichen, F., Rohlmann, A. (1993) Hip joint loading during walking and running measured in two patients, *Journal of Biomechanics*, 26 (8), pp. 969–990.
10. Bills, P., Blunt, L.A., Jiang, X.Q. (2007) Development of a technique for accurately determining clinical wear in explanted total hip replacements, *Wear*, 263 (7–12), pp. 1133–1137.
11. Blunt, L.A., Jiang, X.Q. (2000) Three dimensional measurement of the surface topography of ceramic and metallic orthopaedic joint prostheses, *Journal of Materials Science: Materials in Medicine*, 11 (4), pp. 235–246.
12. Brown, L.T. (2006) *The use of 3D surface analysis techniques to investigate the wear of matt surface finish femoral stems in total hip replacement*. PhD thesis, University of Huddersfield.
13. Brown, L.T., Blunt, L.A., Howell, J.R. (2001) *Use of 3D analysis to investigate the surface replication of PMMA bone cement on stainless steel femoral stems*. Poster presented at National Measurement Conference, Harrogate, UK, November 2001.
14. British Standards Institution (1993) BS 7252–9: 1993 *Metallic materials for surgical implants, part 9: specifications for high-nitrogen stainless steel*. London: BSI.
15. British Standards Institution (1997) BS 7251–4: 1997 *Orthopaedic joint prostheses, part 2: specifications for articulating surfaces made of metallic, ceramic and plastics materials of hip joint prostheses*. London: BSI.
16. British Standards Institution (2000) BS ISO 14242–2: 2000 *Implants for surgery—wear of total hip joint prostheses, part 2: methods of measurement*. London: BSI.

17. British Standards Institution (2002) BS ISO 5833: 2002 *Implants for surgery—acrylic resin cements*. London: BSI.
18. British Standards Institution (2002) BS ISO 7206-4: 2002 *Implants for surgery—partial and total hip joint prostheses, part 4: determination of endurance properties of stemmed femoral components*. London: BSI.
19. Buly, R.L., Huo, M.H., Salvati, E., Brien, W., Bansal, M. (1992) Titanium wear debris in failed cemented total hip arthroplasty: an analysis of 71 cases, *The Journal of Arthroplasty*, 7 (3), pp. 315–323.
20. Bundy, K.J., Penn, R.W. (1987) The effect of surface preparation on metal–bone cement interfacial strength, *Journal of Biomedical Materials Research*, 21 (6), pp. 773–805.
21. Burke, D.W., O’connor, D.O., Zalenski, E.B., Jasty, M., Harris, W.H. (1991) Micromotion of cemented and uncemented femoral components, *Journal of Bone and Joint Surgery*, 73–B (1), pp. 33–37.
22. Cardiner, R.C., Hozack, W.J. (1994) Failure of the cement–bone interface: a consequence of strengthening the cement–prosthesis interface? *Journal of Bone and Joint Surgery*, 76–B (1), pp. 49–52.
23. Chang, P.B., Mann, K.A., Bartel, D.L. (1998) Cemented femoral stem performance: effect of proximal bonding, geometry, and neck length, *Clinical Orthopaedics and Related Research*, 355 (10), pp. 57–69.
24. Charnley, J. (1960) Anchorage of the femoral head prosthesis to the shaft of the femur, *Journal of Bone and Joint Surgery*, 42–B (1), pp. 28–30.
25. Chen, C.Q.L., Scott, W., Barker, T.M. (1999) Effect of metal surface topography on mechanical bonding at simulated total hip stem–cement interfaces, *Journal of Biomedical Materials Research, Part B: Applied Biomaterials*, 48 (4), pp. 440–446.
26. Chen, P.C., Pinto, J.G., Mead, E.H., D’Lima, D.D., Colwell Jr, C.W. (1998) Fatigue model to characterise cement–mantle interface in dynamic shear, *Clinical Orthopaedics and Related Research*, 350 (5), pp. 229–236.
27. Collis, D.K., Mohler, C.G. (2002) Comparison of clinical outcomes in total hip arthroplasty using rough and polished cemented stems with essentially the same geometry, *Journal of Bone and Joint Surgery*, 84–A (4), pp. 586–592.
28. Cook, J.E. (1998) *Fretting wear of total hip replacement femoral stems*. PhD thesis, University of Exeter.
29. Crawford, R.W., Evans, M., Ling, R.S.M., Murray, D.W. (1999) Fluid flow around model femoral components of differing surface finishes, *Acta Orthopaedica Scandinavica*, 70 (6), pp. 589–595.
30. Cristofolini, L., Teutonico, A.S., Monti, L., Cappello, A., Toni, A. (2003) Comparative *in vitro* study on the long term performance of cemented hip stems: validation of a protocol to discriminate between good and bad designs, *Journal of Biomechanics*, 36 (11), pp. 1603–1615.
31. Crowninshield, R.D., Jennings, J.D., Laurent, M.L., Maloney, W.J. (1998) Cemented femoral component surface finish mechanics, *Clinical Orthopaedics and Related Research*, 355 (10), pp. 90–102.
32. Davies, J.P., Singer, G., Harris, W.H. (1992) The effect of a thin coating of polymethylmethacrylate on the torsional fatigue strength of the cement–metal interface, *Journal of Applied Biomaterials*, 3 (1), pp. 45–50.

33. Davy, D.T., Kotzar, G.M., Brown, R.H., Heiple, K.G., Goldberg, V.M., Heiple Jr, K.G., Berilla, J., Burstein, A.H. (1988) Telemetric force measurements across the hip after total arthroplasty, *Journal of Bone and Joint Surgery*, 70–A (1), pp. 45–50.
34. Dobbs, H.S., Robertson, J.L. (1983) The incidence and significance of rub marks on the stem of removed total hip replacements, *Journal of Biomedical Materials Research*, 17 (1), pp. 83–89.
35. Ebramzadeh, E., Billi, F., Sangiorgio, S.N., Mattes, S., Schmoelz, W., Dorr, L. (2005) Simulation of fretting wear at orthopaedic implant interfaces, *Journal of Biomechanical Engineering*, 127 (3), pp. 357–363.
36. Eliades, T., Papadopoulos, J.S., Eliades, G., Silikas, N., Watts, D.C. (2003) Multi-technique characterization of retrieved bone cement from revised total hip arthroplasties, *Journal of Materials science: Material in medicine*, 14 (11), pp. 967–972.
37. Engel, L. & Klingele, H. (1981) *An atlas of metal damage*. Munich: Carl Hanser Verlag.
38. English, T.A., Kilvington, M. (1979) *In vivo* records of hip loads using a femoral implant with telemetric output (a preliminary report), *Journal of Biomedical Engineering*, 1 (2), pp. 111–115.
39. Espehaug, B., Furnes, O., Havelin, L.I., Engesaeter, L.B., Vollset, S.E. (2002) The type of cement and failure of total hip replacements, *Journal of Bone and Joint Surgery*, 84–B (6), pp. 832–838.
40. Firkins, P.J., Tipper, J.L., Ingham, E., Stone, M.H., Farrar, R., Fisher, J. (2001) A novel low wearing differential hardness, ceramic-on-metal hip joint prosthesis, *Journal of Biomechanics*, 34 (10), pp. 1291–1298.
41. Fisher, D.A., Tsang, A.C., Paydar, N., Millionis, S., Turner, C.H. (1997) Cement mantle thickness affects cement strains in total hip replacement, *Journal of Biomechanics*, 30 (11), pp. 1173–1177.
42. Geesink, R.G., de Groot, K., Klein, C.P. (1987) Chemical implant fixation using hydroxyapatite coatings: the development of a human total hip prosthesis for chemical fixation to bone using hydroxyapatite coatings on titanium substrates, *Clinical Orthopaedics and Related Research*, 225 (12), pp. 147–170.
43. Geiger, M.H., Keating, E.M., Ritter, M.A., Ginther, J.A., Faris, P.M., Meding, J.B. (2001) The clinical significance of vacuum mixing bone cement, *Clinical Orthopaedics and Related Research*, 382 (1), pp. 258–266.
44. Geringer, J., Forest, B., Combrade, P. (2005) Fretting corrosion of materials used as orthopaedic implants, *Wear*, 259 (7–12), pp. 943–951.
45. Ginebra, M.P., Aparicio, C., Albuixech, L., Fernandez–Barragan, E., Gil, F.J., Planell, J.A. (1999) Improvement of the mechanical properties of acrylic bone cements by substitution of the radio-opaque agent, *Journal of Materials science: Material in medicine*, 10 (12), pp. 733–737.
46. Gruen, T.A., McNeice, G.M., Amstutz H.C. (1979) “Modes of failure” of cemented stem–type femoral components: a radiographic analysis of loosening, *Clinical Orthopaedics and Related Research*, 141 (6), pp. 17–27.
47. Hansen, D., Steen, J.J. (1992) Mixing does not improve mechanical properties of all bone cements: manual and centrifugation–vacuum mixing compared for 10 cement brands, *Acta Orthopaedica Scandinavica*, 63 (1), pp. 13–18.
48. Harrigan, T.P., Kareh, J., Harris, W.H. (1990) The influence of support conditions in the loading fixture on failure mechanisms in the push out test: a finite element study, *Journal of Orthopaedic Research*, 8 (5), pp. 678–684.

49. Hatton, A., Nevelos, J.E., Nevelos, A.A., Banks, R.E., Fisher, J., Ingham, E. (2002) Alumina-alumina artificial hip joints. Part I: a histological analysis and characterisation of wear debris by laser capture micro-dissection of tissues retrieved at revision, *Biomaterials*, 23 (16), pp. 3429–3440.
50. Havelin, L.I., Engesaeter, L.B., Espehaug, B., Fumes, O., Lie, S.A., Vollset, S.E. (2000) The Norwegian Arthroplasty Register: 11 years and 73,000 arthroplasties, *Acta Orthopaedica Scandinavica*, 71 (4), pp. 337–353.
51. Havelin, L.I., Espehaug, B., Vollset, S.E., Engesaeter, L.B. (1995) The effect of the type of cement on early revision of Charnley total hip prostheses: a review of 8579 primary arthroplasties from the Norwegian arthroplasty register, *Journal of Bone and Joint Surgery*, 77–A (10), pp. 1543–1550.
52. Herberts, P., Malchau, H. (2000) Long term registration has improved the quality of hip replacement: a review of the Swedish THR Register comparing 160,000 cases, *Acta Orthopaedica Scandinavica*, 71 (2), pp. 111–121.
53. Hernigou, Ph., Le Mouël, S. (1999) Do voids in a femoral cement mantle affect the outcome? *The Journal of Arthroplasty*, 14 (8), pp. 1005–1010.
54. Hoepfner, D.W., Chandrasekaran, V. (1994) Fretting in orthopaedic implants: a review, *Wear*, 173 (1), pp. 189–197.
55. Howell, J.R., Blunt, L.A., Ling, R.S.M. (1999) An analysis of fretting damage seen on explanted femoral stems, *Journal of Bone and Joint Surgery*, 81–B (supplement 2), p. 163.
56. Howell, J.R., Blunt, L.A., Doyle, D., Hooper, R.M., Lee, A.J.C., Ling, R.S.M. (2004) *In vivo* surface wear mechanisms of femoral components of cemented total hip arthroplasties, *The Journal of Arthroplasty*, 19 (1), pp. 88–101.
57. Howie, D.W., Middleton, R.G., Costi K. (1998) Loosening of matt and polished cemented femoral stems, *Journal of bone and joint surgery*, 80–B (4), pp. 573–576.
58. Hull, D. (1981) *An introduction to composite materials*. Cambridge: Cambridge University Press.
59. Huiskes, R., Verdonschot, N., Nivbrant, B. (1998) Migration, stem shape, and surface finish in cemented total hip arthroplasty, *Clinical Orthopaedics and Related Research*, 355 (10), pp. 103–112.
60. Hutchings, I.M. (1992) *Tribology: friction and wear of engineering materials*. London: Edward Arnold.
61. Iesaka, K., Jaffè, W.L., Jones, C.M., Kummer, F.J. (2005) The effects of fluid penetration and interfacial porosity on the fixation of cemented femoral components, *Journal of Bone and Joint Surgery*, 87–B (9), pp. 1298–1302.
62. Ingham, E., Fisher, J. (2000) Biological reactions to wear debris in total joint replacement, *Proceedings of the Institution of Mechanical Engineers, Part H: Engineering in Medicine*, 214 (1), pp. 21–37.
63. James, S.P., Schmalzried, T.P., McGarry, F.J., Harris, W.H. (1993) Extensive porosity at the cement–femoral prosthesis interface: a preliminary study, *Journal of Biomedical Materials Research*, 27 (1), pp. 71–78.
64. Jasty, M., Davies, J.P., O’connor, D.O., Burke, D.W., Harrigan, T.P., Harris, W.H. (1990) Porosity of various preparations of acrylic bone cements, *Clinical Orthopaedics and Related Research*, 259 (10), pp. 122–129.

65. Jasty, M., Maloney, W.J., Bragdon, C.R., O'connor, D.O., Haire, T., Harris, W.H. (1991) The initiation of failure in cemented femoral components of hip arthroplasties, *Journal of Bone and Joint Surgery*, 73-B (4), pp. 551–558.
66. Johnsson, R., Franzén, H., Nilsson, L.T. (1994) Combined survivorship and multivariate analysis of revisions in 799 hip prosthesis: a 10 to 20 year review of mechanical loosening, *Journal of Bone and Joint Surgery*, 76-B (3), pp. 439–443.
67. Jones, R.E., Willie, B.M., Hayes, H., Bloebaum, R.D. (2005) Analysis of 16 retrieved proximally cemented femoral stems, *The Journal of Arthroplasty*, 20 (1), pp. 84–93.
68. Karrholm, J., Nivbrant, B., Thanner, J., Anderberg, C. (2000) *Radiostereometric evaluation of hip implant design and surface finish: micromotion of cemented femoral stems*. Scientific exhibit presented at the 67<sup>th</sup> Annual Meeting of the American Academy of Orthopaedic Surgeons, Orlando, USA, March 2000, pp. 1–14.
69. Kiss, J., Murray, D.W., Turner-Smith, A.R., Bithell, J., Bulstrode C.J. (1996) Migration of cemented femoral components after THR: roentgen stereophotogrammetric analysis, *Journal of Bone and Joint Surgery*, 78-B (5), pp. 796–801.
70. Kuehn, K., Ege, W., Gopp, U. (2005) Acrylic bone cements: mechanical and physical properties, *Orthopaedic Clinics of North America*, 36 (1), pp. 29–39.
71. Langlais, F., Kerboull, M., Sedel, L., Ling, R.S.M. (2003) Annotation: the “French paradox”, *Journal of Bone and Joint Surgery*, 85-B (1), pp. 17–20.
72. Lefevre, N., Moussa, H., Kerboull, L., Kerboull, M., Courpied, J.P. (2004) Polished versus matte cemented femoral stems: a minimum of 10-year follow up study, *Journal of Bone and Joint Surgery*, 86-B (supplement 3), p. 250.
73. Lennon, A.B., Prendergast, P.J. (2002) Residual stress due to curing can initiate damage in porous bone cement: experimental and theoretical evidence, *Journal of Biomechanics*, 35 (3), pp. 311–321.
74. Lewis, G. (2000) Relative influence of composition and viscosity of acrylic bone cement on its apparent fracture toughness, *Biomedical Materials and Engineering*, 10 (1), pp. 1–11.
75. Lewis, G. (2002) Fatigue testing and performance of acrylic bone cement materials: state of the art review, *Journal of Biomedical Materials Research, Part B: Applied Biomaterials*, 66 (1), pp. 457–486.
76. Lewis, J.L., Askew, M.J., Wixson, R.L., Kramer, G.M., Tarr R.R. (1984) The influence of prosthetic stem stiffness and of a calcar collar on stresses in the proximal end of the femur with a cemented femoral component, *Journal of Bone and Joint Surgery*, 66-A (2), pp. 280–286.
77. Liu, C., Green, S.M., Watkins, N.D., Gregg, P.J., Mccaskie, A.W. (2001) Some failure modes of four clinical bone cements, *Proceedings of the Institution of Mechanical Engineers, Part H: Engineering in Medicine*, 215 (4), pp. 359–366.
78. Liu, C., Green, S.M., Watkins, N.D., Gregg, P.J., Mccaskie, A.W. (2002) Creep behaviour comparison of CMW 1 and Palacos R-40 clinical bone cements, *Journal of Materials Science: Materials in Medicine*, 13 (11), pp. 1021–1028.
79. Ludema, K.C. (1996) *Friction, wear, lubrication: a textbook in tribology*. Boca Raton: CRC Press.
80. Maher, S.A., Prendergast, P.J. (2002) Discriminating the loosening behaviour of cemented hip prostheses using measurements of migrations and inducible displacement, *Journal of Biomechanics*, 35 (2), 265–275.

81. Maher, S.A., Prendergast, P.J., Lyons, C.G. (2001) Measurement of the migration of a cemented hip prosthesis in an in vitro test, *Clinical Biomechanics*, 16 (4), 307–314.
82. Malchau, H., Herberts, P., Ahnfelt, L. (1993) Prognosis of total hip replacement in Sweden: follow-up of 92,675 operations performed 1978–1990, *Acta Orthopaedica Scandinavica*, 64 (5), pp. 497–506.
83. Maloney, W.J., Jasty, M., Rosenberg, A., Harris, W.H. (1990) Bone lysis in well fixed cemented femoral components, *Journal of Bone and Joint Surgery*, 72–B (6), pp. 966–970.
84. Maloney, W.J., Schmalzried, T., Harris, W.H. (2002) Analysis of long term cemented total hip arthroplasty retrievals, *Clinical Orthopaedics and Related Research*, 405 (12), pp. 70–78.
85. Medical Devices Agency, hazard notice, London: MDA HN 9801, February 1998.
86. Meneghini, R.M., Feinberg, J.R., Capello, W.N. (2003) Primary hybrid total hip arthroplasty with a roughened femoral stem: integrity of the stem cement interface, *The Journal of Arthroplasty*, 18 (3), pp. 299–307.
87. Mjoberg, B. (1997) The theory of early loosening of hip prosthesis, *Orthopaedics*, 20 (12), pp. 1169–1175.
88. Mohler, C.G., Callaghan, J.J., Collis, D.K., Johnston, R.C. (1995) Early loosening of the femoral component at the cement–prosthesis interface after total hip replacement, *Journal of Bone and Joint Surgery*, 77–A (9), pp. 1315–1322.
89. Müller, R.T., Schürmann, N. (1999) Shear strength of the cement metal interface: an experimental study, *Archives of Orthopaedic and Trauma Surgery*, 119 (3–4), pp. 133–138.
90. Mulroy Jr, R.D., Harris, W.H. (1990) The effect of improved cementing techniques on component loosening in total hip replacement: an 11-year radiographic review, *Journal of Bone and Joint Surgery*, 72–B (5), pp. 757–760.
91. Mummery, L. (1990) *Surface texture analysis: the handbook*. Mühlhausen: Hommelwerke GmbH.
92. Murray, D.W., Carr, A.J., Bulstrode, C.J. (1995) Which primary total hip replacement, *Journal of Bone and Joint Surgery*, 77–B (4), pp. 520–527.
93. Musolino, M.C., Pettit, F.S., Burleigh, T.D., Rubash, H.E., Shanbhag, A.S. (1996) *Analysis of corrosion in stainless steel total hip prostheses*. In: Proceedings of the 15<sup>th</sup> Biomedical Engineering Conference, Dayton, USA, March 1996, pp. 5–6.
94. National Joint Registry for England and Wales, 4<sup>th</sup> Annual Report, 26<sup>th</sup> September 2007, pp.18, ISSN 1753–9382.
95. Norman, T.L., Thyagarajan, G., Saligrama, V.C., Gruen, T.A., Blaha, J.D. (2001) Stem surface roughness alters creep induced subsidence and “taper-lock” in a cemented femoral hip prosthesis, *Journal of Biomechanics*, 34 (10), pp. 1325–1333.
96. Nuño, N., Amabili, M. (2002) Modelling debonded stem–cement interface for hip implants: effects of residual stresses, *Clinical Biomechanics*, 17 (1), pp. 41–48.
97. Paul, J.P. (1967) Forces transmitted by joints in the human body, *Proceedings of the Institution of Mechanical Engineers*, 181 (3J), pp. 8–15.
98. Pilliar, R.M., Cameron, H.U., Welsh, R.P., Binnington, A.G. (1981) Radiographic and morphologic studies of load-bearing porous-surfaced structured implants, *Clinical Orthopaedics and Related Research*, 156 (5), pp. 249–257.
99. Pilliar, R.M. (2005) Cementless implant fixation—toward improved reliability, *Orthopaedic*

*Clinics of North America*, 36 (1), pp. 113–119.

100. Porter, A.E., Taak, P., Hobbs, L.W., Coathup, M.J., Blunn, G.W., Spector, M. (2004) Bone bonding to hydroxyapatite and titanium surfaces on femoral stems retrieved from human subjects at autopsy, *Biomaterials*, 25 (21), 5199–5208.

101. Race, A., Miller, M.A., Ayers, D.C., Cleary, R.J., Mann, K.A. (2002) The influence of surface roughness on stem–cement gaps, *Journal of Bone and Joint Surgery*, 84–B (8), pp. 1199–1204.

102. Race, A., Miller, M.A., Clarke, M., Mann, K.A. (2005) Cement–implant interface gaps explain the poor results of CMW 3 for femoral stem fixation, *Acta Orthopaedica*, 76 (5), pp. 679–687.

103. Ramaniraka, N.A., Rakotomanana, L.R., Leyvraz, P.F. (2000) The fixation of the cemented femoral component: effects of stem stiffness, cement thickness and roughness of the cement–bone surface, *Journal of Bone and Joint Surgery*, 82–B (2), pp. 297–303.

104. Raut, V.V., Siney, P.D., Wroblewski, B.M. (1995) Revision for aseptic stem loosening using the cemented Charnley prosthesis: a review of 351 hips, *Journal of Bone and Joint Surgery*, 77–B (1), pp. 23–27.

105. Revell, P.A., AL–Saffar, N., Kobayashi, A. (1997) Biological reaction to debris in relation to joint prostheses, *Proceedings of the Institution of Mechanical Engineers, Part H: Engineering in Medicine*, 211 (2), pp. 187–197.

106. Rockborn, P., Olsson, S.S. (1993) Loosening and bone resorption in Exeter hip arthroplasties: review at a minimum of five years, *Journal of Bone and Joint Surgery*, 75–B (6), pp. 865–868.

107. Rydell, N.W. (1966) Forces acting on the femoral head–prosthesis: a study on strain gauge supplied prostheses in living persons, *Acta Orthopaedica Scandinavica*, 37 (supplement 88), pp. 1–132.

108. Sabokbar, A., Fujikawa, Y., Murray, D.W., Athanasou, N.A. (1997) Radiopaque agents in bone cement increase bone resorption, *Journal of Bone and Joint Surgery*, 79–B (1), pp. 129–134.

109. Salvati, E.A., Betts, F., Doty, S.B. (1993) Particulate metallic debris in cemented total hip arthroplasty, *Clinical Orthopaedics and Related Research*, 293 (8), pp. 160–173.

110. Sanchez–Sotelo, J., Berry, D.J., Harmsen, S. (2002) Long term results of use of a collared matte–finished femoral component fixed with second generation cementing techniques: a 15–year–median follow up study, *Journal of Bone and Joint Surgery*, 84–A (9), pp. 1636–1641.

111. Scheerlinck, T., Casteleyn, P.P. (2006) The design features of cemented femoral hip implants, *Journal of Bone and Joint Surgery*, 88–B (11), pp. 1409–1418.

112. Semlitsch, M., Willert, H.G. (1980) Properties of implant alloys for artificial hip joints, *Medical and Biological Engineering and Computing*, 18 (1), pp. 511–520.

113. Shardlow, D.L., Hailey, J.L., Ingham, E., Stone, M.H., Wroblewski, B.M., Fisher, J. (1997) Fretting wear of Charnley LFA stems: patterns of wear and clinical significance, *Journal of Bone and Joint Surgery*, 79–B (supplement 4), p. 458.

114. Shardlow, D.L., Green, T., Matthews, J.B., Wroblewski, M., Stone, M.H., Fisher, J. (1999) Wear debris from the cement–stem interface of total hip replacement, *Journal of Bone and Joint Surgery*, 81–B (supplement 1), pp. 36–37.

115. Shen, G. (1998) Topic for debate: Femoral stem fixation—an engineering interpretation of the long term outcome of Charnley and Exeter stems, *Journal of bone and joint surgery*, 80–B (5), pp. 754–756.

116. Silva, M., Shepherd, E.F., Jackson, W.O., Dorey, F.J., Schmalzried, T.P. (2002) Average patient walking activity approaches 2 million cycles per year, *The Journal of Arthroplasty*, 17 (6), pp. 693–697.
117. Skinner, J.A., Todo, S., Taylor, M., Wang, J.S., Pinskerova, V., Scott, G. (2003) Should the cement mantle around the femoral component be thick or thin, *Journal of bone and joint surgery*, 85–B (1), pp. 45–51.
118. Smith, D.C. (2005) The genesis and evolution of acrylic bone cement, *Orthopaedic Clinics of North America*, 36 (1), pp. 1–10.
119. Stone, M.H., Wilkinson, R., Stother, I.G. (1989) Some factors affecting the strength of the cement–metal interface, *Journal of Bone and Joint Surgery*, 71–B (2), pp. 217–221.
120. Sutherland, C.J., Wilde, A.H., Borden, L.S., Marks, K.E. (1982) A ten-year follow up of one hundred consecutive Muller curved stem total replacement arthroplasties, *Journal of Bone and Joint Surgery*, 64–A (7), pp. 970–982.
121. Tevelen, G.A., Percy, M.J., Crawford, R.W. (2007) Re-design of the Exeter V40 long stem femoral component for ease of removal, *Proceedings of the Institution of Mechanical Engineers, Part H: Engineering in Medicine*, 221 (2), pp. 195–201.
122. Thomas, S.R., Shukla, D., Latham, P.D. (2004) Corrosion of cemented titanium femoral stems, *Journal of Bone and Joint Surgery*, 86–B (7), pp. 974–978.
123. Thomsen, P.B., Bovling, S., Jacoby, B., Hansen, T.B. (2000) Aseptic loosening of Boneloc cemented Exeter total hip replacement: a 5 year follow up of the first 100 hips, *Hip International*, 10 (2), pp. 102–107.
124. Vail, T.P., Goetz, D., Tanzer, M., Fisher, D.A., Mohler, C.G., Callaghan, J.J. (2003) A prospective randomized trial of cemented femoral components with polished versus grit-blasted surface finish and identical stem geometry, *The Journal of Arthroplasty*, 18 (supplement 1), pp. 95–102.
125. Vázquez, A.S., Garcia, M.A.S., Fernandez, J., Hernandez, D. (2006) Survivorship of the Charnley low friction hip arthroplasty: results in a general hospital, *Journal of Bone and Joint Surgery*, 88–B (supplement 1), p. 73.
126. Verdonschot, N. (2005) Implant choice: stem design philosophies, in: Breusch, S.J., Malchau, H. *The well-cemented total hip arthroplasty*. New York: Springer Berlin Heidelberg.
127. Verdonschot, N., Huiskes, R. (1996) Mechanical effects of stem cement interface characteristics in total hip replacement, *Clinical Orthopaedics and Related Research*, 329 (8), pp. 326–336.
128. Verdonschot, N., Huiskes, R. (1997a) Acrylic cement creeps but does not allow much subsidence of femoral stems, *Journal of Bone and Joint Surgery*, 79–B (4), pp. 665–669.
129. Verdonschot, N., Huiskes, R. (1997b) The effect of cement–stem debonding in THA on the long term failure probability of cement, *Journal of Biomechanics*, 30 (8), 795–802.
130. Walczak, J., Shahgaldi, F., Heatley, F. (1998) *In vivo* corrosion of 316L stainless steel hip implants: morphology and elemental compositions of corrosion products, *Biomaterials*, 19 (1), pp. 229–237.
131. Walker, P.S., Mai, S.F., Cobb, A.G., Bentley, G., Hua, J. (1995) Prediction of clinical outcome of THR from migration measurements on standard radiographs, *Journal of Bone and Joint Surgery*, 77–B (5), pp. 705–714.
132. Wang, J., Toksvig–Larsen, S., Müller–Wille, P., Franzén, H. (1996) Is there any difference

between vacuum mixing systems in reducing bone cement porosity, *Journal of Biomedical Materials Research, Part B: Applied Biomaterials*, 33 (2), pp. 115–119.

133. Wang, J., Franzén, H., Lidgren, L. (1999) Interface gap after implantation of a cemented femoral stem in pigs, *Acta Orthopaedica Scandinavica*, 70 (3), pp. 234–239.

134. Wang, J., Taylor, M., Flivik, G., Lidgren, L. (2003) Factors affecting the static shear strength of the prosthetic stem–bone cement interface, *Journal of Materials Science: Materials in Medicine*, 14 (1), pp. 55–61.

135. Waterhouse, R.B. (1972) *Fretting corrosion*. Oxford: Pergamon Press.

136. Wheeler, J.P.G., Miles, A.W., Clift, S.E. (1997) The influence of the stem–cement interface in total hip replacement: a comparison of experimental and finite element approaches, *Proceedings of the Institution of Mechanical Engineers, Part H: Engineering in Medicine*, 211 (2), pp. 181–186.

137. Whitehouse, D.J. (1982) The parameter rash—is there a cure? *Wear*, 83 (1), pp. 75–78.

138. Willert, H.G., Ludwig, J., Semlitsch, M. (1974) Reaction of bone to methacrylate after hip arthroplasty: a long term gross, light microscopic and scanning electron microscopic study, *Journal of Bone and Joint Surgery*, 56–A (7), pp. 1368–1382.

139. Williams, H.D.W., Browne, G., Gie, G.A., Ling, R.S.M. (2002) The Exeter universal cemented femoral component at 8 to 12 years: a study of the first 325 hips, *Journal of Bone and Joint Surgery*, 84–B (3), pp. 324–334.

140. Wirz, D., Daniels, A.U., Göpfert, B., Morscher, E.W. (2005) Clinical development and current status: Europe, *Orthopaedic Clinics of North America*, 36 (1), pp. 63–73.

141. Wirz, D., Zurfluh, B., Göpfert, B., Li, F., Frick, W., Morscher, E.W. (2002) Results of *in vitro* studies about the mechanism of wear in the stem–cement interface of THR, in: Winters, G.L., Nutt, M.J. *Stainless steels for medical and surgical applications*. West Conshohocken: ASTM International.

142. Witt, J.D., Swann, M. (1991) Metal wear and tissue response in failed titanium alloy total hip replacements, *Journal of Bone and Joint Surgery*, 73–B (4), pp. 559–563.

143. Wroblewski, B.M., Siney, P.D., Dowson, D., Collins, S.N. (1996) Prospective clinical and joint simulator studies of a new total hip arthroplasty using alumina ceramic heads and cross-linked polyethylene, *Journal of Bone and Joint Surgery*, 78–B (2), pp. 280–285.

144. Wroblewski, B.M., Siney, P.D., Fleming, P.A. (2005) Charnley low frictional torque arthroplasty: clinical developments, *Orthopaedic Clinics of North America*, 36 (1), pp. 11–16.

145. Zahiri, C.A., Schmalzried, T.P., Szusczewicz, E.S., Amstutz, H.C. (1998) Assessing activity in joint replacement patients, *The Journal of Arthroplasty*, 13 (8), pp. 890–895.

146. Zhang, H., Blunt, L., Jiang, X., Brown, L., Barrans, S., Zhao, Y. (2008) Review article: femoral stem wear in cemented total hip replacement, *Proceedings of the Institution of Mechanical Engineers, Part H: Engineering in Medicine*, 222 (5), pp. 583–592.

## Appendix I

### Three-way ANOVA of static shear strength, interfacial porosity, and micropore size for bone cements (Section 4.3)

#### (1) Static shear strength (MPa) descriptive statistics and three-way ANOVA

Thickness	Viscosity	Composition	Mean	Std. Deviation	N
Small	Low	Cemfix 3	2.2837	0.87102	5
		Coriplast 3	4.5897	0.42501	5
	Medium	Simplex P	4.3747	1.18029	5
		CMW 3	1.8940	0.84896	5
	High	CMW 1	3.7790	0.53145	5
		Palacos R	2.4179	1.03532	5
Large	Low	Cemfix 3	2.1837	0.13346	5
		Coriplast 3	1.3986	0.10667	5
	Medium	Simplex P	3.1453	0.52352	5
		CMW 3	3.4535	0.42895	5
	High	CMW 1	4.3461	0.69944	5
		Palacos R	1.9986	0.24838	5
<b>Sig.=0.017</b>	<b>Sig.=0.052</b>	<b>Sig.=0.001</b>			

#### (2) Interfacial porosity (%) descriptive statistics and three-way ANOVA

Thickness	Viscosity	Composition	Mean	Std. Deviation	N
Small	Low	Cemfix 3	2.3452	1.01203	5
		Coriplast 3	0.7825	0.79014	5
	Medium	Simplex P	2.7572	1.44670	5
		CMW 3	8.4402	4.90223	5
	High	CMW 1	4.8911	1.97019	5
		Palacos R	13.5138	3.23892	5
Large	Low	Cemfix 3	2.1220	0.95390	5
		Coriplast 3	0.4615	0.36178	5
	Medium	Simplex P	5.3944	3.34977	5
		CMW 3	11.5514	7.43160	5
	High	CMW 1	2.6813	0.89788	5
		Palacos R	9.3382	1.90756	5
<b>Sig.=0.881</b>	<b>Sig.=0.001</b>	<b>Sig.=0.001</b>			

(3) Micropore size ( $\mu\text{m}$ ) descriptive statistics and three-way ANOVA

Thickness	Viscosity	Composition	Mean	Std. Deviation	N
Small	Low	Cemfix 3	212.425	40.93820	5
		Coriplast 3	109.225	54.31485	5
	Medium	Simplex P	136.980	41.05426	5
		CMW 3	179.502	42.31619	5
	High	CMW 1	67.534	16.25208	5
		Palacos R	143.525	8.00557	5
Large	Low	Cemfix 3	209.343	44.90271	5
		Coriplast 3	110.425	44.78343	5
	Medium	Simplex P	155.443	14.95771	5
		CMW 3	161.347	44.97749	5
	High	CMW 1	69.833	10.04208	5
		Palacos R	148.585	34.68598	5
<b>Sig.=0.759</b>	<b>Sig.=0.001</b>	<b>Sig.=0.001</b>			

**Appendix II**

**Unpaired student t-test between Simplex P and Simplex P-T (Section 4.3)**

Bone cement	Small thickness			Large thickness		
	Strength	Porosity	Micropore size	Strength	Porosity	Micropore size
Simplex P	4.3747	2.7572	136.980	3.1453	5.3944	155.443
Simplex P-T	3.5426	5.981	129.154	4.0768	4.6038	140.242
Sig.	<b>0.315</b>	<b>0.037</b>	<b>0.720</b>	<b>0.091</b>	<b>0.650</b>	<b>0.190</b>

**Appendix III**

**One-way ANOVA of interfacial strength and Tukey-Kramer Post Hoc Test for different surface finish rods (Section 4.4)**

**(1) Interfacial Strength (MPa) Descriptive Statistics and ANOVA**

	N	Mean	Std. Deviation	Std. Error	95% Confidence Interval for Mean		Minimum	Maximum	Sig.
					Lower Bound	Upper Bound			
1	4	2.9450	0.31459	0.15729	2.4444	3.4456	2.63	3.38	<b>0.001</b>
2	4	4.3625	0.95311	0.47656	2.8459	5.8791	2.95	5.02	
3	4	5.3050	0.83229	0.41614	3.9806	6.6294	4.18	5.95	
4	4	16.4225	2.95666	1.47833	11.7178	21.1272	12.55	19.36	
Total	16	7.2587	5.71827	1.42957	4.2117	10.3058	2.63	19.36	

**(2) Post Hoc Tests: Multiple Comparisons**

(I) surface finish	(J) surface finish	Mean Difference (I-J)	Std. Error	Sig.	95% Confidence Interval	
					Lower Bound	Upper Bound
1	2	-1.41750	1.14247	0.615	-4.8094	1.9744
	3	-2.36000	1.14247	0.219	-5.7519	1.0319
	4	-13.47750	1.14247	<b>0.001</b>	-16.8694	-10.0856
2	1	1.41750	1.14247	0.615	-1.9744	4.8094
	3	-0.94250	1.14247	0.842	-4.3344	2.4494
	4	-12.06000	1.14247	<b>0.001</b>	-15.4519	-8.6681
3	1	2.36000	1.14247	0.219	-1.0319	5.7519
	2	0.94250	1.14247	0.842	-2.4494	4.3344
	4	-11.11750	1.14247	<b>0.001</b>	-14.5094	-7.7256
4	1	13.47750	1.14247	<b>0.001</b>	10.0856	16.8694
	2	12.06000	1.14247	<b>0.001</b>	8.6681	15.4519
	3	11.11750	1.14247	<b>0.001</b>	7.7256	14.5094

**Note: 1—Polished; 2—Glass bead-blasted; 3—Shot-blasted; 4—Grit-blasted.**

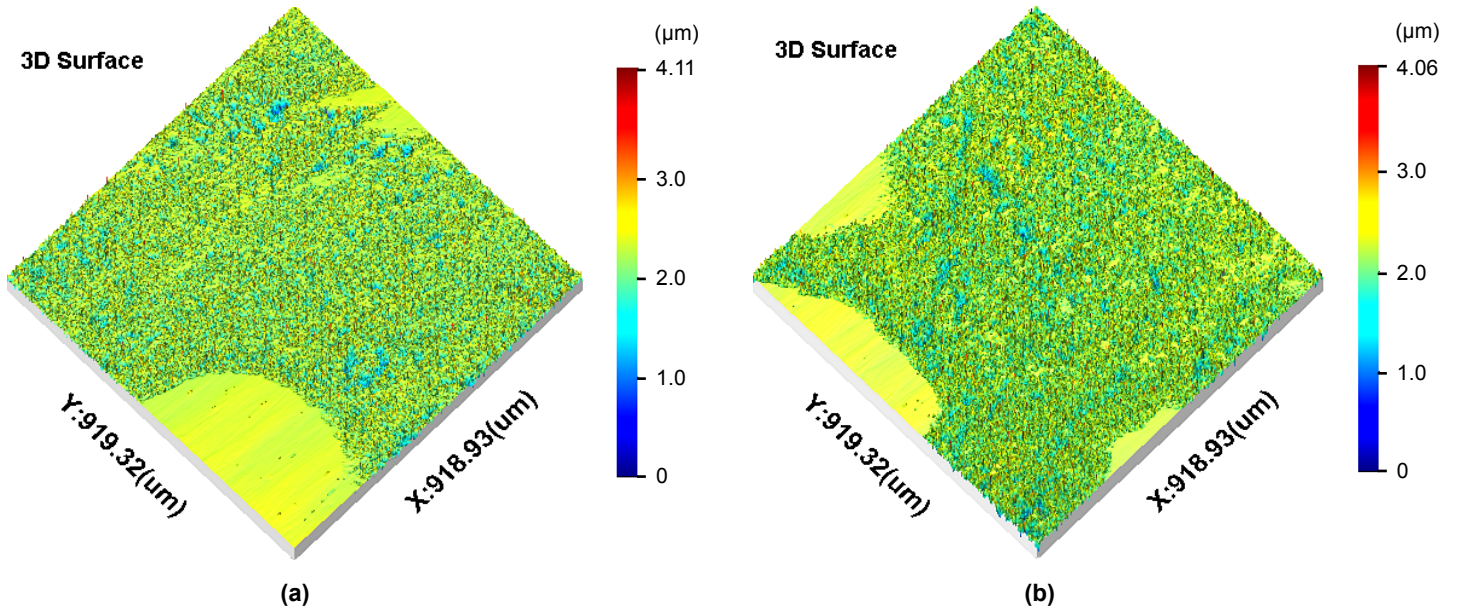
**Appendix IV**

**Summary of the *in vitro* wear simulations to reproduce fretting wear at the stem–cement interface**

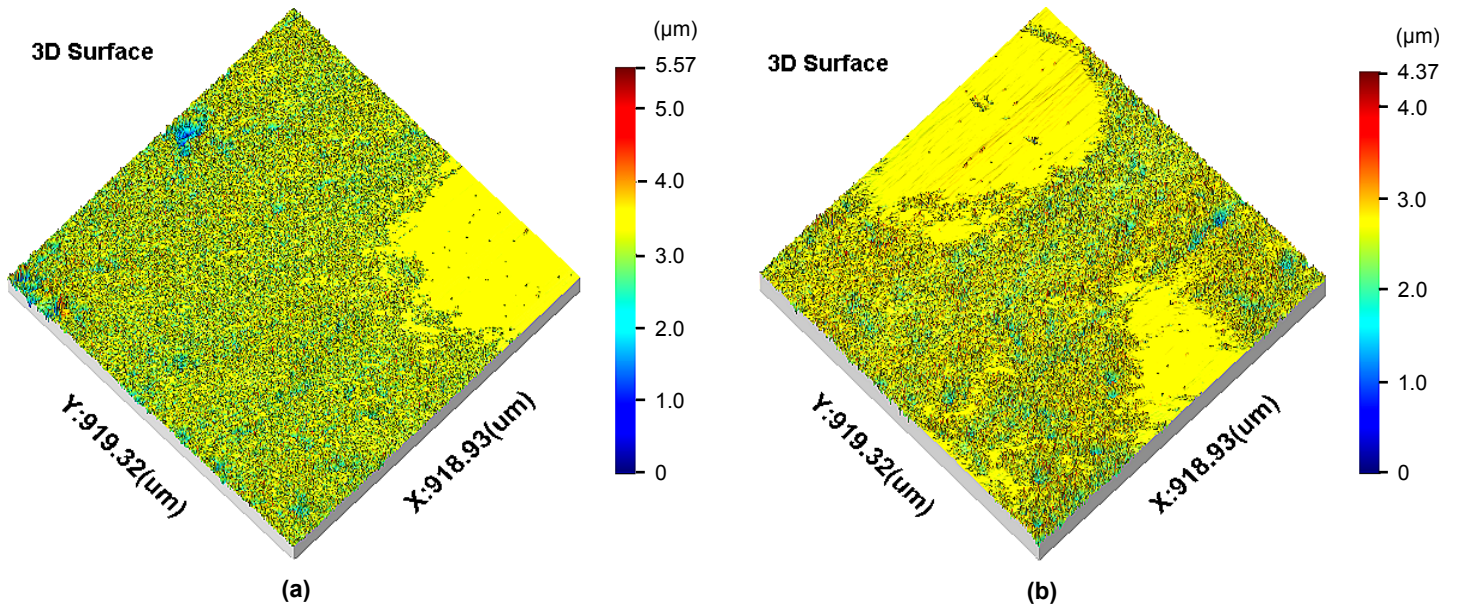
Wear simulations	Femoral stem	Bone cement	Mixing technology	Cycles
Simulation I	Polished Exeter V40™	Simplex P, old	Hand mixed	5 million
Simulation II	Polished Exeter V40™	Simplex P, new	Hand mixed	5 million
Simulation III	Polished Exeter V40™	Simplex P, new	Hand mixed	5 million
Simulation IV	Polished Exeter V40™	Simplex P, new	Hand mixed	10 million
Simulation V	Polished Exeter V40™	CMW 3, new	Hand mixed	5 million
Simulation VI	Polished Exeter V40™	CMW 3, new	Hand mixed	5 million
Simulation VII	Polished Exeter V40™	Palacos R, old	Hand mixed	5 million
Simulation VIII	Polished Exeter V40™	Palacos R, new	Hand mixed	5 million

## Appendix V

### 3D surface topography of the worn areas of Gruen zones 6 and 7 on the femoral stem in simulation I (Section 5.2)



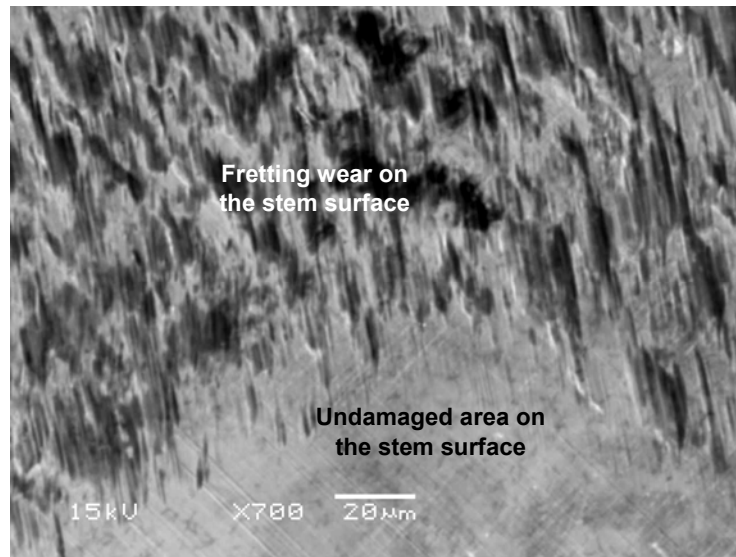
Examples of 3D surface topography of the worn areas of Gruen zone 6 on the femoral stem



Example of 3D surface topography of the worn areas of Gruen zone 7 on the femoral stem

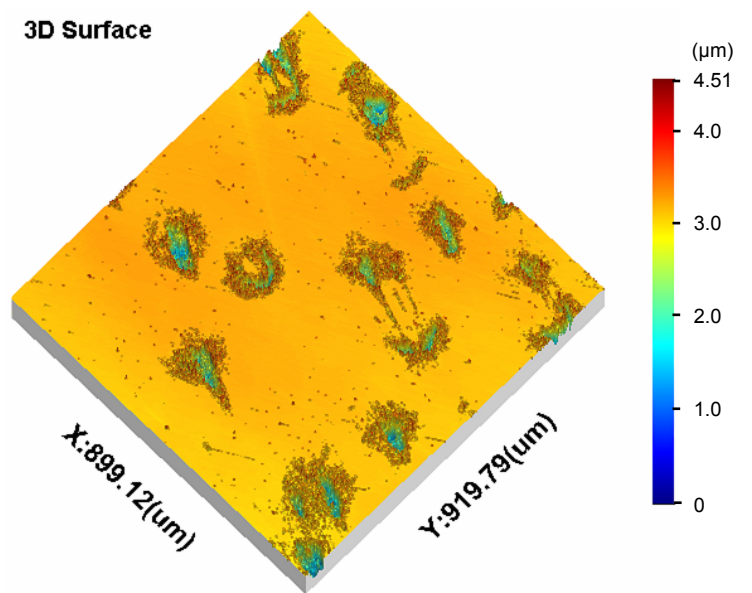
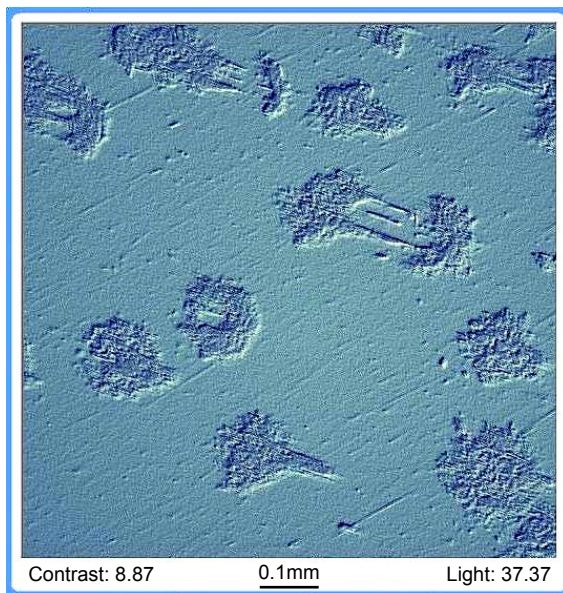
## Appendix VI

Surface topography of fretting zone on the femoral stem from Simulation I measured utilising scanning electron microscope (Section 5.2)



## Appendix VII

Fretting wear scar generated on the femoral stem from Simulation II (Section 5.3)



## Appendix VIII

### Calibration of the new custom-made micromotion sensor (Section 6.2)

Micromotion ( $\mu\text{m}$ )	Output of the strain indicator	Micromotion ( $\mu\text{m}$ )	Output of the strain indicator	Micromotion ( $\mu\text{m}$ )	Output of the strain indicator	Micromotion ( $\mu\text{m}$ )	Output of the strain indicator
4	13	104	306	204	602	304	893
8	25	108	318	208	615	308	905
12	36	112	331	212	627	312	917
16	48	116	342	216	638	316	928
20	60	120	354	220	649	320	941
24	72	124	365	224	659	324	952
28	84	128	378	228	669	328	964
32	96	132	388	232	682	332	975
36	108	136	400	236	693	336	987
40	119	140	412	240	705	340	999
44	130	144	425	244	716	344	1012
48	142	148	437	248	727	348	1023
52	153	152	448	252	740	352	1035
56	165	156	459	256	752	356	1047
60	175	160	471	260	763	360	1061
64	188	164	483	264	774	364	1072
68	200	168	495	268	786	368	1082
72	211	172	506	272	798	372	1094
76	223	176	518	276	810	376	1107
80	236	180	530	280	822	380	1119
84	247	184	542	284	832	384	1130
88	260	188	554	288	845	388	1143
92	270	192	567	292	857	392	1156
96	282	196	578	296	869	396	1167
100	295	200	591	300	881	400	1179

## Appendix IX

### One-way ANOVA of 3D surface parameters of the fretting zones on the stem (Section 7.2)

Wear simulations	Sq ( $\mu\text{m}$ )	Sz ( $\mu\text{m}$ )	Sdq	Sdr (%)
Simulation I	0.3580	3.7248	0.3159	6.5875
Simulation IV	0.3052	3.3890	0.2908	5.4303
Sig.	<b>0.044</b>	<b>0.365</b>	<b>0.136</b>	<b>0.071</b>

## Appendix X

### Microhardness test of the bone cements from the *in vitro* wear simulations (Section 7.3)

#### (1) Simplex P bone cement

Simulation I					Simulation II				
Test	P (kg)	d <sub>1</sub> (μm)	d <sub>2</sub> (μm)	Hardness	Test	P (kg)	d <sub>1</sub> (μm)	d <sub>2</sub> (μm)	Hardness
1	0.3	166.0	164.6	20.36	1	0.3	170.5	170.0	19.19
2	0.3	166.5	163.5	20.43	2	0.3	166.3	164.6	20.32
3	0.3	165.2	165.4	20.36	3	0.3	168.6	167.7	19.68
4	0.3	166.3	166.0	20.15	4	0.3	165.5	164.6	20.42
5	0.3	165.7	165.8	20.25	5	0.3	171.4	168.9	19.11
6	0.3	168.8	164.6	20.02	6	0.3	170.0	164.7	319.86
7	0.3	168.1	165.1	20.04	7	0.3	166.6	163.5	20.42
8	0.3	165.2	164.8	20.43	8	0.3	167.9	167.2	19.82
9	0.3	166.4	165.1	20.25	9	0.3	167.8	166.0	19.97
10	0.3	165.7	164.6	20.27	10	0.3	169.1	164.4	20.00
Mean value				<b>20.30</b>	Mean value				<b>19.88</b>
Simulation III					Simulation IV				
Test	P (kg)	d <sub>1</sub> (μm)	d <sub>2</sub> (μm)	Hardness	Test	P (kg)	d <sub>1</sub> (μm)	d <sub>2</sub> (μm)	Hardness
1	0.3	170.5	168.6	19.35	1	0.3	177.2	169.9	18.47
2	0.3	164.5	166.3	20.33	2	0.3	172.5	170.9	18.87
3	0.3	163.9	171.1	19.83	3	0.3	172.8	169.0	19.05
4	0.3	166.0	169.3	19.79	4	0.3	184.8	175.1	17.18
5	0.3	171.2	166.8	19.48	5	0.3	173.4	170.2	18.85
6	0.3	167.5	168.5	19.71	6	0.3	174.6	172.0	18.52
7	0.3	165.1	166.7	20.12	7	0.3	174.2	171.6	18.61
8	0.3	168.2	167.4	19.76	8	0.3	180.0	174.6	17.70
9	0.3	170.4	168.1	19.42	9	0.3	173.5	173.4	18.49
10	0.3	167.5	166.1	20.00	10	0.3	188.1	182.5	16.20
Mean value				<b>19.78</b>	Mean value				<b>18.40</b>

#### (2) CMW 3 bone cement

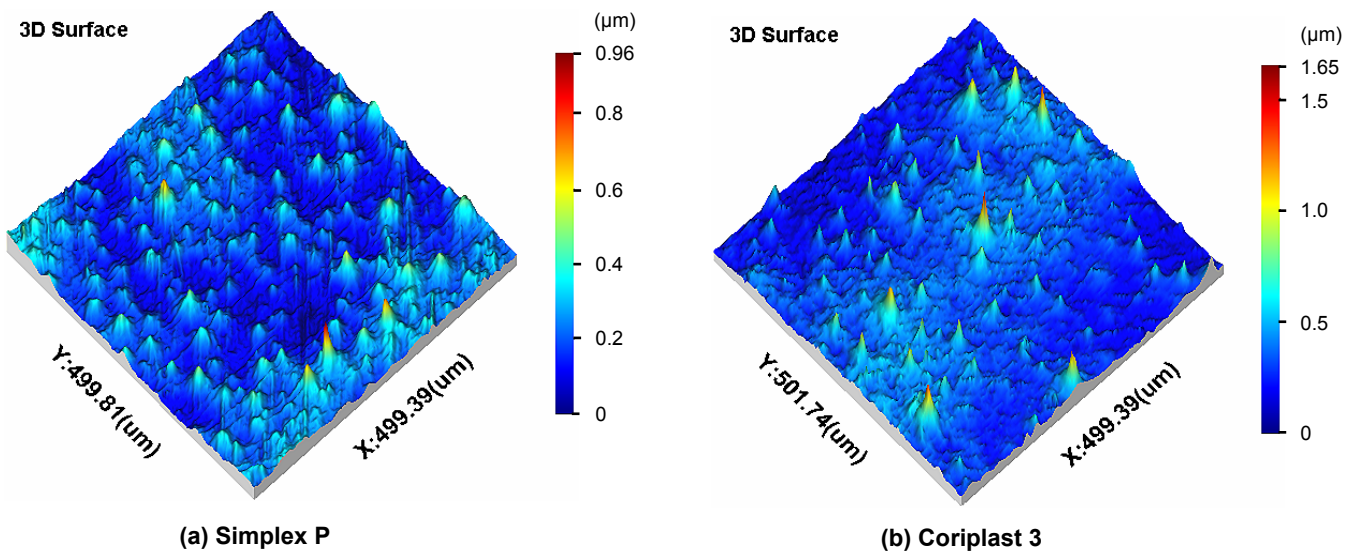
Simulation V					Simulation VI				
Test	P (kg)	d <sub>1</sub> (μm)	d <sub>2</sub> (μm)	Hardness	Test	P (kg)	d <sub>1</sub> (μm)	d <sub>2</sub> (μm)	Hardness
1	0.3	181.6	172.2	17.78	1	0.3	176.6	161.7	19.44
2	0.3	172.9	172.3	18.67	2	0.3	177.9	165.4	18.88
3	0.3	169.0	166.2	19.81	3	0.3	188.1	176.5	16.74
4	0.3	172.3	167.6	19.26	4	0.3	190.3	166.6	17.47
5	0.3	171.0	169.5	19.19	5	0.3	188.2	168.1	17.53
6	0.3	178.8	171.7	18.11	6	0.3	185.7	170.5	17.54
7	0.3	171.8	168.4	19.23	7	0.3	180.8	165.7	18.53
8	0.3	172.5	170.4	18.93	8	0.3	180.3	162.2	18.97
9	0.3	173.9	171.8	18.62	9	0.3	189.5	176.8	16.58
10	0.3	172.5	168.9	19.09	10	0.3	185.9	170.0	17.57
Mean value				<b>18.90</b>	Mean value				<b>17.93</b>

### (3) Palacos R bone cement

Simulation VII					Simulation VIII				
Test	P (kg)	d <sub>1</sub> (μm)	d <sub>2</sub> (μm)	Hardness	Test	P (kg)	d <sub>1</sub> (μm)	d <sub>2</sub> (μm)	Hardness
1	0.3	202.2	193.1	14.24	1	0.3	194.8	186.2	15.33
2	0.3	206.2	192.8	13.98	2	0.3	191.2	185.7	15.67
3	0.3	200.5	194.9	14.23	3	0.3	196.5	190.4	14.87
4	0.3	191.2	187.4	15.52	4	0.3	188.8	183.6	16.05
5	0.3	184.4	180.1	16.75	5	0.3	200.4	193.8	14.32
6	0.3	195.7	193.6	14.68	6	0.3	202.5	193.5	14.19
7	0.3	202.2	189.6	14.50	7	0.3	189.4	180.7	16.25
8	0.3	205.1	195.4	13.87	8	0.3	190.6	178.2	16.36
9	0.3	198.2	190.4	14.84	9	0.3	187.7	178.1	16.63
10	0.3	202.5	192.3	14.28	10	0.3	192.4	187.5	15.42
Mean value				<b>14.70</b>	Mean value				<b>15.51</b>

## Appendix XI

Shrinkage bumps present on Simplex P and Coriplast 3 bone cements following polymerisation (Section 8.3)



## Appendix XII

A selection of publications resulting from this project

### Journals:

1. Brown, L., **Zhang, H.**, Blunt, L., Barrans, S. (2007) Reproduction of fretting wear at the stem-cement interface in total hip replacement, *Proceedings of the Institution of Mechanical Engineers, Part H: Engineering in Medicine*, 221 (8), pp. 963–971.
2. **Zhang, H.**, Brown, L., Blunt, L. (2008) Static shear strength between polished stem and seven commercial acrylic bone cements, *Journal of Materials Science: Material in Medicine*, 19 (2), pp. 591–599.

3. **Zhang, H.**, Brown, L., Blunt, L., Barrans, S. (2008) Influence of femoral stem surface finish on the apparent static shear strength at the stem–cement interface, *Journal of the Mechanical Behavior of Biomedical Materials*, 1 (1), pp. 96–104.
4. **Zhang, H.**, Blunt, L., Jiang, X., Brown, L., Barrans, S., Zhao, Y. (2008) Review article: femoral stem wear in cemented total hip replacement, *Proceedings of the Institution of Mechanical Engineers, Part H: Engineering in Medicine*, 222 (5), pp. 583–592.
5. **Zhang, H.**, Brown, L., Blunt, L., Jiang, X., Barrans, S. (2008) Understanding initiation and propagation of fretting wear on the femoral stem in total hip replacement, *Wear*, in press, doi: 10.1016/j.wear.2008.04.076.
6. Blunt, L., **Zhang, H.**, Barrans, S., Jiang, X., Brown, L. (2008) What results in fretting wear on polished femoral stems, *Tribology International*, accepted, doi: 10.1016/j.triboint.2008.11.007.

#### **Conferences:**

1. **Zhang, H.**, Brown, L., Blunt, L. (2007) *A better understanding of the surface topography at the stem–cement interface*. In: Proceedings of ASME/STLE International Joint Tribology Conference, San Diego, USA, 22<sup>nd</sup>–24<sup>th</sup> October 2007, ISBN 0–7918–3811–0.
2. **Zhang, H.**, Brown, L., Blunt, L., Barrans, S. (2008) *An investigation on generation of debris at the stem–cement interface*. In: Proceedings of the 8<sup>th</sup> World Biomaterials Congress, Amsterdam, The Netherlands, 28<sup>th</sup> May –1<sup>st</sup> June 2008.
3. Blunt, L., **Zhang, H.**, Barrans, S., Brown, L. (2008) *The relative contribution of micropores and shrinkage bumps to fretting wear on polished femoral stems*. In: Proceedings of the 35<sup>th</sup> Leeds–Lyon Symposium on Tribology, Leeds, UK, 9<sup>th</sup>–12<sup>th</sup> September 2008.

# Reproduction of fretting wear at the stem–cement interface in total hip replacement

L Brown, H Zhang\*, L Blunt, and S Barrans

Centre for Precision Technologies, School of Computing and Engineering, University of Huddersfield, Huddersfield, UK

*The manuscript was received on 12 June 2007 and was accepted after revision for publication on 25 July 2007.*

DOI: 10.1243/09544119JEIM333

**Abstract:** The stem–cement interface experiences fretting wear *in vivo* due to low-amplitude oscillatory micromotion under physiological loading, as a consequence it is considered to play an important part in the overall wear of cemented total hip replacement. Despite its potential significance, *in-vitro* simulation to reproduce fretting wear has seldom been attempted and even then with only limited success. In the present study, fretting wear was successfully reproduced at the stem–cement interface through an *in-vitro* wear simulation, which was performed in part with reference to ISO 7206–4: 2002. The wear locations compared well with the results of retrieval studies. There was no evidence of bone cement transfer films on the stem surface and no fatigue cracks in the cement mantle. The cement surface was severely damaged in those areas in contact with the fretting zones on the stem surface, with retention of cement debris in the micropores. Furthermore, it was suggested that these micropores contributed to initiation and propagation of fretting wear. This study gave scope for further comparative study of the influence of stem geometry, stem surface finish, and bone cement brand on generation of fretting wear.

**Keywords:** simulation, fretting wear, stem–cement interface, total hip replacement

## 1 INTRODUCTION

Total hip replacement (THR) is one of the most common and effective procedures performed in the UK and worldwide, with the purpose of dramatically improving the quality of life of patients suffering from hip disorders. With an increasing prevalence of this procedure carried out in younger patients coupled with a longer life expectancy, it is hoped that this total joint system could function well for at least 15–20 years. However, up to 10 per cent of the 60 000 operations performed each year in the UK are to revise prostheses which have failed prematurely. Because of the great efforts made by orthopaedic surgeons and researchers in conducting implant retrieval studies and tissue analyses, aseptic loosening has nowadays been generally accepted as the primary cause of failure of cemented THR, which

predominates mechanical malfunctioning of the stem–cement–bone system [1, 2]. Aseptic loosening can be mainly attributed to bone resorption, which is activated by a macrophage response to particulate debris generated by wear of the components [3, 4]. Theoretically, wear can occur not only at the articulating surface but also at other load-bearing surfaces.

The stem–cement interface has been consistently cited as a weak link in cemented THR [5, 6], which functions as a transitional zone between two materials with significantly different mechanical properties. As a result, a low-amplitude oscillatory micromotion at this interface will happen owing to the unmatched strain when physiological loading is applied [7, 8]. Therefore, there is potential for the stem–cement interface to experience fretting wear *in vivo*. Recently, great progress has been made in reducing wear at the head–cup articulating interface, with the introduction of cross-linked ultra-high-molecular-weight polyethylene (UHMWPE) and hard-on-hard bearing systems [9, 10]. It is thus considered that wear at the stem–cement interface

\*Corresponding author: Centre for Precision Technologies, School of Computing and Engineering, University of Huddersfield, Queensgate, Huddersfield, HD1 3DH, UK. email: h.zhang@hud.ac.uk

## Static shear strength between polished stem and seven commercial acrylic bone cements

Hongyu Zhang · Leigh Brown · Liam Blunt

Received: 22 August 2006 / Accepted: 6 June 2007 / Published online: 10 July 2007  
© Springer Science+Business Media, LLC 2007

**Abstract** The stem–cement interface is one of the most significant sites in cemented total hip replacement and has long been implicated in failure of the whole joint system. However, shear strength at this interface has rarely been compared across a range of commercially available bone cements. The present study seeks to address this issue by carrying out a comparative study. The results indicated that the static shear strength was more dependent on cement type than cement viscosity and volume. However, both cement type and viscosity were contributory factors on porosity and micropore size in the cement surface. There was no significant difference between Simplex P and Simplex P with Tobramycin. Although the bone cements were all hand mixed in this study, the static shear strength was significantly larger than the values recorded by other researchers, and the porosity and micropore size showed much lower values. Bone cement transfer films were detected on the stem surface, typically about 4–10 µm thick. They were considered to be an important factor contributing to high friction at the stem–cement interface after initial debonding.

### Introduction

Acrylic bone cement has been used in cemented total hip replacement (THR) for more than 40 years, the primary

functions of which are as an intermediary material between the prosthesis and the bone to stabilise the femoral stem and to transfer physiological loading of the patient during normal activities [1]. Commercial bone cement is typically supplied as two components: a fine powder consisting of pre-polymerised polymethylmethacrylate (PMMA) or PMMA-based copolymers, benzoylperoxide (BPO) as an initiator for polymerisation reaction, a radiopaque agent commonly barium sulphate ( $\text{BaSO}_4$ ) or zirconium dioxide ( $\text{ZrO}_2$ ), and a vial of liquid composed of Methylmethacrylate (MMA) monomer, *N,N*-dimethyl-*p*-toluidine (DMPT) as an activator for polymerisation reaction and hydroquinone (HQ). Upon mixing the powder and liquid, a dough is formed which is then introduced manually or under mechanical pressure into the bone cavity [2]. Despite clinical application for many years, such problems as thermal necrosis due to exothermic reaction of polymerisation and chemical necrosis as a result of unreacted MMA monomer remain unsolved. “Modern cementing techniques” have been reported to significantly reduce porosity at the stem–cement–bone interfaces as well as in the bulk matrix [3]. Figure 1 displays a scanning electron micrograph (SEM) of Cemfix 3 bone cement surface, where micropores are formed after polymerisation. These micropores are considered to play a critical role in fatigue crack generation and propagation in the cement mantle, and in subsequent aseptic loosening and malfunctioning of cemented THR [4]. The stem–cement interface has consistently been cited as a weak link due to the absence of chemical bonding, and is often a fundamental factor in premature failure of THR [5, 6].

There are many brands of PMMA bone cement commercially available, all are similar in composition but have inherently different characteristics such as viscosity, porosity and mechanical properties during and following

H. Zhang (✉) · L. Brown · L. Blunt  
Centre for Precision Technologies, School of Computing and Engineering, University of Huddersfield, Queensgate, Huddersfield HD1 3DH, UK  
e-mail: H.Zhang@hud.ac.uk

available at [www.sciencedirect.com](http://www.sciencedirect.com)journal homepage: [www.elsevier.com/locate/jmbbm](http://www.elsevier.com/locate/jmbbm)

## Research paper

## Influence of femoral stem surface finish on the apparent static shear strength at the stem–cement interface

H. Zhang\*, L.T. Brown, L.A. Blunt, S.M. Barrans

Centre for Precision Technologies, School of Computing and Engineering, University of Huddersfield, Queensgate, Huddersfield, HD1 3DH, UK

## ARTICLE INFO

## Article history:

Received 29 March 2007

Received in revised form

30 May 2007

Accepted 4 June 2007

Published online 24 July 2007

## Keywords:

Pull out test

Shear strength

Surface finish

Femoral stem

Total hip replacement

## ABSTRACT

The stem–cement interface has long been implicated in failure of cemented total hip replacement. Much research has been performed to study the factors affecting the bond strength between the femoral stem and the bone cement. The present study aims to further investigate the influence of femoral stem surface finish on the apparent static shear strength at the stem–cement interface through a series of pull out tests, where stainless steel rods are employed to represent the femoral stem. The results demonstrated that there was a general tendency for the apparent static shear strength to be increased with the rise of surface roughness. The polished and glass bead-blasted rods illustrated a slip–stick–slip failure whereas the shot-blasted and grit-blasted rods displayed gross interface failure. Following pull out test, cement transfer films were detected on the polished rods, and there was cement debris adhered to the surface of the grit-blasted rods. Micropores, typically 120  $\mu\text{m}$  in diameter, were prevalent in the cement surface interfaced with the polished rods, and the cement surfaces in contact with the shot-blasted and grit-blasted rods were greatly damaged. There was also evidence of metal debris embedding within the cement mantle originating from the tests of the grit-blasted rods, indicating an extremely strong mechanical interlocking at the interface. In summary, this present research demonstrated that the grit-blasted rods with the highest surface roughness were the best in terms of apparent static shear strength. However, it seemed to be most applicable only to the stem designs in which mechanical interlocking of the stem in the initial fixed position was essential.

© 2007 Elsevier Ltd. All rights reserved.

### 1. Introduction

Acrylic bone cement has been clinically employed in cemented total hip replacement (THR) for more than 40 years, and it will continue to be used in total joint replacement especially for those patients with poor bone stock (Charnley, 1960). It is generally accepted that long term durability of cemented THR requires meticulous attention to three elements and two interfaces, which are femoral stem,

stem–cement interface, bone cement, cement–bone interface and bone. The stem–cement interface is a transitional zone which forms a mechanical bonding between the femoral stem and the bone cement, two materials with significantly different mechanical properties. Therefore, this interface has consistently been cited as a weak link in cemented THR. It has been demonstrated in the literature that failure of cemented THR was initiated by debonding at this interface (Jasty et al., 1991; Maloney et al., 2002; Verdonschot and Huiskes, 1997).

\* Corresponding author. Tel.: +44 1484 472769; fax: +44 1484 472161.

E-mail address: [h.zhang@hud.ac.uk](mailto:h.zhang@hud.ac.uk) (H. Zhang).1751-6161/\$ - see front matter © 2007 Elsevier Ltd. All rights reserved.  
doi:10.1016/j.jmbbm.2007.06.001

# Femoral stem wear in cemented total hip replacement

H-Y Zhang<sup>1\*</sup>, L Blunt<sup>1</sup>, X-Q Jiang<sup>1</sup>, L Brown<sup>1</sup>, S Barrans<sup>1</sup>, and Y Zhao<sup>2</sup>

<sup>1</sup>Centre for Precision Technologies, School of Computing and Engineering, University of Huddersfield, Huddersfield, UK

<sup>2</sup>School of Management, Tianjin University, Tianjin, People's Republic of China

The manuscript was received on 24 July 2007 and was accepted after revision for publication on 22 January 2008.

DOI: 10.1243/09544119JEIM346

**Abstract:** The great success of cemented total hip replacement to treat patients with end-stage osteoarthritis and osteonecrosis has been well documented. However, its long-term survivorship has been compromised by progressive development of aseptic loosening, and few hip prostheses could survive beyond 25 years. Aseptic loosening is mainly attributed to bone resorption which is activated by an *in-vivo* macrophage response to particulate debris generated by wear of the hip prosthesis. Theoretically, wear can occur not only at the articulating head–cup interface but also at other load-bearing surfaces, such as the stem–cement interface. Recently, great progress has been made in reducing wear at the head–cup interface through the introduction of new materials and improved manufacture; consequently femoral stem wear is considered to be playing an increasingly significant role in the overall wear of cemented total hip replacement. In this review article, the clinical incidences of femoral stem wear are comprehensively introduced, and its significance is highlighted as a source of generation of wear debris and corrosion products. Additionally, the relationship between femoral stem surface finish and femoral stem wear is discussed and the primary attempts to reproduce femoral stem wear through *in-vitro* wear testing are summarized. Furthermore, the initiation and propagation processes of femoral stem wear are also proposed and a better understanding of the issue is considered to be essential to reduce femoral stem wear and to improve the functionality of cemented total hip replacement.

**Keywords:** wear, femoral stem, bone cement, simulation, total hip replacement

## 1 INTRODUCTION

Cemented total hip replacement (THR) has been performed worldwide to improve the quality of life of patients suffering from debilitating hip disorders, such as end-stage osteoarthritis and osteonecrosis. It is considered to have been a momentous stride forward in orthopaedics since its introduction as a pioneering method to stabilize the femoral stem by Sir John Charnley in the 1960s [1]. The advent of poly(methyl methacrylate) bone cement undoubtedly promoted the great success of cemented THR, and cemented THR still predominates in terms of the number of operations carried out in the UK in

comparison with uncemented THR [2]. However, controversies with regard to bone cement have prevailed across previously published literature, not only because of its inherent shortcomings such as the generation of exothermic heat released by a redox reaction during polymerization and the formation of high residual stresses which could potentially result in initial damage to the bone cement [3], but also owing to a vulnerable interface that has been introduced as a consequence of its application, namely the stem–cement interface. It has been demonstrated in retrieval studies that failure of cemented THR has been initiated at this interface, associated with bone cement fractures and significant areas of osteolysis [4, 5]. In fact, the stem–cement interface, which functions as a transitional zone by mechanical bonding between two materials with significantly different mechanical properties,

\*Corresponding author: Centre for Precision Technologies, School of Computing and Engineering, University of Huddersfield, Huddersfield, UK. email: h.zhang@hud.ac.uk



## Understanding initiation and propagation of fretting wear on the femoral stem in total hip replacement

H. Zhang\*, L.T. Brown, L.A. Blunt, X. Jiang, S.M. Barrans

Centre for Precision Technologies, University of Huddersfield, Queensgate, Huddersfield, HD1 3DH, UK

### ARTICLE INFO

*Article history:*

Received 13 April 2007

Accepted 17 April 2008

Available online xxx

*Keywords:*

Simulation

Femoral stem

Fretting wear

Total hip replacement

### ABSTRACT

The femoral stem–bone cement interface in total hip replacement is supposed to experience low amplitude oscillatory micromotion under physiological loading, consequently leading to fretting wear on the stem surface, which nowadays is considered to play an important part in the overall wear of cemented prosthesis. However, initiation and propagation of fretting wear has been poorly documented and a better understanding concerning this issue has not been established as yet. This present study, on the basis of a profound surface investigation of a polished Exeter V40™ femoral stem and Simplex P bone cement obtained from an in vitro wear simulation, demonstrated that the edges of the micropores in the cement surface matched pretty well to the boundaries of the worn areas on the stem surface. This would indicate that these micropores contributed significantly to the fretting process at the stem–cement interface.

© 2008 Elsevier B.V. All rights reserved.

### 1. Introduction

Cemented total hip replacement (THR) has previously been recognised as a situation that can lead itself to wear, which will happen not only at the articulating head–cup interface but also at other load bearing surfaces. The femoral stem–bone cement interface, which functions as a transitional zone between two materials with significantly different mechanical properties, has consistently been regarded as a weak link in this total joint system [1,2]. Retrieval studies have demonstrated that failed hip prostheses are always associated with debonding at this interface, which is further considered to accelerate aseptic loosening of cemented THR [3,4]. Due to the unmatched strain under physiological loading, the stem–cement interface is supposed to experience low amplitude oscillatory micromotion in vivo. Consequently, fretting wear will inevitably occur at this interface. Recently, great progress has been made to reduce wear at the head–cup interface, with the introduction of cross-linked ultra high molecular weight polyethylene (UHMWPE) and hard–on–hard bearing systems [5,6]. As a result, fretting wear at the stem–cement interface is playing a more and more important part in the overall wear of cemented THR. However, such wear has received relatively little concern and has been poorly documented. Although previous studies have indicated that the wear mechanism at this interface is primarily determined by stem surface finish [7,8], it is considered that a deep insight into

the fretting process has not been gained as yet. This present study therefore aims to establish a better understanding of initiation and propagation of fretting wear on the stem surface by investigating profoundly the femoral stem and bone cement obtained from an in vitro wear simulation.

### 2. Materials and methods

A polished Exeter V40™ femoral stem and Simplex P bone cement were collected following an in vitro wear simulation, which was performed in part with reference to the specifications for endurance of hip prosthesis instructed by ISO standard 7206-4 [9]. The femoral stem and bone cement were first visually evaluated, and then investigated in detail with the use of a Leica stereomicroscope MZ6. Furthermore, the femoral stem was measured employing a Talysurf CCI interferometer, through which the surface features could be delineated more efficiently.

### 3. Results

Fretting wear was successfully reproduced on the stem surface, which mainly concentrated on anterolateral, posteromedial, and under-neck areas (Fig. 1). This complied well with the results of retrieval studies [7,8]. The cement surface was also severely worn in those areas contacting the fretting zones on the stem surface, while the other areas were smooth and appeared undamaged.

The Leica micrographs of the femoral stem demonstrated that many “undamaged islands” were located in the fretting zones. They were entirely surrounded by the worn areas. Additionally, there

\* Corresponding author. Tel.: +44 1484 472769; fax: +44 1484 472161.  
E-mail address: [h.zhang@hud.ac.uk](mailto:h.zhang@hud.ac.uk) (H. Zhang).



Contents lists available at ScienceDirect

Tribology International

journal homepage: [www.elsevier.com/locate/triboint](http://www.elsevier.com/locate/triboint)

## What results in fretting wear on polished femoral stems

Liam A. Blunt<sup>1</sup>, H. Zhang<sup>\*</sup>, Simon M. Barrans<sup>1</sup>, X. Jiang<sup>1</sup>, Leigh T. Brown<sup>1</sup>

Centre for Precision Technologies, University of Huddersfield, Huddersfield HD1 3DH, UK

### ARTICLE INFO

#### Article history:

Received 10 July 2008

Received in revised form

4 November 2008

Accepted 14 November 2008

#### Keywords:

Fretting wear

Total hip replacement

Finite element analysis

### ABSTRACT

Fretting wear on polished femoral stems has previously been observed in retrieval studies, and it is showing an increasing significance in the overall wear of cemented total hip replacement. However, the initiation and propagation process of this wear has not been fully understood, with shrinkage bumps and micropores in the cement surface being potential participants. In the present study, these two factors are investigated through a finite element analysis to determine which contributed more to fretting wear. A 2D finite element model was created to represent the stem–cement interface, and physiological loading was applied on the femoral stem to simulate the situation during patient walking. The analysis indicated that the functionality of the shrinkage bumps was incidental in comparison with the micropores as the relative micromotion between the femoral stem and the shrinkage bumps was significantly lower than that between the femoral stem and the micropores. Additionally, the influence of micropore size and loading level on generation of fretting wear was further investigated, and an effective method was proposed to retard fretting wear and to improve the survivorship of cemented total hip replacement. This study theoretically validated the potential contribution of the micropores to generation of fretting wear.

© 2008 Elsevier Ltd. All rights reserved.

### 1. Introduction

Total hip replacement (THR) has previously been recognised as a tribo-system that can lead itself to wear, especially at the articulating head–cup interface. The wear debris generated due to wear of the ultra high molecular weight polyethylene (UHMWPE) cup can migrate to bone tissue areas surrounding the hip implant, where macrophage response would occur, resulting in further bone resorption. This wear has been suggested as the greatest obstacle to the success of THR [1,2]. Recently, with the renaissance of hard-on-hard bearing couplings, e.g. metal-on-metal and ceramic-on-ceramic configurations, and the advent of cross-linked polyethylene, great progress has been made in reducing wear at the head–cup interface [3–5]. As a consequence, wear at the stem–cement interface has shown an increasing significance in the overall wear of cemented THR [6]. The stem–cement interface has been regarded as a weak link, and wear on the femoral stem surface has been reported in many retrieval studies [7–9] and also in vitro simulations [10]. However, the wear mechanism at this interface has received relatively little concern. It was not until recently when an intensive study on surface

topography of 172 explanted femoral stems was performed that a better understanding of this issue was obtained [11]. It was indicated that wear on the femoral stems was primarily determined by stem surface finish. For polished femoral stems, the morphology of wear indicated a fretting mechanism which generated typical fretting pits below the original stem surface. By contrast, matt femoral stems wore against bone cement through an abrasive mechanism which resulted in generation of both metallic and cement debris before more classical fretting wear ensued.

In spite of the well-documented clinical reports concerning wear on femoral stems, there are few that have been published with regard to the initiation and propagation process of this wear. It has been postulated that the shrinkage bumps on the bone cement surface may act as a potential contributor [12]. These bumps, about 50 µm in width and 1–2.5 µm in height, are formed due to shrinkage of the cement following polymerisation. Fig. 1 shows these bumps on some common bone cement surfaces. It is considered that the stress distribution at the stem–cement interface under physiological loading would be concentrated at these areas. Therefore, fretting wear may be initiated at those sites where the stem is in contact with the shrinkage bumps. In addition, it was shown in another study in which a detailed investigation on surface morphology of the femoral stem and the bone cement was performed that the micropores in the cement surface acted as the wear initiators resulting in generation of fretting wear on polished femoral stems [13]. It is considered that

<sup>\*</sup> Corresponding author at: School of Computing and Engineering, University of Huddersfield, CE1 20, Queensgate, Huddersfield, West Yorkshire HD1 3DH, UK. Tel.: +44 1484 472769; fax: +44 1484 472161.

E-mail address: [h.zhang@hud.ac.uk](mailto:h.zhang@hud.ac.uk) (H. Zhang).

<sup>1</sup> Postal address: LSG/18, Lockside Building, University of Huddersfield, Queensgate, Huddersfield, West Yorkshire, HD1 3DK, UK.

## A BETTER UNDERSTANDING OF THE SURFACE TOPOGRAPHY AT THE STEM-CEMENT INTERFACE

H. Zhang, Centre for Precision Technologies, School of Computing and Engineering, University of Huddersfield, Huddersfield, UK, HD1 3DH

L. Brown, Centre for Precision Technologies, School of Computing and Engineering, University of Huddersfield, Huddersfield, UK, HD1 3DH

L. Blunt, Centre for Precision Technologies, School of Computing and Engineering, University of Huddersfield, Huddersfield, UK, HD1 3DH

### ABSTRACT

The long term stabilization and durability of cemented total hip replacement (THR) depends on not only the bulk properties of the components but also the interfaces through which they interact. The stem-cement interface has been consistently considered as a weak link in the stem-cement-bone system, being a transitional zone between two materials with significantly different mechanical properties. Previous research concerning this interface has been limited to investigation of interfacial shear strength through in vitro test and finite element analysis (FEA). Until now, a deep insight into the contact characteristics at this interface, especially the interaction between femoral stems with various surface finishes and bone cement, has not been established. In addition, it is still an area of debate whether a permanent fixation can be achieved by utilizing a matt femoral stem, and furthermore it is another matter of concern that a matt femoral stem would cause much more damage to the cement mantle, resulting in an acceleration of aseptic loosening of the femoral stem. This present study investigated the surface topography of stainless steel rods and Simplex P bone cement obtained from a series of pull out tests in order to gain a better understanding of the interaction at the stem-cement interface.

### INTRODUCTION

Aseptic loosening has long persisted as the primary cause for premature failure and subsequent revision of cemented THR [1]. It may occur to all types of femoral stem design and it is always associated with debonding at the stem-cement interface, which has been regarded as a weak link in the stem-cement-bone system [2]. As a transitional zone between two materials with significantly different mechanical properties, this interface contributes a lot to the long term durability of the prosthesis. However, in spite of its great importance, the contact characteristics at this interface have received relatively little concern due to the fact that much attention has been paid to studying the bulk properties of the components [3] [4]. Previous research concerning this interface has been limited to investigation of interfacial shear strength through in vitro test and FEA [5] [6]. It is suggested from these studies that bone cement can obtain an excellent contact with the prosthesis

through penetration into the surface features, and this is highly dependent on the surface topography of the femoral stem. In addition, it is generally accepted that matt femoral stems can accomplish a better interfacial strength because of enhanced bone cement integration [7]. However, there is no unanimity of support for the concept that a permanent fixation can be achieved during the long time in vivo service of the prosthesis. In contrast, an inferior clinical outcome has been observed for those femoral stems with a matt surface finish which take advantage of mechanical taper locking of the stem within the cement mantle to acquire re-stabilization. Although previous studies have established the basic contact characteristics at the stem-cement interface, it is considered that a deep insight into the interaction between femoral stem and bone cement is essential to achieve long time survivorship of cemented THR, and thus it should be further investigated.

### MATERIALS AND METHODS

A series of pull out tests, with the use of stainless steel cylindrical rods with polished, glass bead-blasted, shot-blasted, and grit-blasted surface finishes and Simplex P bone cement, were performed to study the simulated stem-cement interfacial shear strength. After the tests, the metallic rods were collected and investigated by a Leica stereomicroscope MZ6 to detect any cement debris present on the surface. In addition, the bone cements were cut longitudinally into two equal parts, the inner surface of which were cleaned with alcohol and then measured employing a Wyko NT 2000 interferometer and a Form Talysurf PGI. The corresponding results were processed using a Surfstand software V3.3 and some selected 3D surface parameters were calculated. Furthermore, these parameters were correlated with the pull out forces at the stem-cement interface.

### RESULTS

The Leica micrographs demonstrated that the polished rod was covered with large areas of bone cement transfer films and there was much cement debris adhered to the surface of the grit-blasted rod (Fig. 1). However, there seemed no bone cement remaining on either the glass bead-blasted rod or the shot-blasted rod.

## An Investigation on Generation of Debris at the Stem Cement Interface

Hongyu Zhang, Leigh Brown, Liam Blunt, Simon Barrans  
 Centre for Precision Technologies, University of Huddersfield, Huddersfield, UK

**Introduction:** Cemented total hip replacement (THR) has been successfully performed worldwide for more than 40 years. However, up to 10% of the 60,000 operations carried out in the UK in 2006 are to revise those prostheses that have failed prematurely. Aseptic loosening is generally accepted as the primary reason for revision. It can be mainly attributed to periprosthetic bone resorption, which is caused by a macrophage response to particulate debris generated by wear of the components. Recently, great progress has been made in reducing wear at the articulating head cup interface, with the renewed interest in use of hard on hard bearing systems. It is therefore considered that fretting wear at the stem cement interface is showing a more and more crucial significance. Indeed, it has been documented concerning particulate debris at this interface across previous literatures [1]. However, few studies have investigated the influence of cement type on it, although cement type has been suggested to affect survivorship of cemented THR [2]. This present work aims to gain insight into this issue by conducting a primary study of bone cements, which are collected from in vitro wear simulations.

**Materials and Methods:** Four simulations were carried out, using polished Exeter V40™ stem and Simplex P (2 simulations), Palacos R (1 simulation) and CMW 3 (1 simulation) cements respectively. The simulations were performed with reference to modifications of ISO 7206-4, which standardises the specifications for endurance test of hip prosthesis. The methodology was discussed in detail elsewhere [3]. One simulation using Simplex P cement was completed at 10 millions cycles, and the others at 5 million cycles. Following each simulation, the cement was evaluated employing an optical stereomicroscope (Leica MZ6) to detect any evidence of wear debris on the surface. Additionally, the cement was gold sputtered to facilitate a scanning electron microscope (SEM, JEOL JSM-6060) study associated with an energy dispersive X-ray analysis (EDXA), from which the composition of the particulate debris can be ascertained. Furthermore, the Vickers hardness of the cement was measured utilising a microhardness tester (Micromet 2101) to correlate it with generation of particulate debris, calculated as the mean value of 10 measurements on the cement surface.

**Results and Discussion:** All the cements demonstrated many micropores in the surface as well as throughout the cement mantle. These micropores showed a large variety of diversities in size and shape. Particularly, there were certain sparking sites around the micropores on Palacos R and CMW 3 cements, which were indicative of metallic particles. In addition, the Simplex P cement surface originating from the simulation with 10 million cycles displayed a similar result (Simplex P-1, fig. 1a). However, there was no evidence of metallic debris on the Simplex P cement surface originating from the simulation with 5 million cycles (Simplex P-2). From the SEM study associated EDXA of the

cement surface, it was demonstrated that both an iron-rich plaque and a chromium-rich plaque were detected around the micropores for Palacos R, CMW 3 and Simplex P-1 cements. This would confirm the presence of metallic debris. This metallic debris could only come from the stem, which was dislodged by fretting process at the stem cement interface during the wear simulation. By contrast, neither an iron-rich nor a chromium-rich plaque was observable for Simplex P-2, which suggested that the particulate debris was just cement particles. These particles were potentially worn off from the cement surface and then retained in the micropores. This indicated that bone cement type as well as loading duration did have some influence on generation of particulate debris. Additionally, the SEM micrograph of Simplex P-1 displayed evidently the presence of micro-cracks at the edge of the micropores (fig. 1b) and these micro-cracks seemed to be initiated from this site and then propagated to its bulk material. This indicated that cement deficiencies will come forth with the increase of loading duration. The Vickers hardness (HV) is 14.7 for Palacos R, 18.9 for CMW 3, 18.4 for Simplex P-1 and 20.3 for Simplex P-2. It seemed that there was no direct relationship between the hardness of the cement and the generation of particulate debris as Palacos R and CMW 3 cements did not show a higher hardness as expected.

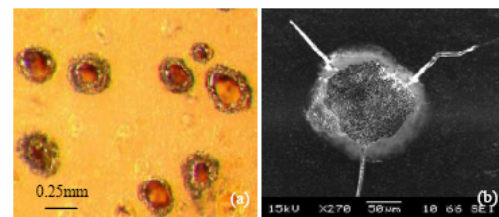


Fig. 1: (a) Optical micrograph of Simplex P-1 cement (b) SEM micrograph of Simplex P-1 cement

**Conclusions:** This present study gained useful insight into the influence of bone cement type on generation of particulate debris at the stem cement interface. Further research is required to validate the current results.

### References:

- Shardlow, D.L., Green, T., Matthews, J., Wroblewski, M., Stone, M.H. and Fisher, J. Wear debris from the cement stem interface of total hip replacement. *J. Bone. Joint. Surg.*, 81B suppl 1, 36, 1999.
- Espehaug, B., Furnes, O., Havelin, L.I., Engesaeter, L.B. and Vollset, S.E. The type of cement and failure of total hip replacements. *J. Bone. Joint. Surg.*, 84B, 832, 2002.
- Brown, L., Zhang, H., Blunt, L. and Barrans, S. Reproduction of fretting wear at the stem cement interface in total hip replacement. *J. Engineering in Medicine*, in press. DOI: 10.1243/09544119JEIM333.

**<The relative contribution of micropores and shrinkage bumps to fretting wear on polished femoral stems>**<Liam Blunt, Hongyu Zhang, Simon Barrans, Leigh Brown><sup>a</sup><sup>a</sup> <Centre for Precision Technologies, University of Huddersfield, Queensgate, Huddersfield, HD1 3DH, UK>**1. INTRODUCTION**

Fretting wear on polished femoral stems has been well documented in clinical reports, but there is little knowledge with regard to its initiation and propagation process. The micropores and shrinkage bumps on bone cement surface has been shown as potential participants in the progression of fretting wear [1, 2], taking into account the differential stress distribution that would be concentrated in these areas at the stem–cement interface. However, it is not clear which one contributes more as no studies have been performed as yet to compare these two factors. This present study thus investigated this issue through a finite element analysis.

**2. METHODS**

A 2D finite element model was created to represent the stem–cement interface using Abaqus 6.6. It encompassed two configurations that simulated the interactions for stem–bumps and stem–micropores respectively, fig. 1 and 2. The stem was 4mm long and 0.75mm wide, and the cement was 3mm long and 0.75mm wide. The bumps were set as 50µm wide and 2.5µm high, and the micropores were set as 0.5mm wide and 0.3mm deep. Such bumps and micropores are common on the cement surface. Totally five bumps and two micropores were defined on the cement surface for the two configurations. The stem was simulated as being made of stainless steel with the Young's modulus of 200GPa and the Poisson's ratio of 0.3. The Young's modulus and the Poisson's ratio for the cement were 2GPa and 0.3.

Both the stem and the cement were assumed to be linearly isotropic and homogeneous, and the element type was CPS4R, i.e. 4-node bilinear plane stress quadrilateral with reduced integration and enhanced hourglass control. A combined loading was applied to the stem, with an axial component 3000N and a transverse component of 250N. The friction coefficient at the stem–cement interface was 0.2, this value was experimentally determined before [3]. A path was defined across the central zone of the cement, and the relative micromotion along the interface was calculated by the following equation,  $\Delta M = M_{\text{cement}} - M_{\text{stem}}$ , where  $M_{\text{cement}}$  is the micromotion of the cement along the path and  $M_{\text{stem}}$  is the micromotion of the stem along the path. In addition, the contact pressure normal to the cement surface was also obtained from the finite element model. These two parameters were then compared to determine the relative contribution of micropores and shrinkage bumps to fretting wear on polished femoral stems.

**3. RESULTS AND DISCUSSION**

The bumps were badly deformed when pressing the stem to the cement, and there existed a gap at the edges of the bumps along the interface before the two materials were in fully contact. Fig. 3 displays the relative micromotion between the stem and the bumps, with the maximum value being less than 0.15µm. It shows an initial low level at the leading edges of the bumps, and then increases significantly towards the central zones with a negative peak in the graph, and finally it reduces again at the trailing edges. Fig 4

demonstrates the contact pressure between the stem and the bumps. It is clear that the contact pressure reaches its peak value of 470Pa at the central zones, and reduces to the minimum at the leading edges and trailing edges of the bumps. It corresponds to the relative micromotion pattern along the interface. It is considered that it is the frictional force that drives the micromotion of the cement, and the frictional force is proportional to the contact pressure. At the leading edges and trailing edges of the bumps where the contact pressure is low, the micromotion of the cement is low as well. Consequently, the relative micromotion at the interface is high because the stem is moving due to the axial loading, and it is negative. In the central zones of the bumps where the contact pressure is higher, the cement moves more, resulting in a decrease of the relative micromotion. Although the relative micromotion does occur between the stem and the bumps, it is too small to initiate fretting wear.

The micropores were badly deformed as well when pressing the stem to the cement, and there was no contact between the stem and the very edge of the micropores. This was caused by the deformation of the micropore edges due to the transverse loading. Fig 5 demonstrates the relative micromotion between the stem and the micropores. It is evident that significantly higher values occur at the edges of the micropores (maximum value 14µm), whilst it is almost zero away from these regions. Fig. 6 shows the contact pressure between the stem and the micropores. It displays zero value at the very edges of the micropores, and reaches its peaks (maximum value 700Pa) at the edges with a small decrease in the central zone. This also corresponds to the relative micromotion pattern along the interface. At the very edges of the micropores where the contact pressure is zero, geometrical deformation of the micropore edges predominates, and the relative micromotion is quite high. Note that the two peaks in fig. 5 refer to opposite sides of adjacent micropores and would therefore have opposite values. As the contact pressure increases at the edges of the micropores, the cement moves more due to the frictional force, resulting in a significant decrease of the relative micromotion. It remains zero although the contact pressure drops off a bit in the central zone.

From the above it is clear that the relative micromotion between the stem and the micropores is significantly larger than that between the stem and the bumps, and it is at a level which could initiate fretting wear. Additionally, it is considered that fretting wear could potentially only initiate at the micropores as the relative micromotion is almost zero in other areas. This theoretically confirms the contribution of the micropores to generation of fretting wear on polished femoral stems.

One limitation involved in the present study is that no non-linear effects were introduced, whilst bone cement is a viscoelastic material and creep occurs when subjected to a constant loading. However, it is considered that the creep behaviour mainly results in relaxation of stress distribution in the cement mantle, and in this study it is the relative micromotion and the contact pressure at the stem–cement interface that are of special interest, therefore the results are not compromised.